

Semileptonic B decays into charmed D(**) mesons from Lattice QCD.

Mariam Atoui

▶ **To cite this version:**

Mariam Atoui. Semileptonic B decays into charmed D(**) mesons from Lattice QCD.. High Energy Physics - Phenomenology [hep-ph]. Université Blaise Pascal - Clermont-Ferrand II, 2013. English. NNT : . tel-00933976v2

HAL Id: tel-00933976

https://theses.hal.science/tel-00933976v2

Submitted on 7 Feb 2014

HAL is a multi-disciplinary open access archive for the deposit and dissemination of scientific research documents, whether they are published or not. The documents may come from teaching and research institutions in France or abroad, or from public or private research centers.

L'archive ouverte pluridisciplinaire **HAL**, est destinée au dépôt et à la diffusion de documents scientifiques de niveau recherche, publiés ou non, émanant des établissements d'enseignement et de recherche français ou étrangers, des laboratoires publics ou privés.

Numéro d'Ordre : DU 2413
EDSF : 776

PCCF T 1307

UNIVERSITÉ BLAISE PASCAL DE
CLERMONT-FERRAND
(U.F.R. Sciences et Technologies)

ÉCOLE DOCTORALE DES SCIENCES FONDAMENTALES

THÈSE

présentée pour obtenir le grade de

DOCTEUR D'UNIVERSITÉ
Spécialité : PHYSIQUE des PARTICULES

par

Mariam ATOUI

Semileptonic B decays into charmed $D^{(**)}$ mesons from Lattice QCD.

Thèse soutenue publiquement le 12 décembre 2013, devant la commission d'examen:

Mme. Asmaa Abada	*Président du jury*
M. Karl Jansen	*Rapporteur*
Mme. Cecilia Tarantino	*Rapporteur*
M. Ziad Ajaltouni	*Examinateur*
M. Jean Orloff	*Examinateur*
M. Vincent Morénas	*Directeur de thèse*

Résumé

Les désintégrations semileptoniques du méson B participent à la détermination de certains paramètres fondamentaux du Modèle Standard. Ce travail décrit essentiellement l'étude des deux canaux de désintégrations $B_s \to D_s \ell \bar{\nu}_\ell$ et $B \to D^{**} \ell \bar{\nu}_\ell$ (où les D^{**} sont les premières excitations orbitales des mésons D ayant une parité positive). Le cadre théorique est celui de la QCD sur réseau qui, en discrétisant l'espace-temps, permet de calculer non perturbativement les fonctions de Green de la théorie. En utilisant l'action à masse twistée avec deux saveurs dégénérées de quarks dynamiques ($N_f = 2$), nous avons commencé par étudier la spectroscopie des états charmés scalaires D_0^* et tenseurs D_2^*. Ensuite, nous avons réalisé la détermination du facteur de forme $\mathscr{G}_s(1)$ décrivant le processus $B_s \to D_s \ell \bar{\nu}_\ell$ dans le Modèle Standard. Ce paramètre offre un moyen d'extraire l'élément de la matrice CKM V_{cb}. Par ailleurs, et pour la première fois en QCD sur réseau, nous avons déterminé les rapports $F_0(q^2)/F_+(q^2)$ et $F_T(q^2)/F_+(q^2)$ dans la région proche du recul nul: ces contributions sont en effet nécessaires afin de discuter ce canal de désintégration dans certains modèles au-delà du Modèle Standard. Enfin, une étude préliminaire du canal de désintégration $B \to D^{**}$ a été abordée où nous avons trouvé une valeur non nulle de l'élément de matrice décrivant la désintégration $B \to D_0^*$ à recul nul contrairement de ce qui est connu à la limite des quarks lourds. Dans le cas du $B \to D_2^*$, nos résultats ont montré un signal indiquant une différence par rapport aux prédictions de masse infinie. Ces calculs sont indispensables afin de tirer une conclusion plus solide concernant le "puzzle 1/2 vs 3/2".

Mots clés: Physique des saveurs lourdes - QCD sur réseau - Phénoménologie des mésons B - Modèle Standard - Facteurs de forme semileptoniques - Excitations orbitales D^{**} - Mésons lourd-légers

Abstract

Semileptonic decays of B mesons provide a rich source of knowledge for determining fundamental parameters of the Standard Model. This work reports mainly on the study of two semileptonic decay channels: the $B_s \to D_s \ell \bar{\nu}_\ell$ and $B \to D^{**} \ell \bar{\nu}_\ell$ (where the D^{**} are the first orbitally excited states of the D mesons having a positive parity). The theoretical framework is Lattice QCD which is considered as the only satisfying approach which calculates in a non perturbative way the transition amplitudes from first principles. By using the twisted mass QCD on the lattice with $N_f = 2$ dynamical flavors we studied, first, the spectroscopy of the scalar D_0^* and the tensor D_2^* states. Then, we determined the normalization $\mathscr{G}_s(1)$ of the form factor dominating $B_s \to D_s \ell \bar{\nu}_\ell$ in the Standard Model which provides a means of extracting the CKM matrix element V_{cb}. Next, we make the first lattice determination of $F_0(q^2)/F_+(q^2)$ and $F_T(q^2)/F_+(q^2)$ near the zero recoil. The obtained results are important for the discussion of this decay in various scenarios of physics beyond the Standard Model. Finally, we did a preliminary study of $B \to D^{**}$ where we have obtained a non vanishing matrix element corresponding to the decay of B into the D_0^* at zero recoil contrary to what was known in the heavy quark limit. Moreover, the computations corresponding to $B \to D_2^*$ show a signal indicating a difference with respect to the infinite mass limit prediction. These results are important to draw a firm conclusion on the "1/2 vs 3/2 puzzle".

Keywords:

Heavy Flavor Physics - Lattice QCD - Phenomenology of B mesons - Standard Model - Semileptonic form factors - Orbital excitations D^{**} - Heavy-light mesons

Remerciements

Mes remerciements s'adressent à toute personne contribuant de près ou de loin à l'élaboration de ce travail. Je commence par remercier Alain Falvard le directeur du Laboratoire de Physique Corpusculaire (LPC-Clermont Ferrand) pour m'avoir accordé la chance de suivre ma thèse jusqu'à sa fin dans des bonnes conditions.

Je suis si heureuse d'avoir fait partie de l'équipe Théorie du LPC. À ce titre, je salue Jean François Mathiot, Jean Orloff, Ana Texeira et je remercie tout spécialement Vincent Morénas qui a supervisé ce travail et qui m'a ouvert la voie pour entrer dans le monde des doctorants. Ce monde qui m'a été une expérience de vie dans laquelle j'ai vécu les plus difficiles mais aussi les plus jolis moments. Vincent, je te remercie pour ton aide ainsi que pour tous les moments que tu m'as consacrés pour discuter, répéter, corriger, etc. J'ai beaucoup appris de ta façon pédagogique de présenter les idées et j'ai profité, grâce à toi, de participer aux conférences internationales, écoles et réunions scientifiques.

J'envoie encore un grand merci à Ana Texeira. Tu m'as écoutée quand j'avais besoin du quelqu'un qui m'écoute. J'apprécie toujours ta façon de "lutter" pour le bien des doctorants. Je te remercie pour tes conseils, tes remarques, l'attention que tu m'as prêtée ainsi que ton encouragement afin que j'aille vers la réussite.

Je m'adresse à Orsay, au Laboratoire de Physique Théorique (LPT), où mon travail a senti son éclosion. En particulier, à Olivier Pène, le "père" de la collaboration qui rassemblait presque tous les mois le groupe Lattice et qui a toujours su montrer disponible, ainsi que Benoît Blossier, pour répondre à mes questions qui ne se terminent jamais. Olivier et Benoît, vous rencontrer et travailler avec vous m'a été une vraie chance. J'ai été guidée par vos explications qui m'ont permis un épanouissement scientifique propice au bon cheminement de cette thèse. Je vous remercie du fond du coeur. Les jours que j'ai passés à Orsay m'ont beaucoup été utiles. J'en profite pour remercier Konstantin Petrov, Francesco Sanfilippo, Jean Pierre Leroy, Alain Le Youanc et Philippe Boucaud pour l'aide qu'ils ont apportée.

Je n'oublierai jamais Damir Becirevic. Avec lui, mes yeux s'ouvraient sur la physique comme je l'aimais. En lisant ses commentaires et ses explications, j'avais l'impression de lire une histoire que je n'aime jamais qu'elle soit terminée. Sa façon d'interpréter, de travailler ainsi que d'expliquer m'a beaucoup

impressionnée. Je n'ai pas mal acquis de ses connaissances et je n'ai jamais hésité de prendre de son trésor. Croiser et travailler avec cet homme a été un beau cadeau que je n'oublierai jamais.

Les lignes suivantes s'adressent à Asmaa Abada, la femme dont j'ai regardé la photo un jour, quand j'étais toujours une étudiante au Liban et que j'avais l'habitude de lire "Sciences et Vie", et je me suis demandée pourrais-je la croiser un jour? pourrais-je être comme elle un jour? pourrais-je être au sein du LPT un jour? Et voilà ... pour certains c'est rien, mais pour moi c'est ce que je "rêvais" il y a cinq ans! Je te remercie Asmaa pour m'avoir honorée de présider le jury. Tu m'as été un modèle sans ce que je te connaissais et tu le resteras.

Aussi, je suis infiniment reconnaissante envers Karl Jansen et Cecilia Tarantino pour avoir accepté d'être rapporteurs de mon travail. Ce fut un honneur de compter des physiciens tels que vous parmi les membres de mon jury. Honneur que je partage également pour la présence dans ce même jury de Ziad Ajaltouni et Jean Orloff. Vous faites partie des physiciens inestimables à la communauté scientifique et je vous remercie pour avoir examiné ce travail.

C'est avec une extrême reconnaissance que je remercie Mme. Zeinab Saad, la doyenne de l'École Doctorale des Sciences et Technologies (EDST) ainsi que Mr. Haitham Zaraket, professeur à l'Université Libanaise (UL) à Beyrouth, pour l'attention et le soutien qu'ils m'ont témoignés et le Conseil National de la Recherche Scientifique au Liban (CNRS-L) qui, en m'attribuant la bourse d'étude, a allégé mon fardeau financier qui me permet de mettre davantage l'accent sur l'aspect le plus important de l'apprentissage. Votre générosité m'a inspirée de redonner à la communauté. J'espère qu'un jour je serai à mesure d'aider les étudiants à atteindre leurs objectifs tout comme vous l'avez fait pour moi.

Je ne pourrai pas retranscrire ici la fierté et la reconnaissance que j'éprouve à l'égard de mes parents. Vous m'avez entourée avec votre attention et votre confiance. Vous m'avez agrandie en m'apprenant que rien ne vaut l'accroissement des connaissances. Vous m'avez appris comment aller au delà des barrières pour atteindre ce que je vise. Bien sûr, je n'oublie pas mes frères et mes soeurs auxquels je dis: vous m'avez réchauffée par votre amour, vos sourires ainsi que vos encouragements. Je me souviens toujours des moments "enfantins" qu'on a passés ensemble et qui me font rire jusqu'à l'instant. Je vous aime tous!

La présence des amis dans nos quotidiens embellit et colorie le trajet suivi. Je tiens également à remercier Zeinab, Fatima, Sarah, Varvara, Meriem et Siavash pour leur encouragement et leur soutien. Je vous souhaite une bonne chance pour la suite.

Finalement, même dans mes révoltes passagères, tu ne m'as donné que l'amour et tu ne m'as éprouvé que la bonté. Sans toi, je ne pourrai espérer la lumière. Je te remercie de me permettre encore aujourd'hui de me grandir avec toi ... mon amour Mostafa.

« ... Et dis : Ô mon Seigneur, accroît mes connaissances.»

Le Coran, Sourate Tâha, verset 114



à ma famille que sa chaleur m'a manquée beaucoup dans les pays froids,

à mon Mostafa,

à toute fille qui suit toujours les rêves qu'elle a dans ses yeux ...



Contents

Introduction **1**

I Phenomenology of beauty mesons 3

1 Flavor in the Standard Model **5**

1.1 The Standard Model 6

1.2 Parameterization of the CKM matrix 13

1.3 The unitarity triangle 15

2 Semileptonic B decays **17**

2.1 A short review on semileptonic B decays 18

2.2 Charmed D meson states 21

2.3 Exclusive $B \to D^{(*)}$ decays 24

2.4 Status of $B \to D^{**}\, \ell\, \bar{\nu}_\ell$ 27

II Lattice gauge theory 33

3 Lattice QCD **35**

3.1 QCD in the continuum 36

3.2 Gauge field on the lattice 38

3.3 Fermion field on the lattice 43

3.4 Twisted-mass action 49

4 Propagator computation in LQCD **55**

4.1 Computation of a physical observable 56

4.2 Hadronic two-point correlation functions 58

4.3 Propagator computation 59

4.4 Resolution of linear systems 67

4.5 Matching to the continuum limit . . . 69
4.6 Non-perturbative renormalization . . . 72

III Spectroscopy and form factors 73

5 Orbital excitations of charmed mesons from tmLQCD 75
5.1 Interpolating fields . . . 76
5.2 Effective mass extraction . . . 80

6 $B_s \to D_s\, \ell\, \bar{\nu}_\ell$ near zero-recoil 89
6.1 Extraction of the form factors . . . 91
6.2 Determination of $\mathcal{G}_s(1)$ . . . 98
6.3 Semileptonic B decay to τ leptons and NP . . . 104

7 $B \to D^{**}\, \ell\, \bar{\nu}_\ell$ transitions using "real" charm quarks 111
7.1 The theoretical framework . . . 112
7.2 Going to the lattice . . . 116
7.3 B transitions to the scalar $D_0^*\,(J^P = 0^+)$ meson . . . 122
7.4 B decays to the tensor D_2^* state . . . 129

Conclusion 137

Appendices 143

A Quantum Field Theory on the Lattice 143
A.1 Short description of relevant notions in the continuum . . . 143
A.2 From Minkowski to Euclidean space . . . 144
A.3 Discretization of the scalar field . . . 145

B Input file 149

C Extraction of the $B \to D^{**}$ form factors 153
C.1 Polarization tensor for the ${}^3P_2$ state . . . 153
C.2 $B \to D_2^*$ form factors . . . 155

D Semileptonic decay widths 159
D.1 Stating the problem . . . 159
D.2 Hadronic tensor $W_{\mu\nu}$ . . . 160

D.3 Measure dΦ of the phase space 162

List of Tables

2.1 The "heavy-light" decomposition of the charm S wave states. The superscript P denotes the parity of the state. 22

2.2 The "heavy-light" decomposition of the D^{**}. The D^{**}'s belonging to the same doublet are related by HQS. The superscript P denotes the parity of the state. 22

2.3 Masses and decay widths of D^{**} [1]. 24

5.1 Basis of the quark bilinear having an angular momentum J^P where the highlighted columns correspond to the scalar $J = 0^+$ state. The matrix γ_4 is the Euclidean equivalent of the γ_0 matrix. 76

5.2 Basis of the quark bilinear having an angular momentum J^P and its corresponding representation spaces. 79

5.3 Basis of gauge links for each required IR. 79

5.4 Meson interpolating fields for the 2^+ states. The colored rows contain the expressions we chose for our study. The spatial indices i and k are all different when appearing in a formula. In the last row, $\phi_1 = (s_2 - s_3)/2$ and $\phi_2 = (2s_1 - s_2 - s_3)/\sqrt{8}$. 80

6.1 Simulation details for the correlator computations at four values of the gauge coupling $\boldsymbol{\beta} =$ 3.80, 3.90, 4.05 and 4.20. The quantities $a\mu_\ell$, $a\mu_s$ and $a\mu_h$ stand for light, strange-like and heavy (i.e. charm-like and heavier) bare valence quark mass values respectively, expressed in lattice units. 94

6.2 The renormalization constants Z_V, Z_A, and Z_T in the $\overline{\text{MS}}$ scheme at 2 GeV, and lattice spacing estimates for each value of the inverse gauge coupling $\boldsymbol{\beta}$. 95

6.3 The values of the ratio $\sigma^{(i)}$ extrapolated to the continuum limit using Eq. (6.44) for each heavy valence quark masses $m_h^{(i)} = \lambda^i m_c$. Results of extrapolation with $\beta_s^{(i)}$ as a free parameter are shown separately from those in which the observed independence on the sea quark mass is imposed in the fit (6.44) by setting $\beta_s^{(i)} = 0$. 101

6.4 Results for $\mathscr{G}_s(w)$, the dominant factor governing the hadronic matrix element relevant to $B_s \to D_s \ell \bar{\nu}_\ell$ ($\ell \in \{e, \mu\}$), computed at zero-recoil and at non-zero recoil. 104

6.5 Results for the ratios of F_T with respect to F_+ at different small recoils. 107

6.6 Results for the ratios of $\mathscr{R}_0(q^2)$ at different non-zero recoils. 109

7.1 Parameters of the simulations. The quantities $a\mu_\ell$, $a\mu_c$ and $a\mu_b$ stand for light, charm and heavy bare valence quark mass values respectively, expressed in lattice units. The lattice spacing $a_{\beta=3.9}$ is fixed by the matching of f_π obtained on the lattice to its experimental value [2] and $a_{\beta=4.05}$ is rescaled using the parameter $\Lambda^{\mathrm{N_f}=2}_{\overline{\mathrm{MS}}}$ [3]. 117

7.2 Masses and energies extracted from the two-point correlation functions. The parameters μ_{h1}, μ_{h2} and μ_{h3} correspond to the heavy "b" quark masses given in Table 7.1. At $\beta = 3.9$, time intervals for the fits are [8, 23] (D), [6, 9] (D_0^* and D_2^*), [11, 17] (small momenta, $B(\mu_{h_1})$ and $B(\mu_{h_2})$), [9, 15] (large momenta, $B(\mu_{h_1})$ and $B(\mu_{h_2})$) and [9, 13] ($B(\mu_{h_3})$). At $\beta = 4.05$, time ranges for the fits are [10, 26] (D), [14, 26] (small momenta, $B(\mu_{h_1})$ and $B(\mu_{h_2})$), [9, 26] (large momenta, $B(\mu_{h_1})$ and $B(\mu_{h_2})$), [14, 22] (small momenta, $B(\mu_{h_3})$) and [9, 22] (large momenta, $B(\mu_{h_3})$). 121

7.3 Values of the eigenvectors $v^{(1)}$ and $v^{(2)}$, for $\beta = 3.9$, $t_0 = t_s = 3$, $t = 7$ and $t_p = 14$. We can notice that they are close to being orthogonal ($v^{(1)}v^{(2)\dagger} \simeq 0$). 126

7.4 Ratios defined in Eq. (7.42). The b quark masses range from the lightest to the heaviest from left to right. They correspond to the B meson mass $m_B \in \{2.5, 3, 3.7\}$ GeV. 128

7.5 Relations between interpolating fields and corresponding combinations of transition amplitudes for each IR ($\mathscr{T}^A_{i(\lambda)} = \langle {}^3P_2 \,|\, A_i \,|\, B\rangle$ where $i = 1, 2, 3$). 131

C.1 Contribution of the terms $\varepsilon^{(\lambda)}_{\mu\nu} p_B^\nu$ and $\varepsilon^{\mu\nu}_{(\lambda)} p_{B\,\nu}$ to the $B \to {}^3P_2$ transition amplitude. 156

C.2 Contribution of the term $\varepsilon^{\mu\nu}_{(\lambda)} p_{B\,\mu} p_{B\,\nu}$ to the $B \to {}^3P_2$ transition amplitude. 156

List of Figures

1.1 Charged current vertices describing the coupling of fermion pairs (quarks or leptons) to vector boson $W^{\pm}$. . . . 12

1.2 Neutral current vertices describing the coupling of fermion pairs (quarks or leptons) to Z^0 boson. . . . 13

1.3 The Bjorken triangle. . . . 15

1.4 UT fit . . . 16

2.1 Feynman diagram representing the exclusive decay $B \to D\ell\bar{\nu}_\ell$. . . . 18

2.2 Feynman diagram representing the semileptonic process $b \to c\,\ell\,\bar{\nu}_\ell$ at tree-level. . . . 19

2.3 Spectroscopy of D-meson excitations. The lines show possible single pion transitions. . . . 24

2.4 Feynman Diagram with a charged Higgs contributing to $B \to \tau\bar{\nu}_\tau$ and $B \to D^{(*)}\tau\bar{\nu}_\tau$. . . . 26

3.1 Lattice QCD symbolic description. . . . 36

3.2 Feynman diagrams of the QCD Lagrangian for cubic and quartic self-interactions and for the quark-gluons vertex. . . . 38

3.3 Gauge links on the lattice. . . . 39

3.4 Representation of a 1×1 Wilson loop known as plaquette. . . . 40

3.5 Six-link loops: from left to right, planar, twisted and L shaped. . . . 42

4.1 Pictorial representation of a two-point correlation function. . . . 59

4.2 Illustration of the difference between quenched (l.h.s.) and unquenched (or full) QCD (r.h.s.). 62

4.3 Smearing at the source for the propagators (l.h.s) Source-sink smeared quark propagators (r.h.s). . . . 65

4.4 Smearing at the sink for the propagators. . . . 65

4.5 Gauge link with APE smearing. . . . 66

4.6 Two-point correlation functions containing Smeared-Smeared (SS) ▲, Smeared-Local (SL) ● and Local-Local (LL) ■ propagators 67

5.1 Results of the fit parameters of the correlation function $\mathscr{C}^{(2)}(t)$ with the function (5.18) together with the constant fit of the effective mass, plotted over the effective mass. In this plot, correlation functions were computed with $a\mu_c = 0.25$. 82

5.2 Effective masses of scalar (●) and pseudoscalar (▲) charmed D meson obtained by solving GEVP as a function of time in lattice units. Results correspond to a simulation using 100 configurations. The valence quark masses are $a\mu_c = 0.25$ and $a\mu_l = 0.0085$. 86

5.3 The plot on the left represents the effective mass $m(T_2^+)$ as a function of time and, on the right, the effective mass $m(E^+)$. In this analysis, we use 240 gauge configurations. The valence charm quark has a mass $a\mu_c = 0.215$ which corresponds to the physical charm quark. 86

6.1 Feynman diagram representing the semileptonic process $B_s \to D_s \ell \bar{\nu}_\ell$. 91

6.2 Valence quark flow in the form factor of $B \to D\ell\bar{\nu}_\ell$ 96

6.3 Example of the plateaus for the $B_s \to D_s$ transition amplitudes, leading to the determination of the relevant form factors, at two different gauge couplings: (a) vector (V_0 is represented by ● and V_k by ●) and tensor (●) hadronic matrix elements corresponding to $\beta = 3.90$, $a\mu_h = 0.4114$, $a\mu_l = 0.0085$. (b) vector and tensor matrix elements corresponding to $\beta = 4.20$, $a\mu_h = 0.3525$, $a\mu_l = 0.0065$. 97

6.4 Values of Σ_3 as obtained on all of the lattice configurations used in this work and shown as a function of μ_l^{sea}/μ_s. Various symbols are used to distinguish the lattice data obtained at different lattice spacings: ○ for $\beta = 3.80$, □ for $\beta = 3.90$ (24^3), ■ for $\beta = 3.90$ (32^3), ● for $\beta = 4.05$, and ▷ for $\beta = 4.20$. The result of the continuum extrapolation is also indicated at the point corresponding to the physical $\mu_{ud}/\mu_s \equiv m_{ud}/m_s = 0.037(1)$. 100

6.5 Heavy quark mass dependence of the ratio σ extrapolated to the physical value of the heavy quark mass and to the continuum limit. The vertical line represents the value of the inverse physical b quark mass. Filled symbols correspond to $\sigma(1, m_h)$ extrapolated to the continuum limit by using Eq. (6.37) with all parameters free, whereas the empty symbols refer to the results obtained by imposing $\beta_s = 0$. 102

6.6 (a) The relevant form factors F_T and F_+ of $B_s \to D_s$ decay channel in lattice units at different non zero recoils corresponding to the ensemble $\beta = 3.9$, $a\mu_l = 0.0085$, $a\mu_h = 0.4114$. (b) The ratio F_T/F_+ in lattice units, as a function of q^2, obtained using the same ensemble. . . 105

6.7 Ratio σ_T as a function of the inverse heavy quark mass. The vertical line represents the value of the inverse physical b quark mass. Filled symbols correspond to $\sigma_T(w, m_h)$ extrapolated to the continuum limit by using Eq. (6.55) with all parameters free, whereas the empty symbols refer to the results obtained by imposing $\beta_s^{(i)\prime} = 0$. 106

6.8 Fit of our data to Eq. (6.65). Empty symbols denote the results computed in the continuum by setting $\beta_s^{(i)\prime\prime} = 0$ in Eq. (6.59). Filled symbols are obtained after allowing $\beta_s^{(i)\prime\prime} \neq 0$. Plotted are the data with $w = w_3 = 1.016$. We see that the data obtained by assuming the independence of $\mathscr{R}_0$ on the sea quark scale is better with the heavy quark mass than the values obtained by letting the parameter $\beta_s^{(i)\prime\prime}$ to be free. 108

6.9 Results for $\mathscr{R}_0(q^2)$ presented in the case where $B_s \to D_s$ are linearly fit to the form $\mathscr{R}_0(q^2) = 1 - \alpha q^2$. The empty (filled) symbols correspond to the results obtained with $\beta_s^{(i)\prime\prime}(w) = 0$ ($\beta_s^{(i)\prime\prime} \neq 0$). 109

7.1 Kinematical configuration of the two-point correlators. 119

7.2 Effective energies of "B"-mesons measured with the ETMC ensemble $\beta = 3.9$ 120

7.3 Comparison of the "B"-mesons energies with the dispersion relation, with the ETMC ensemble ($\beta = 3.9$, $\mu_{\rm sea} = \mu_l = 0.0085$). 120

7.4 Effective mass of the D_0^* meson measured with the ETMC ensemble $\beta = 3.9$ 122

7.5 Kinematical configuration of the three-point correlators. 123

7.6 The ratio $\frac{\langle \boldsymbol{D_0^*} \mid \boldsymbol{A_0} \mid \boldsymbol{B} \rangle}{\langle \boldsymbol{D} \mid \boldsymbol{V_0} \mid \boldsymbol{B} \rangle}$ once symmetrized according to (7.44) for the three b quark masses (i.e. for the three B meson masses as indicated in the plots) and for both lattice spacings. Here, the values are computed using $t_0 = 4$ for $\beta = 3.9$ and $t_0 = 5$ for $\beta = 4.05$. 128

7.7 The ratio of $\tilde{k}/\tilde{k}_\infty$ for $B \to D_2^*$, at $\beta = 3.9$ and $t_p = 14$, to the value derived from the infinite mass limit as a function of time in lattice units for all "B" masses. We present results obtained by considering the average of the diagonal contributions ● (Eqs. (7.56) and (7.57)), and the non-diagonal contributions ● (Eqs. (7.58), (7.59) and (7.60)). The full average is presented by the ■ data points. 134

7.8 Same as Fig. 7.7 but for $\beta = 4.05$ and $t_p = 18$. 135

A.1 The discretization of the lattice in two dimensions. 145

List of Abbreviations

2HDM	Two Higgs Doublet Model
APE	Array Processor Experiment (APE Collaboration)
BC	Boundary conditions
BSM	Beyond the Standard Model
BT	Bakamjian-Thomas
CC	Charged currents
CG	Conjugate gradient
ChPT	Chiral perturbation theory
CKM	Cabbibo Kobayashi Maskawa
CP	Conjugation Parity
EM	Electromagnetic
ETMC	European Twisted Mass Collaboration
EW	Electroweak
GEVP	Generalized Eigenvalue Problem
GI	Godfrey Isgur
HFAG	Heavy Flavor Average Group
HQET	Heavy Quark Effective Theory
HQS	Heavy Quark Symmetry
IR	Irreducible Representation
IW	Isgur-Wise

LHC	Large Hadron Collider
LQCD	Lattice Quantum Chromodynamics
MSM	Minimal Standard Model
MSSM	Minimal SuperSymmetric Model
NC	Neutral Currents
NP	New Physics
OPE	Operator Product Expansion
PCAC	Partially Conserved Axial Current
QCD	Quantum Chromodynamics
QFT	Quantum Field Theory
RC	Renormalization Constant
RI-MOM	Regularization-Invariant Momentum subtraction schemes
SM	Standard Model
SSB	Spontaneous Symmetry Breaking
tmLQCD	twisted mass Lattice Quantum Chromodynamics
tmQCD	twisted mass Quantum Chromodynamics
VEV	Vacuum expectation value

Introduction

The Standard Model (SM) of particle physics provides a successful description of almost all of the so-far observed phenomena. Its predictions are in good agreement with a wide variety of experimental results. However, there are many questions left unanswered and observations unaccounted for: among the observational caveats are the problem of massive neutrinos, the relic dark matter abundance of the Universe and its baryon asymmetry. On the theoretical side, one encounters issues such as the so-called hierarchy problem, the unification of gauge couplings as well as the flavor and CP puzzles.

B-physics is a valuable tool to check the validity of the SM concerning the flavor sector, and thus to search for possible signals of New Physics (NP). At the Large Hadron Collider (LHC), the LHCb experiment is dedicated to the study of B-meson physics. B-meson decays may be mediated by new particles; hence any deviation from the SM predictions might hint towards the presence of NP. Although most of the experimental measurements agree with SM predictions, there are some observables [4–7] suggesting some (small) deviations.

One of the most pressing flavor physics problems is the precise determination of the hadronic matrix elements relevant for B physics, which requires the extraction of the values of the Cabbibo-Kobayashi-Maskawa (CKM) matrix elements from numerous experimental inputs and from different theoretical calculations and assumptions.
Even though experimental measurements still have non-negligible statistical and systematical uncertainties (expected to be improved in a near future), current experimental errors are clearly subdominant with respect to the theoretical uncertainties. For instance, a precise theoretical determination (at the 1% level of accuracy) of the hadronic matrix elements related to b quarks would be needed to render relevant the statistically improved measurement of B (B_s) meson leptonic and semileptonic decay widths.

Experiments measuring semileptonic decay amplitudes of the B system, together with lattice calculations of the semileptonic form factors of $B \to D^{(*,**)}$, give access to the V_{cb} element of the CKM matrix. The theoretical computation of many $B(B_s)$ quantities, such as the form factors, the decay constants, or numerous matrix elements, are challenging due to the effects of strong interactions. The strength of strong interactions, described by Quantum Chromodynamics (QCD), increases with the increase of the distance (or with the decrease of the energy), and at distances larger than $\sim$1 fm (i.e. energies lower than $\sim$1 GeV) the theory is no longer perturbative. Hence, every calculation involving low-energy

hadronic states requires a non-perturbative treatment.
The only available method to calculate physical observables in a non-perturbative way from first principles, where all sources of systematic errors can be kept under control and whose accuracy can be arbitrarily increased with time, is Lattice QCD (LQCD).

The aim of this thesis is to address a small number of theoretical aspects related to B physics. It is based on works done in collaboration with the "Laboratoire de Physique Théorique d'Orsay" and the "European Twisted Mass Collaboration (ETMC)". It focuses mainly on the determination of the form factors of the $B_s \to D_s$ decay channel and the branching ratios of $B \to D^{**}$ semileptonic transitions.

This manuscript is organized as follows: the first chapter is meant to serve as an introduction to the Standard Model of particle physics and to flavor violation in weak interactions as parameterized by the CKM matrix.

The second chapter introduces the notations used to represent the heavy meson states (B and D mesons) and summarizes the current theoretical and experimental status of the $B \to D\,\ell\,\bar{\nu}_\ell$ and $B \to D^{**}\ell\bar{\nu}_\ell$ transitions.

Chapters 3, 4 and 5 describe the formalism of Quantum Field Theory on the Lattice (how to construct fermion and gluon actions (twisted mass fermions), deal with gauge invariance, go to the continuum, renormalize,...). Moreover, some aspects of Lattice simulations (algorithms, propagator computation, smearing techniques, stochastic sources,...) will also be discussed.

Chapter 6 presents an example of calculations made in LQCD: how to extract the mass of fundamental and orbitally excited charmed D states. The whole strategy related to the meson mass determination, especially for the excited D meson states, will be presented in detail.

Finally, Chapters 7 and 8 are devoted to another example of LQCD calculations namely the determination of the transition amplitudes and form factors. In particular, Chapter 7 discusses the phenomenology of B_s transitions into charmed D_s mesons. The form factor parametrizing this weak decay is determined and we also investigate the possibility of having a tensor operator in the effective weak Hamiltonian. Such study leads to better constrain the NP effects as well as to check the SM prediction. Finally, in Chapter 8, we discuss the effect of a finite charm quark mass in the determination of $B \to D^{**}$ branching ratios. We focus on two D^{**} states: the scalar D_0^* and the tensor D_2^*.

Chapter 9 presents an overview and concluding remarks.

Many formulae and technical details are collected in the appendices.

Part I

Phenomenology of beauty mesons

Chapter 1

Flavor in the Standard Model

Our present understanding of the microscopic world is defined in terms of quantum fields and the interactions between them. The best description we have of the fields and their interactions is given by the SM of particle physics. The SM is one of the crowning achievements of twentieth century science: at the time of this writing, the SM is able to explain results of most of the experiments that probed the behavior of matter at the smallest scales. Only gravity remains outside the remit of the SM (in particle physics, experiments are dealing with very tiny masses and the gravitational effects do not need to be taken into account).

This chapter introduces some of the key concepts of the SM. The electroweak theory of weak and electromagnetic interactions is presented. Particular attention is paid to the symmetries of the Lagrangian and the particle content of the model. A description of the different representations of the CKM matrix is given, and finally, the unitarity triangle is presented.

1.1 The Standard Model

The SM describes our current understanding of matter and interactions. It introduces basic constituents, called *quarks* and *leptons*, out of which all matter is made. These fundamental particles experience only three interactions, strong, weak, and electromagnetic, which are mediated by the fundamental *bosons*: the photon, the three weak bosons (W^+, W^-, and Z^0), and the eight gluons. The SM combines the QCD - the theory of strong interaction - and the electroweak (EW) theory - the theory of weak and electromagnetic interactions - in a single gauge theory based on the symmetry group $SU(3)_C \otimes SU(2)_L \otimes U(1)_Y$.

1.1.1 Basic properties of leptons and quarks

1. *Leptons*
   In the SM, three families of leptons are known: the electron e and its neutrino partner ν_e, the muon μ and its neutrino ν_μ, and the τ-lepton accompanied by yet another neutrino ν_τ

$$L_{iL} \equiv \begin{pmatrix} \nu_{\ell_i} \\ \ell_i \end{pmatrix}_L \equiv \begin{pmatrix} \nu_e \\ e \end{pmatrix}_L , \begin{pmatrix} \nu_\mu \\ \mu \end{pmatrix}_L , \begin{pmatrix} \nu_\tau \\ \tau \end{pmatrix}_L \quad L_{iR} \equiv \ e_R \ , \ \mu_R \ , \ \tau_R$$

   where $i = 1, 2, 3$. Here L stands for "left-handed" and R for "right-handed" fermion fields.

$$\psi(x) = \frac{1}{2}(1 - \gamma_5)\psi(x) \ + \ \frac{1}{2}(1 + \gamma_5)\psi(x) \equiv \psi_L(x) + \psi_R(x) \tag{1.1}$$

   Each of the three lepton families carries its own additive quantum number L_ℓ (lepton number) which is the only distinctive characteristic for the family (ℓ_i, ν_{ℓ_i}) and which is strictly conserved in all interactions involving leptons.

2. *Quarks*
   The known quarks are the up and down quarks, the charm and strange quarks, and the top and bottom quarks. They come in three generations and are the constituents of the physical meson and baryon states

$$Q_{iL} \equiv \begin{pmatrix} Q_i^u \\ Q_i^d \end{pmatrix}_L \equiv \begin{pmatrix} u \\ d \end{pmatrix}_L , \begin{pmatrix} c \\ s \end{pmatrix}_L , \begin{pmatrix} b \\ t \end{pmatrix}_L , \quad Q_{iR}^u \equiv u_R,\ c_R,\ b_R, \quad Q_{iR}^d \equiv d_R,\ s_R,\ t_R$$

   The quarks of type up U i.e. (u, c, b) have a charge $Q = 2/3$ (in units of e), while quarks of type down D (d, s, t) have $Q = -1/3$.

A guiding principle in constructing a physical quantum theory is the invariance under some group of local gauge symmetry transformations. In what follows, we illustrate this for the case of EW interactions[1] [8].
The EW theory inherits the phenomenological successes of the four-fermion low-energy description of weak interactions, and provides a well-defined and consistent theoretical framework including weak interactions and quantum electrodynamics in a unified picture. The weak interactions derive their name from their intensity. At low energy the strength of the effective four-fermion interaction of charged currents is determined by the Fermi coupling constant[2] G_F.

The EW interactions are based on the $SU(2)_L \otimes U(1)_Y$ gauge group. The fermion fields are described through their left-handed and right-handed components

$$\psi_{R,L} \ = \ \left(\frac{1 \pm \gamma_5}{2}\right)\psi \qquad\qquad \bar{\psi}_{R,L} \ = \ \bar{\psi}\left(\frac{1 \mp \gamma_5}{2}\right) \tag{1.2}$$

In the SM the left and right fermions have different transformation properties under the gauge group. Thus, mass terms for fermions (of the form $\bar{\psi}_L\psi_R + \text{h.c.}$) are forbidden in the $SU(2) \times U(1)$ symmetric phase. In particular, all ψ_R are singlets in the Minimal Standard Model (MSM).

$$\begin{cases} \psi'(x)_L \ = \exp\left(i\alpha(x)\dfrac{Y_W}{2}\right)\ U_L\ \psi(x)_L & \text{(doublet state)} \\ \psi'(x)_R \ = \exp\left(i\alpha(x)\dfrac{Y_W}{2}\right)\ \psi(x)_R & \text{(singlet state)} \end{cases} \tag{1.3}$$

where the $SU(2)_L$ transformation (non abelian) is

$$U_L \ \equiv \ \exp\left(i\vec{\theta}(x) \cdot \frac{\vec{\tau}}{2}\right) \tag{1.4}$$

and τ_i are the $SU(2)_L$ generators in its fundamental representation satisfying

$$[\tau_i, \tau_j] \ = \varepsilon_{ijk}\,\tau_k \tag{1.5}$$

[1] The QCD part of the SM will be presented in Chapter 3.
[2] $G_F = 11.16639(1)10^{-5}$ GeV^{-2} in natural units $\hbar = c = 1$.

The phase $\vec{\theta}(x) \in \mathbb{R}^3$ parameterizes the $SU(2)$ gauge transformation, and $\alpha(x) \in \mathbb{R}$ parameterizes the $U(1)$ gauge transformation. The parameter Y_W is called the hypercharge of the $U(1)$ group.
The standard EW theory is a chiral theory, in the sense that ψ_R and ψ_L behave differently under the gauge group. In the absence of mass terms, there are only vector and axial-vector interactions in the Lagrangian which have the property of not mixing ψ_L and ψ_R.

Let us summarize the structure of the EW Lagrangian.
The free Lagrangian with fermion matter fields reads

$$\mathscr{L}_0 = \bar{\psi}_L \, i\gamma^\mu D_\mu \psi_L + \bar{\psi}_R \, i\gamma^\mu D_\mu \, \psi_R \tag{1.6}$$

The requirement for local gauge invariance entails the redefinition of the partial derivatives $D_\mu \psi_{L,R}$

$$\begin{cases} D_\mu \psi_L = \left[\partial_\mu + i g_1 \sum_{a=1}^{3} \tau^a W_\mu^a + i g_2 \frac{1}{2} Y_W(\psi_L) B_\mu \right] \psi_L \\ D_\mu \psi_R = \left[\partial_\mu + i g_2 \frac{1}{2} Y_W(\psi_R) B_\mu \right] \psi_R \end{cases} \tag{1.7}$$

The two real numbers g_1 and g_2 are the couplings associated with $SU(2)$ and $U(1)$ respectively, and Y_W is the $U(1)$ hypercharge.
We thus have four gauge fields: W^a, corresponding to the three $SU(2)$ generators, and B corresponding to $U(1)$. Introducing the field strengths

$$B_{\mu\nu} = \partial_\mu B_\nu - \partial_\nu B_\mu \tag{1.8}$$

$$\mathscr{W}_{\mu\nu}^A = \partial_\mu W_\nu^A - \partial_\nu W_\mu^A - g_1 \varepsilon_{ABC} W_\mu^B \, W_\nu^C \tag{1.9}$$

where ε_{ABC} is the totally antisymmetric Levi-Civita tensor, one can then construct the kinetic Lagrangian of the gauge fields

$$\mathscr{L}_{\text{kin}} = -\frac{1}{4} B_{\mu\nu} B^{\mu\nu} - \frac{1}{4} \sum_{a=1}^{3} \mathscr{W}_{\mu\nu}^a \mathscr{W}^{a\mu\nu} \tag{1.10}$$

Gauge symmetry forbids mass terms for the gauge bosons and the fermions. Thus, the $SU(2)_L \otimes U(1)_Y$ Lagrangian contains only massless fields.

The interactions of the fermions with the gauge bosons are given by

$$\mathscr{L}_{\text{int}} = -g_1 \bar{\psi}_L \gamma^\mu \widetilde{W}_\mu \psi_L - g_2 \, B_\mu \sum_{\substack{\psi_j \in \ell_j, \nu_{\ell_j}, \\ Q_j^u, Q_j^d}} y(\psi_j) \bar{\psi}_j \gamma^\mu \psi_j \tag{1.11}$$

where we have defined $\widetilde{W}_\mu(x) \equiv \tau^a W_\mu^a(x)/2$ and $y(\psi_j) \equiv Y_W(\psi_j)/2$.

However, the $SU(2)_L \otimes U(1)_Y$ Lagrangian cannot describe the observed dynamics because the gauge bosons and the fermions are still massless. In what follows, we will describe the mechanism of EW symmetry breaking which gives masses to the fermions and introduces the massive ($W^{\pm}$ and Z) gauge bosons.

1.1.2 Higgs sector

In order to generate masses, one needs to break the gauge symmetry. The origin of mass in the SM is a consequence of the spontaneous symmetry breaking (SSB) of the $SU(2)_L \otimes U(1)_Y$ triggered by the Higgs mechanism (developed by Higgs, Brout, Englert, Guralnik, Hagen and Kibble) [9–12]. To describe it, let us introduce an $SU(2)_L$ doublet of complex scalar fields

$$\phi \equiv \begin{pmatrix} \phi^{(+)} \\ \phi^{(0)} \end{pmatrix} \tag{1.12}$$

The scalar Lagrangian is

$$\mathscr{L}_S = (D_\mu \phi)^\dagger D^\mu \phi - \mu^2 \phi^\dagger \phi - h \left(\phi^\dagger \phi\right)^2 \qquad (h > 0, \mu^2 < 0) \tag{1.13}$$

with the covariant derivative

$$D^\mu \phi = \left[\partial^\mu + i g_1 \widetilde{W}_\mu + i g_2 y(\phi) B^\mu\right] \phi \qquad \text{with} \quad y(\phi) = \frac{1}{2} \tag{1.14}$$

The Lagrangian $\mathscr{L}_S$ is invariant under local $SU(2)_L \otimes U(1)_Y$ transformations.
There is an infinite set ($\mathscr{S}$) of degenerate states with minimum energy, satisfying

$$\langle 0 \,|\, \phi^{(0)} \,|\, 0 \rangle = \sqrt{\frac{-\mu^2}{2h}} \equiv \frac{v}{\sqrt{2}} \tag{1.15}$$

where v is the vacuum expectation value (VEV) of the neutral scalar. Since the electric charge is conserved, the VEV of ϕ^+ must vanish. Once the system has chosen a particular state belonging to ($\mathscr{S}$), the $SU(2)_L \otimes U(1)_Y$ symmetry is spontaneously broken to the electromagnetic group $U(1)_{\text{em}}$ which remains a true symmetry of the vacuum, i.e.

$$SU(2)_L \otimes U(1)_Y \to U(1)_{\text{em}} \tag{1.16}$$

Let us parameterize the scalar doublet as follows

$$\phi(x) = \exp\left\{i \frac{\sigma_i \theta^i}{2}\right\} \frac{1}{\sqrt{2}} \begin{pmatrix} 0 \\ v + H(x) \end{pmatrix} \tag{1.17}$$

with four real fields $\theta^1(x)$, $\theta^2(x)$, $\theta^3(x)$ and $H(x)$.
Local $SU(2)_L$ invariance allows to rotate away any dependence on $\theta^i(x)$. These three fields are precisely the would-be massless Goldstone bosons associated with the SSB mechanism (the condition $\theta^i(x) = 0$ is called the physical (unitary) gauge).

Gauge field masses

The covariant derivative couples the scalar doublet to the gauge bosons. The kinetic piece of the scalar Lagrangian is

$$\begin{aligned}(D_\mu\phi)^\dagger\, D^\mu\phi \xrightarrow{\theta^i=0} \frac{1}{2}\partial_\mu H\partial^\mu H \;+\; \frac{g_1^2\, v^2}{8}\,\left[\left(W_\mu^1\right)^2 \;+\left(W_\mu^2\right)^2\right] \\ +\,\frac{v^2}{8}\;\left[g_1 W_\mu^3 \,-\, g_2 B_\mu\right]^2 \;+\text{cubic}\;+\text{quartic terms}\end{aligned} \tag{1.18}$$

If one redefines cleverly the fields as follows

$$W_\mu^\pm \;=\; \frac{W_\mu^1 \,\mp\, i W_\mu^2}{2} \tag{1.19}$$

and rotates the B_μ and W_μ^3 fields as

$$\begin{pmatrix} W_\mu^3 \\ B_\mu \end{pmatrix} \;\equiv\; \begin{pmatrix} \cos\theta_W & \sin\theta_W \\ -\sin\theta_W & \cos\theta_W \end{pmatrix} \begin{pmatrix} Z_\mu \\ A_\mu \end{pmatrix} \tag{1.20}$$

where θ_W is the weak-mixing angle defined as

$$\tan\theta_W \;=\; \frac{g_2}{g_1} \tag{1.21}$$

one verifies that the kinetic part of the scalar Lagrangian written in terms of Z_μ, A_μ and $W_\mu^\pm$ now contains quadratic terms for the $W_\mu^\pm$ and the Z. In other words, the $W^\pm$ and Z gauge bosons acquire masses

$$M_Z\cos\theta_W \;=\; M_{W^\pm} \;=\; \frac{1}{2}\, v\, g_1 \tag{1.22}$$

while A_μ is identified with the electromagnetic vector potential and remains massless. The electromagnetic current is thus conserved: the coupling of the electromagnetic interaction is identified with the electron charge e

$$g_1 \sin\theta_W \;=\; g_2\cos\theta_w \;=\; e \tag{1.23}$$

and the conserved quantum number is

$$Q'^f \;=\; T_3^f \;+\; \frac{Y_W^f}{2} \tag{1.24}$$

where Q'^f is the electric charge generator (in units of e), T_f^3 is the third component of the weak isospin and Y_W^f is the hypercharge of the fermionic field f.

Fermion masses

A fermionic mass term $\mathscr{L}_m \;= -m\overline{\psi}\psi \;= -m(\overline{\psi}_L\psi_R \;+\overline{\psi}_R\psi_L)$ is not allowed, because it explicitly breaks the gauge symmetry: left- and right-handed fields transform differently under $SU(2)_L \otimes U(1)_Y$.

However, the bilinear Yukawa interactions of left- and right-handed fermions with the scalar field are invariant under $SU(2)_L \times U(1)_Y$

$$\mathscr{L}_{\text{Yukawa}} \;=\; Y^u_{ij}\;\bar{Q}_{iL}\;\phi^c\;Q^u_{jR} \;+\; Y^d_{ij}\;\bar{Q}_{iL}\;\phi\;Q^d_{jR} \;+\; Y^\ell_{ij}\;\bar{L}_{iL}\;\phi\;\ell_{jR} \;+\; \text{h.c.} \tag{1.25}$$

where the first term involves the charge-conjugate scalar field $\phi^c \equiv i\tau^2\phi^*$. The matrices $Y^{u(d)}_{ij}$ and Y^ℓ_{ij} are the Yukawa couplings for the up (down) quarks and the charged leptons, respectively. After EW symmetry breaking, quarks and leptons become massive and their masses are described by the Lagrangian[3]

$$\mathscr{L}_{\text{mass}} \;=\; \bar{Q}^u_{iL}\;M^u_{ij}\;Q^u_{jR} \;+\; \bar{Q}^d_{iL}\;M^d_{ij}\;Q^d_{jR} \;+\; \bar{\ell}_{iL}\;M^\ell_{ij}\;\ell_{jR} \;+\; \text{h.c.} \tag{1.26}$$

with the mass matrices defined by

$$M^u_{ij} \;=\; vY^u_{ij}\;,\; M^d_{ij} \;=\; vY^d_{ij}\;,\; M^\ell_{ij} \;=\; vY^\ell_{ij} \tag{1.27}$$

In general, the Yukawa couplings and hence the mass matrices are not diagonal. The above mass matrices can be diagonalized through the bi-unitary transformations

$$\begin{aligned} V^{u\dagger}_L\;M_u\;U^u_R &= \text{diag}(m_u,\;m_c,\;m_t) \;\equiv\; d_u \\ V^{d\dagger}_L\;M_d\;U^d_R &= \text{diag}(m_d,\;m_s,\;m_b) \;\equiv\; d_d \\ V^{\ell\dagger}_L\;M_\ell\;U^\ell_R &= \text{diag}(m_\ell,\;m_\mu,\;m_\tau) \;\equiv\; d_\ell \end{aligned} \tag{1.28}$$

where the U and V are the 3×3 unitary matrices which relate flavor (unprimed) and mass eigenstates (primed). Applying the transformations

$$Q^u_L \;\to\; V^u_L\;Q'^u_L\;,\quad Q^d_L \;\to\; V^d_L\;Q'^d_L\;,\quad \ell_L \;\to\; V^\ell_L\;\ell'_L \tag{1.29}$$

$$Q^u_R \;\to\; U^u_R\;Q'^u_R\;,\quad Q^d_R \;\to\; U^d_R\;Q'^d_R\;,\quad \ell_R \;\to\; U^\ell_R\;\ell'_R \tag{1.30}$$

to the Lagrangian given in Eq. (1.26), one obtains

$$\mathscr{L}_{\text{mass}} \;=\; \sum_{Q^u_i,Q^d_i,\ell_i} \Big(m_{Q^u_i}\;\bar{Q}'^u_{iL}\;Q'^u_{iR} \;+\; m_{Q^D_i}\;\bar{Q}'^d_{iL}\;Q'^d_{iR} \;+\; m_{\ell_i}\;\bar{\ell}'_{iL}\;\ell'_{iR} \;+\; \text{h.c.}\Big) \tag{1.31}$$

Thus we have generated a mass-term for the fermions.

In terms of the physical fermion and boson states, one can now proceed to study neutral and charged currents.

[3]Since the original formulation of the SM did not include right-handed neutrinos (nor Higgs triplets), neutrinos remain strictly massless to all orders in perturbation theory.

Charged Currents

The charged current (CC) Lagrangian will now read

$$\mathscr{L}_{CC}^{(q)} \;=\; -\frac{g_1}{\sqrt{2}}\left[W_\mu^+\;\overline{Q}_{iL}^{\prime u}\;\gamma^\mu\;\left(V_{\rm CKM}\right)_{ij}\;Q_{jL}^{\prime d}\;+\;W_\mu^-\;\overline{\ell}_{iL}^{\prime}\;\gamma^\mu\;\left(\delta\right)_{ij}\;\nu_{\ell_j\,L}^{\prime}\;+\;\text{h.c.}\right] \tag{1.32}$$

where the unitary matrix $V_{\rm CKM} \;=\; V_L^{u\prime}\,V_L^d$ is the so-called Cabibbo-Kobayashi-Maskawa matrix [13,14] which encodes flavor violation in CC. In the case of three quark generations, it is a 3×3 unitary mixing matrix [14]

$$V_{\rm CKM} \;=\; \begin{pmatrix} V_{ud} & V_{us} & V_{ub} \\ V_{cd} & V_{cs} & V_{cb} \\ V_{td} & V_{ts} & V_{tb} \end{pmatrix} \tag{1.33}$$

It can be shown that it depends on four parameters: three angles and a phase. In the absence of a fundamental theory of flavor, there is no theoretical prediction for the values of these parameters which should be determined experimentally. We will describe the different parametrizations of this matrix in the next section.



Figure 1.1: Charged current vertices describing the coupling of fermion pairs (quarks or leptons) to vector boson $W^\pm$.

Weak charged currents are the only tree-level interactions in the SM that change flavor. On the leptonic sector, there is no analogue of the CKM matrix because, in the SM, neutrinos are massless: since they are degenerate states, any rotation between the different flavors has no physical effect. Fig. 1.1 depicts the CC vertices in the SM.

Neutral Currents

In terms of the mass eigenstate fields Z_μ and A_μ, the neutral part of the weak interaction Lagrangian is

$$\begin{aligned}\mathscr{L}_{\rm NC} \;=\; -\sum_{\psi_j}\bar{\psi}_j\gamma^\mu\Big\{A_\mu\left[g_1\frac{\tau_3}{2}\sin\theta_W\;+\;g_2\;y(\psi_j)\cos\theta_W\right] \\ +Z_\mu\left[g_1\frac{\tau_3}{2}\cos\theta_W\;-\;g_2\;y(\psi_j)\;\cos\theta_W\right]\Big\}\psi_j\end{aligned} \tag{1.34}$$

This neutral current (NC) Lagrangian can be decomposed as

$$\mathscr{L}_{\rm NC} \;=\; \mathscr{L}_{\rm QED} + \;\mathscr{L}^{Z}_{\rm NC} \tag{1.35}$$

where $\mathscr{L}_{\rm QED}$ is the usual QED Lagrangian, and

$$\mathscr{L}^{Z}_{\rm NC} \;=\; -\frac{e}{2\sin\theta_W\cos\theta_W}\, J^{\mu}_{Z}\, Z_{\mu} \tag{1.36}$$

which contains the interaction of the boson with the neutral fermionic current J^{μ}_{Z}. Equivalently, $\mathscr{L}^{Z}_{\rm NC}$ has the form (see Fig. 1.2)

$$\mathscr{L}^{Z}_{\rm NC} \;=\; -\frac{e}{2\sin\theta_W\cos\theta_W}\, Z_{\mu} \sum_{f} \bar{\psi}_f \gamma^{u}(v_f - a_f\gamma_5)\psi_f \tag{1.37}$$

where the coefficients $a_f = T^f_3$ and $v_f = T^f_3 \left(1 - 2Q'^{\,f}\sin^2\theta_W\right)$ represent the axial (A) and vector (V) couplings of the Z^0 boson to fermions.



Figure 1.2: Neutral current vertices describing the coupling of fermion pairs (quarks or leptons) to Z^0 boson.

Now that we have introduced the neutral as well as the charged currents, let us proceed to present the different parameterizations used for the CKM matrix.

1.2 Parameterization of the CKM matrix

There are several parameterizations of the CKM matrix. We will only present two of them: the standard parameterization and a generalization of the Wolfenstein parametri- zation.

The standard parameterization: the "standard" parameterization [15] of $V_{\rm CKM}$ involves three angles $\theta_{12},\ \theta_{23},\ \theta_{13}$ and a phase δ_{13}

$$\begin{pmatrix} c_{12}\,c_{13} & s_{12}\,c_{13} & s_{13}\,e^{-i\delta_{13}} \\ -s_{12}\,c_{23} \;-\; c_{12}\,s_{23}\,s_{13}\,e^{i\delta_{13}} & c_{12}\,c_{23} \;-\; s_{12}\,s_{23}\,s_{13}\,e^{i\delta_{13}} & s_{23}\,c_{13} \\ s_{12}\,s_{23} \;-\; c_{12}\,c_{23}\,s_{13}\,e^{i\delta_{13}} & -c_{12}\,s_{23} \;-\; s_{12}\,c_{23}\,s_{13}\,e^{i\delta_{13}} & c_{23}\,c_{13} \end{pmatrix} \tag{1.38}$$

where $c_{ij} = \cos\theta_{ij}$ and $s_{ij} = \sin\theta_{ij}$ for the generation labels i, $j = 1, 2, 3$.

This parameterization offers numerous advantages when it comes to physical interpretation. The angles are defined and labeled in a way which relates them to the mixing of two specific generations, and if one of these angles vanishes, the mixing between those two generations vanishes. In the limit $\theta_{23} = \theta_{13} = 0$, the third generation decouples and the situation reduces to the Cabibbo mixing of the first two generations, with θ_{12} identified as the Cabibbo angle [13]. The real angles θ_{12}, θ_{23}, θ_{13} can all be chosen to lie in the first quadrant by an appropriate redefinition of the quark field phases.

The matrix elements in the first row and third column, which have been directly measured in decay processes, are all of a simple form. The CP violating phase δ_{13} may vary in the range $0 \leq \delta_{13} < 2\pi$. However, measurements of CP violation in K decays force δ_{13} to be in the range $0 < \delta_{13} < \pi$. From phenomenological studies we know that s_{13} and s_{23} are small numbers: $\mathcal{O}(10^{-3})$ and $\mathcal{O}(10^{-2})$ respectively. Consequently, the parameters

$$|V_{ud}| = c_{12}, \;\; |V_{us}| = s_{12}, \;\; |V_{ub}| = s_{13}e^{-i\delta_{13}}, \;\; |V_{cb}| = s_{23} \;\text{ and }\; |V_{tb}| = c_{23} \tag{1.39}$$

are known to an excellent approximation. The above parameters c_{12}, s_{12}, s_{13} and s_{23} can be extracted from tree-level decays mediated by the transitions $d \to u$, $s \to u$, $b \to u$, and $b \to c$ respectively. The phase δ_{13} can be extracted from CP violating transitions or loop processes sensitive to $|V_{td}|$.
In Chapter 2, we will present the determination of the CKM matrix element V_{cb} from semileptonic B decays, and in the next chapters we will discuss how lattice computations can help in performing such tasks.

The Wolfenstein parameterization: a considerable simplification is gained if one takes into account that, from experiment, $s_{12} = |V_{us}| \simeq 0.22$, i.e. s_{12} is a small number. Thus, following Wolfenstein [16] one can set

$$s_{12} \equiv \lambda, \qquad s_{23} = A\lambda^2, \qquad s_{13}e^{-i\phi} = A\lambda^3(\rho - i\eta) \tag{1.40}$$

As a result, by neglecting terms of higher order in λ, one can write down

$$V = \begin{pmatrix} V_{ud} & V_{us} & V_{ub} \\ V_{cd} & V_{cs} & V_{cb} \\ V_{td} & V_{ts} & V_{tb} \end{pmatrix} \sim \begin{pmatrix} 1 - \frac{\lambda^2}{2} & \lambda & A\lambda^3(\rho - i\eta) \\ -\lambda & 1 - \frac{\lambda^2}{2} & A\lambda^2 \\ A\lambda^3(1 - \rho - i\eta) & -A\lambda^2 & 1 \end{pmatrix} \tag{1.41}$$

where A, ρ and η are real numbers that are of order unity. This approximate form is widely used, mainly in B physics, but care must be taken, especially for CP-violating effects in K physics, since the phase enters V_{cd} and V_{cs} through terms that are of higher order in λ.
A survey of the current status of the CKM parameters can be found in ref. [1]. In the SM, the non-vanishing of the η parameter is the only source of CP violation.

1.3 The unitarity triangle

The unitarity of the CKM matrix can be expressed by several relations. In particular, the sum of squared entries of each row (or column) must be equal to 1. Given the fact that different entries of CKM matrix can be independently measured, it is possible to test the SM by verifying that such relations are experimentally satisfied. In particular the most precise bound comes from the analysis of the first line of the matrix

$$|V_{ud}|^2 + |V_{us}|^2 + |V_{ub}|^2 = 1 \tag{1.42}$$

The value of V_{ud} is known from the measurement of nuclear β decays [17], and the remaining two parameters can be determined experimentally from leptonic and semileptonic decays of K, D and B mesons.

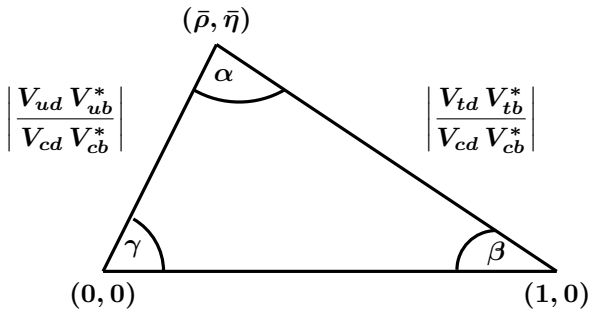


Figure 1.3: The Bjorken triangle corresponding to Eq. (1.45) in the $(\bar{\rho}, \bar{\eta})$ plane.

Orthogonality of rows and columns gives

$$\sum_a V_{ba} V_{ca}^* = \delta_{bc} \tag{1.43}$$

which allows to construct six (unitarity) triangles whose common area is given by the Jarlskog invariant [18]

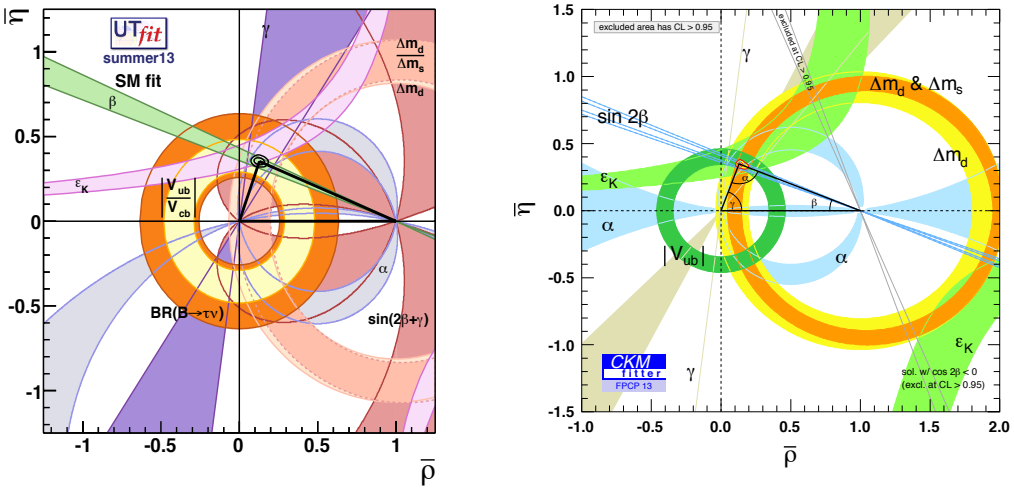
$$J_{\text{inv.}} \sim \eta\, A^2\, \lambda^6 \tag{1.44}$$

Notice that $J_{\text{inv.}}$ (or equivalently the area of the triangles) vanishes[4] in the case $\delta_{13} = 0$.
Of particular phenomenological interest is the Bjorken triangle (the "$b-d$" triangle displayed in Fig. 1.3) constructed from

$$V_{ud} V_{ub}^* + V_{cd} V_{cb}^* + V_{td} V_{tb}^* = 0 \tag{1.45}$$

since the three sides are all of the same order (λ^3).

[4] A direct evidence that J is non vanishing is obtained from the measurement of $\sin 2\beta$ in B decays.



(a) UTfit global fit (from [19]). (b) CKMfitter global fit (from [20]).

Figure 1.4: Unitarity triangle in the $\bar{\rho}$ and $\bar{\eta}$ parameters fitted to the information on angles and by constraining other parameters from semileptonic B decays, B_d^0 oscillations and K mixing.

The angles of the unitarity triangle are given by

$$\begin{cases} \alpha = \arg\left(\dfrac{V_{cd}\,V_{cb}^*}{V_{td}\,V_{tb}^*}\right) \\ \beta = \arg\left(\dfrac{V_{td}\,V_{tb}^*}{V_{ud}\,V_{ub}^*}\right) \\ \gamma = \arg\left(\dfrac{V_{ud}\,V_{ub}^*}{V_{cd}\,V_{cb}^*}\right) \end{cases} \tag{1.46}$$

Various experimental results are used to overconstrain the vertex of the unitarity triangle. In Fig. 1.4, we show the fit of all present bounds to the values of $\bar{\rho}$ and $\bar{\eta}$ performed by the UTfit and the CKMfitter collaborations. All the constraints to the triangle intersect in the same region, thus indicating a good agreement between the SM interpretation of flavor violation and experimental data. The increase in precision, both on the theoretical and the experimental side, will allow to perform more and more stringent fits and possibly unveil the presence of NP.

Note that we have only discussed flavor mixing for quarks since, in the SM, lepton flavor is strictly conserved ($m_\nu = 0$). Once massive neutrinos are incorporated, charged current interactions will also violate lepton flavor.

Chapter 2

Semileptonic B decays

Semileptonic B decays are of primary importance in Heavy Flavor Physics since, for example, they participate very strongly in the accurate determination of the CKM matrix element V_{cb}. Moreover, improving the accuracy of the CKM parameters is at the basis of many new physics analysis.

However, there are many puzzling features associated with the semileptonic $b \to c$ data, which have appeared during the last ten years. Let us quote for instance the so-called "1/2 versus 3/2 puzzle" which corresponds to the difference between theoretical predictions and experimental measurements of semileptonic branching ratios of $B \to D^{**}\ell\bar{\nu}_\ell$ [21, 22]. One can also find that in non-leptonic decays, there is not a fair agreement between experimental results on D_0^* production in $B^0 \to \overline{D}^0\,\pi^+\,\pi^-$ [23].

In the present chapter, we will introduce the notations that will be used in this manuscript, especially for the B and the charmed $D^{(*,**)}$ meson states. We will then proceed with the phenomenology of the weak transitions of the B meson into D and D^{**} focusing on previous theoretical approaches used when working with such semileptonic decays. Finally, the "1/2 versus 3/2 puzzle" will be discussed and some proposals to elucidate the contradiction between theory and experiment will be suggested.

2.1 A short review on semileptonic B decays

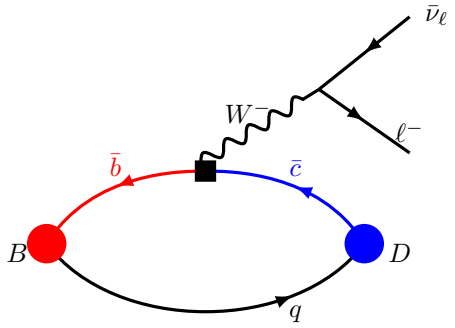


Figure 2.1: Feynman diagram representing the exclusive decay $B \to D\ell\bar{\nu}_\ell$.

In the past years, B factories such as BaBar and experiments such as ALEPH, DELPHI, LHCb etc., collected vast amounts of data on B mesons making it possible to study their various decay modes, such as the semileptonic decays into the charmed D meson states (D^{**}, D_s,...). From the experimental point of view, there are two different approaches:

exclusive approach, where the final state is well defined and one can consider a particular decay as, for example, $B \to D^{**}\,\ell\bar{\nu}_\ell$ or $B \to D\ell\,\bar{\nu}_\ell$ (Fig. 2.1).

inclusive approach, where the decays are treated at the quark level ($b \to c\ell\bar{\nu}_\ell$ as shown in Fig. 2.2) while the other quark is considered as a spectator. The fact that inclusive decays do not depend

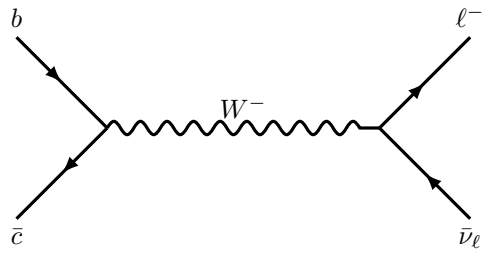


Figure 2.2: Feynman diagram representing the semileptonic process $b \to c\,\ell\,\bar{\nu}_\ell$ at tree-level.

on the final state, allows us to study semileptonic processes of the type $B \to X_c\,\ell\,\bar{\nu}_\ell$ (where X_c is any hadronic state containing a charm quark c).

Inclusive and exclusive decays of heavy flavors play a complementary rôle in the determination of fundamental parameters of the electroweak standard model and in the development of a deeper understanding of QCD. The theory of both inclusive and exclusive processes is based on an operator product expansion (OPE) which allows to separate the dynamics at short and long distances. At a very large scale, $\mu = \mathcal{O}(m_W)$, charm and beauty decays are described by second order weak interactions involving $W^\pm$ exchanges. Since the momentum transfer $p^2 \ll m_W^2$, one effectively has four-fermion interactions given by a hamiltonian of the form

$$H_{\text{eff}} = \frac{G_F}{\sqrt{2}} \sum_i c_i(\mu)\,\mathcal{O}_i(\mu) \tag{2.1}$$

It involves a sum of local operators $\mathcal{O}_i$s, which incorporate the long-distance effects, with coefficients c_is. The c_is are the Wilson coefficients which encode all the physics on momentum scales greater than μ and which can be calculated in perturbation theory as long as $\mu \gg \Lambda_{\text{QCD}}$. They include the full effects of Ws, Zs and top quarks, as well as any Beyond Standard Model (BSM) physics, plus short-distance-effects of QCD. The scale μ is arbitrary; we have introduced it only to separate short and long distance physics.
Armed with H_{eff}, the matrix elements between two hadronic states $|B\rangle$ and $|X_c\rangle$ are given by

$$A(B \to X_c) = \frac{G_F}{\sqrt{2}} \sum_i c_i(\mu)\,\langle X_c\,|\,\mathcal{O}_i(\mu)\,|\,B\rangle \tag{2.2}$$

In the above expression, the matrix element $\langle X_c\,|\,\mathcal{O}_i(\mu)\,|\,B\rangle$ must be computed outside perturbation theory.
There are a variety of approaches to deal with the calculations of hadronic matrix element. Current ones include lattice calculations, QCD sum rules, Heavy Quark Effective Theory (HQET), and phenomenological quark models. Each of these approaches has advantages and disadvantages. For example, quark models are easy to use and good for intuition. However, their relation to QCD is unclear. On the other hand, lattice calculations are rigorous from the point of view of QCD, but they suffer from lattice artifacts and statistical uncertainties among other things. Furthermore, effective theories are usually

applicable only to a restricted class of problems, and sometimes require substantial corrections which cannot be calculated within the same framework. For example, due to the large mass of the b-quark, it will be possible to use the systematic framework provided by HQET [24]. It describes the dynamics of hadrons containing a heavy quark, and is very powerful in treating heavy-to-heavy transitions such as $b \to c$, but a priori less suitable for heavy-to-light $b \to u$ transitions. It is a valid description of the physics at momenta much smaller than the mass of the heavy quark m_Q. HQET is constructed so that only inverse powers of m_Q appear in the effective Lagrangian.
Heavy meson decay constants as well as form factors are examples of the simplest quantities that can be studied with the above approaches.

Consider the semileptonic B decays into D mesons. They are induced by the weak annihilation process $b \to c\,\ell\bar{\nu}_\ell$ where $\ell = e, \mu, \tau$. The relevant tree-level weak hamiltonian is given by

$$H_{\text{eff}} \;=\; \frac{G_F}{\sqrt{2}}\, V_{cb}\, (\bar{c}\Gamma^\mu b)_L\, (\bar{\ell}\Gamma_\mu \nu_\ell)_L \;+\; \text{h.c.} + \;\cdots \tag{2.3}$$

where $\Gamma_\mu = \gamma_\mu(1-\gamma_5)$ and "$\cdots$" are higher-dimensional operators that contain the momentum dependence. This result is an example of an operator product expansion. In this simple case, there is one $c(\mu)$, which we take to be unity.
The corresponding transition amplitude factorizes into the product of leptonic and hadronic matrix elements

$$A(B \to X_c\,\ell\bar{\nu}) \;= \frac{G_F}{\sqrt{2}}\, V_{cb}\, \underbrace{\langle D \,|\, \bar{c}\Gamma^\mu b \,|\, B\rangle}_{\text{hadronic part}}\, \underbrace{\langle \ell \,|\, \bar{\ell}\Gamma_\mu \nu_\ell \,|\, \nu_\ell\rangle}_{\text{leptonic part}} \tag{2.4}$$

The hadronic part is the matrix element of the vector or axial vector currents $V_\mu = \bar{c}\,\gamma_\mu\, b$ and $A_\mu = \bar{c}\,\gamma_\mu\gamma_5\, b$ between B and D states.
It is convenient to write the structure of a matrix element in terms of a few Lorentz invariant quantities called "form factors". The most general vector current matrix element for $B \to D$ must transform as a Lorentz four vector. The only four vectors available are the momenta p_B and p_D of the initial and final mesons, so the matrix element must have the structure $F_1\, p_{D\mu} + F_2\, p_{B\mu}$. The form factors "$F_1$" and "$F_2$" are Lorentz invariant functions that can only depend on the invariants, p_B^2, p_D^2 and $p_B \cdot p_D$. Two of the variables are fixed, $p_B^2 = m_B^2$ and $p_D^2 = m_D^2$, and it is conventional to choose $q^2 = (p_B - p_D)^2$ as the only independent variable. A similar analysis can be carried out for the other matrix elements. The conventional choice of form factors allowed by the parity and time-reversal invariance of QCD is

$$\langle D(p_D) \,|\, V_\mu \,|\, B(p_B)\rangle \;= f_+(q^2)(p_B + p_D)_\mu \;+ f_-(q^2)(p_B - p_D)_\mu \tag{2.5}$$

The form factors f_+ and f_- are real[1]. The same type of reasoning can be applied to any other semileptonic decay to find the parametrization of the hadronic matrix elements in terms of the corresponding form factors.

[1] This can be shown using, for example, the time reversal symmetry on the hadronic matrix element.

2.2 Charmed D meson states

We are interested, throughout this work, in the charmed D mesonic state as a final product of the semileptonic B decays. So, we will recall the two different ways to characterize charmed mesons.

2.2.1 The "spin-orbit" decomposition

The mesonic system can be classified as

$$\left|n\,^{2S+1}L_J\right\rangle \tag{2.6}$$

where n represents the radial quantum number, S stands for the total spin of the meson, L is the orbital angular momentum and J is the total angular momentum ($\vec{J} = \vec{L} + \vec{S}$).
The Eq. (2.6) represents the "**spin-orbit**" decomposition. When L is non zero, the states are said orbitally excited. The first orbitally excited bound state corresponds to the $1P\,(L = 1)$ wave function of the charmed system. We have the following four $1P$ states

$$\left|1\,^3P_0\right\rangle \quad ; \quad \left|1\,^1P_1\right\rangle \quad ; \quad \left|1\,^3P_1\right\rangle \quad ; \quad \left|1\,^3P_2\right\rangle \tag{2.7}$$

Other excited states are associated, for example, with $2S\,(n = 2, L = 0)$ and $1D\,(n = 1, L = 2)$ wave functions for the charmed system.
For simplicity, the index n will be henceforth omitted when there are no radial excitations.

2.2.2 The "heavy-light" decomposition

There is another decomposition called the "**heavy-light**" decomposition. In this case, in the rest frame of a heavy meson, the total angular momentum $\vec{J}$ reads

$$\vec{J} \;=\; \vec{s}_h \;+\; \vec{j} \tag{2.8}$$

where $\vec{s}_h$ is the spin of the heavy quark and $\vec{j}$ is the angular momentum of the "light component" of the meson. The "light component" (or the "light degrees of freedom" or the "light cloud") consists of the superposition of the light quark, the sea quarks and gluons. In quark models, $\vec{j}$ can be decomposed as

$$\vec{j} \;=\; \vec{s}_l \;+\; \vec{l} \tag{2.9}$$

where $\vec{s}_l$ represents the spin of the light quark and $\vec{l}$ stands for the orbital angular momentum of the light cloud. The states are denoted as

$$\left|n\,jJ^P\right\rangle \tag{2.10}$$

This decomposition displays an interesting feature in the limit where the heavy quark of the meson has an infinite mass: a new symmetry appears (the heavy quark symmetry (HQS) [25]) which leads to the conservation of the spin of the heavy quark s_h, and hence to the conservation of the "light component" $\vec{j}$ of the meson (since $\vec{J}$ in Eq. (2.8) is conserved due to the rotational invariance of the system). Therefore,

it is convenient to use j as an index to order heavy-light meson states.
We will use this decomposition to classify the charmed D states

***S* wave states ($l = 0$):** heavy mesons satisfying this property are listed in table 2.1.

doublet	J^P values	notation $\left\vert j\ J^P\right\rangle$	experimental notation
$j^P = 1/2^-$	0^-	$\left\vert \frac{1}{2}\ 0^-\right\rangle$	D (c heavy quark), B (b heavy quark)
	1^-	$\left\vert \frac{1}{2}\ 1^-\right\rangle$	D^*, B^*

Table 2.1: The "heavy-light" decomposition of the charm S wave states. The superscript P denotes the parity of the state.

***P* wave states ($l = 1$):** the heavy P-wave mesons are represented by M^{**}. The index j has two values, $1/2$ and $3/2$, and each of these values forms a doublet. In the case where the heavy quark is the charm, we obtain the D^{**} presented in table 2.2.

doublet	J^P values	notation $\left\vert jJ^P\right\rangle$	experimental notation
$j^P = 1/2^+$	0^+	$\left\vert \frac{1}{2}\ 0^+\right\rangle$	D_0^*
	1^+	$\left\vert \frac{1}{2}\ 1^+\right\rangle$	D_1'
$j^P = 3/2^+$	1^+	$\left\vert \frac{3}{2}\ 1^+\right\rangle$	D_1
	2^+	$\left\vert \frac{3}{2}\ 2^+\right\rangle$	D_2^*

Table 2.2: The "heavy-light" decomposition of the D^{**}. The D^{**}'s belonging to the same doublet are related by HQS. The superscript P denotes the parity of the state.

Experimentalists usually refer to the charmed D mesons by the notations indicated in Tables 2.1 and 2.2. We will use them when needed.

However when we consider finite quark masses, the classification used at the static approximation (i.e. at the infinite mass limit) does not hold. Indeed, in such a case, the spin of the heavy quark is no longer conserved. The angular momentum of the light cloud j is not a good quantum number anymore, i.e. states must be labeled by their total angular momentum J. For example, we have two S wave states (notation D_J: D_0, D_1) but they do not form a $j^P = 1/2^-$ doublet.
Moreover, one can relate states classified in the "spin-orbit" decomposition to those represented in the "heavy-light" one by using the so-called "6j" Wigner coefficients [26]

$$\left\vert jJ\right\rangle \ = \ \sum_S (-)^{s_Q+s_q+L+J}\ \sqrt{(2S+1)(2j+1)}\ \begin{Bmatrix} s_Q & s_q & S \\ L & J & j \end{Bmatrix}\ \left\vert n\ ^{2S+1}L_J\right\rangle \tag{2.11}$$

where s_q represents the spin of the light quark. When applied in the present case to the four D^{**}s, we

get

$$\begin{cases} \left|\tfrac{1}{2}\,0^+\right\rangle &= \left|{}^3P_0\right\rangle \\ \left|\tfrac{1}{2}\,1^+\right\rangle &= -\dfrac{1}{\sqrt{3}}\left|{}^1P_1\right\rangle \;+\; \sqrt{\dfrac{2}{3}}\left|{}^3P_1\right\rangle \\ \left|\tfrac{3}{2}\,1^+\right\rangle &= \sqrt{\dfrac{2}{3}}\left|{}^1P_1\right\rangle \;+\; \dfrac{1}{\sqrt{3}}\left|{}^3P_1\right\rangle \\ \left|\tfrac{3}{2}\,2^+\right\rangle &= \left|{}^3P_2\right\rangle \end{cases} \tag{2.12}$$

We can see that, for the 0^+ and 2^+ states, both decompositions are equivalent. This explains why we will choose to study the $\left|\frac{1}{2}\,0^+\right\rangle$ and the $\left|\frac{3}{2}\,2^+\right\rangle$ states amongst the D^{**} mesons. For the two 1^+ states, more work is needed in order to disentangle them because of their dependence on $\left|{}^1P_1\right\rangle$ and $\left|{}^3P_1\right\rangle$.

2.2.3 Properties of the D^{**} states

The charmed D^{**} states have been mostly observed in nonleptonic $B \to D^{**}\,\pi$ decays from where their properties like widths and masses are extracted (Table 2.3). Parity and angular momentum conservation constrain the decays allowed for each state, helping to identify experimentally the D^{**} candidates (Fig. 2.3). The main decay channels of such states are the nonleptonic decays

$$D^{**} \;\to D^*\,\pi \tag{2.13}$$

Parity is conserved, thus the pion must have an even orbital angular momentum l. Angular momentum conservation implies that $l \;=\; 0,\,2$. Hence the $j = 1/2$ states decay through an S-wave to $D^*\,\pi$, and are both expected to be broad (large decay widths)

$$D^{**}_{j=1/2} \;\to\; D^{(*)}_{j=1/2}\,\pi \tag{2.14}$$

whereas $j = 3/2$ states are only allowed through an $l = 2$ (D-wave channel) and are expected to be narrower (small widths)

$$D^{**}_{j=3/2} \;\to\; D^{(*)}_{j=1/2}\,\pi \tag{2.15}$$

Among the expected non-strange D^{**}s, two have been observed experimentally [27]

$$D_1(2420)^{\pm} \qquad \text{with} \qquad I(J^P) = \tfrac{1}{2}(1^+) \tag{2.16}$$

$$D_2^*(2460)^{\pm} \qquad \text{with} \qquad I(J^P) = \tfrac{1}{2}(2^+) \tag{2.17}$$

where I is the isospin quantum number. These states have rather small widths. This is the reason why this doublet has been identified while the doublet $j \;= 1/2$ has not (broad resonances).

In the next section, we will summarize some relevant results arising from the study of $D^{(*)}$ and D^{**} states created by the semileptonic decay of B mesons.

D^{**}	Mass [MeV]	width [MeV]
D_0^*	2318±29	267 ± 40
D_1'	2427 ± 26 ± 25	$384^{+107}_{-75} \pm 74$
D_1	2421.3± 0.6	27.1 ± 2.7
D_2^*	2464.4 ± 1.9	37 ± 6

Table 2.3: Masses and decay widths of D^{**} [1].

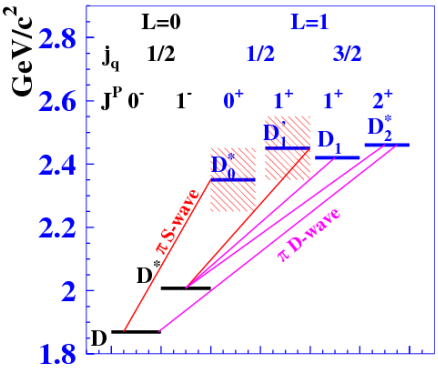


Figure 2.3: Spectroscopy of D-meson excitations. The lines show possible single pion transitions [27].

2.3 Exclusive $B \to D^{(*)}$ decays

A precise knowledge of semileptonic decays of B mesons brings several advantages to flavor physics. For example, exclusive semileptonic B decays into D and D^* mesons allow two independent estimates of the CKM matrix element V_{cb} and contribute considerably to the analysis of the unitarity triangle.

Case of a massless lepton: in the limit of vanishing lepton mass, the differential decay rates of $B \to D\ell\bar{\nu}_\ell$ and $B \to D^*\ell\bar{\nu}_\ell$ write [24]

$$\begin{cases} \dfrac{d\Gamma}{dw}(B \to D\,\ell\bar{\nu}_\ell) &= \dfrac{G_F^2}{48\pi^3}\,(m_B + m_D)^2\, m_D^3 (w^2-1)^{3/2}\,|V_{cb}|^2\,|\mathscr{G}(w)|^2 \\ \dfrac{d\Gamma}{dw}(B \to D^*\ell\bar{\nu}_\ell) &= \dfrac{G_F^2}{48\pi^3}\,(m_B)^5\,(1-r^2)r^3\,\sqrt{w^2-1}(1+w^2)\,\lambda(w)\,|V_{cb}|^2\,|\mathscr{F}(w)|^2 \end{cases} \tag{2.18}$$

where $\mathscr{F}(w)$ and $\mathscr{G}(w)$ are functions of the form factors entering the $B \to D^{(*)}$ transition amplitudes [24], and w is the product of the velocities of the hadrons in the HQET framework

$$w = v_B \cdot v_D \;=\; \frac{m_B^2 + m_{D^{(*)}}^2 - q^2}{2\,m_B\,m_{D^{(*)}}} \tag{2.19}$$

For a momentum transfer q^2 that verifies

$$q^2_{\rm min} \le q^2 \le q^2_{\rm max}, \qquad q^2_{\rm min} = m_\ell^2 \approx 0 \quad \text{and} \quad q^2_{\rm max} = (m_B - m_{D^{(*)}})^2 \tag{2.20}$$

w varies in the range

$$1 \;\le w \;\lesssim \frac{m_B^2 + m_{D^{(*)}}^2}{2\,m_B\,m_{D^{(*)}}} \tag{2.21}$$

The term $\lambda(w)$ reads

$$\lambda(w) = 1 + \frac{4w}{w+1}\,t^2(w) \quad \text{with} \quad t^2(w) = \frac{1-2wr+r^2}{(1-r)^2} \quad \text{and} \quad r = m_{D^*}/m_B \tag{2.22}$$

By exploiting Eq. (2.18), one can derive information on the shape of

$$|\text{CKM matrix element} \times \text{form factor}| \tag{2.23}$$

from the experimentally measured differential decay rates.

The main theoretical problem is the determination of these form factors. At the zero recoil point, $w = 1$, heavy quark symmetries play a useful rôle in setting the normalization $\mathscr{F}(1) = \mathscr{G}(1)$ [28], even though this point is not directly accessible from experiments due to the kinematic suppression in Eqs. (2.18). Let us compare the latest determinations of the $|V_{cb}|$ value extracted from $B \to D\ell\bar{\nu}_\ell$ decays. The most recent unquenched[2] lattice calculation dates back to 2005 [29] and gives

$$\mathscr{G}(1) \;=\; 1.074 \pm 0.024 \tag{2.24}$$

Using the above value along with the latest HFAG average [30] that includes older Aleph, CLEO and Belle measurements, as well as the new 2008-2009 BaBar data, one finds

$$|V_{cb}|\,|\mathscr{G}(1)| \;=\; (42.64 \pm 1.53) \times 10^{-3} \tag{2.25}$$

The resulting estimate of $|V_{cb}|$ is

$$|V_{cb}| \;=\; (39.70 \pm 1.42_{\rm exp} \pm 0.89_{\rm th}) \times 10^{-3} \tag{2.26}$$

in good agreement with the lattice determination of $\mathscr{F}(1)$ [31, 32] from $B \to D^*\ell\bar{\nu}_\ell$ [30]

$$|V_{cb}| \;=\; (39.54 \pm 0.5_{\rm exp} \pm 0.74_{\rm th}) \times 10^{-3} \tag{2.27}$$

but with an experimental error which is more than twice larger. In the case of $B \to D$ decays, the experimental error overcomes the theoretical one arising from the determination of $\mathscr{G}(1)$. However, in the case of B transitions into D^*, the theoretical uncertainty is larger than the experimental one. Therefore, any precise determination of the form factors is important to get a more precise value of the CKM matrix element V_{cb}.
An alternate lattice determination, currently available only in the quenched approximation, consists in calculating the form factor directly at non zero recoils $w > 1$, avoiding the extrapolation to $w = 1$ [33,34]. Using only 2009 BaBar data [35], this approach gives a slightly higher value than the unquenched lattice results (2.26)

$$|V_{cb}| \;=\; (41.6 \pm 1.8_{\rm exp} \pm 0.77_{\rm th}) \times 10^{-3} \tag{2.28}$$

The most recent non lattice calculation combines the heavy quark expansion with a "BPS" expansion [36] giving in this limit

$$\mathscr{G}(1) \;=\; 1.04 \pm 0.02 \tag{2.29}$$

[2]The "unquenched" notion will be discussed later on.

With such an estimate, one finds [1]

$$|V_{cb}| \;=\; (40.7 \pm 1.5_{\rm exp} \pm 0.8_{\rm th}) \times 10^{-3} \tag{2.30}$$

in agreement, within the errors, with both lattice determinations in (2.26) and (2.28).

Case of a massive lepton: until 2007, only decays where the final lepton was an electron or a muon had been observed. When the mass of the charged lepton is no longer negligible[3], the relations (2.18)

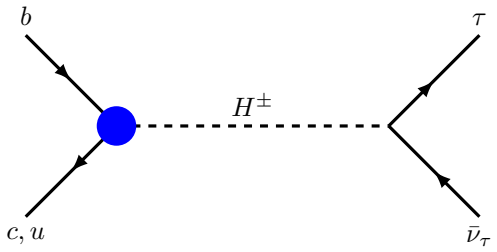


Figure 2.4: Feynman Diagram with a charged Higgs contributing to $B \to \tau\bar{\nu}_\tau$ and $B \to D^{(*)}\tau\bar{\nu}_\tau$.

do not hold and experimental measurements of $B \to D^{(*)}\tau\bar{\nu}_\tau$ are sensitive to other form factors.
The first observation of the $B \to D^*\tau^-\bar{\nu}_\tau$ decay, by the Belle Collaboration [37], was followed by improved measurements and evidence for $B \to D\tau^-\nu_\tau$, by both Babar and Belle Collaborations [38,39]. Recently, BaBar has updated its older measurements [38] by using its full data sample. The obtained results of $B \to D^{(*)}\tau\bar{\nu}_\tau$ branching ratios normalized to the corresponding $B \to D^{(*)}\ell\bar{\nu}_\ell$ modes ($\ell = \mu, e$) are

$$\begin{aligned} R(D) \;=\; \frac{\mathscr{B}(B \to D\tau\bar{\nu}_\tau)}{\mathscr{B}(B \to D\ell\bar{\nu}_\ell)} \;&= 0.440 \pm 0.072 \quad \text{and} \\ R(D^*) \;=\; \frac{\mathscr{B}(B \to D^*\tau\bar{\nu}_\tau)}{\mathscr{B}(B \to D^*\ell\bar{\nu}_\ell)} \;&= 0.332 \pm 0.03 \end{aligned} \tag{2.31}$$

where the statistical and systematic uncertainties have been combined quadratically. The results (2.31) have been compared with the SM predictions [40, 41]

$$R(D)_{\rm SM} \;= 0.297 \pm 0.017 \quad \text{and} \quad R(D^*)_{\rm SM} \;= 0.252 \pm 0.003 \tag{2.32}$$

which are averaged over electrons and muons.
One can see clearly that experimental measurements exceed the SM expectations by 2.0σ for $R(D)$ and by 2.7σ for $R(D^*)$; taken together, they disagree at the 3.4σ level. In a recent full $N_f = 2+1$ flavor Lattice QCD calculation[4], the authors of Ref. [42] found $R(D) = 0.316 \pm 0.012 \pm 0.007$. Another recent phenomenological approach challenges the SM determination for $R(D)$, giving $R(D) = 0.31 \pm 0.02$ [4]: both analyses reduce the discrepancy below 2σ.
Current experimental measurements of $R(D)$ are statistics-limited, so the luminosities available at fu-

[3] We will always use massless neutrinos.
[4] This N_f number will be explained in a coming chapter.

ture flavor facilities should allow significant improvements. If the experimental results for $R(D)$ and $R(D^*)$ are to be confirmed, they might point to NP effects in semitauonic B decays. It has been excluded that the excess in $R(D^{(*)})$ over the SM be explained within type II two Higgs doublet model (2HDM) [43] and in the context of the Minimal Supersymmetric Standard Model (MSSM) with flavor violation [44]. Instead, it is deemed possible in other extensions, e.g. in type III [45] and Aligned [46] two Higgs doublet models, by adopting effective Lagrangians [47]. (Fig. 2.4 represents charged Higgs mediated contributions to the taunic B decays.)

In the following, we propose to study the decay $B_s \to D_s\,\ell\bar{\nu}_\ell$. We will revisit the SM predictions by computing the normalization of the vector form factor relevant to the extraction of the CKM matrix element $|V_{cb}|$ from $\mathscr{B}(B_s \to D_s\ell\bar{\nu}_\ell)$ with $\ell \in \{e, \mu\}$. Moreover, in the models with two Higgs doublets, the charged Higgs boson can mediate tree-level processes, including $B \to D\ell\bar{\nu}_\ell$, and considerably enhance the coefficient multiplying the scalar form factor in the decay amplitude. So, we need to estimate the scalar form factor to interpret the recent discrepancy between the experimentally measured $R(D)$ and its theoretical prediction within the SM. Finally, in the models of physics BSM in which a tensor coupling to a vector boson is allowed, a third form factor might become important. We will perform the first Lattice QCD estimate of this (tensor) form factor.

2.4 Status of $B \to D^{**}\,\ell\,\bar{\nu}_\ell$

In what follows, we will discuss the theoretical approaches used to describe the semileptonic decay of B mesons into D^{**} as well as the values obtained for the corresponding branching ratios from the theoretical and the experimental sides. Important results will be collected in Sections 2.4.2 and 2.4.3.

2.4.1 Infinite mass limit approaches

In the heavy quark limit for the b and c quarks, all the transition amplitudes associated with $B \to D^{**}\,\ell\,\bar{\nu}_\ell$ decays are proportional to one of the two Isgur-Wise (IW)[5] functions $\tau_{1/2}$ and $\tau_{3/2}$ [25]. For example

$$\langle D^{**}(0^+)\,|\,A_\mu\,|\,B(0^-)\rangle \quad \equiv \quad -\,(v_\mu - v'_\mu)\;\tau_{1/2}(w) \tag{2.33}$$

$$\langle D^{**}(2^+)\,|\,A_\mu\,|\,B(0^-)\rangle \quad \equiv \quad \sqrt{3}\;\;\tau_{3/2}(w)\;\;\left[(1+w)\epsilon^*_{\mu\nu}\,v^\nu\;\;-\,v'_\mu\,v^\nu\,v^\rho\epsilon^*_{\nu\rho}\right] \tag{2.34}$$

where v and v' are the four velocities of the initial and final mesons, $\epsilon_{\mu\nu}$ is the polarization tensor of the 2^+ state and the mesonic states are normalized according to

$$\left\langle M(\vec{v}',\,\varepsilon_\beta)\,\middle|\,M(\vec{v},\,\varepsilon_\alpha)\right\rangle \;=\; (2\pi)^3\,2v_0\,\delta_{\alpha\beta}\,\delta^3(\vec{v}'-\vec{v}) \tag{2.35}$$

[5] A third IW function $\xi(w)$ is also introduced for the $B \to D^{(*)}$ transitions.

Quark model predictions

The characterization of the IW functions relies on theoretical predictions. The IWs are bounded by sum rules, such as the so-called Uraltsev sum rule [48]

$$\sum_n |\tau_{3/2}^{(n)}(1)|^2 - |\tau_{1/2}^{(n)}(1)|^2 = \frac{1}{4} \tag{2.36}$$

with n labeling the radial excitations. The functions $\tau_{1/2}(1)$ and $\tau_{3/2}(1)$ are the IW form factors at zero recoil ($w = 1$). Focusing only on the ground states suggests the inequality $|\tau_{1/2}(1)| < |\tau_{3/2}(1)|$, which is also confirmed by the similar sum rule studied in Ref. [49]. This is not a theorem but relies on the assumption that the lowest state dominates in each channel.
The IW functions were also determined using a quark model having very interesting features in the heavy quark limit: this particular class of models, called à la Bakamjian-Thomas (BT) [50], provides a method for writing in a covariant way the transition amplitudes. It also exhibits the correct behavior in the infinite mass limit and satisfies the heavy-quark symmetry relations discovered by Isgur and Wise. Within the BT quark model approach, one finds that the difference $|\tau_{3/2}(1)| - |\tau_{1/2}(1)|$ is positive and large [51]. This difference between $\tau_{1/2}(1)$ and $\tau_{3/2}(1)$ comes from the Wigner rotations of the light spectator quark, which acts differently for the $j = 1/2$ and $j = 3/2$ states. In addition, since the matrix elements are written in terms of the wave functions of the bound states which depend on the dynamics, one also has to choose a necessarily relativistic potential model to fix the wave functions at rest. The guiding principle in choosing the potential is obviously the requirement to describe as broad a range of observed hadrons as possible. In that respect, the standard Godfrey-Isgur (GI) potential model [52] provides the best description of the whole spectroscopy. By using the wave functions fixed by the GI potential model, the BT approach leads to the following results [53]

$$\tau_{3/2}(1) \simeq 0.54 \qquad\qquad \tau_{1/2}(1) \simeq 0.22 \tag{2.37}$$

In what follows, we will compare the above values to those obtained using other theoretical approaches.

Lattice QCD predictions

The only known way to systematically and rigorously solve the quantum theory of strong interactions, allowing us to compute these form factors without uncontrolled hypothesis, is Lattice QCD. The IW form factor at zero recoil, $\tau_{1/2}(1)$, was first calculated in Ref. [54] and the computation was later improved in Ref. [55], where the results were obtained for a given lattice spacing and using $N_f = 2$ flavors of dynamical quarks. The results read

$$\tau_{3/2}(1) = 0.528(23) \qquad\qquad \tau_{1/2}(1) = 0.297(26) \tag{2.38}$$

The agreement between the results obtained in the static limit of Lattice QCD (2.38) (i.e. lattice computations using the infinite mass limit of the charm quark) and the results obtained using the BT approach with a suitable potential model (2.37) is striking. A similar agreement has been observed for the distribution of the axial, scalar and vector charges in the heavy-light mesons with either $L = 0$, or $L = 1$ [56]. The advantage of quark models is that one can easily calculate the w-dependence of $\tau_{1/2}(w)$

and $\tau_{3/2}(w)$, needed when computing the branching ratios.

QCD sum rules

The $\tau_j(1)$ results from QCD sum rules depend on the choice of the creation and annihilation operators for the D^{**} states and do not agree among themselves. The first calculation of $\tau_j(1)$ was made in Ref. [57, 58]

$$\tau_{3/2}(1) \sim 0.25 \qquad\qquad \tau_{1/2}(1) \simeq 0.35(8) \tag{2.39}$$

Other results based on QCD sum rules were presented in Ref. [59]

$$\tau_{3/2}(1) \simeq 0.43(8) \qquad\qquad \tau_{1/2}(1) \simeq 0.13(4) \tag{2.40}$$

The hierarchy $|\tau_{1/2}(1)| < |\tau_{3/2}(1)|$ is similar to the one found in Lattice QCD and in the quark model discussed above. However, the value $\tau_{1/2}(1) \simeq 0.13(4)$ is considered to be incompatible with the value given in Eq. (2.39) or with the results in Eqs. (2.38) and (2.37). The difference between the values obtained using QCD sum rules and between these values and the results coming from other theoretical approaches (LQCD, quark models) is considered to be an indicator of a possible uncertainty of the method.

2.4.2 Theoretical summary

From the previous discussion, one can calculate the ratio of the values of the IW functions involving the D^{**} states at $w = 1$ in the heavy quark limit

$$\frac{|\tau_{1/2}(1)|^2}{|\tau_{3/2}(1)|^2} \simeq 0.17 \tag{2.41}$$

It indicates that the branching ratio of the semileptonic B decay to a $j^P = (1/2)^+$ state should be small compared to the decay to a $j^P = (3/2)^+$ meson, provided the phase space contribution does not reverse the trend. Using the results of the quark model calculation in the BT formalism with the GI potential model, one has [51]

$$\begin{aligned}
\mathscr{B}(B_d^0 \to D_2^{*-} \ell \bar{\nu}_\ell)_{\rm th} &\simeq 0.7 \times 10^{-2} \\
\mathscr{B}(B_d^0 \to D_{1\ (3/2)}^{-} \ell \bar{\nu}_\ell)_{\rm th} &\simeq 0.45 \times 10^{-2} \\
\mathscr{B}(B_d^0 \to D_{1\ (1/2)}^{\prime -} \ell \bar{\nu}_\ell)_{\rm th} &\simeq 0.7 \times 10^{-3} \\
\mathscr{B}(B_d^0 \to D_0^{*-} \ell \bar{\nu}_\ell)_{\rm th} &\simeq 0.6 \times 10^{-3}
\end{aligned} \tag{2.42}$$

which confirms that the production of the broad resonances is much lower than the one of narrow states. Let us confront these results with the experimentally measured branching fractions.

2.4.3 Experimental situation

The experimental status of the weak transitions between B and the broad D^{**} states reveals a different situation.

Narrow states: decays to the narrow D^{**} states have been experimentally measured with good accuracy[6]

$$\mathscr{B}(B_d^0 \to D_2^* \ell^+ \bar{\nu}_\ell) = (0.26 \pm 0.03)\% \tag{2.43}$$

$$\mathscr{B}(B_d^0 \to D_1 \ell^+ \bar{\nu}_\ell) = (0.59 \pm 0.05)\% \tag{2.44}$$

giving

$$\mathscr{B}(B_d^0 \to D^{**}_{\text{narrow}} \ell^+ \bar{\nu}_\ell) = (0.85 \pm 0.06)\% \tag{2.45}$$

There is an excess in the theoretical prediction, by a factor of 2, for $\mathscr{B}(B_d^0 \to D_2^* \ell^+ \bar{\nu}_\ell)$, but there is also an overall success for the sum $\mathscr{B}(B_d^0 \to D^{**}_{\text{narrow}} \ell^+ \bar{\nu}_\ell)$ which indicates that there is a qualitative agreement between theory and experiment in B decays to a $j_{3/2}$ state.

Broad states: the measured value for the D_0^* is

$$\mathscr{B}(B_d^0 \to D_0^* \ell^+ \bar{\nu}_\ell) = (0.40 \pm 0.07)\% \tag{2.46}$$

The semileptonic experimental data contradicts the theoretical estimate for the decay to a $j = 1/2$ state, with a huge discrepancy, of one order of magnitude. For the broad D_1' state, the situation is different because the two experiments disagree. Belle does not see any broad D_1' component, while BaBar gives

$$\mathscr{B}(B_d^0 \to D_1' \ell^+ \bar{\nu}_\ell) = (0.38 \pm 0.06 \pm 0.06)\%$$

HFAG [30] also gives

$$\mathscr{B}(B_d^0 \to D_1' \ell^+ \nu_\ell) = (0.18 \pm 0.06)\%$$

Finally, the relation found in the heavy mass limit [60–62]

$$\mathscr{B}\left(B \to D^{**}_{j=3/2}\, \ell\, \bar{\nu}\right) \gg \mathscr{B}\left(B \to D^{**}_{j=1/2}\, \ell\, \bar{\nu}\right) \tag{2.47}$$

is violated: this is known as "**1/2 vs 3/2 puzzle**" [21, 22]. It is one of the longstanding puzzling features of semileptonic $b \to c$ data.

2.4.4 Conclusion and proposals

The broad $B \to D^{**}_{1/2}$ decays remain a controversial topic on both experimental and theoretical front. Measurements done by BaBar and Belle for the D_1' are incompatible. Moreover, experimental data also indicate that the production of D_0^* states does not verify the theoretical predictions.

[6] The numbers presented are taken from [23] where the values are given by the HFAG Collaboration [30] and averaged by taking measurements from neutral and charged B mesons using isospin symmetry. Obtained values are quoted for the B_d^0 meson.

The broadness of $j = 1/2$ states may be one of the reasons causing the disagreement between experiments as well as between theory and experiment, since it has always been difficult to disentangle very broad resonances.
In order to clarify the comparison between theory and experiment, it has been suggested to analyze states analogous to the controversial D^{**} (i.e. D_0^* and D_1') but having narrow widths (i.e. D_{s0}^* and D_{s1}'), in particular studying the non-leptonic decays $B_s^0 \to \overline{D}_s\, \pi$ [23] which would provide an important check of the observations made in the corresponding non-strange modes. Other theoretical suggestions to ease or solve the previous problems include taking into account an unexpectedly large B-decay rate to the first radially excited $D^{'(*)}$ [63–65].

In many theoretical approaches (HQET, heavy quark expansion, quark model, Lattice QCD with quenched calculation, etc...), branching ratios corresponding to the decay $B \to D^{**}\ell\bar{\nu}_\ell$ were calculated using the infinite mass limit. The impact of the corrections arising from the finiteness of the heavy quark mass in the process of B into the D^{**} has not been much discussed, and until now there is no available Lattice QCD result that would help to assess the size of these corrections. That is the reason why, in order to address the aforementioned questions, we propose in this doctoral work to determine for the first time the physical parameters and then the form factors from Lattice QCD using "real" charmed quarks having a finite mass.

Part II

Lattice gauge theory

Chapter 3

Lattice QCD

The Standard Model is a gauge theory based on $SU(2) \times U(1) \times SU(3)$. The $SU(2)$ and $U(1)$ components have weak couplings and can be studied with perturbative methods, but the $SU(3)$ part (QCD) can be studied with perturbative techniques at high energies only. In the infrared regime, the strong coupling grows and thus the use of non-perturbative techniques is inevitable in order to determine accurately the low energy properties of QCD.

One possibility is to discretize the space-time in order to "put" the QCD Lagrangian on a finite lattice: the method was proposed by Wilson in 1974 and is called "Lattice gauge theory". It is a means of regularizing a field theory by moving from a continuous infinite world to a discretized finite volume where quark fields are placed on the sites separated by the lattice spacing "a" and gauge fields are the links between these sites (Fig. 3.1). In this theory truncated to a finite number of degrees of freedom, masses, decay constants and hadronic transition amplitudes can, in principle, be calculated by averaging, in the statistical sense, over gauge configurations generated numerically on a computer. The continuum limit is then recovered, for example, by taking the limit of a vanishing lattice spacing and the volume to infinity.

In the first section we will review the continuous QCD action. Then we will introduce the discretization of QCD on the lattice which proceeds in many steps: we begin with the lattice action for gluons followed by the discretization of the fermionic part of the QCD action. Finally, we discuss the twisted mass action, the adopted choice in our simulation, and we will show some of its implications.

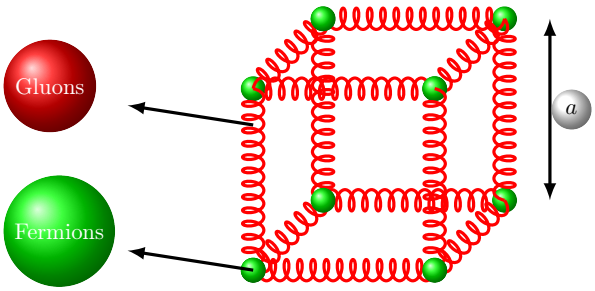


Figure 3.1: Lattice QCD symbolic description.

3.1 QCD in the continuum

Quantum chromodynamics is a relativistic Quantum Field Theory which describes the strong interaction in terms of fundamental degrees of freedom (quarks and gluons). In Euclidean space[1], the continuum

[1]The reasons for going to Euclidean space are given in Appendix A.

action for QCD with a set of n_f flavours of quarks is

$$S[\psi,\,\bar{\psi},\,A^{\mu}] \,=\, \int\, d^4x \,\sum_{f=1}^{n_f}\, \bar{\psi}_f(x)\,(\gamma_\mu\, D_\mu +\, m_f)\,\psi_f(x) \,-\, \frac{1}{4}\mathrm{Tr}\,[\mathscr{F}_{\mu\nu}\mathscr{F}^{\mu\nu}] \tag{3.1}$$

If we explicitly write all the indices, we arrive at

$$\begin{aligned} S[\psi,\,\bar{\psi},\,A^{\mu}] \,=\, \sum_{f=1}^{n_f}\, \int\, d^4x\; \bar{\psi}^f(x)_{\alpha,A}\, \Big\{(\gamma^\mu)_{\alpha\beta}\,[\partial_\mu\delta_{AB} \,+\, ig\; A_\mu(x)_{AB}] \\ +m_f\delta_{AB}\delta_{\alpha\beta}\Big\}\;\psi^f(x)_{\beta,B} - \,\frac{1}{4}\mathscr{F}^a_{\mu\nu}\mathscr{F}^{\mu\nu}_a \end{aligned} \tag{3.2}$$

where γ_μ are the Dirac-matrices, $\alpha,\beta \in \{1,2,3,4\}$ are the Dirac indices, $A, B \in \{1,2,3\}$ stands for the color indices of the fermion fields, $a \in \{1,\cdots,8\}$ denotes the gluon color indices and $\mu,\nu \in \{1,2,3,4\}$ the Lorentz indices.
The $SU(3)$ gauge invariance of QCD requires the action to be invariant under the transformation

$$\psi(x) \rightsquigarrow \psi'(x) = G(x)\,\psi(x)\;,\;\; \bar{\psi}(x) \to \bar{\psi}'(x) \,=\, \bar{\psi}(x)G^\dagger(x) \tag{3.3}$$

where $G(x)$ is a complex 3×3 matrix at each space-time point x. Being unitary and special, it can be decomposed as

$$G(x) \;=\; \exp[-i\;\mathbf{T}\cdot\mathbf{\Theta(x)}] \tag{3.4}$$

where $\mathbf{T}$ represents the generators of the $SU(3)$ group and $\mathbf{\Theta}(x)$ is a local phase.
By definition, they satisfy

$$G^\dagger(x) = G^{-1}(x) \quad \text{and} \quad \det\,[G(x)] = 1 \tag{3.5}$$

The local invariance of the fermionic action under the gauge transformation (3.3) generates a gauge field $A_\mu(x)$ having the transformation property

$$A_\mu(x) \rightsquigarrow A'_\mu(x) \;=\; G(x)A_\mu(x)G^\dagger(x) \,+\, i(\partial_\mu\, G(x))\, G^\dagger(x) \tag{3.6}$$

Note that A_μ lies in the Lie algebra of $SU(3)$ which implies

$$A_\mu(x) \,=\, \sum_{a=1}^{8}\, A^a_\mu(x)\;\mathbf{T_a} \tag{3.7}$$

Moreover, $D_\mu(x)$ is the covariant derivative defined by

$$D_\mu(x) \,=\, \partial_\mu \,+\, i\,g\,A_\mu(x) \tag{3.8}$$

and transforms as

$$D_\mu(x) \rightsquigarrow D'_\mu(x) \,=\, \partial_\mu \,+\, i\,g\,A'_\mu(x) \,=\, G(x)D_\mu G^\dagger(x) \tag{3.9}$$

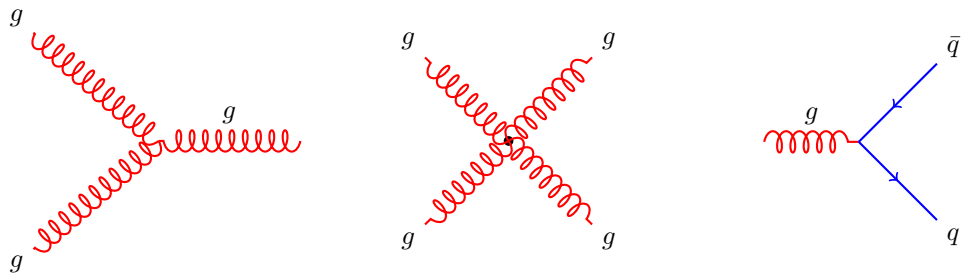


Figure 3.2: Feynman diagrams of the QCD Lagrangian for cubic and quartic self-interactions and for the quark-gluons vertex.

Finally, $\mathscr{F}^a_{\mu\nu}$, the field strength tensor, is the commutator of two covariant derivatives expressed in terms of the gauge fields A^a_μ

$$\mathscr{F}^a_{\mu\nu} \;=\; -i[D_\nu(x), D_\mu(x)] \;=\; \partial_\mu A^a_\nu(x) - \partial_\nu\, A^a_\mu(x) \;+\; i\, g\, [A^a_\mu(x),\, A^a_\nu(x)] \tag{3.10}$$

It transforms according to

$$\mathscr{F}^a_{\mu\nu}(x) \rightsquigarrow \mathscr{F}'^a_{\mu\nu}(x) \;=\; G(x)\, \mathscr{F}^a_{\mu\nu}(x) G^\dagger(x) \tag{3.11}$$

Because the commutator in (3.11) does not vanish ($SU(3)$ is a non abelian group), the term representing the gauge action

$$\frac{1}{4} \int d^4x \sum_{a=1}^{8} \mathscr{F}^a_{\mu\nu}\, \mathscr{F}^{\mu\nu}_a \tag{3.12}$$

gives rise to self-interactions of the gluons, making QCD a highly non trivial theory. Self-interactions (cf. figure 3.2) are responsible for confinement of color, the most prominent feature of QCD.

3.2 Gauge field on the lattice

Using local gauge invariance and requiring the locality of interactions, one can construct lattice actions whose continuum limits reproduce the Yang-Mills Theory and whose strong coupling limits confine quarks. The discussion of the possible gauge actions constitutes the core of the forthcoming sections.

3.2.1 Lattice transcription of gauge field variable

In the continuum, the gauge fields $A_\mu(x)$ carry 4-vector Lorentz indices and mediate interactions between fermions. To transfer them to a lattice, Wilson noted [66] that in the continuum, a fermion moving

from x to y in presence of a gauge field $A_\mu(x)$ picks up a phase factor given by the path ordered product

$$\Psi(y) \;=\; \mathscr{P} \exp\left(ig \int_x^y A_\mu(x_\mu)\, dx^\mu \right) \Psi(x) \tag{3.13}$$

where g is the gauge coupling constant.
From here arises the idea that gauge field variables can be associated with links that connect sites on the lattice. So, Wilson introduced a discretized version of a path ordered product, the *gauge link* $U(x, x + a\hat{\mu})$

$$\begin{aligned} U(x, x + a\hat{\mu}) \quad &= \quad \mathscr{P} \exp\left(iga \int_0^1 A_\mu(x + \tau\hat{\mu})\, d\tau \right) \\ &\equiv \quad \exp\left(igaA_\mu(x + \frac{\hat{\mu}}{2}) \right) \end{aligned} \tag{3.14}$$

where $\hat{\mu}$ is a unit vector pointing in the μ direction and A_μ is the average field defined at the midpoint of the link. The link matrix is the path dependent gauge connection that relates the color space at site x to the site $x + a\hat{\mu}$, and is denoted by

$$U(x, x + a\hat{\mu}) \;\equiv\; U_\mu(x) \tag{3.15}$$

$U_\mu(x)$ are forward connections and $U_{-\mu}(x)$ are backward connections (see Fig. 3.3). They satisfy relations such as

$$U(x, x - a\hat{\mu}) \;\equiv\; U_{-\mu}(x) \;= \exp\left(-i\, g\, a\, A_\mu(x - \frac{\hat{\mu}}{2}) \right) = \; U^\dagger(x - a\hat{\mu}, x) \tag{3.16}$$



Figure 3.3: Gauge links on the lattice.

The set of $U_\mu(x)$ for all μ and all lattice points x will be called "*gauge configuration*". A configuration represents a possible value of the gluon fields on the lattice.
Finally, we introduce the discretized forward covariant derivative

$$\overrightarrow{\nabla}_\mu \psi(x) \;=\; \frac{U(x, x + a\hat{\mu})\psi(x + a\hat{\mu}) - \psi(x)}{a} \tag{3.17}$$

as well as the backward covariant derivative

$$\overrightarrow{\nabla}^*_\mu \psi(x) \;=\; \frac{\psi(x) - U_{-\mu}(x)\psi(x - a\hat{\mu})}{a} \tag{3.18}$$

Usually, when discretizing the continuum Dirac action, we replace the derivative with the following

symmetric difference

$$\nabla\psi(x) \;=\; \frac{1}{2}(\overrightarrow{\nabla}_\mu + \overrightarrow{\nabla}^*_\mu)\,\psi(x) \;=\; \frac{U(x,x+a\hat{\mu})\psi(x+a\hat{\mu}) - U_{-\mu}(x)\psi(x-a\hat{\mu})}{2a} \tag{3.19}$$

The latter ensures the anti-hermiticity of the Dirac operator[2].

3.2.2 Gauge invariance and gluon action

We are now going to discuss how to construct gauge invariant quantities (observables) on the lattice. A rotation in color space can be done at each site with an $SU(3)$ matrix $G(x)$. Then, the link variable $U_\mu(x)$ transforms according to

$$U_\mu(x) \to G(x)\; U_\mu(x)\; G^\dagger(x+a\mu) \tag{3.20}$$

Since the action needs to be invariant with respect to this transformation law, it has to be constructed from traces of products of U matrices around closed paths, known as Wilson loops.

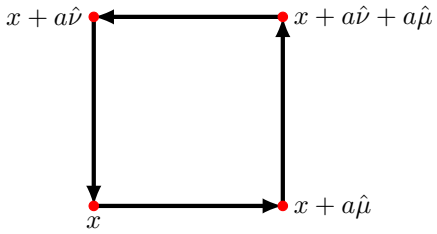


Figure 3.4: Representation of a 1×1 Wilson loop known as plaquette.

The simplest example is the 1×1 loop, shown in Fig. 3.4, which defines the gauge invariant quantity called "plaquette"

$$\mathrm{Re}\big[\mathrm{Tr}\,\big(U_\mu(x)\,U_\nu(x+a\hat{\mu})\,U^\dagger_\mu(x+a\hat{\nu})\,U^\dagger_\nu(x)\big)\big] \tag{3.21}$$

whose invariance is obvious from (3.20). The trace of any Wilson loop in the fundamental representation is complex, with the two possible path-orderings giving complex conjugate values. Thus, taking the trace ensures gauge invariance and taking the real part is equivalent to averaging the loop and its charge conjugate.

Formulation of the Lattice action: as a pedagogical example, we will outline the construction of the lattice gauge action for QED ($U(1)$ symmetry), in which the link variables are commuting complex numbers instead of $SU(3)$ matrices. Closed loops

$$L^{1\times1}_{\mu\nu} = U_\mu(x)\,U_\nu(x+a\hat{\mu})\,U^\dagger_\mu(x+a\hat{\mu})\,U^\dagger_\nu(x) \tag{3.22}$$

[2]The notion of Dirac operator will be introduced in Section 3.3

are expressed, using Eq. (3.14), as

$$L_{\mu\nu}^{1\times1} = \exp\left[iag\left(A_\mu\big(x+\frac{\hat{\mu}}{2}\big) + A_\nu\big(x+\hat{\mu}+\frac{\hat{\nu}}{2}\big) - A_\mu\big(x+\hat{\nu}+\frac{\hat{\mu}}{2}\big) - A_\nu\big(x+\frac{\hat{\nu}}{2}\big)\right)\right] \tag{3.23}$$

and can be used to construct the gauge action. Expanding (3.23) about $x + \dfrac{\hat{\mu}+\hat{\nu}}{2}$ gives

$$L_{\mu\nu}^{1\times1} = \exp\left[ia^2 g(\partial_\mu A_\nu - \partial_\nu A_\mu) + \frac{ia^4 g}{12}\left(\partial_\mu^3 A_\nu - \partial_\nu^3 A_\mu\right) + \cdots\right] \tag{3.24}$$

and expanding the exponential, we obtain

$$L_{\mu\nu}^{1\times1} = 1 + ia^2 g\mathscr{F}_{\mu\nu} - \frac{a^4 g^2}{2}\mathscr{F}_{\mu\nu}\mathscr{F}^{\mu\nu} + \mathscr{O}(a^6) \tag{3.25}$$

The real part of the loop reads

$$\mathrm{Re}\left[\ \mathrm{Tr}\,(1 - L_{\mu\nu}^{1\times1})\right] = \frac{a^4 g^2}{2}\mathscr{F}_{\mu\nu}\mathscr{F}^{\mu\nu} + \mathscr{O}(a^6) \tag{3.26}$$

while the imaginary part gives

$$\mathrm{Im}\,(L_{\mu\nu}^{1\times1}) = a^2 g\,\mathscr{F}_{\mu\nu} + \mathscr{O}(a^4) \tag{3.27}$$

Note that, since the electric and magnetic fields E and B are proportional to $F_{\mu\nu}$, Eq. (3.27) shows that they are given by the imaginary part of the Wilson loop $L_\mu^{1\times1}$.
There are 6 distinct positively oriented plaquettes, $\{\mu < \nu\}$, associated with each site. Summing over them and taking into account the double counting by an extra factor of $\frac{1}{2}$, gives, to the lowest order in a

$$\begin{aligned}\frac{1}{g^2}\sum_x\sum_{\mu<\nu}\mathrm{Re\ Tr}\ \left[(1 - L_{\mu\nu}^{1\times1})\right] &= \frac{a^4}{4}\sum_x\sum_{\mu<\nu}\mathscr{F}_{\mu\nu}\mathscr{F}^{\mu\nu} + \mathscr{O}(a^2)\\ &\xrightarrow{a\to0} \quad \frac{1}{4}\int d^4x\,\mathscr{F}_{\mu\nu}\mathscr{F}^{\mu\nu}\end{aligned} \tag{3.28}$$

Note that the factor a^4 together with the sum over x is just the discretization of the space-time integral[3] and thus the expansion of the *plaquette* reproduces the continuum action when a goes to zero.
The gauge action for the non-abelian case can be similarly constructed: the result for $SU(3)$, defined in terms of *plaquette* and called the gauge part of the Wilson action, is

$$S_G = \frac{\beta}{3}\sum_x\sum_{\mu<\nu}\mathrm{Re}\ \left[\mathrm{Tr}\,(\mathbb{1} - L_{\mu\nu}^{1\times1})\right] \tag{3.29}$$

where $\beta = \dfrac{6}{g^2}$ is the *inverse coupling*[4].

[3] That is also the reason why the $\mathscr{O}(a^6)$ correction term in Eq. (3.25) becomes an $\mathscr{O}(a^2)$ correction term in Eq. (3.28).
[4] For a general group $SU(N \geq 3)$, $\beta = \frac{2N}{g^2}$ and the plaquette $L_{\mu\nu}^{1\times1}(N)$ corresponds to the same ordered product as for $SU(3)$.

Improved gauge actions: we have already shown that the Wilson gauge action (3.28) reproduces the continuum limit up to terms $\mathcal{O}(a^2)$. So lattice artifacts contribute at $\mathcal{O}(a^2)$. Since it is impossible to choose arbitrary small lattice spacings, it is advisable to use any strategy which can minimize discretization effects and make the extrapolation to the continuum simpler. We will present in the following the basis of the *Symanzik improvement program* [67–69]. The main idea of this program is to cancel the leading order corrections and reduce lattice artifacts at non-zero lattice spacing.
We start from the above construction of the gauge action. We see clearly that the first terms in the expansion of the *plaquette* in power of the lattice spacing is, for the $SU(N)$ theory

$$\mathrm{Re}\left[\mathrm{Tr}\left(L_{\mu\nu}^{1\times 1}\right)\right] \;=\; N \;+\; \frac{1}{2}\,a^4\,O_4 \;+\; a^6\,O_6 \;+\cdots \tag{3.30}$$

where N is the trace of the $\mathbb{1}_{N\times N}$ identity matrix. Here, O_4 is the dimension-four operator corresponding to the continuum gauge action

$$O_4 \;=\; g^2 \sum_{\mu\nu} \mathrm{Tr}\,\mathscr{F}_{\mu\nu}\,\mathscr{F}^{\mu\nu} \tag{3.31}$$

There are no dimension-five operators, and $O_6 \;= \sum_j r_j\,O_6^j$, where O_6^j are the dimension-six operators allowed by lattice symmetries. The dimension-six operators present in the discretized lattice gauge part of the Wilson action lead to discretization errors proportional to a^2.

One wants to reduce discretization errors as much as possible in order to achieve a better convergence to the continuum limit, and to make a more efficient simulation of QCD. Classical improvements of the lattice action, i.e. decreasing discretization errors by removing the $\mathcal{O}(a^2)$ term, can be achieved by adding to the lattice action operators which go to zero when $a \to 0$, and tuning their coefficients to eliminate dimension-six operators present in the action. The lattice action then becomes

$$S_{\mathrm{latt}} \;\rightsquigarrow S_{\mathrm{cont}} \;+\mathcal{O}(a^3) \tag{3.32}$$

In order to apply this program to the gauge part of the Wilson action of QCD, one adds six-link loops involving six gauge links to define $\mathcal{O}(a^2)$ improved actions. There are only three six-link loops that one can draw on the lattice. These, shown in Fig. 3.5, are the planar, the twisted and the L shaped loop.

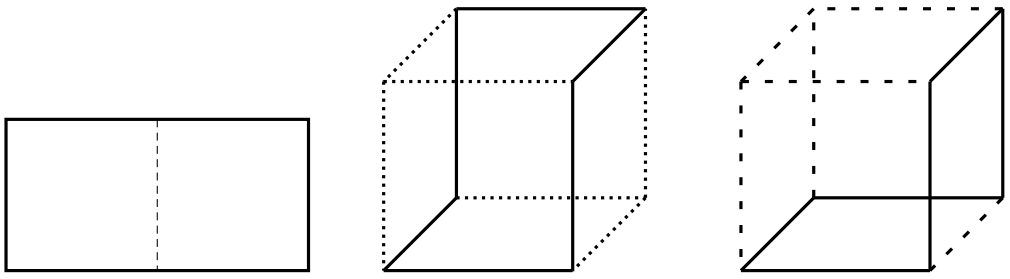


Figure 3.5: Six-link loops: from left to right, planar, twisted and L shaped.

For example, the lattice gauge action called *the tree-level Symanzik action* is the linear combination of

the plaquette $L_{\mu\nu}^{1\times1}$ and the planar loop $L_{\mu\nu}^{1\times2}$

$$S_G \;=\; \frac{\beta}{3}\,\sum_x\,\left(b_0\,\sum_{\mu,\nu}^{4}\,\left[1-\mathrm{Re}\left(\mathrm{Tr}\;L_{\mu\nu}^{1\times1}\right)\right]\;+\;b_1\,\sum_{\mu,\nu}^{4}\left[1-\mathrm{Re}\left(\mathrm{Tr}\;L_{\mu\nu}^{1\times2}\right)\right]\right) \tag{3.33}$$

with $b_0 = 1 - 8b_1$. We recover the gauge part of the Wilson action for $b_1 = 0$ and the tree-level Symanzik improved action for $b_1 = -1/12$ [69] which corresponds to the form of the gauge action used by the European Twisted Mass Collaboration (ETMC)

$$\boxed{S_G \;=\; \frac{\beta}{3}\,\sum_x\,\left(\frac{5}{3}\,\sum_{\mu,\nu}^{4}\,\left[1-\mathrm{Re}\left(\mathrm{Tr}\;L_{\mu\nu}^{1\times1}\right)\right]\;-\;\frac{1}{12}\,\sum_{\mu,\nu}^{4}\,\left[1-\mathrm{Re}\left(\mathrm{Tr}\;L_{\mu\nu}^{1\times2}\right)\right]\right)} \tag{3.34}$$

Other popular action is the Iwasaki action [70] where $b_1 = -0.331$.

3.3 Fermion field on the lattice

Putting fermions on the lattice is a much more difficult task. Many approaches to lattice fermions have been developed over the years, none of which is completely free from issues. In the following, we will illustrate some of the fermionic actions and we will identify some of the underlying problems.

Let us start with the lattice transcription of the fermion fields $\psi(x)$. In the continuum, the quark fields are represented by anti-commuting Grassmann variables. On the lattice, they will be attached to lattice points so that the fermionic field is defined as $\psi_x,\ x \in \{n\}$. It belongs to the fundamental representation of $SU(3)$.

3.3.1 The *naïve action* and the doublers problem

Naïve fermions are the simplest implementation of fermions on the lattice. They are rarely used in simulations, but nevertheless it is interesting to discuss them. In order to get the action for a free fermion field ψ_x, we start from its action in the continuum and in Euclidean space[5]

$$S_F^{\mathrm{cont}}[\psi,\,\bar{\psi}] \;=\; \int\,d^4x\,\left[\bar{\psi}(x)\gamma_\mu\partial_\mu\psi(x)\;+\;m\bar{\psi}(x)\psi(x)\right] \tag{3.35}$$

The naïve lattice fermions are constructed by simply replacing the derivatives by symmetric differences

$$S_F^{\mathrm{naïve}}[\psi,\bar{\psi},U] = a^4\,\sum_{x\in\{n\}}\,\bar{\psi}_x\,D^{\mathrm{naive}}\psi_x = a^4\,\left(\sum_{x\in\{n\}}\,\sum_{\mu=1}^{4}\,\bar{\psi}_x\gamma_\mu\nabla_\mu\,\psi_x\;+\;m\,\sum_{x\in\{n\}}\,\bar{\psi}_x\psi_x\right) \tag{3.36}$$

[5] As was mentioned in Section 3.1, the reasons for going into Euclidean space are presented in Appendix A.

where the symmetric lattice derivative is given by Eq. (3.19). Since the action is bilinear in $\bar{\psi}$ and ψ, we can write it in the form

$$S_F[\psi,\bar{\psi},U] \;=\; a^4 \sum_{x,y\in\{n\}} \sum_{\alpha,\beta,a,b} \bar{\psi}_{x,a,\,\alpha}\; D(x,y)^{ab}_{\alpha\beta}\; \psi_{y,b,\,\beta} \tag{3.37}$$

where we have introduced the *naïve* Dirac operator

$$D(x,y)^{ab}_{\alpha\beta} \;=\; \sum_{\mu=1}^{4} (\gamma_\mu)_{\alpha\beta}\; \frac{U_\mu(x)_{ab}\delta_{x+\hat{\mu},y} - U_{-\mu}(x)_{ab}\delta_{x-\hat{\mu},y}}{2a} \;+\; m\;\delta_{\alpha\beta}\delta_{ab}\delta_{x,y} \tag{3.38}$$

The doubling problem

In order to identify the doublers, which is one of the fermion lattice regularization problems, let us calculate the Fourier transform of the quark propagator for the trivial gauge field configuration $U_\mu(x) = \mathbb{1}$ (this is the case when we neglect the quark-gluon interaction). We will omit the color indices for notational convenience and use vector/matrix notation in Dirac space.

For free fermions the inverse D^{-1}_{xy} of the lattice Dirac operator is the *quark propagator* G^F_{yx} (lattice Green function)

$$\sum_{y\in\{n\}} D_{xy}\, G^F_{yz} \;=\; \delta_{x,z} \tag{3.39}$$

By inserting (3.38) and the inverse Fourier transform, we arrive at

$$G^F_{yz} \;=\; \frac{1}{V} \sum_{p\in\{\tilde{n}\}} \tilde{G}^F(p)\; e^{ip\cdot(y-z)} \tag{3.40}$$

where V is the total number of lattice points.

In Eq. (3.39), we get the Fourier transform of the quark propagator

$$\frac{1}{V} \sum_{p\in\{\tilde{n}\}} \sum_{\mu} \gamma_\mu \left(\frac{e^{ip\cdot(x+\hat{\mu}-z)} - e^{ip\cdot(x-\hat{\mu}-z)}}{2a} \;+\; m\, e^{ip\cdot(x-z)} \right) \tilde{G}^F(p) \quad = \quad \delta_{x,z} \tag{3.41}$$

$$\Leftrightarrow \quad \frac{1}{V} \sum_{p\in\{\tilde{n}\}} e^{ip\cdot(x-z)} \sum_{\mu} \gamma_\mu \left(\frac{e^{iap_\mu} - e^{-iap_\mu}}{2a} \;+\; m\cdot\mathbb{1} \right) \tilde{G}^F(p) \quad = \quad \delta_{x,z} \tag{3.42}$$

Replacing $\delta_{x,z}$ by its discretized expression, $\frac{1}{V}\sum_{p\in\tilde{n}} e^{ip\cdot(x-z)}$, we finally get the inverse of the quark propagator in momentum space

$$\tilde{G}^F(p)^{-1} \;= m\mathbb{1} \;+\; \frac{i}{a} \sum_{\mu=1}^{4} \gamma_\mu \sin(p_\mu a) \tag{3.43}$$

which is nothing but $\tilde{D}(p)$, the naïve Dirac operator in momentum space.

The matrix $\tilde{G}^F(p)$ can be calculated easily

$$\tilde{G}^F(p) \;=\; \frac{m\mathbb{1} \;-\; \dfrac{i}{a}\displaystyle\sum_\mu \gamma_\mu \sin\left(p_\mu a\right)}{m^2 \;+\; \dfrac{1}{a^2}\displaystyle\sum_\mu \sin^2\left(p_\mu a\right)} \tag{3.44}$$

In the continuum, the propagator for a massless fermion has a pole in momentum space

$$\tilde{G}^F(p)\Big|_{m=0} \;=\; \frac{\dfrac{i}{a}\displaystyle\sum_\mu \gamma_\mu \sin\left(p_\mu a\right)}{\dfrac{1}{a^2}\displaystyle\sum_\mu \sin^2\left(p_\mu a\right)} \;\xrightarrow{a\to 0}\; \frac{-i\sum_\mu \gamma_\mu p_\mu}{p^2} \;= -i\,\frac{\not{p}}{p^2} \tag{3.45}$$

corresponding to

$$p \;=\; (0,0,0,0) \tag{3.46}$$

However, on the lattice, the situation is different because the propagator for free fermions has 15 additional poles $p = (\pi/a,0,0,0),(0,\pi/a,0,0),\cdots,(\pi/a,\pi/a,\pi/a,\pi/a)$, which are known as *doublers*. It is then mandatory to devise ways to circumvent the problem of doublers, at least in the continuum limit.

3.3.2 The Wilson lattice regularized action

One possible solution to avoid doublers was suggested by Wilson [71] who proposed to add a momentum-dependent "mass term" to the fermion action. This is equivalent to raising the masses of the unwanted doublers to values of the order of the cutoff ($E \sim 1/a$), so that they become very heavy as a is taken to zero. It is a second derivative operator which vanishes in the continuum limit

$$-\frac{ar}{2}\sum_\mu \nabla^*_\mu \nabla_\mu \,\psi_x \tag{3.47}$$

where r is the Wilson parameter which is taken equal to 1 in our simulations. We can now combine the Wilson term (3.47) with the naïve fermion action to obtain Wilson's complete fermion action

$$\begin{aligned} S_W = {} & m\sum_x \bar{\psi}_{x,\alpha,a}\psi_{y,\beta,b}\delta_{xy}\delta_{\alpha\beta}\delta_{ab} \\ & + \frac{1}{2a}\sum_{x,\mu} \bar{\psi}_{x,\alpha,a}(\gamma_\mu)_{\alpha\beta}[U_\mu(x)_{ab}\psi_{x+\hat{\mu},\,\beta,b} \;-\; U^\dagger_\mu(x-\hat{\mu})_{ab}\psi_{x-\hat{\mu},\,\beta,b}] \\ & - \frac{ar}{2a^2}\sum_{x,\mu} \bar{\psi}_{x,\,\alpha,a}[U_\mu(x)_{ab}\psi_{x+\hat{\mu},\,\beta,b}\delta_{\alpha\beta} \;- 2\psi_{x,\,\beta,b}\delta_{ab}\delta_{\alpha\beta} + U^\dagger_\mu(x-\hat{\mu})_{ab}\psi_{x-\hat{\mu},\,\beta,b}] \end{aligned} \tag{3.48}$$

which can also be written as

$$S_W \equiv \sum_{x,y} \sum_{\alpha,\beta,a,b} \bar{\psi}_{x\,\alpha,a}\, D^W(x,y)^{ab}_{\alpha\beta}\, \psi_{y,\,\beta,b} \tag{3.49}$$

with the Dirac operator

$$D^W(x,y)^{ab}_{\alpha\beta} = \frac{1}{2a}\Bigg\{\kappa^{-1}\delta_{xy}\delta_{\alpha\beta}\delta_{ab} - \sum_{\mu}\Big[\Big(\mathbb{1}-\gamma_\mu\Big)_{\alpha\beta}\delta_{x,y-\hat{\mu}}\,U_\mu(x)_{ab} + \Big(1+\gamma_\mu\Big)_{\alpha\beta}\delta_{x,y+\hat{\mu}}\,U^\dagger_\mu(x-\hat{\mu})_{ab}\Big]\Bigg\} \tag{3.50}$$

where κ is the *hopping parameter*

$$\kappa^{-1} = 2ma + 8r \tag{3.51}$$

By making the same kind of reasoning as in the preceding section, we find an additional term in the propagator

$$\tilde{S}(p) = \frac{E(p) - \frac{i}{a}\sum_\mu \gamma_\mu \sin(ap_\mu)}{E^2(p) + \frac{1}{a^2}\sum_\mu \sin^2(ap_\mu)} \tag{3.52}$$

where

$$E(p) = \mathbb{1}m + \mathbb{1}\frac{1}{a}\sum_\mu (1-\cos(ap_\mu)) \tag{3.53}$$

For components with $p_\mu = 0$, the additional term, $\mathbb{1}\frac{1}{a}\sum_\mu (1-\cos(ap_\mu))$, vanishes. Whereas, with $p_\mu = \pi/a$ it provides an extra contribution $2/a$. This term acts as an additional mass term, and the total mass of the doublers is now given by

$$m + \frac{2l}{a} \tag{3.54}$$

where l is the number of momentum components with $p_\mu = \pi/a$.

3.3.3 Chiral symmetry considerations

The *chiral symmetry* is a symmetry of the Lagrangian for massless fermions. The corresponding Lagrangian, in Euclidean space, is

$$\mathscr{L} = \sum_f \bar{\psi}_f\, \gamma_\mu\, D_\mu\, \psi_f \equiv \sum_f \bar{\psi}_f\, D\, \psi_f \tag{3.55}$$

where D is the massless Dirac operator and $\psi_f \equiv \psi$ is a vector fermion field in color space. For the two flavors (up u and down d), we have

$$\psi_f \;=\; \begin{pmatrix}\psi_u\\ \psi_d\end{pmatrix} \tag{3.56}$$

Any spinor field can be decomposed into "*chiral fields*" as follows

$$\psi \;=\; \psi_L \;+\psi_R \;=\; \frac{1}{2}\,(1-\gamma_5)\,\psi \;+\frac{1}{2}\,(1+\gamma_5)\,\psi \;=\; P_L\,\psi \;+P_R\,\psi \tag{3.57}$$

where $P_L(P_R)$ is the left(right)-handed projector obeying

$$P_L^2 \;+P_R^2 \;=1 \quad ; \quad P_L\,P_R=0 \quad ; \quad P_L^2=P_L \quad ; \quad P_R^2=P_R \tag{3.58}$$

The Lagrangian can be rewritten as

$$\mathscr{L} \;=\; \bar{\psi}_L\,D\,\psi_L \;+\; \bar{\psi}_R\,D\,\psi_R \tag{3.59}$$

and is invariant[6] under the following set of transformations

$$\begin{cases} \psi_L \;\to\; \psi'_L \;=\; \exp\left[-i\sum\limits_a \alpha_L^a\tau^a\right]\,\psi_L \\ \psi_R \;\to\; \psi'_R \;=\; \exp\left[-i\sum\limits_a \alpha_R^a\tau^a\right]\,\psi_R \end{cases} \tag{3.60}$$

which forms the $SU(2)_L \times SU(2)_R$ global symmetry group. This symmetry is called "chiral symmetry" and transforms a fermion state according to

$$|\psi\rangle \;\to\; |\psi'\rangle \;=\; \exp\left[-i\sum_a(\alpha_L^a\tau^a)\,P_L\right]\,\exp\left[-i\sum_a(\alpha_R^a\tau^a)\,P_R\right]\,|\psi\rangle \tag{3.61}$$

With a bit algebra, Eq. (3.61) can be rearranged to exhibit the axial and vector nature of the transformation

$$|\psi\rangle \;\to\; |\psi'\rangle \;=\; \exp\left[-i\sum_a(\alpha_V^a\tau^a)\right]\,\exp\left[-i\gamma_5\,\sum_a(\alpha_A^a\tau^a)\right]\,|\psi\rangle \tag{3.62}$$

This corresponds to the following set of transformations for the fields

$$\text{vector transformation} \qquad \begin{cases} \psi \;\to\; \psi' \;=\; \exp\left[-i\sum\limits_a \alpha_V^a\tau^a\right]\,\psi \\ \bar{\psi} \;\to\; \bar{\psi}' \;=\; \bar{\psi}\exp\left[+i\sum\limits_a \alpha_V^a\tau^a\right] \end{cases} \tag{3.63}$$

[6]There are two additional groups $U(1)_V \times U(1)_A$. $U(1)_V$ is related to the baryon number conservation while $U(1)_A$ is broken due to the abelian anomaly (at the quantum level).

$$\text{axial transformation} \quad \begin{cases} \psi \;\rightarrow\; \psi' \;=\; \exp\left[-i\gamma_5 \sum_a \alpha_A^a \tau^a\right] \psi \\ \bar{\psi} \;\rightarrow\; \bar{\psi}' \;=\; \bar{\psi} \exp\left[+i\gamma_5 \sum_a \alpha_A^a \tau^a\right] \end{cases} \tag{3.64}$$

which also leaves the Lagrangian of Eq. (3.55) invariant (global $SU(2)_V \times SU(2)_A$ symmetry group). Finally, since we have (Eqs. (3.55) and (3.59))

$$\mathscr{L} \;=\; \bar{\psi} D \psi \;= \bar{\psi}_L D \psi_L \;+ \bar{\psi}_R D \psi_R \tag{3.65}$$

then by substituting the relations given in Eq. (3.57), we obtain the following equation which can be considered as the essence of the chiral symmetry in the continuum

$$D\gamma_5 \;+\; \gamma_5 D \;=\; 0 \tag{3.66}$$

and which states that the massless Dirac operator anticommutes with γ_5.

Going back to the lattice: in order to ensure that lattice results correspond to the continuum limit of massless fermions, the chiral symmetry has to be respected for $a \neq 0$. Although the Wilson term, which we add to the naïve action, helps in removing the doublers, the Wilson Dirac operator D^W does not obey Eq. (3.66). Since it breaks the chiral symmetry, the Wilson operator introduces $\mathscr{O}(a)$ artifacts that were not present in the naïve quark action. Simulations at very small lattice spacings by keeping reasonably large physical volume would be necessary to reach a decent level of accuracy. Such simulations are very costly and the Symanzik $\mathscr{O}(a)$ improvement procedure is often necessary. For more details about how the improvement program is implemented in lattice QCD with Wilson quarks, we refer to [67, 68].

Many attempts were made to find a discretized fermion action, free of doublers and respecting the chiral symmetry at the same time. A very important step was the derivation of the fundamental "*no-go theorem*" by Nielsen and Ninomiya [72, 73] which can be summarized as follows: a discretized theory without unwanted doublers will necessarily violate chiral symmetry.

To find a fermion lattice action respecting the chiral symmetry, Ginsparg and Wilson [74,75] formulated, in 1982, the *Ginsparg-Wilson relation*, an essential condition for chiral symmetry on the lattice

$$D\gamma_5 \;+\; \gamma_5 D \;=\; a\, D\, \gamma_5\, D \tag{3.67}$$

The right-hand side vanishes for $a \rightarrow 0$ and so the chiral symmetry is recovered in the continuum limit. Moreover, this equation also allows to define chiral symmetry on the lattice for finite a.

In current simulations, two types of Ginsparg-Wilson fermions are being used: the first are *domain-wall fermions* (DWF) which are defined on a five-dimensional space, in which the fifth dimension is fictitious [76–78]. The second type are *overlap fermions* which appeared from a completely different context and have an explicit form that exactly satisfies the Ginsparg-Wilson relation. However, their numerical implementation has unfortunately a computational cost which is at least an order of magnitude greater than for other choices.

3.4 Twisted-mass action

An alternate regularization of QCD, which does not suffer from unphysical zero mode fermion and preserves chiral symmetry is the "*twisted mass QCD (tmQCD) action*" [79, 80]. The results presented in the forthcoming chapters will mostly deal with the case of two degenerate light quarks in the sea, that is $N_f = 2$ simulations[7], this section will mainly focus on the description of the action related to such computations.

3.4.1 Twisted mass QCD in the continuum

Let ψ be a fermion field which, in addition to Dirac and color indices, carries also a flavor index which can assume $N_f = 2$ values. The index structure of ψ is $\psi_{a,\alpha,i}$, where a stands for the color index, α is the Dirac index and i represents the flavor index. In such a basis, the fermionic twisted mass QCD action, in Euclidean space, reads

$$\begin{aligned} S_F[\psi,\bar{\psi},G] \;=\; \int d^4x\; \bar{\psi}_{a,\alpha,i}(x) \Big[(\gamma_\mu)_{\alpha\,\beta}\,(D_\mu)_{ab}\,\delta_{ij} \;+\; \underbrace{(m_q)\delta_{ab}\,\delta_{\alpha\beta}\,\delta_{ij}}_{\text{conventional mass term}} \\ + \underbrace{(i\mu_q)(\gamma_5)_{\alpha\beta}(\tau^3)_{ij}\delta_{ab}}_{\text{twisted mass term}} \Big]\, \psi_{b,\beta,j}(x) \end{aligned} \tag{3.68}$$

The real parameter μ_q is called the twisted mass. The conventional mass term m_q is trivial in color, Dirac and flavor space, while the twisted mass term is trivial only in color space. It also has a γ_5 in Dirac space, and the third Pauli matrix τ^3 which acts in $SU(2)$ flavor space. The mass term of the twisted-mass action can be rearranged according to

$$m_q \;+\; i\mu_q\gamma_5\tau^3 \;=\; M\exp\left(i\omega\tau^3\gamma_5\right) \tag{3.69}$$

where $M = \sqrt{m_q^2 \,+\, \mu_q^2}$ is called the invariant mass. We also define the twist angle ω via

$$\tan\omega = \frac{\mu_q}{m_q} \tag{3.70}$$

In the following, the indices will be suppressed for notational simplicity.
In terms of these quantities, the Lagrangian of Eq. (3.68) can be written as

$$\mathscr{L} \;=\; \bar{\psi}\left[\not{D} + M\exp\left(i\omega\tau^3\gamma_5\right)\right]\psi \tag{3.71}$$

It breaks parity, isospin (flavor) and has an extra term when compared to the QCD Lagrangian. Let us consider the chiral rotation around the third axis, $I_3(\alpha)$, defined by

$$\psi' \;=\; \exp\left(i\gamma_5\frac{\alpha}{2}\tau^3\right)\psi \qquad\qquad \bar{\psi}' \;=\; \bar{\psi}\exp\left(i\gamma_5\frac{\alpha}{2}\tau^3\right) \tag{3.72}$$

[7] For the generalization of tmQCD to the case of quarks with different masses, we refer to [81, 82].

where α is the chiral rotation angle.
Redefining the mass parameters through the following transformations

$$\begin{cases} m_q \to m'_q = m_q \cos\omega + \mu_q \sin\omega \\ \mu_q \to \mu'_q = -m_q \sin\omega + \mu_q \cos\omega \end{cases} \tag{3.73}$$

it is straightforward to see that the Lagrangian in Eq. (3.68) is invariant under the combination of these two transformations. In terms of Eq. (3.72) this means

$$\mathscr{L} = \bar{\psi}' \left[\not{D} + M \exp\left(i\omega' \tau^3 \gamma_5\right) \right] \psi' \tag{3.74}$$

i.e. $M = M'$ (which justifies the name "invariant mass") and $\tan\omega' = \mu'_q/m'_q$, where $\omega' = \omega - \alpha$.

This implies that we can define a family of theories parametrized by their twist angle. They are all equivalent because they are related by field and mass redefinitions only. The quark mass is given by the invariant mass M.
One can immediately see that by choosing $I_3(\alpha = \omega)$, we obtain $\omega' = 0$, which is equivalent to $\mu'_q = 0$ and $m'_q = M$. More explicitly, the special case of tmQCD with zero twist angle is simply QCD[8].
Another interesting case is obtained with the $I_3(\omega - \pi/2)$ rotations, i.e. when $\omega' = \pi/2$, so that $m'_q = 0$ and $\mu'_q = M$. This case is known as fully twisted or maximally twisted QCD [83].

Symmetries: tmQCD exhibits, for a generic angle ω, the discrete symmetries that involve axis reflection (parity and time reversal) [80].

- The twisted parity P_ω is defined as

$$\begin{cases} x = (x^0, \vec{x}) \to x' = (x^0, -\vec{x}) \\ \qquad \psi(x) \to \gamma_0 \exp\left[i\omega\gamma_5\tau^3\right] \psi(x') \\ \qquad \bar{\psi}(x) \to \bar{\psi}(x') \exp\left[i\omega\gamma_5\tau^3\right] \gamma_0 \end{cases} \tag{3.75}$$

- The twisted time reversal T_ω is defined as

$$\begin{cases} x = (x^0, \vec{x}) \to x' = (-x^0, \vec{x}) \\ \qquad \psi(x) \to i\,\gamma_0\gamma_5 \exp\left[i\omega\gamma_5\tau^3\right] \psi(x') \\ \qquad \bar{\psi}(x) \to -i\,\bar{\psi}(x') \exp\left[i\omega\gamma_5\tau^3\right] \gamma_0\gamma_5 \end{cases} \tag{3.76}$$

The $SU(2)$ vector and axial twisted transformations take the form:

[8] The basis $\{\psi', \bar{\psi}'\}$ of Eq. (3.72) is thus called the "physical basis" because it is the basis where tmQCD takes the form of QCD when $\alpha = \omega$. $\{\psi, \bar{\psi}\}$ is called the "twisted basis".

- Twisted vector (isospin) symmetry $SU(2)^{\omega}_{V}$

$$\begin{cases} \psi(x) \to & \exp\left[-i\frac{\omega}{2}\gamma_5\tau^3\right] \exp\left[i\frac{\theta^a_V}{2}\tau^a\gamma_5\right] \exp\left[i\frac{\omega}{2}\gamma_5\tau^3\right]\psi(x) \\ \bar{\psi}(x) \to & \bar{\psi}(x) \exp\left[i\frac{\omega}{2}\gamma_5\tau^3\right] \exp\left[-i\frac{\theta^a_V}{2}\tau^a\gamma_5\right] \exp\left[-i\frac{\omega}{2}\gamma_5\tau^3\right] \end{cases} \tag{3.77}$$

- Twisted axial (isospin) symmetry $SU(2)^{\omega}_{A}$

$$\begin{cases} \psi(x) \to & \exp\left[-i\frac{\omega}{2}\gamma_5\tau^3\right] \exp\left[i\frac{\theta^a_A}{2}\tau^a\gamma_5\right] \exp\left[i\frac{\omega}{2}\gamma_5\tau^3\right]\psi(x) \\ \bar{\psi}(x) \to & \bar{\psi}(x) \exp\left[i\frac{\omega}{2}\gamma_5\tau^3\right] \exp\left[i\frac{\theta^a_A}{2}\tau^a\gamma_5\right] \exp\left[-i\frac{\omega}{2}\gamma_5\tau^3\right] \end{cases} \tag{3.78}$$

  which is however only valid for $M = 0$.

3.4.2 Lattice formulation of twisted mass Lattice QCD

We now replace the continuum Euclidean space-time by a hypercubic lattice of spacing a.

Complete tmLQCD action: following references [83–85], a lattice formulation of QCD with an $SU(2)_f$ flavor doublet of degenerate quarks is given by the action

$$S = S_g[U] + S_F^{(w)}[\psi, \bar{\psi}, U] \tag{3.79}$$

$S_g[U]$ stands for the lattice gauge action and $S_F^{(w)}$ for the tmQCD action on the lattice with Wilson fermions.

Fermion tmLQCD action: the tmQCD action on the lattice (tmLQCD action) $S_F^{(w)}$ reads

$$S_F^{(w)}\left[\psi, \bar{\psi}, U\right] = a^4 \sum_x \bar{\psi}_x \left[D_W \ + m_0 \ + i\mu_q\gamma_5\tau^3\right]\psi_x \tag{3.80}$$

where

$$D_W \ = \frac{1}{2}\sum_\mu \gamma_\mu(\nabla^*_\mu + \nabla_\mu) - a\frac{r}{2}\sum_\mu \nabla^*_\mu\nabla_\mu \tag{3.81}$$

∇ and ∇^* are the standard gauge covariant forward and backward derivatives, m_0 and μ_q are respectively the bare untwisted and twisted quark masses. The parameter r is the Wilson parameter. The term D_W is a standard symmetric discretization of the lattice derivative and the term $ar\sum_\mu \nabla^*_\mu\nabla_\mu$ is the Wilson term needed to remove the doublers from the spectrum of the theory.

The twisted-mass fermionic action, written in terms of the *hopping parameter* κ, is given by

$$\boxed{\begin{aligned}\sum_x \Big\{ & \bar{\psi}_x \, (1 \, + 2\, i\, \kappa\, \mu\, \gamma_5\, \tau_3)\psi_x \\ & -\kappa\, \bar{\psi}_x \sum_{\mu=0}^{3} \left[U_\mu(x)(r+\gamma_\mu)\, \psi_{x+a\hat{\mu}} \, + \, U_\mu^\dagger(x-a\hat{\mu})\,(r-\gamma_\mu)\, \psi_{x-a\hat{\mu}} \right] \Big\}\end{aligned}} \tag{3.82}$$

The hopping parameter κ is related to the untwisted quark mass m_0 ($\kappa = 1/(8 + 2am_0)$). The above expression corresponds to the action implemented in our codes.

In terms of the symmetries described in the previous section, one can see that the Wilson term breaks the twisted parity P_ω and the time reversal T_ω symmetries. However the ordinary parity P survives as a symmetry if it is combined with a discrete flavor rotation (the combination being denoted as P_F^1 and P_F^2)

$$\begin{cases} P_F^1 : \; \psi_x \to i\, \gamma_0\, \tau^1\, \psi_{x'} & \bar{\psi}_x \to \; -i\, \bar{\psi}_{x'}\, \gamma_0 \tau^1 \\ P_F^2 : \; \psi_x \to i\, \gamma_0\, \tau^2\, \psi_{x'} & \bar{\psi}_x \to \; -i\, \bar{\psi}_{x'}\, \gamma_0 \tau^2 \end{cases} \tag{3.83}$$

or if it is combined with the sign flip of the twisted mass ($\tilde{P} = P \otimes [\mu_q \to -\mu_q]$)

$$\tilde{P} : \; \psi_x \to i\, \gamma_0\, \psi_{x'} \qquad \bar{\psi}_x \to \; -i\, \bar{\psi}_{x'}\, \gamma_0 \qquad \mu_q \to \; -\mu_q \tag{3.84}$$

where $x' = P\, x$.
The same holds for time reversal T: T_F^1, T_F^2 and $T \otimes [\mu_q \to -\mu_q]$ are also symmetries of the lattice action. Moreover, the Wilson term breaks the twisted vector and axial symmetries $SU(2)_V^w$. This is however a discretization effect (triggered by the presence of the Wilson term) and vanishes in the continuum limit.

Renormalization with Wilson fermions may be complicated due to the loss of chiral symmetry. In tmQCD this can be simplified by a clever choice of the twist angle: $w = \pi/2$. In the following, we will describe how to tune the twist angle to the maximal twist.

Tuning to maximal (or full) twist: the twist angle can be defined in the renormalized theory, analogously to the continuum theory by

$$\tan\omega \; = \frac{\mu_R}{m_R} \tag{3.85}$$

where μ_R and m_R are respectively the renormalized twisted and untwisted quark masses given by

$$\mu_R = Z_\mu \; \mu_q \qquad\qquad m_R = Z_m \; m_q \tag{3.86}$$

Z_μ is the renormalization constant for the twisted mass quark and Z_m stands for the renormalization constant for the untwisted quark mass m_0 ($m_q = m_0 - m_{\rm cri}$). Without chiral symmetry at finite lattice

spacing, the bare untwisted mass term renormalizes with a counter term $m_{\rm cri}$ [80]. The $m_{\rm cri}$[9] is the value of m_0 where the untwisted quark mass m_R vanishes. Thus, to tune the value of ω, one has to determine the ratio Z_μ/Z_m and the critical mass $m_{\rm cri}$. One possible way to determine the critical mass is to use the "Partially Conserved Axial Current" (PCAC) relation

$$m_R = \frac{Z_A\langle \partial_\mu A^a_\mu(x)\ P^a(0)\rangle}{2Z_P\ \langle P^a(x)P^a(0)\rangle} \qquad (a=1,2) \tag{3.87}$$

where A_μ is the axial current, and P^a is the pseudoscalar density $P^a = \bar\psi\gamma_5\frac{\tau^a}{2}\psi$.
Tuning to maximal twist (when the twist angle ω is equal to $\frac{\pi}{2}$), that is taking m_0 to the critical value $m_{\rm cri}$ and thus obtaining $m_R = 0$, can be achieved by tuning κ to a particular value $\kappa_{\rm cri}$ so that we get a vanishing value of the correlation function

$$\langle \partial_\mu A^a_\mu(x)\ P^a(0)\rangle \tag{3.88}$$

Then it is not necessary to compute any renormalization constant, but only the critical mass.
Note that the fermionic action at maximal twist is obtained by replacing m_0 by $m_{\rm cri}$ in Eq. (3.80).

Equivalence between tmQCD and QCD: the equivalence between QCD and tmQCD reflects itself in the correspondence between the correlation functions computed in the two theories. The relation between correlation functions in QCD and tmQCD can be inferred by the set of transformations of Eq. (3.72), i.e.

$$\langle \mathscr{O}\rangle[\bar\psi',\psi']_{\rm (QCD)} = \langle \mathscr{O}\rangle[\bar\psi,\psi]_{\rm tmQCD} \tag{3.89}$$

and is valid for Wilson fermions at finite lattice spacing up to cutoff effects if the theory is renormalized in a mass independent scheme [79]. Using Ginsparg-Wilson fermions, it is possible to prove [79] that tmQCD and QCD are equivalent, i.e. given a lattice regularization that preserves chiral symmetry, the equivalence between QCD and tmQCD is preserved at finite lattice spacing: consequently they have the same continuum limit. Based on universality arguments, we expect that this equivalence is also satisfied for renormalized correlation functions computed with Wilson twisted mass fermions [79].
The equation which relates the correlators in the two theories depends on how the twist angle is defined. Hence a given standard correlation function in QCD can be written as a linear combination of correlation functions computed in tmQCD at a given twist ω. The procedure of computing correlation functions can be summarized by:

- We start with the QCD correlation function we are interested in.
- We perform the axial rotation that in the continuum brings the action from the physical basis to the twisted basis on the fields appearing in the correlation function.
- We then compute the resulting correlation function with the Wilson twisted mass lattice action in the twisted basis, with a relevant choice of quark masses.

[9] The term $m_{\rm cri}$ is the amount of mass induced by the Wilson term that should be subtracted to have a good chiral limit. The corresponding $\kappa_{\rm cri}$ is called the critical parameter, which ensures that in the chiral limit the quark mass vanishes.

- Finally, we perform the continuum limit.

The final result will be exactly the desired QCD correlation function in the continuum with quark mass $M_R = \sqrt{m_R^2 + \mu_R^2}$.

Advantages: each fermion formulation has its own advantages and disadvantages. The advantages of using the tmQCD regularization are described in great detail in Ref. [79]. For the tmQCD action, choosing full twist is special since it simplifies, in most situations, the renormalization of the weak interaction matrix elements. This is a major simplification, not only in terms of computational difficulty, but also in terms of the uncertainty entering the computation of the observables on the lattice, like for example the decay constants. The error associated with the computation of the renormalization constants does enter the systematics. Also, choosing the full twist implies an important property called $\mathcal{O}(a)$ improvement, i.e. the discretization effects of $\mathcal{O}(a)$ vanish and the leading corrections appear only at $\mathcal{O}(a^2)$: by simply tuning one parameter we realize the non-perturbative Symanzik improvement program mentioned in Section 3.2.
More precisely, parity-even correlation functions (which include all the physical correlation functions) are automatically $\mathcal{O}(a)$ improved (for example, this is the case of the correlators used to compute the masses), and $\mathcal{O}(a)$ discretization effects will affect only parity-odd (unphysical) correlation functions [86].

Disadvantages: the price to pay is that twisted terms break explicitly the parity and isospin at finite lattice spacing [83], as we have explained above. However, these terms are $\mathcal{O}(a^2)$ and they disappear in the continuum limit: those symmetries are restored in the continuum.
This violation of parity will have some unpleasant consequences when studying meson spectroscopy as will be seen in a forthcoming chapter.
In general, the effect of isospin breaking is large when working with pions. The lack of this symmetry at finite lattice spacing means that there is a mass splitting between the charged and neutral pions ($m_{\pi^+} = m_{\pi^-} \neq m_{\pi^0}$) leading to $\mathcal{O}(a^2)$ discretization which are exceptionally large [87].

Conclusion

We have discussed the discretization strategy of gauge and fermion actions on the lattice as well as several issues arising when looking for a less "controversial" fermionic action. Finally, we choose to work with the tmQCD action because of its advantages and simplifications, as well as with the Symanzik gauge improved action in order to compute some physical observables. The techniques of computation on the lattice, and simulation results, will be the topic of the next chapters.

Chapter 4

Propagator computation in LQCD

From the path integral formalism one can see the analogy between QFT and statistical mechanics, and how a Green's function in Minkowskian space can be calculated in Euclidean space as a statistical mean value (see Appendix A). However, such integrals cannot be solved analytically and have to be computed numerically. So, we have to perform computations in a finite discretized lattice by using a numerical integration procedure, and then extrapolate observables to the "real world".

In this chapter, we will review the procedure to calculate correlation functions and thus physical observables in Lattice QCD. We will start with a general example and then proceed to explain some of the tools used to compute the propagators of the theory.

4.1 Computation of a physical observable

Calculating an observable in LQCD implies finding its vacuum expectation value expressed in terms of path integrals as

$$\langle O \rangle \;=\; \frac{\int [d\psi]\,[d\bar{\psi}]\,[dU]\; O\; e^{-S(\psi,\bar{\psi},U)}}{\mathscr{Z}} \tag{4.1}$$

where $S = S_G \; + S_F$ and $[d\psi]\,[d\bar{\psi}]\,[dU]$ are the integration measures of the fermion and gauge link variables. $\mathscr{Z}$ is the partition function of the theory

$$\mathscr{Z} \;= \int [d\psi]\,[d\bar{\psi}]\,[dU]\, e^{-S[\psi,\bar{\psi},U]} \tag{4.2}$$

The fermion action, S_F, is written as

$$\bar{\psi}\, D[U]\, \psi \tag{4.3}$$

where $D[U]$ represents the Dirac operator corresponding to the "particular" fermion action we use[1]. Since fermion fields are treated as Grassmann variables, we use the property

$$\int [d\psi]\,[d\bar{\psi}]\, e^{-\bar{\psi}\, D[U]\, \psi} \;= \mathrm{Det}[D[U]] \tag{4.4}$$

which comes from a particular case of the Wick theorem. In this way, one gets rid of the integrals over the quark fields at the cost of having to deal with an integrand which is not local. The statistical weight e^{-S} is now replaced by

$$e^{-S_G}\; \mathrm{Det}[D[U]] \tag{4.5}$$

and we are left with the integral over the gauge fields. Due to the large number of degrees of freedom on a lattice grid, we cannot evaluate "by hand" integrals of the form (4.1) with standard approaches such as Simpson integration.

[1] In our work it is the twisted mass Wilson Dirac operator.

If we look at the dimension of a typical path integral discretized on a lattice of geometry ($L^3 \times T = 24^3 \times 48$)

$$\int [d\psi]\,[d\bar{\psi}]\,[dA]\cdots \Rightarrow \prod_{x_\mu}\left(\int\, d\psi(x_\mu)\, d\bar{\psi}(x_\mu)\, dU(x_\mu)\right)\cdots \tag{4.6}$$

we find

- $x_\mu : 24^3 \times 48 \simeq 7 \times 10^5$ lattice sites.
- $\psi \equiv \psi_A^{a,(f)}$: 24 quark degrees of freedom for every flavor ($N_f = 2$) ($\times 2$ particle/antiparticle, $\times 3$ colors, $\times 4$ spins)
- $U = U_\mu^{ab}$: 32 gluon degrees of freedom ($\times$ 8 colors, $\times$ 4 spin)

  $\Longrightarrow$ In total: $24^3 \times 48 \times (2 \times 24 + 32) \simeq 53 \times 10^6$ integrals

Thus, due to the huge size of the manifold over which the integrals are computed, we need to rely on Monte Carlo techniques which are in fact the unique method to perform such integrations. This class of numerical integration methods can be applied whenever the integral assumes the form of a weighted average over the integrand space, and is very suitable when the weight is highly peaked over a limited region of the integrand space. In fact, it is a statistical physics technique: one replaces the average over an experiment by the arithmetic mean of the results obtained from an infinite number of experiments. In twisted mass Wilson discretization, it can be shown that $\mathrm{Det}[D[U]]$ is real and positive [88] so that $\langle O \rangle$ can be regarded as the average value of O over the space of the gauge configuration U, weighted with the probability distribution $\mathscr{P}[U]$

$$\begin{cases} \langle O \rangle &= \displaystyle\int [DU]\; O\; \mathscr{P}[U] \\ \mathscr{P}[U] &= \dfrac{1}{\mathscr{Z}} \displaystyle\prod_f \mathrm{Det}[D[U]]_f\, e^{-S_G} \end{cases} \tag{4.7}$$

The first part of the evaluation of O consists in generating a set of N_{conf} gauge configurations[2]

$$U_i, i \in [1, \cdots, N_{\mathrm{conf}}] \tag{4.8}$$

according to the distribution function $\mathscr{P}[U_i]$. This is performed by making use of hybrid techniques which mix normal Monte Carlo methods with molecular dynamics in order to avoid the explicit evaluation of the fermionic matrix determinant. Being a very technical point which is not the subject of this thesis work, we will not review it and we will assume that the generation of such a set is possible [89].

Then, for each gauge configuration U_i, one measures the value of the observable $O|_{U_i}$. An approximate estimate $\langle O[U] \rangle$ of the observable is given by the simple arithmetic average over the N_{conf} determinations

[2]The generated gauge configurations can be used many times in order to determine different quantities of interest.

$O|_{U_i}$

$$\langle O[U] \rangle \; = \frac{1}{N_{\text{conf}}} \sum_{i=1}^{N_{\text{conf}}} O|_{U_i} \quad \text{as} \quad N_{\text{conf}} \to \infty \tag{4.9}$$

Computing $O|_{U_i}$ costs less computer power than producing ensembles of gauge configurations.
Under the assumptions of the central limit theorem, for a sufficiently large N_{conf} we estimate the error on $\langle O \rangle$ to be about $1/\sqrt{N_{\text{conf}}}$ with respect to $\langle O[U] \rangle$. In order to make an accurate estimate of the error, *Jackknive* techniques, that we will explain later, have been used.

4.2 Hadronic two-point correlation functions

The discretized two-point correlation function is useful when extracting the masses of the states and studying their spectroscopy. Let us introduce for example the two-point correlation function of the charmed pseudoscalar D meson

$$\mathscr{C}^{(2)}(t_x - t_y) \; = \langle T\{\mathscr{O}_D^\dagger(t_x)\, \mathscr{O}_D(t_y)\} \rangle \tag{4.10}$$

where the creation operator $\mathscr{O}_D(t)$ is defined as

$$\mathscr{O}_D(t_x) \; = \sum_{\vec{x}} \bar{\psi}_u(\vec{x}, t_x)\, \gamma_5\, \psi_c(\vec{x}, t_x) \tag{4.11}$$

ψ_u and ψ_c are respectively the u and c quark fields defined on the lattice[3]. The operator $\mathscr{O}_D$ creates a meson having a vanishing momentum with the correct quantum numbers.
Two-point correlation functions can also be written in terms of path integrals as

$$\begin{aligned} \mathscr{C}^{(2)}(t_x - t_y) \; &= \frac{1}{\mathscr{Z}} \int \Big(\prod_f [d\bar{\psi}_f][d\psi_f]\, [dU] \Big)\, \mathscr{O}_D^\dagger(t_x)\, \mathscr{O}_D(t_y)\, e^{-\sum_f S(\psi_f, \bar{\psi}_f, U)} \\ &= \frac{1}{\mathscr{Z}} \sum_{\vec{x},\vec{y}} \int \Big(\prod_f [d\bar{\psi}_f][d\psi_f]\, [dU] \Big) \\ &\qquad \times (\bar{\psi}_c\, \gamma_5 \psi_u)(\vec{x}, t_x) \;\cdot\; (\bar{\psi}_u \gamma_5 \psi_c)(\vec{y}, t_y) \;\cdot\; e^{-\sum_f S(\psi_f, \bar{\psi}_f, U)} \end{aligned} \tag{4.12}$$

Fortunately, owing to the bilinear nature of the Lagrangian, we can use Eq. (4.4) to integrate over the fermion fields

$$\begin{aligned} \mathscr{C}^{(2)}(t_x - t_y) \; = \frac{1}{\mathscr{Z}} \int [dU] \; & \overbrace{\bar{\psi}_c^\alpha(\vec{x}, t_x)\, \gamma_5^{\alpha\beta} \overbrace{\psi_u^\beta(\vec{x}, t_x) \bar{\psi}_u^\delta}(\vec{y}, t_y) \gamma_5^{\delta\gamma} \psi_c^\gamma}(\vec{y}, t_y) \\ & \times \left(\prod_f \text{Det}[D[U]] \right) e^{-S_G[U]} \end{aligned} \tag{4.13}$$

[3]For convenience, we will adopt the notation $\psi_x \equiv \psi(x)$ which should not be mistaken for the continuum case.

After performing the Wick contractions, correlation functions are expressed as traces over products of quark propagators, Dirac matrices and color structures

$$\mathscr{C}^{(2)}(t \equiv t_x - t_y) \; = - \sum_{\vec{x}\vec{y}} \left\langle \mathrm{Tr}\, [\gamma_5\, S_u(\vec{x}, t_x; \vec{y}, t_y)\, \gamma_5\, S_c(\vec{y}, t_y; \vec{x}, t_x)] \right\rangle \tag{4.14}$$

where $S_q(x, y)$ is the propagator of the q quark from the lattice point[4] y to the lattice point x for a given gauge configuration U and is the solution of

$$D_q(x, y) S_q(y, z) \; = \; \delta^4(x, z) \tag{4.15}$$

The Eq. (4.14) has a simple physical interpretation: $S_u(\vec{x}, t_1; \vec{y}, t_2) \equiv \; D_u^{-1}(\vec{x}, t_1; \vec{y}, t_2)$ propagates an up quark from $(\vec{y}, t_2)$ to the point $(\vec{x}, t_1)$ while $S_c(\vec{y}, t_y; \vec{x}, t_x)] \equiv D_c^{-1}(y; x)$ propagates a charm quark in the opposite direction, as depicted in Fig. 4.1.

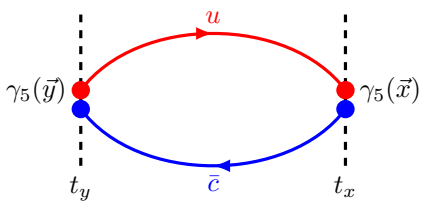


Figure 4.1: Pictorial representation of a two-point correlation function.

From the properties of the Dirac operator under discrete symmetry transformations, one can deduce several important and useful properties of the associated quark propagator. One of the symmetries is the so called H-symmetry, or γ_5-hermiticity. It is a property of the Euclidean QCD Dirac operator, which in terms of the quark propagator means that

$$S_u(x, y) \; = \gamma_5\, S_u^\dagger(y, x)\, \gamma_5 \tag{4.16}$$

The H-symmetry is extremely useful as it relates propagators "$x \to y$" and "$y \to x$", so that the number of propagators to be computed is decreased by a huge amount. With that in mind, Eq. (4.14) simplifies to

$$\mathscr{C}^{(2)}(t) \; = - \sum_{\vec{x}\vec{y}} \left\langle \mathrm{Tr}\, [S_u^\dagger(\vec{y}, t_y; \vec{x}, t_x)\, S_c(\vec{y}, t_y; \vec{x}, t_x)\,] \right\rangle \tag{4.17}$$

4.3 Propagator computation

From Eq. (4.14), one can see that meson correlation functions can be calculated as a product of inverse Dirac operators. However, even on a lattice of modest size, the propagator matrix is extremely large ($12N \times 12N$ where N is the number of lattice points) and thus one can only calculate a subset of each matrix.

[4]Here the "point" notion relates to site as well as to Dirac and color indices.

The quark propagator in coordinate space, which we will denote by ϕ in the following, can be computed as the solution of the linear system

$$D\,\phi = \eta \tag{4.18}$$

where D is the lattice Dirac operator and η is a source vector. This equation generalizes (4.15) for a generic source η.
In its simplest form, η is one of the twelve point sources located at the space-time point x (each source being non zero for one color-spin combination $(a;\,\alpha)$ only). It is a function of spin α, color a and lattice point x

$$\eta[\tilde{a},\tilde{\alpha},\tilde{x}]^a_\alpha(x) \;= \delta^{a,\tilde{a}}\,\delta_{\alpha,\tilde{\alpha}}\delta(x-\tilde{x}) \tag{4.19}$$

The point sources are placed at the position $\tilde{x}$ of the *source* interpolator $\mathscr{O}^\dagger_D(\tilde{x})$ and the solution ϕ of (4.18) yields the quark propagator from a **single point** $\tilde{x}$ to **any other point** y of the *sink* operator $\mathscr{O}_D(y)$, which corresponds to just one column of the propagator matrix. This type of solutions is referred to as "*one-to-all propagators*" which is just a fraction of the set of propagators connecting any two lattice points.
As a means to access the full propagator matrix, we propose to estimate stochastically the propagators by implementing the *one-end trick* method [90, 91]:

1. The starting point of all stochastic approaches is to consider random sources which, for reasons that will become clear later on, are taken diluted in spin variable

$$\eta[n,\tilde{\alpha},\tilde{t}]^a_\alpha(x) \equiv \delta_{\alpha,\tilde{\alpha}}\cdot\,\Xi[n,\tilde{t}]^a(x) \quad\text{with}\quad \Xi[n,\tilde{t}]^a(x) \;=\; \delta(t-\tilde{t})\,\frac{\pm 1 \,\pm i}{\sqrt{2}} \tag{4.20}$$

   where $n = 1,\cdots N_r$ labels the noise samples generated for each gauge configuration. The factor

$$\frac{\pm 1 \,\pm i}{\sqrt{2}} \tag{4.21}$$

   represents a random number. It is the so-called $\mathbb{Z}_2 \times \mathbb{Z}_2$ noise [92]; other forms of noise exist. The sources are non zero in a single time-slice[5] $\tilde{t}$. All entries of Ξ on time slice $\tilde{t}$ are chosen independently. The random numbers in Ξ are then copied to four sources η, where they appear in different spin components. The optimal way to choose the time-slice $(\tilde{t})$ at which the stochastic source is located, is to change it randomly as the gauge configuration is changed.
   The sources satisfy

$$\begin{aligned}\lim_{N_r\to\infty}\frac{1}{N_r}\sum_{i=1}^{N_r}\eta[i,\tilde{\alpha},\tilde{t}]^a_\alpha(x)\,\eta^*[i,\tilde{\beta},\tilde{t}]^b_\beta(y) \\ = \delta_{ab}\,\delta_{\alpha\beta}\,\delta_{\alpha\tilde{\alpha}}\,\delta_{\beta\tilde{\beta}}\,\delta(x-y)\,\delta(t_x-\tilde{t})\,\delta(t_y-\tilde{t})\end{aligned} \tag{4.22}$$

2. As a next step, we invert the lattice Dirac operator D (for one given flavor) on each sample of

[5] To keep the noise-to-signal ratio reasonable, it is mandatory to use time-slice sources rather than volume sources.

this source. To this end, one introduces the *ϕ-propagator* which is a solution of the equation

$$\sum_y D[f,r]^{ab}_{\alpha\beta}(x,y)\ \ \phi[n,f,r,\tilde{\alpha},\tilde{t}]^b_\beta(y)\ = \eta[n,\tilde{\alpha},\tilde{t}]^a_\alpha(x) \tag{4.23}$$

where f represents the fermion flavour and $r = \pm 1$.
Then, using Eq. (4.22) and the above equation, one can obtain an unbiased estimator of the *all-to-all propagator* $S_f(r,x,y)|^{ab}_{\alpha\beta}$, which is the inverse of the Dirac operator, by computing the quantity

$$\frac{1}{N_r}\sum_{n=1}^{N_r} \phi[n,f,r,\tilde{\alpha},\tilde{t}]^b_\beta(x)\ \ \eta[n,\tilde{\alpha},\tilde{t}]^a_\alpha(y)^* \tag{4.24}$$

Two-point correlation functions with the one-end-trick method
For the interpolating fields of B and D mesons, having arbitrary Dirac structures[6] Γ, an improved estimator for the "charged" two-point correlators is obtained by

$$\begin{aligned}\mathscr{C}^{(2)}_{hl}(t) &= \frac{1}{2}\sum_{r=\pm1}\left\langle \mathrm{Tr}\sum_{\vec{x},\vec{y}}\Gamma_1\, S_l(r;\,\vec{y},\,\tilde{t};\,\vec{x},\,\tilde{t}+t)\,\Gamma\, S_h(-r;\,\vec{x},\,\tilde{t}+t;\,\vec{y},\,\tilde{t})\right\rangle \\ &= \frac{1}{2}\sum_{r=\pm1}\frac{1}{N_r}\sum_{i=1}^{N_r}\left\langle \mathrm{Tr}\left\{\sum_{\vec{x}}(\Gamma_1\gamma_5)_{\tilde{\alpha}\tilde{\beta}}\,\phi^*\big[i,\,l,\,r,\,\tilde{\beta},\,\tilde{t}\big]^b_\alpha(\vec{x},\tilde{t}+t)\right.\right. \\ &\qquad\left.\left.\times(\gamma_5\Gamma)_{\alpha\beta}\phi\big[i,\,h,\,r,\,\tilde{\alpha},\,\tilde{t}\big]^b_\beta(\vec{x},\tilde{t}+t)\right\}\right\rangle\end{aligned} \tag{4.25}$$

where the Dirac structure Γ_1 is equal to $\gamma_0\Gamma^\dagger\gamma_0$ and $\langle ...\rangle$ stands for the gauge ensemble average. Here h represents the heavy quark (b or c) and l is the light one.
In this case, the signal is of order V (the volume of the lattice), while the noise is of order $V/\sqrt{N_r}$ so that it is sufficient to employ one random source per gauge configuration.
The stochastic estimate of the three-point correlation functions follows the same idea and is also evaluated using the *one-end-trick*.

Equation (4.7) states that a physical observable can be evaluated, after the Grassmann integration, by computing a ratio of purely bosonic integrals over the gauge fields. We stress again that the fermion determinants depend on U and one has to perform a Monte Carlo simulation using

$$\mathscr{Z}^{-1}\exp[-S_G[U]]\prod_f \mathrm{Det}[D[U]]_f \tag{4.26}$$

as the distribution weight for the gauge fields. However, computing the determinant of the Dirac operator matrix is highly nontrivial. In the following, we will discuss how to deal with such a determinant.

[6]The Dirac structure Γ is a 4×4 matrix acting in spin space; usually it could be one or a product of γ-matrices.

4.3.1 Quenching and partial quenching

Figure 4.2 displays two Feynman diagrams in which solid lines represent the valence quarks propagating in the vacuum. These quarks are created and annihilated by the operator $\mathscr{O}$ which enters the calculation of correlation functions by means of path integrals. The red loop in the diagram on the right illustrates a typical contribution to the determinant in Eq. (4.7), i.e. processes involving "sea quarks" (also known as dynamical quarks).

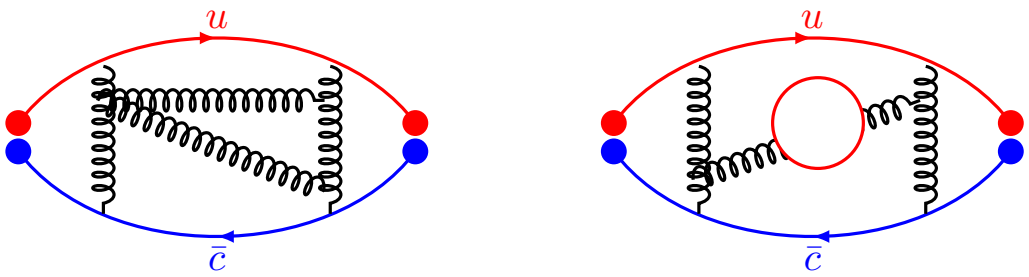


Figure 4.2: Illustration of the difference between quenched (l.h.s.) and unquenched (or full) QCD (r.h.s.).

However, computing determinants is time-consuming and requires huge computing power. There is an approximation called the "*quenched approximation*" which consists in neglecting the effects of the determinant by setting it to unity in the functional integral, so that only valence quarks are retained in correlators (diagram on the left). The quenched approximation is therefore also called "*valence approximation*" and a simulation with quenched dynamical quarks is called an $N_f = 0$ simulation. However, the quenched approximation, by neglecting the contribution of the sea quarks, necessarily leads to predictions with huge systematical errors. Thus, it would be highly preferable to work with the unquenched theory for the purpose of precise predictions and subsequent experimental confrontations of Lattice QCD.

Light quark unquenching: in the last ten years the development of algorithms and machines made it possible to perform computations by including the fermionic determinant that arises from integrating over (Grassmann) quark fields. Since the historical term for omitting this determinant is "quenching", its inclusion is called "unquenching". When we take into account the effect of the vacuum light quark loops (the up u and the down d quarks assumed to be degenerate), we talk about $N_f = 2$ lattice simulations. However, when we work with lower quark masses:

- the computation time increases.
- the number of lattice points has to be increased in such a way that the lattice discretization effects are negligible when compared to the statistical ones.

So we choose to do the computations assuming a larger (unphysical) mass for the light quarks which, in the end, will be extrapolated to the real physical mass.
Computations with $N_f = 2$ are affected by a quenching effect which is expected to be much smaller than the already quantified light quark quenching ($N_f = 0$).

Nonetheless, ultimately, one would like to get rid also of this effect. For this reason, the ETM Collaboration has begun to generate a set of $N_f = 2 + 1 + 1$ gauge ensembles including also the unquenching of the strange and charm quarks. The impact of the heavy quarks on the long distance QCD vacuum fluctuation is expected to be much less important, because their mass is much larger than the typical scale $\mathcal{O}(\Lambda_{\mathrm{QCD}})$.

Partial quenching and chiral limit: in *partial quenching*, only a subset of flavors of dynamical quarks is kept but these do not have the same number nor the same mass as valence quarks. In our work, we perform partial quenching of the two up and down light sea quarks ($N_f = 2$ simulations). As we mentioned above, we have to extrapolate to the physical light quark mass. From chiral symmetry, we know that, at leading order, the pion mass squared is proportional to the light quark mass

$$m_\pi^2 \propto m_q \quad \text{where} \quad m_q = \frac{m_u + m_d}{2} \tag{4.27}$$

so we will use the pion mass (which is a physical quantity) as an indicator of the light quark masses.

Now that we have discussed the techniques for computing the propagators needed for the hadron correlator present in Section 4.2, we will describe in the next section the smearing techniques which improve the overlap of the lattice hadron interpolators with the physical state.

4.3.2 Smearing techniques

Since one is interested in the properties of a single hadron, the problem of isolating one single state occurs. One possibility to tackle this problem is to take a lattice sufficiently large in the time direction and study the behavior of the correlation functions at very large time separations $t_x - t_y$. However, larger lattices need more computer time and the signal over noise ratio worsens at large time separations because the signal decays exponentially.
So, one needs to look for other methods to extract fundamental states without having an increase in noise.

In the following, we will present two types of smearing designed to improve the correlation function signal. We will start by the Gaussian smearing applied on the fermion fields and then proceed to the APE smearing, a type of smearing applied on the gauge fields.

Gaussian smearing

A promising ansatz to extract the ground state consists in constructing an operator that has a large overlap with the state under study. The contribution of the fundamental state will dominate even at small time separations. Then we can expect an accurate determination of the ground state because the signal to noise ratio is usually large for small times.
The basic idea is to construct hadron operators by *smearing* the fermion field $\psi(\vec{x}, t)$ with a suitable

wave function $F(\vec{x},\vec{x}')$

$$\psi^S(\vec{x},t) = \sum_{\vec{x}'} F(\vec{x},t\,;\vec{x}',t)\;\psi(\vec{x}',t) \tag{4.28}$$

The conjugate of the smeared quark field is

$$\bar{\psi}^S(\vec{x},t) = \sum_{\vec{x}'} \bar{\psi}(\vec{x}',t)\;\gamma_0\,[F(\vec{x}',t\,;\vec{x},t)]^\dagger\,\gamma_0 \tag{4.29}$$

The variable $\vec{x}$ denotes space points as well as color and Dirac indices. There are many options for smearing. The *Jacobi smearing* [93] is one of the most popular ones, and has also the good property of being gauge invariant. The Jacobi smearing function is computed using a recursive procedure. We start with

$$F(\vec{x},\vec{y}) \;= \alpha\;(\delta_{\vec{x},\vec{y}} \;+ \kappa_s H'(\vec{x},\vec{y})) \tag{4.30}$$

where $H'(\vec{x},\vec{y})$ is called the hopping matrix

$$H' \;= \sum_{\mu=1}^{3} U_\mu(\vec{x})\;\delta_{\vec{y},x+\hat{\mu}} \;+ U_\mu^\dagger(x-\hat{\mu})\;\delta_{\vec{y},\vec{x}-\hat{\mu}} \tag{4.31}$$

with κ_s being the coupling strength of the nearest neighbor in space directions, and α the normalization factor

$$\alpha \;= \frac{1}{1+6\kappa_s} \tag{4.32}$$

In the following, we will see how this type of smearing is implemented when computing the propagators. The construction of the smeared quark propagator is done in three steps

1. Using the fact that F is hermitian, we create a smeared source[7] $S^{(N)}$

$$\begin{aligned} S^{(1)} &= S^{(0)}\;F \\ S^{(2)} &= S^{(1)}\;F \\ &\cdots \\ S^{(N)} &= S^{(N-1)}\;F \end{aligned} \tag{4.33}$$

   where $S^{(0)}$ is the source used when calculating the Local-Local (LL) quark propagator G_{LL} (neither the source nor the sink are smeared).
   After N^{th} iterations, the smeared source is $S^{(N)} = S^{(0)}\,F^N$.

2. Then we solve the Dirac equation (cf. diagram on the left of Fig. 4.3)

$$\sum_y D(\vec{z},t_z\;\vec{y},t_y)\;G_{\mathrm{SL}}(\vec{y},t_y\,;\vec{x},t_x) \;= S^N(z,x)\delta_{t_z,t_x} \tag{4.34}$$

[7] From now on in this chapter, we will denote the source by S and the propagator by G.

where $D(z, y)$ is the Dirac matrix and G_{SL} is the Smeared-source and Local-sink (SL) quark propagator computed using the smeared source $S^{(N)}$. It is related to the local quark propagator by

$$G_{\mathrm{SL}}(y, x) = \sum_z G_{\mathrm{LL}}(y, z) F(z, x) \tag{4.35}$$

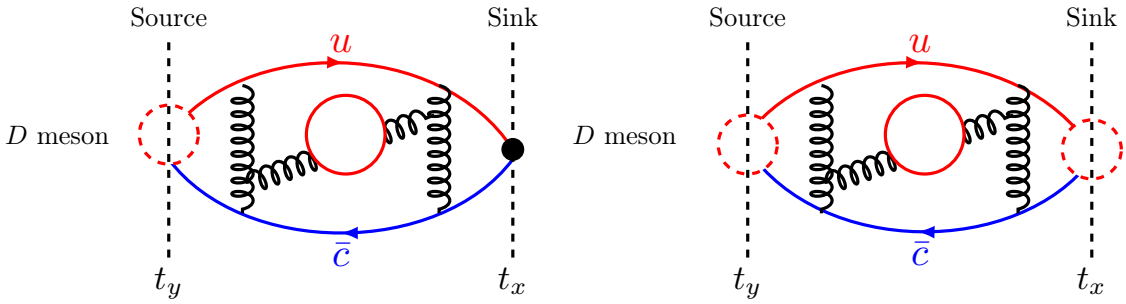


Figure 4.3: Smearing at the source for the propagators (l.h.s) Source-sink smeared quark propagators (r.h.s).

3. Finally, we multiply by the wave function to obtain the Source-Sink smeared (SS) quark propagator G_{SS} (diagram on the right of Fig. 4.3)

$$G_{\mathrm{SS}}(y, x) = \sum_z F^N(y, z)\, G_{\mathrm{SL}}(z, x) \tag{4.36}$$

The construction of a smeared propagator does not take much more computer time than the calculation of a local propagator.

The propagator obtained without smearing the source but only the sink is called Local-source and Smeared-sink (LS) propagator G_{LS} (Fig. 4.4). It can be obtained by replacing the source-smeared propagator G_{SL} in Eq. (4.36) by the local one G_{LL}.

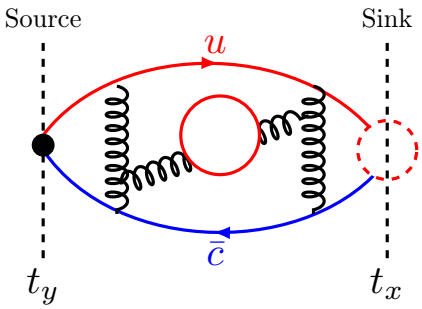


Figure 4.4: Smearing at the sink for the propagators.

The Jacobi smearing depends on two parameters N and κ_s. These can be tuned to optimize the overlap

of the hadron operators with their respective ground states.

We now describe a different type of smearing applied on gauge fields. It is called the APE smearing.

APE smearing

This kind of smearing is applied on the gauge fields present in the gaussian smearing function [94]. The gauge fields of the QCD action will remain unchanged. The idea is to remove, from the gauge links, the fluctuations which have short wavelengths by averaging them with their nearest neighbors. In other words, we suppress the unphysical ultraviolet fluctuations in the gauge invariant sector. The method we will use is an iterative method based on the following steps

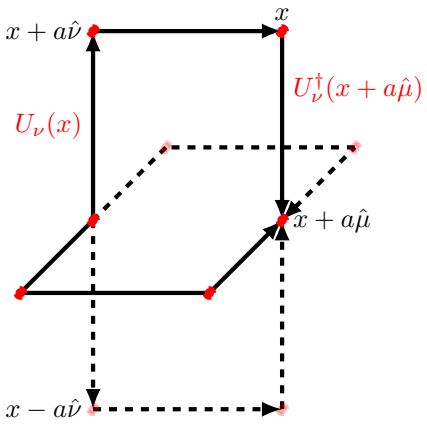


Figure 4.5: Gauge link with APE smearing.

1. Initialization from the original links: $U_\mu^{(0)}(x) \; = U_\mu(x)$
2. Construction of the link as shown in Fig. 4.5 in the spatial directions only ($\mu \neq 0$)

$$U_\mu^{(n+1)}(x) \; = U_\mu^{(n)}(x) \; + \alpha_{\mathrm{APE}} \sum_{\mu \neq \nu} U_\nu^{(n)}(x)\, U_\mu^{(n)}(x+\nu)\, U_\nu^{(n)\dagger}(x+\mu) \tag{4.37}$$

   where α_{APE} is called the APE smearing parameter.
3. Projection of $U_\mu^{n+1}(x)$ in $SU(3)$.
4. Repetition of the second and third steps N_{APE} times.

Application

Figure 4.6 shows the behavior of the D meson two-point correlation functions computed in a lattice of size $24^3 \times 48$ at $\beta = 3.9$ for different types of smearing. The parameters of the gaussian smearing are $\kappa_s = 0.15$ and $N = 30$ and those of the APE smearing are $\alpha_{\mathrm{APE}} = 0.5$ and $N_{\mathrm{APE}} = 10$. It is obvious

that these correlators decay exponentially with time and one can see that the SS, SL and LL correlation functions have different exponential behaviors at small time. For reasons we will mention in the next chapter, we prefer to use the smeared-smeared propagators when computing correlation functions.
There is also an approach followed by the ETMC aiming at combining information coming from smeared-local and smeared-smeared operators. It is called the "*w-method*" [95].

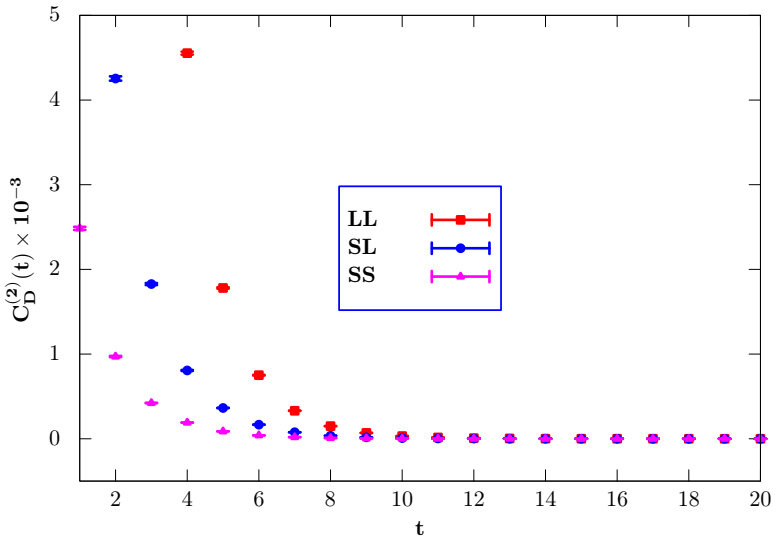


Figure 4.6: Two-point correlation functions containing Smeared-Smeared (SS) ▲, Smeared-Local (SL) ● and Local-Local (LL) ■ propagators .

Having prepared our smeared sources S, we need to compute the propagator G, i.e., we need $G = D^{-1} S$. Let us see how one can solve such an equation algorithmically .

4.4 Resolution of linear systems

In practice, when we look for propagators, we solve linear systems. In addition, there are many types of propagators, each corresponding to the used source. The general form of the linear system is

$$D^{ab}_{\alpha\beta}(x,y)\, G^{bc}_{\beta\gamma}(y,z) = S^{ac}_{\alpha\gamma}(x,z) \tag{4.38}$$

where D is the Dirac matrix operator, S is the so-called *source* and G the unknown propagator vector. As we already mentioned, the Dirac operator is a large matrix. In order to find numerical solutions for any particular system of linear equations, whose matrix is symmetric and positive-definite, we use the conjugate gradient (CG) method [96]. It is an iterative method, so it can be applied to sparse systems that are too large to be handled by direct methods such as the Cholesky decomposition. Such systems often arise when we solve partial differential equations numerically.
We consider the following system of linear equations

$$A\,x = b \tag{4.39}$$

for the vector x, where the known $n \times n$ matrix A is symmetric, positive definite and real, and b is known as well. We choose to work with the CG method because it is the simplest algorithm, and in fact the only one which applies to the case of a twisted mass Dirac operator.
The idea is to minimize the following quadratic function

$$f \ : x \mapsto \ \frac{1}{2} \, (Ax, \, x) \ - \ (b, x) \tag{4.40}$$

The symbol $(,)$ represents the inner product defined as followed: let u and v be two non-zero vectors, then $(u, v) := u^T v$. So we have $(Ax, \, x) \ = x^T \, A \, x$ and $(b, x) \ = x^T b$.
The vectors u and v are conjugate if they are orthogonal with respect to this inner product: $\left(u^T v\right) \ = 0$. Moreover, this conjugation is a symmetric relation.

We start with an input vector x_0 which can be either an approximate initial solution or 0. The next optimal solution x_{k+1} is given by

$$x_{k+1} \ = x_k \ + \alpha_k p_k \tag{4.41}$$

where α_k is a coefficient determined by minimizing the function f, and the direction p_k is chosen to be the conjugate, with respect to A, of the previous ones, i.e.

$$(p_i, \ Ap_k) \ = 0 \quad \text{when } i < k \tag{4.42}$$

$r_0 = b - Ax_0$;
$p_0 = r_0$;
$k = 0$;
while $k < k_{\max}$ **do**
  $\alpha_k \ = \dfrac{r_k^T \, r_k}{p_k^T \, A \, p_k}$;
  $x_{k+1} \ = x_k \ + \ \alpha_k \, p_k$;
  $r_{k+1} \ = r_k \ - \ \alpha_k \, A \, p_k$;
  if $(r_{k+1}, r_{k+1}) \ < \epsilon^2 (r_0, r_0)$ **then**
    exit loop;
  else
    $\beta_k \ = \dfrac{r_{k+1}^T \, r_{k+1}}{r_k^T \, r_k}$;
    $p_{k+1} \ = r_{k+1} + \beta_k \, p_k$;
    $k \ = k + 1$;
  end
end
Return x_{k+1};

Conjugate Gradient algorithm.

The "CG algorithm" gives the most straightforward explanation of the conjugate gradient method. The

maximal number of iterations is given by $k_{\max}$ and the needed precision by ϵ. In most cases, preconditioning is necessary to ensure fast convergence of the conjugate gradient method. Preconditioning is an application of a transformation, called the preconditioner, that conditions a given problem into a form that is more suitable for numerical solution. For example, the even/odd preconditioning uses a decomposition of the matrix into blocks according to the parity of each site, i.e. according to the parity of $x + y + z + t$.

All numerical lattice results are obtained in a discretized space-time. However, we want to obtain results for continuous space-time. Hence, the next section describes how the physical results are obtained in the continuum limit.

4.5 Matching to the continuum limit

Let us recall first that the configurations used in lattice simulations are generated with a probability distribution

$$e^{-S_G} \tag{4.43}$$

The Yang-Mills action is proportional to $\beta \equiv \frac{6}{g^2}$ where g is the bare gauge coupling constant.
We then compute the mean value of the correlation functions and finally, when analyzing data, one has to relate results to experimental values. This can be done by converting them from lattice units to physical ones. For example, we have the hadron mass given by

$$m_{\text{phys.}} = a^{-1}\, m_{\text{latt.}}(g(a)) \tag{4.44}$$

where $m_{\text{latt.}}(g(a))$ is the effective mass in lattice units[8] extracted from the analysis of two-point correlation functions computed for different values of the gauge coupling g. Since the gauge coupling constant and the lattice spacing are implicitly related, this means that we measure the quantities for different values of the lattice spacing a and then we do the extrapolation to the continuum limit by making $a \to 0$.

The determination of the lattice spacing a is thus crucial. Let us see the procedure to determine it.

4.5.1 Lattice spacing determination

First we have to know how the coupling g behaves as a function of a. The Renormalisation Group Equations (RGE) give the relation between the running of g and a

$$-a\,\frac{\partial g}{\partial a} \;=\; \beta(g) \;=\; -\beta_0\, g^3 \;-\; \beta_1\, g^5 \;+\cdots \tag{4.45}$$

where $\beta(g)$ is called the β-function and determines, up to an integration constant, how the coupling g depends on the cutoff a. The β function is only known perturbatively up to few orders in g: $\beta_0 =$

[8] For converting results to MeV one uses $\hbar c = 179.327$ MeV fm $\Rightarrow 1$ fm$^{-1} = 197.327$ MeV.

$\frac{11}{3}\frac{N}{16\pi^2}$ [66] and $\beta_1 = \frac{34}{3}\frac{N}{16\pi^2}^2$ [97], where N is the number of the active flavors. The minus sign before g^3 is very important since it indicates that the theory is asymptotically free.
The solution of Eq (4.45) is

$$a(g) = \exp\left(-\int_0^g \frac{dg'}{\beta(g')}\right) \Lambda_L^{-1} \exp(-\frac{1}{2\,\beta_0\,g^2})(\beta_0 g^2)^{-\frac{\beta_1}{2\beta_0^2}} (1+\mathscr{O}(g^2)) \tag{4.46}$$

In the above, Λ_L is an integration constant having the dimension of a mass and is defined by

$$\Lambda_L = \lim_{g\to 0} \frac{1}{a} \exp(-\frac{1}{2\,\beta_0\,g^2})\,(\beta_0 g^2)^{-\frac{\beta_1}{2\beta_0^2}} \tag{4.47}$$

By inverting the relation (4.46) one obtains the coupling g as a function of the scale a, the so-called running coupling,

$$g(a)^{-2} = \beta_0 \log(a^{-2}\Lambda_L^{-2}) + \frac{\beta_1}{\beta_0} \ln\left(\ln\left(a^{-2}\,\Lambda_L^{-2}\right)\right) + \cdots \tag{4.48}$$

Changing a thus implies a changing of g such that the physical observable remains independent of the scale-fixing procedure. Moreover, for shrinking lattice spacings the coupling g also decreases. Vanishing lattice spacings correspond to a vanishing coupling g. This behavior is called the "*asymptotic freedom*".
A good knowledge of the lattice spacing is needed to extract physical quantities, so after performing the computations one needs to "calibrate" the lattice spacing a. This can be done by choosing a quantity $O^{\exp}$ of dimension d and computing its extrapolated value O in lattice units. The lattice spacing will then be given by the ratio

$$a = (O/O^{\exp})^{1/d} \tag{4.49}$$

This scaling can be directly used to obtain masses m in units of eV from am in the lattice.
In order to fix the lattice spacing a, we have to find a physical quantity that we can use to compare with our results. Valid candidates are the decay constant of a pion f_π, a hadron mass (it could be the nucleon or the ρ meson) or the Sommer parameter r_0 [98]. However, the determination of such observables is not the same due to the difficulty of their evaluation. For example, if we choose the nucleon mass as a reference, it is necessary to extrapolate the result to the physical mass of quarks, which correspond to $m_\pi \simeq 139$ MeV; because of the limitation in computer power, we performed computations with a pion mass $m_\pi \gtrsim 300$ MeV, which induces systematic errors.
A simple parameter to calculate is r_0, the Sommer parameter, defined by solving the equation

$$r_0^2 \frac{\partial V(r)}{\partial r}|_{r_0} = 1.65 \tag{4.50}$$

where $V(r)$ is the static potential between quarks and antiquarks parametrized as

$$A + \frac{B}{r} + \sigma\, r \tag{4.51}$$

It can be calculated through the Wilson loop $L_{r\times t}$, i.e. the trace of an ordered product of gauge link variables along a rectangle of length (r, T). The mean value in the vacuum is related to the potential by

$$V(r) \;=\; \lim_{T\to\infty} \frac{1}{T} \log\left\langle L_{r\times t}\right\rangle \tag{4.52}$$

This potential leads to the determination of the energy scale $r_0 = 0.440(12)$ fm.
In our work, the lattice spacing is fixed by using the parameter r_0/a [98], with r_0 determined by matching f_π obtained on the same lattices with its physical value [2].

When analyzing lattice data, the obtained results have statistical and systematical errors. The errors have to be quantified in order to confront the result with the physical experimental one. The statistical error is due to the use of Monte Carlo importance sampling to evaluate the path integral and its estimation will be detailed in the next chapter. There are, in addition, a different types of systematic errors which are always present to some degree in lattice calculations. The most common lattice errors are reviewed below.

4.5.2 Sources of systematic error

Discretization effects
Observables calculated at finite lattice spacing will differ from their continuum physical value by finite terms. These additional terms are called, in general, discretization errors.
The continuum limit of physical quantities is reached by computing the same quantities at various lattice spacings and then extrapolating to $a \to 0$. One should try, at the smaller possible lattice spacings, to get rid of errors induced by this extrapolation. However, decreasing the lattice spacing for a fixed number of lattice points shrinks the physical volume. Thus, as we decrease a, we have to increase the number of lattice points which in turn increases the numerical cost of the computations. The minimal value of the lattice spacing is then determined by the computational power at our disposal.
In our simulation, we will be left with effects of order a^2 and above. Discretization effects are then parametrized as polynomials in a^2 (we prefer to use the term $a^2/a^2_{\beta=3.9}$ since it is a dimensionless quantity), thus we fit the data computed at finite lattice spacing with such polynomials and numerically extrapolate the fitted function.
We will not concentrate here on extrapolating the masses since our ultimate goal is the computation of the form factors. In the next chapters, we will show qualitatively how such extrapolations are done. Typical simulations try to afford three or four values of a. Discretization errors are expected to be larger for quantities involving larger scales, for example form factors or decays involving particles with momenta larger than $\Lambda_{\rm QCD}$.

Finite size effects
The lattice volume represents the infrared cut-off of the non-perturbative regularized theory. Since all computations are obtained using a finite volume, when analyzing the observables, one has to remove the volume effect and, if possible, extrapolate to infinite spatial volume.
Once the volume exceeds about 2 fm (so that the particle is not "squeezed"), the dominant finite-

volume effect comes from virtual pions wrapping around the lattice in the spatial directions. This effect is exponentially suppressed as the volume becomes large (roughly as $\sim \exp(-m_\pi L)$) and has been estimated using Chiral Perturbation Theory (ChPT) [99] or other methods [100]. The estimates suggest that finite volume shifts are sub-percent effects when $m_\pi L \gtrsim 4$, and most large-scale simulations use lattices satisfying this condition. This becomes challenging as one approaches the physical pion mass, for which $L \simeq 5$ fm is required. At present, this can only be achieved by using relatively coarse lattices, $a \simeq 0.07$ fm. In our computations, the parameter $m_\pi\, L$ is larger than 4, so finite size effects are expected to be small and therefore can be ignored. One can check explicitly the amount of finite size effects by performing two simulations using the same parameters but different lattice volumes and comparing the results.

4.6 Non-perturbative renormalization

An observable calculated in Lattice QCD is a bare quantity. The path integral estimated by Monte Carlo contains all the bare parameters of the theory (mass, couplings) and operators. Hence, we have to apply a renormalization procedure, perturbative or non-perturbative, depending on the scheme, using Feynman diagrams or the numerical ratio of quantities determined on the lattice.
An operator $\mathscr{O}$ can be renormalized as

$$\mathscr{O}_{\rm ren}(a) = Z_{\mathscr{O}}(a)\, \mathscr{O} \tag{4.53}$$

where $Z_{\mathscr{O}}$ is, in general, a function of the ultraviolet cut-off a.
The calculation of renormalization factors $Z_{\mathscr{O}}$ can be carried out using lattice perturbation theory. Although perturbation theory on the lattice is computationally more complex than in the continuum, these calculations can be extended beyond one-loop order [101–103].
Renormalization constants, used in the present thesis, are taken from [104] where the Rome-Southampton method (also known as the RI-MOM scheme) [105] was used to compute non-perturbatively the renormalization coefficients of arbitrary quark-antiquark operators. In the RI-MOM approach, the procedure is similar to the one used in the continuum perturbation theory. In particular, the renormalization conditions are defined similarly in perturbative and non-perturbative calculations. The renormalization factors, obtained for different values of the renormalization scale, are evolved perturbatively to a reference scale $\mu = 2$ GeV. Since, at the end, one wants to make contact with phenomenological studies, which almost exclusively refer to operators renormalized in the $\overline{\rm MS}$ scheme, one needs to connect the RI-MOM quantities to those defined in this $\overline{\rm MS}$ scheme, which is accomplished in continuum perturbation theory [106].

Part III

Spectroscopy and form factors

Chapter 5

Orbital excitations of charmed mesons from tmLQCD

A first task in numerical simulations of Lattice QCD is the determination of the lowest hadron masses. Since most of these masses are experimentally known to high precision, the comparison to the numerical results is an important check of non-perturbative QCD.

The essential idea of this chapter will be to look for the masses of the first orbital excitations of the D meson, called D^{**}, having $J^P = 0^+$ and $J^P = 2^+$ as total angular momentum J and parity P. We first discuss the procedure followed to construct creation operators with the correct quantum numbers, in particular for the first orbitally excited states D^{**}. Then, we explain how we extract the meson masses from the two-point correlation functions as well as how to estimate the corresponding errors.

5.1 Interpolating fields

Interpolating fields are meson (or baryon) creation and annihilation operators having the quantum numbers of the considered states. They are mandatory in order to compute the correlation functions used in the determination of the masses of the mesons, or the transition amplitudes of the semileptonic channels to be studied in the next chapters. In the following, we will explain how one can find the interpolating operators entering the $B \to D^{**}\,\ell\bar{\nu}_\ell$ processes, while focusing on the scalar D_0^* ($J^P = 0^+$) and the tensor D_2^* ($J^P = 2^+$) states.

5.1.1 Interpolating field for the scalar D_0^* ($J^P = 0^+$) state

The set of states with total angular momentum J and parity P in the range $J^P = (0,1)^\pm$ can be described by *local* interpolating fields

$$\mathcal{O}(t) \;=\; \bar{\psi}_{q_1}(t,\vec{x}_{q_1})\,\Gamma\,\psi_{q_2}(t,\vec{x}_{q_2}) \tag{5.1}$$

where $\bar{\psi}_{q_1}(t,\vec{x}_{q_1})$ creates an antiquark at the position $\vec{x}_{q_1}$ and $\psi_{q_2}(t,\vec{x}_{q_2})$ creates a quark at the position $\vec{x}_{q_2}$. The Dirac structure Γ, constructed out of Dirac γ_μ matrices, determines the quantum numbers of the state. In the following table are collected the different structures pertaining to the $J^P = (0,1)^\pm$ states. We added the possibility of taking into account charge conjugation, but since we will only be interested in the $J^P = 0^+$ meson, we will choose $C = +1$.

	$C=+1$			$C=-1$		
J^P	0^+	0^-	1^+	0^+	1^+	1^-
Γ	$\mathbb{1}$	γ^5, $\gamma^5\gamma^4$	$\gamma^5\gamma_i$	γ_4	$\gamma_5\gamma_4\gamma_i$	γ_i, $\gamma_i\,\gamma_4$

Table 5.1: Basis of the quark bilinear having an angular momentum J^P where the highlighted columns correspond to the scalar $J = 0^+$ state. The matrix γ_4 is the Euclidean equivalent of the γ_0 matrix.

To summarize, the chosen interpolating field for the D_0^* meson is

$$\mathscr{O}_{D_0^*}(t) \;=\; \bar{\psi}_q(t,\vec{x}_q)\,\psi_c(t,\vec{x}_c) \tag{5.2}$$

5.1.2 Interpolating field for the tensor D_2^* ($J^P = 2^+$) state

When dealing with angular momenta J strictly greater than one, it is no longer possible to consider local interpolating fields: we need a *non-local* structure for these operators which can be summarized in the following way

$$\mathscr{O}(t) \;= \bar{\psi}_{q_1}(t,\vec{x}_{q_1})\;\mathscr{P}_{\mathbf{t}}(\tilde{\mathbf{x}}_{\mathbf{q_1}},\tilde{\mathbf{x}}_{\mathbf{q_2}})\;\mathbf{\Gamma}\;\psi_{q_2}(t,\vec{x}_{q_2}) \tag{5.3}$$

where $\mathscr{P}_{\mathbf{t}}(\tilde{\mathbf{x}}_{\mathbf{q_1}},\tilde{\mathbf{x}}_{\mathbf{q_2}})\mathbf{\Gamma}$ is a suitable combination of gauge links and Dirac matrices which conspires to give the angular momentum of the meson state. In order to determine this combination, we will rely on group theoretical techniques described in the following section.

Group theory and angular momentum J states on the lattice

In the continuum, a state with an integer angular momentum J belongs to a specific irreducible representation (IR), denoted by $D^{(J)}$, of the symmetry group $SO(3)$. More rigourously, it belongs to the representation space of the IR which produces the momentum J. Moreover, since J is any integer, there is an infinite number of states of angular momentum J because there is an infinite number of IRs of $SO(3)$.

On the lattice, the rotation group is no longer $SO(3)$ but the cubic group[1] O, which has five IRs only, namely A_1 and A_2 (one-dimensional), E (two-dimensional) and T_1 and T_2 (three-dimensional). Hence the problem: how can an infinite number of states in the continuum be described by a finite number of states on the lattice? In other words, how can we recognize a state of angular momentum J inside the state computed on the lattice?

According to group theory, a state $|\psi_R\rangle$ on the lattice is related to the states $|\psi\rangle_{J,\,m}$ of angular momentum J in the continuum by

$$|\psi_R\rangle \;=\; \sum_{J,\,m} c^R_{J,\,m}\,|\psi\rangle_{J,\,m} \tag{5.4}$$

An angular momentum J state contributes to the r.h.s. of this equation if and only if $|\psi_R\rangle$ belongs to the subduced representation [107], noted $D^{(J)}\downarrow O$, of $D^{(J)}$ in the cubic group O. It is a representation of a sub-group of O and is reducible in terms of the IRs of O. The decomposition for different values of

[1] The cubic group O contains 24 elements.

J are listed in the following table

J	$D^{(J)} \downarrow O$
0	A_1
1	T_1
2	$E \oplus T_2$
3	$A_2 \oplus T_1 \oplus T_2$
4	$A_1 \oplus E \oplus T_1 \oplus T_2$
5	$E \oplus 2\,T_1 \oplus T_2$
6	$A_1 \oplus A_2 \oplus E \oplus T_1 \oplus 2\,T_2$
etc	etc

So, in our case, the tensor meson will be studied using E and T_2. Though these two IRs also appear in the description of higher angular momenta, we expect the corresponding contributions to be small because the $J = 2$ state is "fundamental" compared to the $J \geqslant 3$ states.

Construction of the interpolating field for the $J^P = 2^+$ state

Adding the parity states P is equivalent to enlarging the symmetry group of the lattice to O_h by including the reflexions ($O_h = O \otimes$ reflexions). This new group O_h possesses 10 IRs which are $A_1^\pm$ and $A_2^\pm$ (one-dimensional), $E^\pm$ (two-dimensional) and $T_1^\pm$ and $T_2^\pm$ (three-dimensional). The $J^P = 2^+$ state will then be studied using the subduced representation $D^{(2^+)} \downarrow O_h$, which gives

$$J^P = 2^+ \quad \text{(in the continuum)} \quad \rightsquigarrow \quad E^+ \oplus T_2^+ \quad \text{(on the lattice)} \tag{5.5}$$

Following (5.3), the interpolating field is constructed by combining a Dirac structure Γ (quark bilinears) with a combination of paths on the lattice. In the language of group theory, we must combine the corresponding IRs in order to obtain E^+ and T_2^+. The different possibilities are

$$\begin{cases} A_1^+ \otimes E^+ = \boxed{E^+} & T_1^+ \otimes E^+ = T_1^+ \oplus \boxed{T_2^+} \\ A_1^+ \otimes T_2^+ = \boxed{T_2^+} & T_1^+ \otimes T_1^+ = A_1^+ \oplus \boxed{E^+} \oplus T_1^+ \oplus \boxed{T_2^+} \\ & T_1^+ \otimes T_2^+ = A_2^+ \oplus \boxed{E^+} \oplus T_1^+ \oplus \boxed{T_2^+} \\ & T_1^+ \otimes A_2^+ = \boxed{T_2^+} \end{cases} \tag{5.6a}$$

$$\begin{cases} A_1^- \otimes E^- = \boxed{E^+} & T_1^- \otimes E^- = T_1^+ \oplus \boxed{T_2^+} \\ A_1^- \otimes T_2^- = \boxed{T_2^+} & T_1^- \otimes T_1^- = A_1^+ \oplus \boxed{E^+} \oplus T_1^+ \oplus \boxed{T_2^+} \\ & T_1^- \otimes T_2^- = A_2^+ \oplus \boxed{E^+} \oplus T_1^+ \oplus \boxed{T_2^+} \\ & T_1^- \otimes A_2^- = \boxed{T_2^+} \end{cases} \tag{5.6b}$$

with the notation "J^P Dirac structure $\otimes$ path on the lattice".

Basis of J^P *Dirac structures*: according to the previous equations, we need *a priori* Dirac structures that belong to the IR space of $A_1^\pm$ and $T_1^\pm$. Expanding Table 5.1 to include the space of the IRs corresponding to the given Dirac structures, we have

	$C=+1$			$C=-1$		
J^P	0^+	0^-	1^+	0^+	1^+	1^-
Γ	$\mathbb{1}$	γ^5, $\gamma^5\gamma^4$	$\gamma^5\gamma_i$	γ_4	$\gamma_5\gamma_4\gamma_i$	γ_i, $\gamma_i\,\gamma_4$
IR space of O_h	A_1^+	A_1^-	T_1^+	A_1^+	T_1^+	T_1^-

Table 5.2: Basis of the quark bilinear having an angular momentum J^P and its corresponding representation spaces.

Basis of paths on the lattice: following Eqs. (5.6), we *a priori* need to find paths which belong to the representation space of $A_2^\pm$, $T_1^\pm$, $T_2^\pm$ and $E^\pm$. The two-step method proceeds as follows [107]:

(i) We start from a basis of links on the lattice. The choice we made is the dimension 6 base consisting of all spatial links oriented in all senses $\{1,\ \bar{1},\ 2,\ \bar{2},\ 3,\ \bar{3}\}$ where i represents a link oriented in the $+i$ sense, whereas $\bar{\imath}$ represents a link oriented in the opposite one $-i$.

(ii) Using the projection operators in each representation space, we then find a corresponding basis for each IR expressed in terms of the original spatial links. The results are collected in Table 5.3 where we have used the following notations

$$s_i = (i + \bar{\imath}) \qquad \text{and} \qquad p_i = (i - \bar{\imath}) \tag{5.7}$$

Notice that many of the relevant IRs cannot be assigned a basis of paths expressed in terms of the i and $\bar{\imath}$ variables, which eliminates many possibilities to be considered in Eq. (5.6).

IR	A_2^+	A_2^-	T_1^+	T_1^-	T_2^+	T_2^-	E^+	E^-
Basis	none	none	none	$\begin{cases} \frac{1}{\sqrt{2}}\,p_1 \\ \frac{1}{\sqrt{2}}\,p_2 \\ \frac{1}{\sqrt{2}}\,p_3 \end{cases}$	none	none	$\begin{cases} \frac{1}{2}\,(s_2 - s_3) \\ \frac{1}{\sqrt{8}}\,(2s_1 - s_2 - s_3) \end{cases}$	none

Table 5.3: Basis of gauge links for each required IR.

Results

Combining the Dirac basis with the remaining path basis, we are left with the only possible structures that can provide the E^+ and T_2^+ IRs. The results are listed in Table 5.4. We will choose the interpolating fields with the p_i variables: indeed, being the difference of links having opposite senses, they are

closely related to derivatives on the lattice.

IR for Γ	IR for paths	IR of O_h	interpolating field	J^P
T_1^-	T_1^-	T_2^+	$\frac{1}{\sqrt{3}}\bar{\psi}_{q_1}(\gamma_k p_i + \gamma_i p_k)\psi_{q_2}$	$2^+,\ 3^+$
T_1^-	T_1^-	E^+	$\frac{1}{\sqrt{2}}\bar{\psi}_{q_1}(\gamma_1 p_1 - \gamma_2 p_2)\psi_{q_2}$ $\frac{1}{\sqrt{6}}\bar{\psi}_{q_1}(2\gamma_3 p_3 - \gamma_1 p_1 - \gamma_2 p_2)\psi_{q_2}$	$2^+,\ 4^+$
A_1^+	E^+	E^+	$\frac{1}{\sqrt{2}}\bar{\psi}_{q_1}(s_1 - s_2)\psi_{q_2}$ $\frac{1}{\sqrt{6}}\bar{\psi}_{q_1}(2s_3 - s_1 - s_2)\psi_{q_2}$	$2^+,\ 4^+$
T_1^+	E^+	T_2^+	$\frac{1}{2}\bar{\psi}_{q_1}\gamma_5\gamma_1(\phi_2 + \sqrt{3}\phi_1)\psi_{q_2}$ $\frac{1}{2}\bar{\psi}_{q_1}\gamma_5\gamma_2(\phi_2 - \sqrt{3}\phi_1)\psi_{q_2}$ $-\bar{\psi}_{q_1}\gamma_5\gamma_3\phi_2\psi_{q_2}$	$2^+,\ 3^+$

Table 5.4: Meson interpolating fields for the 2^+ states. The colored rows contain the expressions we chose for our study. The spatial indices i and k are all different when appearing in a formula. In the last row, $\phi_1 = (s_2 - s_3)/2$ and $\phi_2 = (2s_1 - s_2 - s_3)/\sqrt{8}$.

5.2 Effective mass extraction

The mesonic masses are determined from the exponential fall of the Euclidean-time two-point correlation functions (or vacuum expectation value) of appropriate creation operators $\mathscr{O}(\tau)$ at large time separation as follows: having chosen the interpolating operator, we can write the formal expression of its two-point correlation function

$$\mathscr{C}_{ij}^{(2)}(\tau) \equiv \sum_{x,y} \left\langle \mathscr{O}_i^\dagger(\tau)\ \mathscr{O}_j(0) \right\rangle_T = \frac{1}{Z}\ \mathrm{Tr}\left[e^{-H\,(T-\tau)}\ \mathscr{O}_i^\dagger(0)\, e^{-H\,\tau}\, O_j(0)\right] \tag{5.8}$$

where H is the Hamiltonian of the theory and the partition function Z is defined to be

$$\mathrm{Tr}\left[e^{-T\,H}\right] \tag{5.9}$$

The parameter τ is the actual distance of interest to us and T is the time extent of the system. In the limit of large T, it is possible to show that $\mathscr{C}_{ij}(t)$ corresponds to the vacuum matrix element of the operator $\mathscr{O}_i^\dagger(\tau)\ \mathscr{O}_j(0)$ [86]

$$\lim_{T\to\infty}\ \mathscr{C}_{ij}^{(2)}(\tau) = \langle\Omega\,|\,\mathscr{O}_i^\dagger(\tau)\ \mathscr{O}_j(0)\,|\,\Omega\rangle \qquad \text{where} \qquad |\Omega\rangle \equiv \text{vacuum} \tag{5.10}$$

After inserting a complete set of energy eigenstates of the Hamiltonian

$$\sum_n \frac{|n\rangle\langle n|}{2n} = \mathbb{1} \tag{5.11}$$

and using

$$\mathscr{O}_i^\dagger(\tau) = e^{H\tau}\,\mathscr{O}_i^\dagger(0)\,e^{-H\tau} \qquad \text{(time-translation invariance)} \tag{5.12}$$

we get

$$\begin{aligned}\mathscr{C}_{ij}^{(2)}(\tau) &= \sum_n \langle\Omega\,|\,\mathscr{O}_i^\dagger(\tau)\left(\frac{|n\rangle\langle n|}{2E_n}\right)\mathscr{O}_j(0)\,|\,\Omega\rangle \\ &= \sum_n \frac{e^{-\tau\,(\delta E_n)}}{2E_n}\,\langle\Omega\,|\,\mathscr{O}_i^\dagger(0)\,|\,n\rangle\,\langle n\,|\,\mathscr{O}_j(0)\,|\,\Omega\rangle\end{aligned} \tag{5.13}$$

where $\delta E_n = E_n - E_\Omega$. From now on we use E_n to denote the energy differences relative to the vacuum $|\Omega\rangle$ instead of δE_n. This implies that the energy E_Ω of the vacuum $|\Omega\rangle$ is shifted to zero.
The final expression is a sum of exponentials: each exponent corresponds to an energy level of the state n predicted by the theory and is multiplied by the product of the matrix elements of $\mathscr{O}_i^\dagger$ and $\mathscr{O}_j$. In the case where the matrix $\mathscr{C}_{ij}^{(2)}$ is diagonal, we have

$$\begin{aligned}\mathscr{C}^{(2)}(\tau) &= \sum_n \frac{1}{2E_n}\,|\langle\Omega\,|\,\mathscr{O}\,|\,n\rangle|^2\,e^{-E_n\,\tau} \\ &= \sum_n \frac{e^{-E_n\,\tau}}{2E_n}\,|\mathscr{Z}_n|^2\end{aligned} \tag{5.14}$$

where we defined the matrix elements

$$\mathscr{Z}_n \equiv \langle\Omega\,|\,\mathscr{O}\,|\,n\rangle \tag{5.15}$$

The relation (5.14) has the following structure

$$\mathscr{C}^{(2)}(t) = c_0 e^{-E_0\,t}\left(1 + \frac{c_1}{c_0}e^{-\delta E_1 t} + \cdots\right) \quad \text{with} \quad \delta E_1 = E_1 - E_0 \tag{5.16}$$

where E_1 is the first excited state. At small times, all the terms contribute to the sum, but at times t larger than the inverse of the first energy gap ($\frac{1}{\delta E_1}$) all the terms inside the brackets are suppressed, so that only the contribution of the ground state survives. The fundamental energy can then be determined by looking at the slope of the logarithm of the correlation function at larger times

$$\log\mathscr{C}^{(2)}(t) \xrightarrow{t>>\frac{1}{\delta E_1}} \log c_0 - E_0\,t \tag{5.17}$$

So, if we are interested in the lowest energy E_0, we look for the time interval $[t_{\min}, t_{\max}]$ with $t_{\min}$ high enough so that the lowest mass dominates the correlation function.
In general, the operator $\mathscr{O}$ creates states propagating from $t = 0$ both in the positive and in the negative

temporal direction, so that meson correlators are symmetric with respect to the exchange $t \longleftrightarrow T-t$. In this case the correlator exhibits the following time dependence

$$\mathscr{C}^{(2)}(t) = \frac{|\mathscr{Z}_0|^2}{E_0} \cosh[E_0(\frac{T}{2}-t)]\, e^{-T\ E_0/2} \tag{5.18}$$

where T is the time extent of the lattice. Neglecting the symmetric behavior of the correlation function leads to an error which becomes larger and larger as t approaches $T/2$. Therefore, we prefer to use Eq. (5.18) when analyzing two-point correlators.
Also, in order to analyze in which time range the contribution of the sub-leading exponentials in Eq. (5.14) can be safely neglected, one defines an *effective mass* as

$$\frac{\mathscr{C}^{(2)}(t)}{\mathscr{C}^{(2)}(t+1)} = \frac{\cosh(m_{\text{eff}}(t-T/2))}{\cosh(m_{\text{eff}}(t+1-T/2))} \tag{5.19}$$

The determination of the effective mass for a certain time t is done iteratively in terms of the ratio $\frac{\mathscr{C}(t)}{\mathscr{C}(t+1)}$, hence the effective mass is always defined up to $t = T/2-1$. A plot of the parameter $m_{\text{eff}}(t)$ as a function of time will hopefully show a *plateau* where the low-lying state dominates and the fitting range of the mass term can be set.

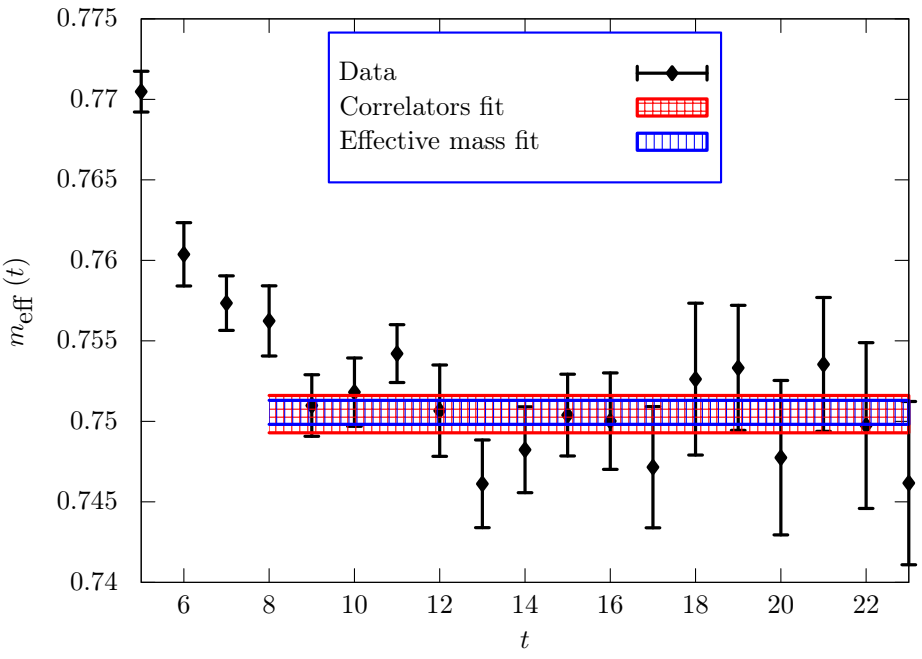


Figure 5.1: Results of the fit parameters of the correlation function $\mathscr{C}^{(2)}(t)$ with the function (5.18) together with the constant fit of the effective mass, plotted over the effective mass. In this plot, correlation functions were computed with $a\mu_c = 0.25$.

This is not the only way to determine hadron masses. In fact, if one is interested in the determination of both the matrix elements $\mathscr{Z}_0$ and the hadron mass E_0, a two-parameter fit of the two-point correlation

function is necessary. If, instead, one is only interested in the determination of the hadron mass, it is possible to perform a constant fit of the effective mass m_{eff} extracted from the ratio between $\mathscr{C}^{(2)}(t)$ and $\mathscr{C}^{(2)}(t+1)$.
Let us illustrate the previous two methods with an explicit numerical example for the case of the lower lying states of the D meson. Figure 5.1 displays a comparison between the determination of the D meson mass from a two-parameter fit of the correlation function (5.18) and from a constant fit of the effective mass. It is clear that the latter provides a more precise estimate of E_0.
When we only needed the energy determination of the hadrons (or the masses), we have used the effective mass method. In the cases where both energy and matrix element $\mathscr{Z}$ were needed, we have used the direct fit of the correlation function (5.18) in order to have a better control of the correlation between the errors of the energy E and the matrix element $\mathscr{Z}$.

5.2.1 Error estimation

In Monte Carlo simulations, we measure different quantities from the same configurations. Thus, the measurements are naturally correlated. In this case, the expression for the error has to take this fact into account so it is recommended to use *Jackknife* or *Bootstrap* analysis methods [108].

Jackknife method: it provides a systematic way to obtain the "standard deviation" error of a set of stochastic measurements

1. We calculate the average $\bar{m}$ of the full set of data (σ) determined from simulation.

2. We divide data (σ) into N blocks, with block length greater than the correlation time $\tau_{\text{corr.}}$ in order to get rid of autocorrelations. If there are no correlations, the block length can be set to one.

3. For each $n = 1 \cdots N$, we remove block n and calculate the average $\bar{m}_{(n)}$ using the data from all the other blocks

$$\bar{m}_{(n)} = \frac{1}{N-1} \sum_{n' \neq n} \bar{m}_{(n')} \tag{5.20}$$

4. We estimate the error on m by calculating the deviation of the $\bar{m}_{(n)}$s from $\bar{m}$

$$\delta m = \sqrt{\frac{N-1}{N} \sum_{n=1}^{N} (\bar{m}_{(n)} - \bar{m})^2} \tag{5.21}$$

(The factor $(N-1)/N$ is there to give the correct result if we look at the errors of simple observables.)

We often want an estimate of some function of the expectation value of σ', $f(\langle\sigma'\rangle)$, where σ' is some quantity which we measure from simulation. Note that this is in general very different from $\langle f(\sigma')\rangle$.

The Jackknife error estimate is then

$$\delta f \ = \sqrt{\frac{N-1}{N} \ \sum_{m} (f_{(n)} - \left\langle f \right\rangle)^2} \tag{5.22}$$

where $f_{(n)} \ = f(\sigma'_{(n)})$. This is typically a good approximation, because $f_{(n)}$ is close to $\left\langle f \right\rangle$. (Here $\left\langle f \right\rangle$ is usually $\sum_{n} \frac{f_{(n)}}{N}$ but it could also be defined as $\left\langle f \right\rangle \ = f(\left\langle \sigma' \right\rangle)$.)

Bootstrap method: it is closely related to the *Jackknife* method, but it mimics the resampling more closely. It works as follows

1. We divide data (σ) into N blocks, with block length greater than the correlation time $\tau_{\text{corr.}}$.
2. From the set of the N blocks, we pick randomly N' blocks (i.e. a bootstrap sample). Some blocks may not get selected at all, some once, some twice, etc..
3. We calculate the quantity of interest σ' over the selected data.
4. We repeat steps 2 and 3 a large number of times, say n_B times, each time using random numbers to generate the bootstrap sample. The calculated quantities are $\sigma'_1, \sigma'_2, \cdots, \sigma'_{n_B}$.
5. Finally, we estimate the standard deviation

$$\delta\sigma' \ = \ \sqrt{\frac{1}{n_B - 1} \ \sum_{i} \left(\sigma'_i - \left\langle \sigma' \right\rangle\right)} \quad \text{where} \quad \left\langle \sigma' \right\rangle = \frac{\sum_i \sigma'_i}{n_B} \tag{5.23}$$

One should have at least several tens of samples, preferably hundreds. In the bootstrap n_B can go up to 1000.

Let us now proceed to describe the determination of the mass of the first orbitally excited states ($L = 1$) of the charmed D meson, with orbital angular momentum $J^P = 0^+, 2^+$, from their corresponding two-point correlation functions. We will refer to these two states as the *scalar* D_0^* ($J^P \ = \ 0^+$) and the *tensor* D_2^* ($J^P = 2^+$) states[2].

5.2.2 Spectroscopy of the scalar D_0^* state

After describing how we can extract the meson masses from two-point correlators, we will now address the charm *scalar* mesonic state. As parity is broken by the lattice twisted-mass action [83] and the states we consider are not made out of quarks of the same flavor doublet (contrary to what is discussed in section 5.2 of [80]), the scalar D_0^* meson can in principle mix with the pseudoscalar D meson. In order to disentangle these states, we will use the Generalized EigenValue Problem (GEVP) [110].

[2]There are also two D^{**} with $J^P = 1^+$ but we will omit them from the current study since disentangling them demands more work. First results on $J^P = 1^+$ in the D_s sector from $N_f = 2 + 1 + 1$ tmLQCD can be found in [109].

Description of the Generalized Eigenvalue Problem

To implement this method in the present case, we consider a 2×2 correlation matrix

$$\mathscr{C}_{ij}^{(2)}(t) \ = \left\langle \mathscr{O}_i^{\dagger} \, \mathscr{O}_j \right\rangle \ = \sum_n \langle \Omega \,|\, \mathscr{O}_i^{\dagger} \,|\, n \rangle \, \langle n \,|\, \mathscr{O}_j \,|\, \Omega \rangle \, e^{-E_n t} \tag{5.24}$$

composed of a set of scalar and pseudoscalar operators, having the quantum numbers of the state one is interested in. In the twisted basis we take

$$\mathscr{O}_j \ \in \left\{ \bar{\chi}_c \, \gamma_5 \, \chi_u, \ \bar{\chi}_c \, \chi_u \right\} \tag{5.25}$$

Using the right-hand side of Eq. (5.24), it has been shown that diagonalizing the correlation matrix $\mathscr{C}_{ij}^{(2)}(t)$ allows to disentangle the physical states to some extent. Indeed, we solve the following equation

$$\sum_k \mathscr{C}_{jk}^{(2)}(t) \, v_k^{(n)}(t, t_0) \ = \sum_k \lambda^{(n)}(t, t_0) C_{jk}(t_0) v_k^{(n)}(t, t_0) \tag{5.26}$$

in order to find the eigenvectors and eigenvalues of the system. In GEVP, the normalization at some time slice $t_0 < t$ ought to improve the signal by suppressing the contributions from higher excited states. The method improves when the number of interpolators is increased, but including more operators enhances the statistical noise and thus affects the diagonalization.
When solving the GEVP, we obtain n masses from the following ratio of the eigenvalues at consecutive times

$$\frac{\lambda^{(n)}(t, t_0)}{\lambda^{(n)}(t+1, t_0)} \ = \ \frac{e^{-m^{(n)}\, t} + e^{-m^{(n)}\,(T-t)}}{e^{-m^{(n)}\,(t+1)} + e^{-m^{(n)}\,(T-(t+1))}} \tag{5.27}$$

From the above ratio one can extract the effective masses as a function of time in lattice units. Finally, fitting the data points in a defined time interval allows to extract the effective masse of the state n.

Simulation setup

In what follows, we present our results for the pseudoscalar D and the scalar D_0^* meson masses obtained using GEVP. In this analysis, correlation functions were computed using a sample of 100 gauge configurations produced by the ETMC [111, 112] with $N_f = 2$ twisted-mass fermions tuned at maximal twist. The lattice volume is $24^3 \times 48$ in lattice units. We implement non-degenerate valence quarks in the twisted mass formulation of Lattice QCD, as discussed in [113], by formally introducing a twisted doublets for each non-degenerate quark flavor. In this analysis, we thus include in the valence sector two twisted doublets (u, d) and (c, c') with masses $a\mu_q = 0.0085$ and $a\mu_c = 0.25$ (which corresponds to m_D at $\beta = 3.9$) respectively.
We use, in our analysis, smeared-smeared two-point correlators because they are less noisy. As expected, the effective mass of the scalar excited state (D_0^*) in Fig. 5.2 is greater than the pseudoscalar (D) one. The effective mass plateaus are represented by the shaded band within defined intervals of time. The plateau coming from the pseudoscalar state is found in a wider interval of time than the scalar one: in Fig. 5.2 we choose $t \in [4, 7]$ for the scalars and $t \in [5, 14]$ for the pseudoscalars. Also, as t approaches

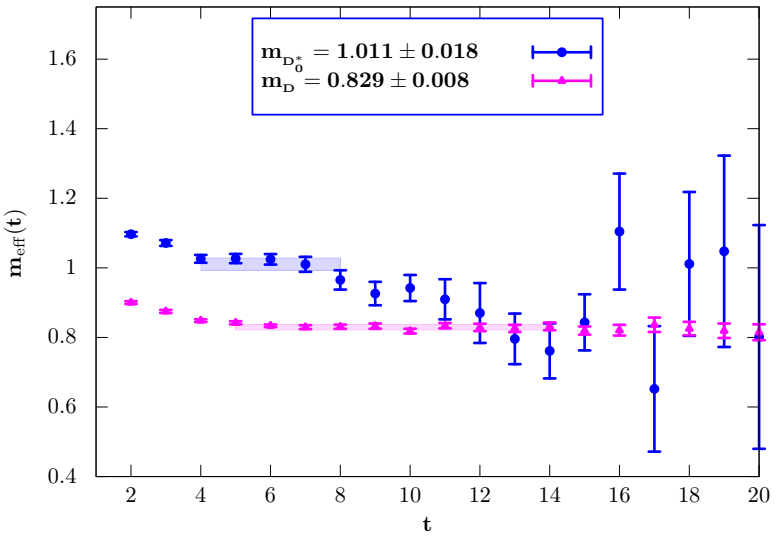


Figure 5.2: Effective masses of scalar (●) and pseudoscalar (▲) charmed D meson obtained by solving GEVP as a function of time in lattice units. Results correspond to a simulation using 100 configurations. The valence quark masses are $a\mu_c = 0.25$ and $a\mu_l = 0.0085$.

11, the data points tend to mix and the scalar mass exhibits larger error bars than the pseudoscalar.

5.2.3 Lower tensor D_2^* states

As explained before, one can obtain the $J = 2$ states by considering the E^+ and T_2^+ IRs. The appropriate operators for $J^P = 2^+$ were given in Table 5.4. We separately combine the two diagonal interpolators contributing to the E^+-representation and the three non-diagonal interpolators of the T_2^+-representation. So we have two masses, $m(E^+)$ and $m(T_2^+)$. The extracted masses are, in principle,

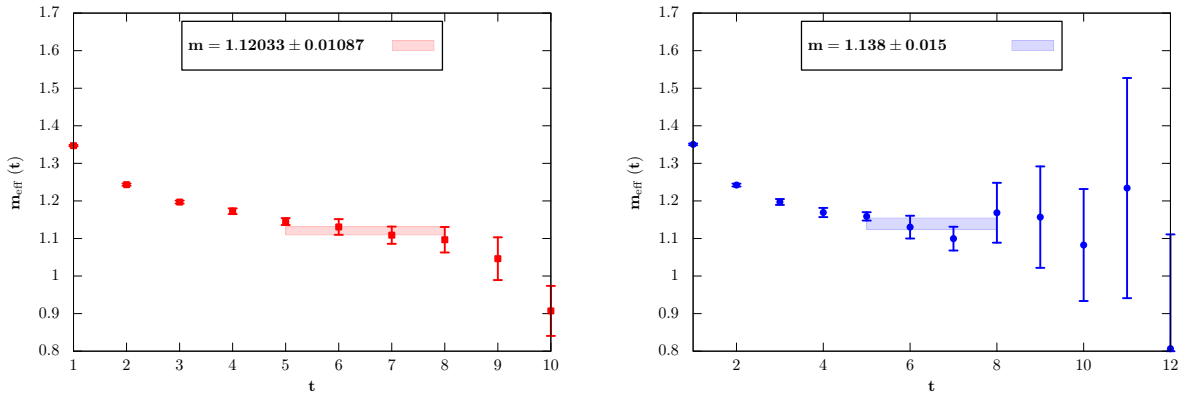


Figure 5.3: The plot on the left represents the effective mass $m(T_2^+)$ as a function of time and, on the right, the effective mass $m(E^+)$. In this analysis, we use 240 gauge configurations. The valence charm quark has a mass $a\mu_c = 0.215$ which corresponds to the physical charm quark.

equal in the continuum: any discrepancy comes from the cut-off effects. We show in Fig. 5.3 that,

indeed, lattice artifacts are present and that the signal to noise ratio decreases when approaching the center of the lattice.
These plots allow not only the determination of the effective masses of $J^P = 2^+$ states, but also enable the determination of the time range needed for the fit of the two-point correlation functions from which we will extract the energy as well as the constant $\mathscr{Z}$ required in the calculation of form factors.

5.2.4 Discussion of results

From the above results, it is clear that working with excited D meson states is a delicate issue. The noise increases when looking for higher orbital angular momentum J masses. However, the corresponding plateaus, though not that large, are enough for a qualitative study of form factors.
We will compare the values we obtain from lattice simulations with the experimental determinations of the masses by studying the quantity $\Delta m = (m_{D^{**}} - m_D)$ where D^{**} stands for the scalar D_0^* (the tensor D_2^*) state and D is the pseudoscalar charmed meson.

$J = 0^+$ state: since the results presented in this chapter are obtained in lattice units, we use the value of the lattice spacing $a = 0.085$ fm, fixed as explained in Chapter 4, or more precisely its inverse $a^{-1} \sim 2.3$ GeV to get the difference Δm. In the case of the scalar D_0^*, Δm is about $[369 - 442]$ MeV. If we compare this with the experimentally measured masses in the D_s sector (where the light quark is not the (u, d) but the strange s), we get ratios $\Delta m^{\text{th.}}/\Delta m^{\text{exp.}}$ varying from 1.13 up to 1.26.

$J = 2^+$ state: using Fig. 5.3, one can determine that the mass $m(E) \sim 2.6$ GeV and $m(T_2) \sim 2.75$ GeV. The uncertainty is large here due to the noise. The computed mass difference ratio to its experimental value is almost 1.4.

Regardless of the fact that these results are not extrapolated to the continuum, they offer some insight on the magnitude of the discretization errors for our currently used lattice spacing. For both scalar and tensor states, we see a systematic trend for the mass difference Δm to exceed the experimental one ($\sim 30\%$). This excess diminishes when going to the continuum limit[3]($\sim$10%).

[3]We confronted our results with those of [114] where an extrapolation to the continuum was performed: both results were compatible at $\beta = 3.9$.

Chapter 6

$B_s \to D_s\, \ell\, \bar{\nu}_\ell$ near zero recoil from the SM and beyond

The two semileptonic decay channels $B \to D\ell\bar{\nu}_\ell$ and $B \to D^*\ell\bar{\nu}_\ell$, where the resulting lepton is either an electron or a muon, allow two independent estimates of the CKM matrix element V_{cb}. The main uncertainty on V_{cb} comes from the theoretical determination of the form factors that parametrize the hadronic weak current, hence, any precise determination of the form factors lead to an accurate determination of the CKM matrix elements.

In the first chapter, we presented a brief introduction to the exclusive decay $B \to D\ell\bar{\nu}_\ell$, giving recent results for the ratio of branching fractions of $B \to D^{(*)}\mu\bar{\nu}_\mu$ and $B \to D^{(*)}\tau\bar{\nu}_\tau$ decays. The experimental result for this ratio came as a surprise and suggests a disagreement with respect to the SM predictions. This discrepancy, which is around 2σ, might provide the first evidence for NP in semitauonic B decays. One possibility to accommodate this fact is to consider additional operators in the effective weak Hamiltonian which describes the system, and, in parallel, revisit the SM predictions.

With the aim of revealing and quantifying the effects of new physics in semileptonic B decays, we propose in this chapter to focus on the study of $B_s \to D_s$ transitions. The decay mode $B_s^0 \to D_s^+\ell\bar{\nu}_\ell$ could be studied in B-factories like LHCb or especially at Super Belle. One more advantage in studying B_s decay is that there is no averaging between neutral and charged modes so that the soft photon problem is less important [115]

$$\frac{\mathscr{B}(B_s \to D_s\gamma_{\rm soft}\,\ell\,\bar{\nu}_\ell)}{\mathscr{B}(B_s \to D_s\ell\bar{\nu}_\ell)} < \frac{\mathscr{B}(B \to D^0\gamma_{\rm soft}\ell\bar{\nu}_\ell)}{\mathscr{B}(B \to D^0\gamma\,\ell\,\bar{\nu}_\ell)} \tag{6.1}$$

Moreover, from the lattice point of view, the non-strange heavy-light mesons are more difficult because a chiral extrapolation in the valence light quark is required, which is a source of systematic uncertainties. Working with the strange case is simpler because the light spectator is fixed to its known mass (m_s) and no extrapolation in the light quark mass is needed when computing the relevant form factors on the lattice.

With the available computer power it is not possible to simulate quark masses in the range of the physical b mass and at the same time keep the finite volume and discretization effects under control. In order to circumvent these problems, many different methods have been proposed (for a recent review see [116]). The physical b quark mass expressed in lattice units, am_b is larger than 1 for all ensembles used in our simulation, and one expects large discretization effects (in principle of order 100%) when computing directly quantities with a physical b quark mass. In our work we have avoided computing the quantities of interest directly at the physical b quark, and have instead performed an interpolation of the data computed from the c quark region together with information coming from the static limit (heavy quark mass $m_h \to \infty$).

In the present chapter we study the form factors entering the $B_s \to D_s$ decay channel. We proceed as follows: first, we present the determination of the form factors parametrizing the weak matrix elements. Then, we present the simulation details as well as the strategy for the lattice computation. Finally, we explore what will be referred to as the "ratio method" which we implement in order to extrapolate to the

physical b quark mass without performing any static calculation.

The analysis presented here is the object of a publication [117].

6.1 Extraction of the form factors

The amplitude for the hadronic transition $B_s \to D_s$ is parametrized in the SM through the vector and the scalar form factors, $F_+(q^2)$ and $F_0(q^2)$, defined as

$$\begin{aligned}\left\langle D_s(p_{D_s}) \left| (V-A)_\mu \right| \bar{B}_s(p_{B_s}) \right\rangle = \; & F_+(q^2)\,(p_{B_s}+p_{D_s})_\mu \\ & + q_\mu \; \left[F_0(q^2) - F_+(q^2)\right] \left(\frac{m^2_{B_s} - m^2_{D_s}}{q^2}\right)\end{aligned} \tag{6.2}$$

where the momentum transfer is $q = (p_{B_s} - p_{D_s})$, and $q^2 \in]0, q^2_{\rm max}]$, with $q^2_{\rm max} = (m_{B_s} - m_{D_s})^2$. In the above expression, the matrix element of the axial current is zero due to parity conservation.

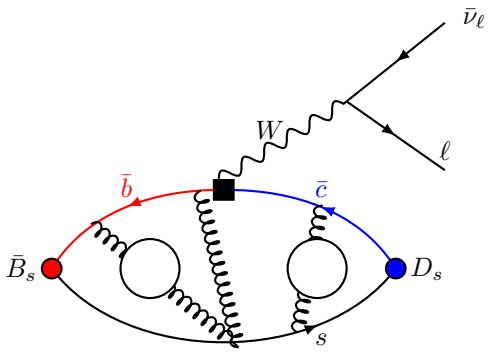


Figure 6.1: Feynman diagram representing the semileptonic process $B_s \to D_s\,\ell\,\bar{\nu}_\ell$.

The SM effective Hamiltonian can be extended to include new operators. In a generic NP scenario, not accounting for leptonic mixing and which preserves the lepton flavor universality (LFU), the effective Hamiltonian can be written by adding, to the SM one, scalar, vector and tensor operators [4]

$$\begin{aligned}H_{\rm eff} \; = \; -\sqrt{2}\,G_F\,V_{cb} \; \Big[& (\bar{c}\gamma_\mu b)\;(\bar{\ell}_L\gamma^\mu\nu_L) \; + \boxed{g_V}\;(\bar{c}\gamma_\mu b)\;(\bar{\ell}_L\gamma^\mu\nu_L) \\ & + \boxed{g_S}\;(\bar{c}b)\;(\bar{\ell}_R\nu_L) \; + \boxed{g_T}\;(\bar{c}\sigma_{\mu\nu}b)\;(\bar{\ell}_R\sigma^{\mu\nu}\nu_L)\Big] + \text{h.c.}\end{aligned} \tag{6.3}$$

where g_S, g_T and g_V are the dimensionless couplings proportional to $m^2_W/m^2_{\rm NP}$, with $m_{\rm NP}$ being the New Physics scale. Though appearing in physical observables such as the $B \to D\ell\bar{\nu}_\ell$ decay rate, the extra scalar and vector parts do not provide any extra form factors. On the contrary, the tensor term

leads to a new form factor $F_T(q^2)$ whose corresponding hadronic matrix element is defined as [118]

$$\langle D_s(p_{D_s})|\bar{c}\sigma_{\mu\nu}b|B_s(p_{B_s})\rangle = -i(p_{B_s\mu}\, p_{D_s\nu} - p_{D_s\mu}\, p_{B_s\nu})\, \frac{2F_T(q^2)}{m_{B_s} + m_{D_s}} \tag{6.4}$$

Let us proceed to describe the strategy for the extraction of these form factors from lattice simulations. As a first step, we choose a suitable kinematics.

6.1.1 Kinematics

When both mesons are at rest, only the scalar form factor contributes to the transition matrix element. In other words, in order to "see" $F_+(q^2)$ one should give a momentum to one of the meson states which we choose to be D_s. Moreover, we will assume that this momentum has symmetrical spatial components

$$p_{B_s} = \left(m_{B_s}\,, \vec{0}\right) \qquad \text{and} \qquad p_{D_s} = (E_{D_s}, p, p, p) \tag{6.5}$$

We also use the twisted boundary conditions (BCs) [119,120] for the quark field in order to increase the kinematical region accessible for the investigation of momentum dependent quantities like, for example, form factors. This allows to shift the quantized values of p by a continuous amount

$$p = \frac{\theta\pi}{L} \quad \text{so that} \quad |\vec{q}| = \sqrt{3}\,\frac{\theta\pi}{L} \tag{6.6}$$

The chosen θs correspond to small momenta, thus we are discussing the decay matrix element near zero-recoil. More specifically, our θs correspond to the following recoils w for $B_s \to D_s\ell\bar{\nu}_\ell$

$$w \in \{1,\, 1.004,\, 1.016,\, 1.036,\, 1.062\} \tag{6.7}$$

Note that $w_{\max}$ for this decay mode is 1.546.
The D_s mesons, to which a three momentum is given, obey the free-boson lattice dispersion relation that describes the data at fixed lattice spacing

$$4\sinh^2\frac{E_D}{2} = 4\left(3\sin^2\frac{\theta\pi}{2L}\right) + 4\sinh^2\frac{m_D}{2} \tag{6.8}$$

In the continuum limit, the latter becomes the continuum dispersion relation

$$E_{D_s}^2 = |\vec{q}|^2 + m_{D_s}^2 \tag{6.9}$$

Since our B-meson is always at rest, it is easy to see that

$$w = \sqrt{1 + \frac{3\theta^2\pi^2}{(m_{D_s}L)^2}} \tag{6.10}$$

This is a very welcome feature because w does not depend on the B_s mass. So we can vary m_{B_s} to reach its physical value while keeping m_{D_s} fixed. In other words, we will indeed be able to extrapolate to physical $B_{(s)} \to D_{(s)}$ at fixed values of w.

Using the above kinematics, we find the expressions of the form factors in terms of the corresponding matrix elements. The factor $F_0(q^2)$ is determined from the vector transition amplitude by

$$\begin{cases} P_\mu^0 \langle D(p_{D_s})|V_\mu|B(p_{B_s})\rangle = \dfrac{m_{B_s}+m_{D_s}}{m_{B_s}-m_{D_s}}\, F_0(q^2)\,, \\ \qquad\qquad \text{with} \quad P_\mu^0 = \dfrac{q_\mu}{q^2_{\max}}, \quad \text{and} \quad q_\mu = (m_{B_s}-E_{D_s}, -\vec{p}_{D_s}) \end{cases} \tag{6.11}$$

The vector form factor $F_+(q^2)$ can be written as

$$\begin{cases} P_\mu^+ \langle D(p_{D_s})|V_\mu|B(p_{B_s})\rangle = \vec{q}^{\,2}\dfrac{2m_{B_s}}{m_{B_s}-E_{D_s}}\, F_+(q^2)\,, \\ \qquad\qquad \text{with} \quad P_\mu^+ = \left(\dfrac{\vec{q}^{\,2}}{m_{B_s}-E_{D_s}}, \vec{q}\right) \end{cases} \tag{6.12}$$

For the tensor operator $T_{\mu\nu} = \bar{c}\sigma_{\mu\nu}b$, the component which contributes to the tensor form factor in the B_s rest frame is T_{0k}

$$\langle D(p_{D_s})|T_{0k}|B(p_{B_s})\rangle = \frac{-2i\left(m_{B_s}\, p_{D_s\, k}\right)}{m_{B_s}+m_{D_s}}\, F_T(q^2)\,. \tag{6.13}$$

The form factor F_T is then determined by using the imaginary part of the tensor hadronic matrix element.

6.1.2 Lattice setup and simulation details

In this analysis, we use gauge ensembles produced by the European Twisted Mass Collaboration [111, 112] at four values of the inverse bare gauge coupling β, and different light sea quark masses. The values of the simulated lattice spacings lie in the interval $[0.05, 0.1]$ fm.
Dynamical quark simulations have been performed using the tree-level improved Symanzik gauge action [69] and the Wilson twisted mass action [79] tuned to maximal twist [83] (already discussed in Chapter 3). Let us recall that the use of maximally twisted fermionic action offers the advantage of automatic $\mathcal{O}(a)$ improvement for all the interesting physical observables computed on the lattice [83].
Bare quark mass parameters, corresponding to a degenerate bare mass value of the u/d quark, are chosen to have the light pseudoscalar mesons in the range $280 \leq m_{\rm PS} \leq 500$ MeV. We have computed two- and three-point correlation functions using valence quark masses whose range is extended from the light sea quark mass up to $2.5-3$ times the physical charm quark mass. We implement non-degenerate valence quarks in the twisted mass formulation by formally introducing a twisted doublet for each non-degenerate quark flavor. We thus add in the valence sector three twisted doublets, $(s, s'), (c, c')$ and (b, b') with masses $a\mu_s$, $a\mu_c$ and $a\mu_b$, respectively. Within each doublet, the two valence quarks are regularized in the physical basis with Wilson parameters of opposite values, $r = -r' = 1$.
Here, we implement twisted BCs for the c doublet

$$\chi_c(x + L\hat{e}_i) = e^{i\theta L}\chi_c(x) \tag{6.14}$$

β	$(L/a,\ T/a)$	$a\mu_\ell$	$a\mu_s$	$a\mu_h$
3.80	(24, 48)	0.0080, 0.0110	0.0194	0.2331, 0.2742, 0.3225, 0.3793, 0.4461, 0.5246, 0.6170, 0.7257, 0.8536, 1.0040
3.90	(32, 64)	0.0030, 0.0040	0.0177	0.2150, 0.2529, 0.2974, 0.3498,
	(24, 48)	0.0040, 0.0064 0.0085, 0.0100		0.4114, 0.4839, 0.5691, 0.6694, 0.7873, 0.9260
4.05	(32, 64)	0.0030, 0.0080	0.0154	0.1849, 0.2175, 0.2558, 0.3008, 0.3538, 0.4162, 0.4895, 0.5757, 0.6771,0.7963
4.20	(48, 96)	0.0020	0.0129	0.1566, 0.1842, 0.2166, 0.2548,
	(32, 64)	0.0065		0.2997, 0.3525, 0.4145, 0.4876, 0.5734,0.6745

Table 6.1: Simulation details for the correlator computations at four values of the gauge coupling $\beta = 3.80$, 3.90, 4.05 and 4.20. The quantities $a\mu_\ell$, $a\mu_s$ and $a\mu_h$ stand for light, strange-like and heavy (i.e. charm-like and heavier) bare valence quark mass values respectively, expressed in lattice units.

This is equivalent to define an auxiliary field

$$\chi_c^{\vec{\theta}}(x) = e^{-i\vec{\theta}\cdot\vec{x}}\chi_c(x) \tag{6.15}$$

and a Dirac operator

$$D^{\vec{\theta}}(\chi_c, \bar{\chi}_c, U) \equiv D(\chi_c^{\vec{\theta}}, \bar{\chi}_c^{\vec{\theta}}, U^{\vec{\theta}}) \qquad \text{with} \qquad U_i^{\vec{\theta}}(x) = e^{ia\theta}U_i(x) \tag{6.16}$$

The whole fermionic action finally reads

$$S^{\rm val} \;=\; S_{\rm F}[\chi_s,\, \bar{\chi}_s,\, U] \;+\; S_{\rm F}[\chi_b,\, \bar{\chi}_b,\, U] \;+\; S_{\rm F}\big[\chi_c^{\vec{\theta}},\, \bar{\chi}_c^{\vec{\theta}},\, U^{\vec{\theta}}\big] \tag{6.17}$$

where $S_F[\chi_q, \bar{\chi}_q, U]$ represents the twisted mass action of fermions tuned to maximal twist.
Simulation details are given in Table 6.1, where μ_ℓ, μ_s and μ_h indicate the bare light, strange-like and heavy (i.e. charm-like and heavier) valence quark masses respectively. We have set the light valence quark masses equal to the light sea ones, $a\mu_\ell = a\mu_{\rm sea}$.

Renormalized currents are obtained from the bare ones using renormalization constants (RC), whose values have been computed in [104, 121] using RI-MOM techniques and then transferred to the $\overline{\rm MS}$ scheme. In Table 6.2 we collect the values of Z_V, Z_A and Z_T at each value of β as well as the corresponding estimates of the lattice spacing [2].

Quark propagators with different valence masses are obtained using the multiple mass-solver method [96], which allows to invert the Dirac operator for several valence masses at the same time, with a mild increase in computational cost with respect to the computation of the single propagator.

β	3.80	3.90	4.05	4.20
Z_V	0.5816(2)	0.6103(3)	0.6451(3)	0.686(1)
Z_A	0.746(11)	0.746(6)	0.772(6)	0.780(6)
Z_T	0.73(2)	0.750(9)	0.798(7)	0.822(4)
a (fm)	0.098(3)	0.085(3)	0.067(2)	0.054(1)

Table 6.2: The renormalization constants Z_V, Z_A, and Z_T in the $\overline{\text{MS}}$ scheme at 2 GeV, and lattice spacing estimates for each value of the inverse gauge coupling $\boldsymbol{\beta}$.

The statistical accuracy of the meson correlators is significantly improved by using the *one-end* stochastic method [122, 123] already described in Chapter 4.
Two- and three-point correlation functions were then computed by employing smearing techniques on a set of 100-240 independent gauge configurations for each ensemble. We evaluated the statistical errors using the *Jackknife* method.
Smeared interpolating operators become mandatory in the cases where relativistic heavy quarks are involved. Smearing proves to be beneficial in reducing the coupling of the interpolating field with the excited states, thus increasing its projection onto the lowest energy eigenstate. The usual drawback, i.e. the increase of the gauge noise due to the fluctuations of the links entering the smeared fields, is controlled by replacing thin gauge links with APE smeared ones. With this technical improvement, we can extract heavy-light meson masses and matrix elements at relatively small temporal separations, while keeping the noise-to-signal ratio under control. We employed the Gaussian smearing [124, 125] for heavy-light meson interpolating fields at the source and/or the sink. The smeared field is of the form

$$S^{(N)} = (1 + 6\kappa_s)^{-N}(1 + \kappa_s a^2 \nabla^2_{\rm APE})^N S^{(0)} \tag{6.18}$$

where $S^{(0)}$ is a standard local source and $\nabla_{\rm APE}$ is the lattice covariant derivative with APE smeared gauge links characterized by the parameters $\alpha_{\rm APE} = 0.5$ and $N_{\rm APE} = 20$. We have taken $\kappa_s = 4$ and $N = 30$.

6.1.3 Hadronic matrix elements from LQCD

The first step in exploring the form factors of Eqs. (6.2) and (6.4) in Lattice QCD, and getting information on semileptonic decays, is to find the matrix elements of vector or axial vector currents between single hadron states. In order to access matrix elements, one starts by computing the following three-point correlation functions

$$\mathscr{C}^{(3)}(t, t_i, t_f, \vec{p}_i, \vec{p}_f) = \sum_{\text{positions}} \langle \mathscr{O}^\dagger_{D_s}(t_f, \vec{x}_f)\, J_\mu(t, \vec{x})\, \mathscr{O}_{B_s}(t_i, \vec{x}_i)\rangle \cdot e^{i(\vec{x}-\vec{x}_f)\cdot\vec{p}_f} \cdot e^{-i(\vec{x}-\vec{x}_i)\cdot\vec{p}_i} \tag{6.19}$$

where $\mathscr{O}^\dagger_{D_s}$, $\mathscr{O}_{B_s}$ are respectively the annihilation and creation operators of the D_s and B_s mesons, J_μ is the vector or axial current. Figure 6.2 represents the diagram corresponding to such correlation functions.

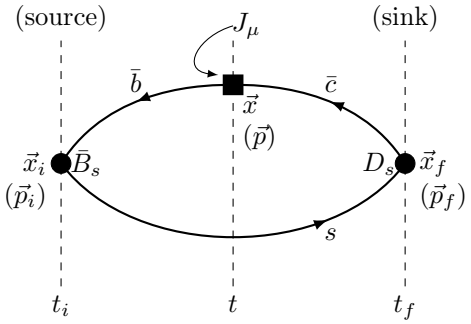


Figure 6.2: Valence quark flow in the form factor of $B \to D\ell\bar{\nu}_\ell$

In terms of the *all-to-all* propagators, the three-point function for the $B_s \to D_s$ process becomes

$$\mathscr{C}^{(3)}(t, t_i, t_f, \vec{p}_i, \vec{p}_f) = \sum_{\text{positions}} \left\langle \text{Tr}\left[S^b(x, x_i)\, \gamma_5\, S^s(x_i, x_f)\, \gamma_5\, S^c(x_f, x)\Gamma_{\text{ins.}}\right] \right\rangle \times \exp\left[-i\vec{p}_f \cdot (\vec{x}_f - \vec{x})\right] \cdot \exp\left[-i\vec{p}_i \cdot (\vec{x} - \vec{x}_i)\right] \tag{6.20}$$

where $\Gamma_{\text{ins.}}$ stands for the spin structure of the current. The standard way to calculate semileptonic three-point functions in LQCD is the sequential propagator method. The *sequential propagator* method provides a means of computing a heavy-quark propagator (i.e. $S^c(x_f, x)$) that connects all spatial sites x_f at the sink time slice t_f, to all sites x and t at the vector current insertion. Algorithmically, this amounts to taking the spectator quark propagator $S^s(x_i, x_f)$ and projecting it onto the sink momentum p_f, the sink smearing and the sink matrix structure, which is here γ_5.

Let

$$\tilde{\Sigma}_{cs}(x_i, x; t_2, \vec{p}_f) = \gamma_5[\Sigma_{cs}(x, x_i; t_2, \vec{p}_f)]^\dagger \gamma_5 \tag{6.21}$$

where

$$\Sigma_{cs}(x, x_i; t_2, \vec{p}_f) \;=\; \sum_{x_f} S^c(x, x_f)\gamma_5 S^s(x_f, x_i)\delta_{t_2, t_f - t_i} e^{-i\vec{p}_f \cdot (\vec{x}_f - \vec{x}_i)} \tag{6.22}$$

The *sequential propagator* $\Sigma_{cs}(x, x_i; t_2, \vec{p}_f)$ can be combined with the beauty-quark propagator $S^b(x, x_i)$ and appropriate γ-matrices to arrive at Equation (6.20)

$$\mathscr{C}^{(3)}(t_1, t_2, \vec{p}_i, \vec{p_f}) = \sum_{x, x_i} \left\langle \text{Tr}\,\left[S^b(x, x_i)\, \gamma_5\, \tilde{\Sigma}_{cs}(x_i, x; t_2, \vec{p}_f)\; \Gamma_{\text{ins.}}\right] \right\rangle \times\; \exp\left[i\vec{p}_f \cdot (\vec{x} - \vec{x}_i)\right] \exp\left[-i\vec{p}_i \cdot (\vec{x} - \vec{x}_i)\right]\; \delta_{t_1, t - t_i} \tag{6.23}$$

Using

$$\sum_x D^c(y, x)\, S^c(x, z) = \; \delta_{y,z} \tag{6.24}$$

the *sequential propagator* $\Sigma_{cs}(x, x_i; t_2, \vec{p}_f)$ satisfies the relation

$$\sum_x D^c(y,x)\Sigma_{cs}(x,x_i;t_2,\vec{p}_f) = \gamma_5\, S^s(y,x_i)\, e^{-i\vec{p}_f\cdot(\vec{y}-\vec{x}_i)}\, \delta_{t_2,t_f-t_i} \tag{6.25}$$

Thus to get the *sequential propagator* $\Sigma_{cs}(x, x_i; t_2, \vec{p}_f)$, the heavy-quark Dirac operator is inverted on the "*sequential source*", $\gamma_5\, S^s(y, x_i)\, e^{-i\vec{p}_f\cdot(\vec{y}-\vec{x}_i)}\, \delta_{t_2,t_f-t_i}$.

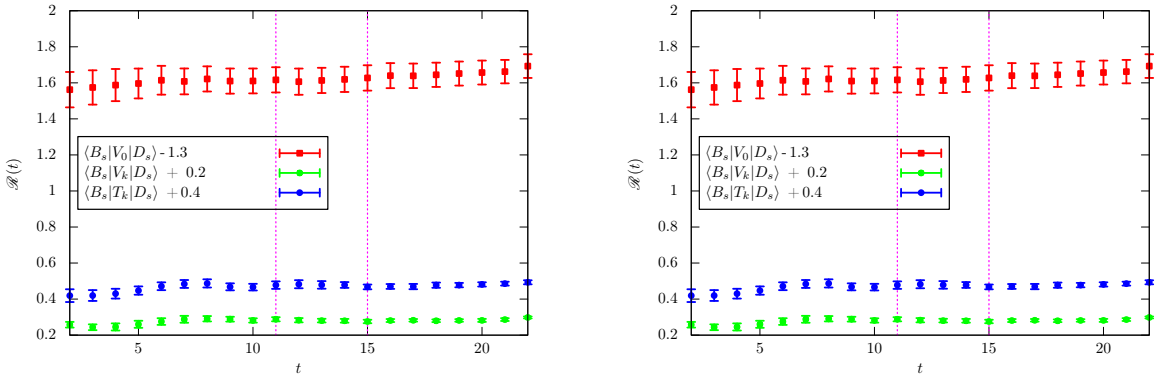
The goal now is to extract the matrix elements from the already computed three-point correlation functions. From the asymptotic behavior of the three-point correlation function, it is clear that the removal of the exponential factors can be achieved by considering the ratio

$$\boxed{\mathscr{R}(t) = \frac{\mathscr{C}^{(3)}(t,t_i,t_f,\vec{p}_i,\vec{p}_f)}{\mathscr{C}^{(2)}_{(B_s)}(t-t_i,\vec{p}_f)\cdot\mathscr{C}^{(2)}_{(D_s)}(t_f-t,\vec{p}_i)}\cdot\mathscr{Z}_{B_s}\cdot\mathscr{Z}_{D_s}} \tag{6.26}$$

where $\mathscr{Z}_M = |\langle 0|\mathscr{O}_M|M\rangle|$ is obtained from the fit with asymptotic behavior of the two-point correlation functions

$$\mathscr{C}^{(2)}(t) \xrightarrow[t\to\infty]{} \frac{\mathscr{Z}^2_{B_s,D_s}}{E_{B_s,D_s}}\, \cosh\left(E_{B_s,D_s}\left[\frac{T}{2}-t\right]\right)\, e^{-E_{B_s,D_s}\frac{T}{2}} \tag{6.27}$$

When the operators in the ratio (6.26) are sufficiently separated in time, one observes a stable signal



(a) (b)

Figure 6.3: Example of the plateaus for the $B_s \to D_s$ transition amplitudes, leading to the determination of the relevant form factors, at two different gauge couplings: (a) vector (V_0 is represented by ● and V_k by ●) and tensor (●) hadronic matrix elements corresponding to $\beta = 3.90$, $a\mu_h = 0.4114$, $a\mu_l = 0.0085$. (b) vector and tensor matrix elements corresponding to $\beta = 4.20$, $a\mu_h = 0.3525$, $a\mu_l = 0.0065$.

(plateau) which is the desired hadronic matrix element

$$\mathscr{R}(t) \xrightarrow[t-t_i\to\infty]{t_f-t\to\infty} \langle D_{s(\vec{p}_f)}|J_\mu|B_{s(\vec{p}_i)}\rangle$$

In this work, the two-point functions entering the ratio of Eq. (6.26) are described by their analytic

expressions and that is why *analytical ratios* are used in the extraction of $B_s \to D_s$ form factors. The quality of the plateaus can be inferred from Fig. 6.3 which shows the hadronic transition amplitudes determined from smeared-smeared two- and three-point correlators for two different gauge ensembles. For clarity, the data points have been shifted as indicated in the label of the plot. For $\beta = 3.9$, the plateaus could be found in the time interval $[11, 15]$ and for $\beta = 4.20$ the time range lies between $t = 16$ and $t = 22$.

6.2 Determination of $\mathscr{G}_s(1)$

In the limit of vanishing lepton mass, the semileptonic decay rate of $B_s \to D_s$ transitions is expressed in terms of a function $\mathscr{G}_s^{(B_s \to D_s)}(w)$. Although the shape of $|V_{cb}|\mathscr{G}(w)$ is experimentally well-determined, lattice input is needed to extract $|V_{cb}|$ (the zero recoil point $\mathscr{G}(1)$ or the Isgur-Wise point). Let us define the form factors in this (HQET inspired) way

$$\frac{1}{\sqrt{m_{B_s} m_{D_s}}} \langle D_s(v_{D_s})|V_\mu|B_s(v_{B_s})\rangle = (v_{B_s} + v_{D_s})_\mu\, h_+(w) + (v_{B_s} - v_{D_s})_\mu\, h_-(w) \tag{6.28}$$

where $v_{B_s} = p_{B_s}/m_{B_s}$, $v_{D_s} = p_{D_s}/m_{D_s}$, and $w = (m_{B_s}^2 + m_{D_s}^2 - q^2)/(2m_{B_s}m_{D_s})$. By comparing Eqs. (6.2) and (6.28), one gets

$$\begin{cases} F_+(q^2) &= \dfrac{m_{B_s} + m_{D_s}}{\sqrt{4 m_{B_s} m_{D_s}}}\, h_+(w) \left[1 - \dfrac{m_{B_s} - m_{D_s}}{m_{B_s} + m_{D_s}}\, \dfrac{h_-(w)}{h_+(w)}\right] \\ F_0(q^2) &= \dfrac{\sqrt{m_{B_s} m_{D_s}}}{m_{B_s} + m_{D_s}}\, (w+1)\, h_+(w) \left[1 - \dfrac{m_{B_s} + m_{D_s}}{m_{B_s} - m_{D_s}}\, \dfrac{w-1}{w+1}\, \dfrac{h_-(w)}{h_+(w)}\right] \end{cases} \tag{6.29}$$

The above-mentioned function $\mathscr{G}_s(w)$ is proportional to $F_+(q^2)$; it is defined by

$$\mathscr{G}(w) = h_+(w)\,[1 - \ H(w)] \tag{6.30}$$

where, for shortness, we introduced the dimensionless ratio

$$H(w) = \frac{m_{B_s} - m_{D_s}}{m_{B_s} + m_{D_s}}\, \frac{h_-(w)}{h_+(w)} \tag{6.31}$$

The dominant term at $w = 1$ is $h_+(1)$, which can be obtained from $F_0(q^2_{\rm max})$

$$h_+(1) = \ \frac{m_{B_s} + m_{D_s}}{\sqrt{4 m_{B_s} m_{D_s}}}\, F_0(q^2_{\rm max}) \tag{6.32}$$

Unfortunately, $H(1)$ is not directly accessible from the lattice at zero-recoil. Instead we need to compute the form factors $F_{0,+}(q^2)$ at few small recoil momenta and then extrapolate to $w = 1$. At $w \neq 1$, it is convenient to work with the ratio of two form factors and to express it in terms of $H(w)$ by using Eqs. (6.29)

$$Y(q^2) \equiv \frac{F_+(q^2)}{F_0(q^2)} = \frac{(m_{B_s} + m_{D_s})^2 - H(w)(m_{B_s} - m_{D_s})^2}{2 m_{B_s} m_{D_s}\,[w + 1 - H(w)(w-1)]} \tag{6.33}$$

from which it is easy to get

$$H(w) = \frac{1 - \dfrac{2m_{B_s}m_{D_s}}{(m_{B_s}+m_{D_s})^2}\left[(w+1)Y(q^2)\right]}{1 - \dfrac{2m_{B_s}m_{D_s}}{(m_{B_s}-m_{D_s})^2}\left[(w-1)Y(q^2)\right]} \tag{6.34}$$

It is therefore sufficient to compute the ratio $Y(q^2)$ for a few $\theta \neq 0$, and then extrapolate the function $H(w)$ towards $H(1)$. If we write

$$H(w) = \alpha + \beta w + \gamma w^2 + \cdots \tag{6.35}$$

then we can get α, β from the fit with our data, and then easily obtain $H(1)$, which is finally combined with the result from Eq. (6.32) to compute

$$\mathscr{G}_s(1) = h_+(1)\,[1 - H(1)] \tag{6.36}$$

for each gauge ensemble and for all light quark masses.

6.2.1 The extrapolation strategy

Since the numerical lattice data that we have are obtained with the strange valence light quark, it is sufficient to determine $\mathscr{G}_s(1)$ for all gauge ensembles and then extrapolate to the continuum limit and to the physical sea quark mass, by fitting with a simple linear function of $m_l^{\rm sea}$ and a^2

$$\mathscr{G}_s^{\rm latt}(1) = \alpha_s + \beta_s \frac{m_l^{\rm sea}}{m_s} + \gamma_s \frac{a^2}{a_{3.9}^2} \tag{6.37}$$

This quantity is calculated for all the fixed values of heavy quark masses we considered in our simulation, which range from the charm region up to the b quark mass. This allows to extrapolate to the physical bottom mass by means of the "ratio method" [126] which was first applied in a calculation of the b quark mass and the decay constants f_B and f_{B_s}. Let us describe the method.

6.2.2 The ratio method

The method that we have used to determine $\mathscr{G}_s(1)$ is suggested by the HQET asymptotic behavior of $\mathscr{G}_s(1)$

$$\lim_{m_h\to\infty} \mathscr{G}_s(1) = \text{constant} \tag{6.38}$$

where m_h is the heavy quark mass.
As a first step, we consider an appropriate sequence of heavy quark masses

$$m_h^{(i)} \qquad i \in \{0, \cdots, 9\} \tag{6.39}$$

with fixed ratios

$$\frac{m_h^{(i+1)}}{m_h^{(i)}} = \lambda \simeq 1.17 \tag{6.40}$$

and ranging from

$$m_c \leq m_h^{(i)} \leq m_b \tag{6.41}$$

where m_c (m_b) corresponds to the physical charm (beauty) quark mass given in the $\overline{\rm MS}$ scheme at a renormalization scale of 2 GeV .
Then one computes the ratios at two subsequent values of the heavy quark mass

$$\Sigma_{(i)}(1, m_h^{(i)}, a^2, m_l^{\rm sea}) = \frac{\mathscr{G}_s(1,\, a^2,\, m_h^{(i+1)},\, m_l^{\rm sea})}{\mathscr{G}_s(1,\, a^2,\, m_h^{(i)},\, m_l^{\rm sea})} \tag{6.42}$$

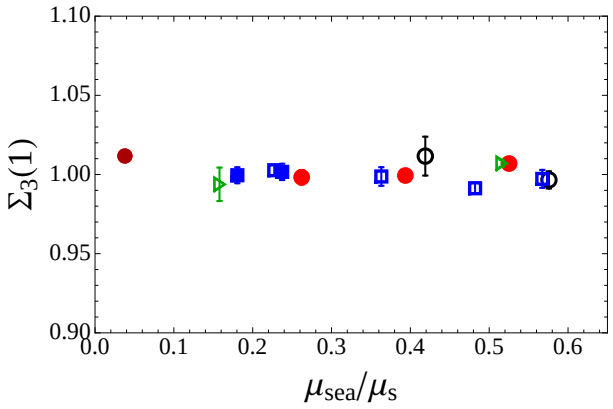


Figure 6.4: Values of Σ_3 as obtained on all of the lattice configurations used in this work and shown as a function of μ_l^{sea}/μ_s. Various symbols are used to distinguish the lattice data obtained at different lattice spacings: ○ for $\beta = 3.80$, □ for $\beta = 3.90$ (24^3), ■ for $\beta = 3.90$ (32^3), ● for $\beta = 4.05$, and ▷ for $\beta = 4.20$. The result of the continuum extrapolation is also indicated at the point corresponding to the physical $\mu_{ud}/\mu_s \equiv m_{ud}/m_s = 0.037(1)$.

The resulting ratio provides a strong cancellation of statistical errors and its values are very accurate. We show in Fig. 6.4 the values of Σ_3 obtained for all the lattice configurations used, as a function of the light sea quark mass divided by the physical strange quark mass.

From Eq. (6.38), it follows that the ratios (6.42) have the following static limit

$$\lim_{m_h\to\infty} \left(\lim_{\substack{m_l^{\rm sea}\to m_{ud} \\ a\to 0}} \Sigma_{(i)}(1, m_h^{(i)}, a^2, m_l^{\rm sea}) \right) \stackrel{\rm def.}{=} \lim_{m_h\to\infty} \sigma^{(i)}(1, m_h^{(i)}) = 1 \tag{6.43}$$

where m_{ud} stands for the average of the physical up and down quark masses ($m_{ud} = (m_u + m_d)/2$) computed on the same lattices [2].

We extrapolate the ratios defined in Eq. (6.42) to the continuum limit according to

$$\Sigma_{(i)}(1, m_h^{(i)}, a^2, m_l^{\rm sea}) \;=\; \alpha_s^{(i)} + \beta_s^{(i)}\,\frac{m_l^{\rm sea}}{m_s} + \gamma_s^{(i)}\,\frac{a^2}{a_{3.9}^2} \tag{6.44}$$

As anticipated from Fig.6.4 the values of $\beta_s^{(i)}$ and $\gamma_s^{(i)}$, as obtained from the fit of our data to Eq. (6.44), are consistent with zero. We observe that the ratios $\sigma^{(i)}$ do not show any significant dependence on the light sea quark mass $m_l^{\rm sea}$: this implies that the value of $\beta_s^{(i)}$ in the fit (6.44) is compatible with zero. We checked the results obtained by imposing $\beta_s^{(i)} = 0$: the result for the ratios $\sigma^{(i)}$ remains practically the same for the first heavy quark masses and compatible within the error bars for the heaviest ones. In Table 6.2.2, we present the values of $\sigma^{(i)}$ for different heavy quark masses. We see that for larger heavy quark masses ($m_h^{(9)} = m_b$ and $m_h^{(8)} = m_b/\lambda$), the continuum value of $\sigma^{(i)}$ will have a larger error. Also, the errors on the form factor obtained at $m_h^{(7)} = m_b/\lambda^2$ are large but they do not alter the convergence of the ratios $\sigma^{(i)}$ to the known static limit (infinite quark mass), equal to 1, as can be seen from Fig. 6.5.

$1/m_h^{(i)}$ [GeV]	$\sigma^{(i)}(m_h)_{(\beta_s^{(i)}\neq 0)}$	$\sigma^{(i)}(m_h)_{(\beta_s^{(i)}\neq 0)}$
$1/m_h^{(1)}$=0.739	0.996(2)	0.991 (1)
$1/m_h^{(2)}$=0.629	1.004(4)	1.007(2)
$1/m_h^{(3)}$=0.534	1.005(5)	1.008(2)
$1/m_h^{(4)}$=0.454	1.005(6)	1.006(2)
$1/m_h^{(5)}$=0.386	1.012(8)	1.013(2)
$1/m_h^{(6)}$=0.328	1.005(10)	1.013(5)
$1/m_h^{(7)}$=0.279	1.006(23)	1.019(6)
$1/m_h^{(8)}$=0.237	0.975(48)	1.022(11)
$1/m_h^{(9)}$=0.202	0.853(48)	1.060(31)

Table 6.3: The values of the ratio $\sigma^{(i)}$ extrapolated to the continuum limit using Eq. (6.44) for each heavy valence quark masses $m_h^{(i)} = \lambda^i\, m_c$. Results of extrapolation with $\beta_s^{(i)}$ as a free parameter are shown separately from those in which the observed independence on the sea quark mass is imposed in the fit (6.44) by setting $\beta_s^{(i)} = 0$.

Interpolation to the static limit

Let us recall that, instead of extrapolating $\mathscr{G}_s(1)$ in inverse heavy quark mass to the physical b mass, we interpolate the ratio $\sigma\,(1, m_h)$ to $\sigma\,(1, m_h = m_b)$ with $\lim\limits_{m_h\to\infty} \sigma\,(1, m_h) = 1$. In practice, after performing the continuum extrapolation of the ratios, we study their dependence on the inverse heavy quark mass. We perform a polynomial fit in $1/m_h$, of the form

$$\sigma\,(1, m_h) \;= 1 \,+\, \frac{s_1}{m_h} \,+\, \frac{s_2}{m_h^2} \tag{6.45}$$

which satisfies the constraint $\sigma = 1$ at the static point. The fit is illustrated in Fig. 6.5 using the extrapolated values $\sigma^{(i)}$ in the continuum. Note that the data points at different heavy quark masses converge to the exactly known static limit.

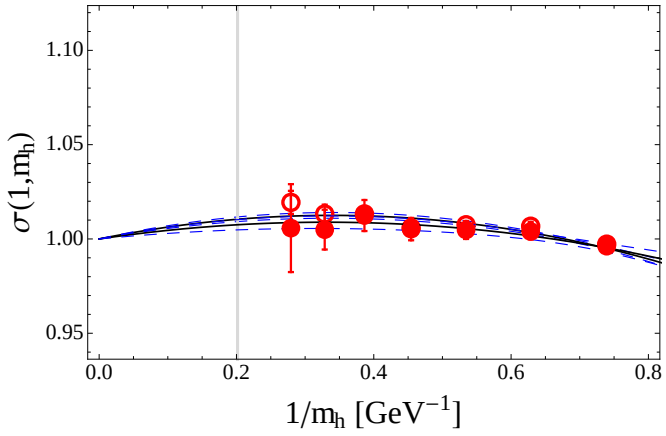


Figure 6.5: Heavy quark mass dependence of the ratio σ extrapolated to the physical value of the heavy quark mass and to the continuum limit. The vertical line represents the value of the inverse physical b quark mass. Filled symbols correspond to $\sigma(1, m_h)$ extrapolated to the continuum limit by using Eq. (6.37) with all parameters free, whereas the empty symbols refer to the results obtained by imposing $\beta_s = 0$.

The physically interesting value of $\mathscr{G}_s(1)$ is finally determined by considering the following equation

$$\mathscr{G}_s(1, m_h = m_b) \;=\; \mathscr{G}_s(1, m_h^{(0)} = m_c)\; \sigma^{(0)}\; \sigma^{(1)}\; \cdots\; \sigma^{(8)} \tag{6.46}$$

where $\sigma^{(i)}$ stands for $\sigma^{(i)}(1,\ \lambda^i m_c)$ and where the initial triggering value $\mathscr{G}_s(1, m_h^{(0)})$ corresponds to the elastic form factor of the $D_s \to D_s$ transitions. In the continuum, it is exactly equal to 1.
Note that we do not need to use the renormalization constant when starting with the elastic form factor at the charm point. We finally obtain

$$\mathscr{G}_s^{\text{phys.}}(1, m_b) \;= 1.052(46) \tag{6.47}$$

which is compatible with the previous lattice prediction for the $B \to D$ decay presented in Section 2.3. If we want to start from the computed $\mathscr{G}_s(1)$, in the continuum, at $m_h = \lambda^{(i)} m_c$ we will apply $\sigma_{i+1} \cdots \sigma_n$ in order to reach the sought value at the b-quark mass. For example, starting from $i = 3$, we get

$$\begin{aligned} \mathscr{G}_s(1, m_h = m_b) \;&=\; \mathscr{G}_s(1, m_h^{(3)} = \lambda^3 m_c)\; \sigma^{(4)}\; \sigma^{(5)}\; \cdots\; \sigma^{(8)} \\ &= 1.059(47) \end{aligned} \tag{6.48}$$

which is compatible with the result given in Eq. (6.47).

6.2.3 Systematic effects

The systematic error associated with the interpolation of the ratio $\sigma(1, m_h)$ as a function of $1/m_h$ can be determined by repeating the analysis and choosing a third order polynomial in $1/m_h$ (rather than a second order one as in (6.45)). This modification results in a decrease of $\mathscr{G}_s(1)$ for the $B_s \to D_s$ decay of about 0.005. The resulting value $\mathscr{G}_s(1) = 1.047(61)$ remains compatible with the value in Eq. (6.47).

The error of $\mathscr{G}_s(1)$ can be significantly reduced if we impose that $\mathscr{G}_s(1)$ does not depend on the mass of the dynamical sea quark, which is what we already observed in Fig. 6.5 with our data at four different lattice spacings. This leads to

$$\mathscr{G}_s(1) \ = 1.073(17) \tag{6.49}$$

Furthermore, although the finite volume effects are not expected to affect the quantities computed in this work, they could appear when the dynamical (sea) quark mass is lowered. In order to check for that effect, we can compare our results obtained on the ensembles with ($\beta = 3.9,\ V = 24^3 \times 48$) and with ($\beta = 3.9,\ V = 32^3 \times 64$) which differ in volume. The situation shown in Fig. 6.4 is a generic illustration of the situation we see with all the other quantities: the form factors are insensitive to a change of the lattice volume. All these checks suggest that our result (6.47) obtained by using $\beta_s^{(i)}$ as a free parameter, remains stable.

The above analysis at zero recoil can also be done at different non zero recoils. In what follows, we will present the determination of $\mathscr{G}_s(w)$.

6.2.4 $\mathscr{G}_s$ at non zero recoil

The analysis of $\mathscr{G}_s(w)$ at non-zero recoil is essentially the same as in the zero-recoil case described above. From the correlation functions (6.19) and by using the projector P_μ^+ (6.12) we get the form factor $F_+(q^2)$ which is proportional to the desired $\mathscr{G}(w, m_h^{(i)})$, cf. Eqs. (6.29) and (6.36). The observations made in the analysis of $\mathscr{G}_s(1)$ concerning the independence on the light sea quark mass and on the lattice spacing remain true after switching from $w = 1$ to $w > 1$.
The values are given in Table 6.4, where we again report our results both in the case where the parameter $\beta_s^{(i)}$ in the continuum extrapolation (6.44) is left free and in the case where $\beta_s^{(i)} = 0$ is imposed. The net effect in the latter case is that the resulting error is considerably smaller.

Using the parameterization of Ref. [127], which expresses $\mathscr{G}_s(w)$ in terms of its slope ρ^2

$$\frac{\mathscr{G}_s(w)}{\mathscr{G}_s(1)} = 1 - 8\rho^2 z + (51\rho^2 - 10)z^2 - (252\rho^2 - 84)z^3 \tag{6.50}$$

with $z = (\sqrt{w+1} - \sqrt{2})/(\sqrt{w+1} + \sqrt{2})$, we extract the slope ρ^2 from our data. Knowing that the window of "w"s we consider here is very narrow (6.7), a clean determination of ρ^2 would require very accurate values of $\mathscr{G}_s(w)$.
In our case, we obtain $\rho^2 = 1.2(8)$. In the case where we dismiss the dependence on the sea quark

w $\left(q^2_{B_s\to D_s}\right)$ [GeV^2]	$\mathscr{G}_s(w)_{\beta_s^{(i)}\neq 0}$	$\mathscr{G}_s(w)_{\beta_s^{(i)}=0}$
1. (11.54)	1.052(47)	1.073(17)
1.004 (11.46)	1.052(47)	1.075(16)
1.016 (11.20)	1.029(49)	1.063(15)
1.036 (10.79)	1.044(51)	1.034(17)
1.062 (10.23)	0.986(57)	1.004(20)

Table 6.4: Results for $\mathscr{G}_s(w)$, the dominant factor governing the hadronic matrix element relevant to $B_s \to D_s \ell \bar{\nu}_\ell$ ($\ell \in \{e, \mu\}$), computed at zero-recoil and at non-zero recoil.

mass (when the errors on $\mathscr{G}_s(w)$ are smaller) we get $\rho^2 = 1.1(3)$. These values are consistent with the experimentally established $\rho^2 = 1.19(4)(4)$ [30]. The same result for ρ^2 is obtained if the data are fit to [128]

$$\frac{\mathscr{G}_s(w)}{\mathscr{G}_s(1)} = \left(\frac{2}{1+w}\right)^{2\rho^2} \tag{6.51}$$

6.3 Semileptonic B decay to τ leptons and New Physics

The BaBar Collaboration has recently measured $\mathscr{B}(B \to D\tau\bar{\nu}_\tau)$ unveiling a discrepancy of about 2σ with respect to the SM estimate [4]. New Physics models can account for such a discrepancy

- either via an enhancement of the coefficient multiplying the scalar form factor in the decay amplitude (as can occur in models where a charged Higgs mediates the tree-level process, e.g. 2HDM);
- or by introducing a non zero coupling in which case an additional form factor appears in the amplitude.

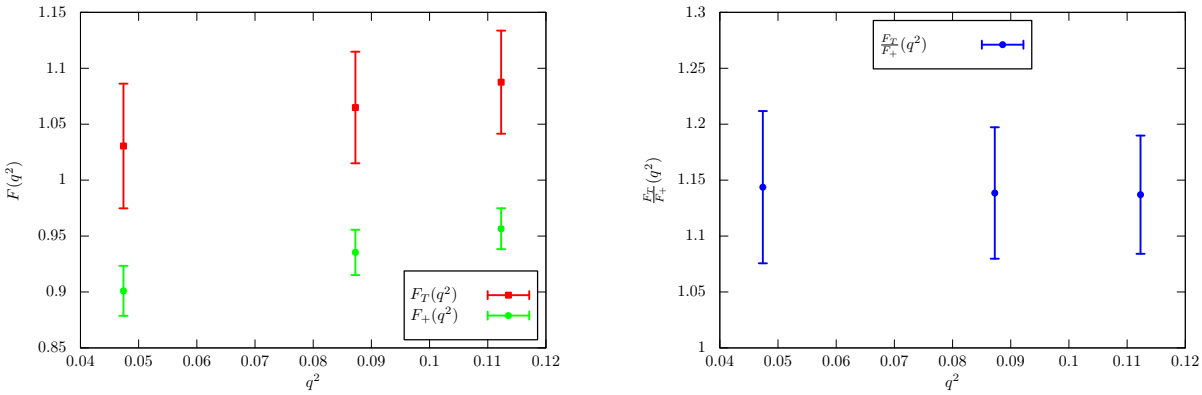
Since the contribution of the scalar form factor $F_0(q^2)$ is helicity suppressed in the SM, it should be more significant in the $B \to D\tau\bar{\nu}_\tau$ than in $B \to D\mu\bar{\nu}_\mu$. So, it is important to study it, as well as its tensor counterpart coming from the form factor $F_T(q^2)$, when considering NP scenarios.
Thus, in this section, we will focus on the determination, at different non zero recoils, of the ratios

$$\mathscr{R}_T(q^2) = \frac{F_T(q^2)}{F_+(q^2)} \quad \text{and} \quad \mathscr{R}_0(q^2) = \frac{F_0(q^2)}{F_+(q^2)} \tag{6.52}$$

which enter the differential decay rates of $B \to D$ process.

$\mathscr{R}_T(q^2)$

To our knowledge, the only existing result is the one of ref. [129] for the non-strange case ($B_{ud} \to D_{ud}\,\ell\,\bar{\nu}_\ell$) in which the constituent quark model was used. Their result for the ratio F_T/F_+ was 1.03(1) and, in their work, this ratio was predicted to be a constant with respect to the momentum transfer q^2 (or the recoil w).



(a) (b)

Figure 6.6: (a) The relevant form factors F_T and F_+ of $B_s \to D_s$ decay channel in lattice units at different non zero recoils corresponding to the ensemble $\beta = 3.9$, $a\mu_l = 0.0085$, $a\mu_h = 0.4114$. (b) The ratio F_T/F_+ in lattice units, as a function of q^2, obtained using the same ensemble.

Indeed, our lattice computations show this behavior, for example in Fig. 6.6(b). However, F_T has larger error bars than the vector and the scalar form factors, F_+ and F_0 (see Fig. 6.6(a)). We begin with the determination of suitable ratios at successive values of heavy quark masses, for a defined value of the recoil w and at all the lattice spacings we considered in our simulation

$$\Sigma^T_{(i)}(w, m_h^{(i)}, a^2, m_l^{\rm sea}) \;=\; \frac{\mathscr{R}_T(w,\, a^2,\, m_h^{(i+1)},\, m_l^{\rm sea})}{\mathscr{R}_T(w,\, a^2,\, m_h^{(i)},\, m_l^{\rm sea})} \tag{6.53}$$

The heavy quark behavior of $F_T(q^2)$ is similar to that of $F_+(q^2)$. Indeed, if we apply the heavy quark equation of motion to the b-quark

$$\frac{1+\not{v}}{2}\, b = b \tag{6.54}$$

which, in the b rest frame, reads $\gamma_0 b = b$. Then, in Eq. (6.13), $T_{0k} = \bar{c}\sigma_{0k}\, b = -i\bar{c}\gamma_k\, b$, so that the heavy quark behavior of the form factor $F_T(q^2)$ resembles that of $F_+(q^2)$.

Hence, in order to determine the physical values of $\mathscr{R}_T(q^2)$ near zero recoil, we follow the same strategy of extrapolation presented in Section 6.2.

We first need to extrapolate the ratios Σ^T as well as the variables $\mathscr{R}_T$ to the continuum limit by using a fit analogous to Eq. (6.37)

$$\Sigma^T_{(i)}(w, m_l^{\rm sea}, a^2) \;= \alpha_s^{(i)\prime}(w) + \beta_s^{(i)\prime}(w)\,\frac{m_l^{\rm sea}}{m_s} + \gamma_s^{(i)\prime}(w)\,\frac{a^2}{a^2_{3.9}} \tag{6.55}$$

thus assuming a linear dependence on the dynamical ("sea") quark mass and on the square of the lattice spacing. Since we work with maximally twisted QCD on the lattice, the leading discretization errors are proportional to a^2. We find again that our results depend very little on the lattice spacing and that the form factors (and their ratios) do not depend on the sea quark mass. For that reason we made the continuum extrapolation by imposing $\beta_s^{(i)\prime}(w) = 0$ and by leaving $\beta_s^{(i)\prime}(w)$ as a free parameter.

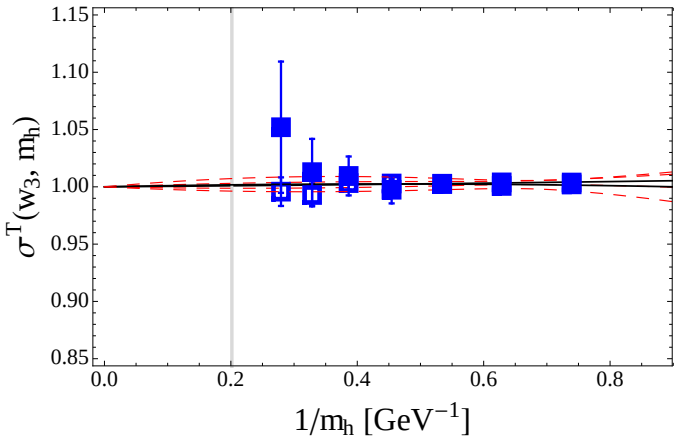


Figure 6.7: Ratio σ_T as a function of the inverse heavy quark mass. The vertical line represents the value of the inverse physical b quark mass. Filled symbols correspond to $\sigma_T(w, m_h)$ extrapolated to the continuum limit by using Eq. (6.55) with all parameters free, whereas the empty symbols refer to the results obtained by imposing $\beta_s^{(i)\prime} = 0$.

Using the extrapolated values in the continuum, $\sigma_T^{(i)}(w) \;=\; \sigma_T(w, m_h^{(i)})$ with $m_h = \lambda^i m_c$, we proceed to interpolate to the physical b quark mass according to

$$\sigma_T(w, m_h) \;=\; 1 \;+\; \frac{s_1'}{m_h} \;+\; \frac{s_2'}{m_h^2} \tag{6.56}$$

This interpolation is illustrated in Fig. 6.7.

Finally, we compute $\mathscr{R}_T(w, m_b)$ by considering the equation

$$\mathscr{R}_T(1, m_h = m_b) \;=\; \mathscr{R}_T(1, m_h^{(i)})\;\sigma_T^{(i)}\;\sigma_T^{(i+1)}\;\cdots\;\sigma_T^{(8)} \tag{6.57}$$

and taking $i = 3$. The main values at different momenta are collected in Table 6.5. These results are consistent with those obtained when taking $i = 2$ or 4.

w	$q^2_{B_s\to D_s}$ (GeV^2)	$\mathscr{R}_T(q^2)$ with $\beta_s^{(i)\prime} \neq 0$	$\mathscr{R}_T(q^2)$ with $\beta_s^{(i)\prime} = 0$
1.004	11.46	1.076(68)	1.078(43)
1.016	11.20	1.062(76)	1.064(49)
1.036	10.79	0.975(94)	0.997(64)
1.062	10.23	0.920(111)	1.004(76)

Table 6.5: Results for the ratios of F_T with respect to F_+ at different small recoils.

Notice that the error on $\mathscr{R}_T(q^2)$ increases when going to higher values of w. We are therefore unable to check the flatness of $\mathscr{R}_T(q^2)$ which occurs in the infinite mass limit.

$\mathscr{R}_0(q^2)$

We consider in this case various ratios of $\mathscr{R}_0$ at successive heavy quark masses, different lattice spacings and recoil w

$$\Sigma^0_{(i)}(w, m_h^{(i)}, a^2, m_l^{\rm sea}) \; = \frac{\mathscr{R}_0(w,\, a^2,\, m_h^{(i+1)},\, m_l^{\rm sea})}{\mathscr{R}_0(w,\, a^2,\, m_h^{(i)},\, m_l^{\rm sea})} \tag{6.58}$$

Then, in order to reach the continuum values $\sigma_0^{(i)}(w, m_h^{(i)})$ of $\Sigma^0_{(i)}(w, m_h^{(i)}, a^2, m_l^{\rm sea})$, we apply the continuum extrapolation using

$$\Sigma^0_{(i)}(w, m_l^{\rm sea}, a^2) \; = \alpha_s^{(i)\prime\prime}(w) + \beta_s^{(i)\prime\prime}(w)\, \frac{m_l^{\rm sea}}{m_s} + \gamma_s^{(i)\prime\prime}(w)\, \frac{a^2}{a^2_{3.9}} \tag{6.59}$$

After inspection, we found again that the dependence of the form factors on the sea quark mass is indiscernible in our data and that our results depend very mildly on the lattice spacing. Since the dependence on the sea quark mass is negligible, we again consider the continuum extrapolation by setting $\beta_s^{(i)\prime\prime}(w) = 0$, separately from the case in which $\beta_s^{(i)\prime\prime}(w)$ are left as free parameters. The net effect is that the error on $\sigma_0^{(i)}(w) = \Sigma^0_{(i)}(w, 0, 0)$ is considerably smaller in the case with $\beta_s^{(i)\prime\prime} = 0$ and the data better respect the heavy quark mass dependence.
Now we want to discuss the heavy quark interpolation. We consider the ratio of form factors $\mathscr{R}_0$ which depends mainly on m_{B_s,D_s} and on the ratio of form factors $\dfrac{h_-(w)}{h_+(w)}$. Using the HQET mass formula [130]

$$m_{B_s,D_s} = m_{b,c} + \overline{\Lambda} + (\lambda_1 + 3\lambda_2)/m_{b,c} \tag{6.60}$$

where λ_1, λ_2 and Λ are expressed in terms of hadronic matrix elements defined in the framework of HQET, and knowing that $h_+(w)$ scales as a constant with the inverse heavy quark mass, we deduce that, for the charm mass fixed to its physical value,

$$\mathscr{R}_0(w, m_h, m_c) \propto 1/m_h \tag{6.61}$$

Consequenty, we consider the ratio $\mathscr{R}'_0(w, m_h)$

$$\mathscr{R}'_0(w, m_h) = m_h\, \mathscr{R}_0(w, m_h) \tag{6.62}$$

which scales as a constant in the heavy quark mass limit. The corresponding σ' can then be described by a relation similar to Eq. (6.45) and $\mathscr{R}'_0(1, m_h = m_b)$ obtained by

$$\mathscr{R}'_0(1, m_h = m_b) \;= \mathscr{R}'_0(1, m_h^{(i)})\; \sigma_0^{'(i)}\; \sigma_0^{'(i+1)}\; \cdots\; \sigma_0^{'(8)} \tag{6.63}$$

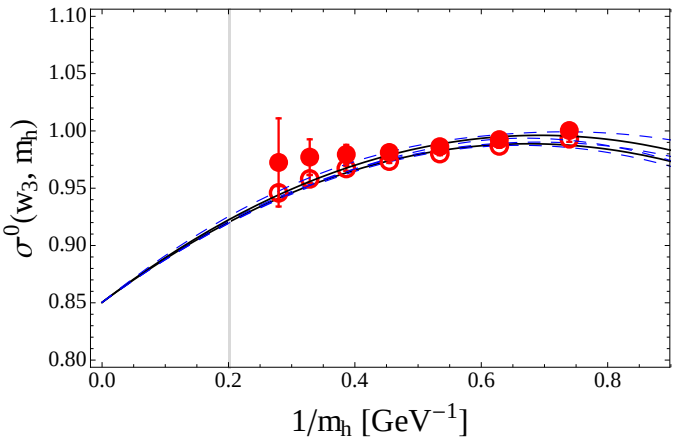


Figure 6.8: Fit of our data to Eq. (6.65). Empty symbols denote the results computed in the continuum by setting $\beta_s^{(i)\prime\prime} = 0$ in Eq. (6.59). Filled symbols are obtained after allowing $\beta_s^{(i)\prime\prime} \neq 0$. Plotted are the data with $w = w_3 = 1.016$. We see that the data obtained by assuming the independence of $\mathscr{R}_0$ on the sea quark scale is better with the heavy quark mass than the values obtained by letting the parameter $\beta_s^{(i)\prime\prime}$ to be free.

which is written in terms of $\mathscr{R}_0(w, m_h, m_c)$ as

$$\begin{aligned} \lambda^9 m_c\, \mathscr{R}_0(w, m_h = m_b) &= \sigma_0^{'(i)}\; \sigma_0^{'(i+1)}\; \cdots\; \sigma_0^{'(8)}\; \lambda^i m_c\, \mathscr{R}_0(w, \lambda^i m_c) \\ \Rightarrow \mathscr{R}_0(w, m_h = m_b) &= \underbrace{\lambda^{i-9}\; \sigma_0^{'(i)}\; \sigma_0^{'(i+1)}\; \cdots\; \sigma_0^{'(8)}}_{\sigma_0^{(i)}\; \sigma_0^{(i+1)}\; \cdots\; \sigma_0^{(8)}}\; \mathscr{R}_0(w, \lambda^i m_c) \end{aligned} \tag{6.64}$$

Therefore $\sigma_0 = \sigma'_0/\lambda$.
Hence, we perform the heavy quark interpolation using

$$\sigma_0(w, m_h) = \frac{1}{\lambda} + \frac{s''_1(w)}{m_h} + \frac{s''_2(w)}{m_h^2} \tag{6.65}$$

where we recall that $\lambda = 1.176$.
In Fig. 6.8, we illustrate the ratio σ_0 for one specific value of $w = 1.016$ showing the data obtained by assuming both the dependence and the independence of $\mathscr{R}_0(w)$ on the sea quark scale. We see that our results obtained by assuming the independence of $\mathscr{R}_0(w)$ on the sea quark scale respect better the heavy quark mass dependence than those obtained by letting the parameter $\beta_s^{(i)\prime\prime}$ in Eq. (6.59) free,

although both are compatible within the error bars.
The results obtained for $\mathscr{R}_0(q^2)$ are listed in Table 6.6.

w	$q^2_{B_s\to D_s}$ (GeV^2)	$\mathscr{R}_0(q^2)$ with $\beta_s^{(i)\prime\prime} \neq 0$	$\mathscr{R}_0(q^2)$ with $\beta_s^{(i)\prime\prime} = 0$
1.004	11.46	0.766(19)	0.752(7)
1.016	11.20	0.781(24)	0.757(9)
1.036	10.79	0.787(34)	0.760(16)
1.062	10.23	0.825(59)	0.761(34)

Table 6.6: Results for the ratios of $\mathscr{R}_0(q^2)$ at different non-zero recoils.

Knowing that the form factors satisfy the constraint $F_0(0) = F_+(0)$, one can then attempt to fit $\mathscr{R}_0(q^2)$ linearly in q^2

$$\mathscr{R}_0(q^2) \ = 1 - \ \alpha q^2 \tag{6.66}$$

From the results obtained with $\beta_s^{(i)\prime\prime}(w)$, we get $\alpha = 0.021(1)$ GeV^{-2}, while from the data with $\beta_s^{(i)\prime\prime}(w)$ free, α is equal to 0.020(1) GeV^{-2}. This is illustrated in Fig. 6.9. It is interesting to note that these

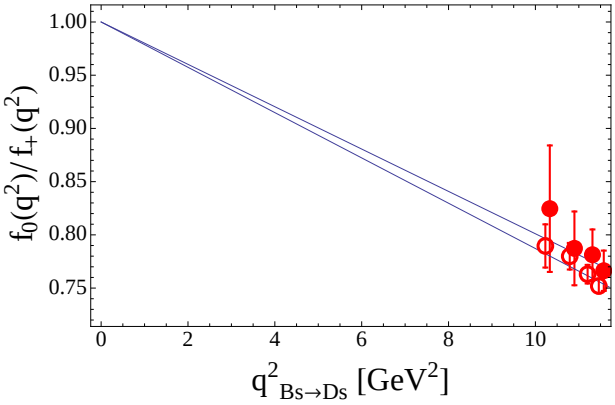


Figure 6.9: Results for $\mathscr{R}_0(q^2)$ presented in the case where $B_s \to D_s$ are linearly fit to the form $\mathscr{R}_0(q^2) = 1 - \alpha q^2$. The empty (filled) symbols correspond to the results obtained with $\beta_s^{(i)\prime\prime}(w) = 0$ ($\beta_s^{(i)\prime\prime} \neq 0$).

results are consistent with the values that can be obtained from the results quoted in recent works (in the non-strange case). More specifically, from the lattice results of Refs. [33, 34] one finds $\alpha = 0.020(1)$ GeV^{-2}, while from those reported in Ref. [131] one finds $\alpha = 0.022(1)$ GeV^{-2}. Recent QCD sum rule analyses give $\alpha = 0.021(2)$ GeV^{-2} [132, 133]. Note also that near zero recoil, the central value of our result ($\mathscr{R}_0(q^2) = 0.77(2)$), coincides with the quark model results of Refs. [129, 134].

Concluding remarks: we have computed the relevant form factors entering the semileptonic decay channel $B_s \to D_s$ near the zero-recoil limit using fully propagating heavy quarks and renormalization

constants, in a non-perturbative way. We applied a method which allows the interpolation to the physical b quark mass without doing any calculation in the static limit.

We first computed the normalization of the vector factor relevant to the extraction of the CKM matrix element $|V_{cb}|$ from $\mathscr{B}(B_s \to D_s \ell \bar{\nu}_\ell)$ with the light lepton $\ell \in \{e, \mu\}$ in the final state. We obtained

$$\mathscr{G}_s(1) \;=\; 1.052(46) \tag{6.67}$$

Then, we determined for the first time in LQCD the form factor $F_T(q^2)$ with respect to $F_+(q^2)$. In the $\overline{\text{MS}}$ renormalization scheme and at $\mu = m_b$ we obtained

$$\left.\frac{F_T(q^2)}{F_+(q^2)}\right|_{q^2=11.5\text{GeV}^2} = 1.08(7) \tag{6.68}$$

This allows a better constrained study of NP effects. Finally, we computed the ratio of the scalar to the vector form factors, $F_0(q^2)/F_+(q^2)$, required to interpret the recent discrepancy between the experimentally measured $\mathscr{B}(B \to D\tau\bar{\nu}_\tau)/\mathscr{B}(B \to D\mu\bar{\nu}_\mu)$ and its theoretical prediction within the SM (cf. Chapter 2). Of several considered recoils "w", we quote

$$\left.\frac{F_0(q^2)}{F_+(q^2)}\right|_{q^2=11.5\text{GeV}^2} = 0.77(2) \tag{6.69}$$

We observe that the errors on the above quantities can be significantly reduced if one imposes that the form factor ratios and the form factors themselves do not depend on the mass of the dynamical (sea) quark, which is essentially what we see at all values of the lattice spacing.
The above strategy could also be applied to the semileptonic $B \to D$ transitions with an additional chiral extrapolation.

Chapter 7

$B \to D^{**}\, \ell\, \bar{\nu}_\ell$ transitions using "real" charm quarks

Contents

7.1 The theoretical framework 112
7.1.1 Definition of the form factors 112
7.1.2 Extraction of the form factors 113
7.1.3 Decay rates 116
7.1.4 Strategy 116
7.2 Going to the lattice 116
7.2.1 The setup 116
7.2.2 Computing the meson energies 117
7.3 B transitions to the scalar D_0^* ($J^P = 0^+$) meson 122
7.3.1 Three-point correlators 122
7.3.2 Determination of $\frac{\mathscr{B}(B \to D_0^*)}{\mathscr{B}(B \to D)}$ at zero recoil 123
7.4 B decays to the tensor D_2^* state 129
7.4.1 Contribution of the form factors to the ${}^3P_2$ decay width 129
7.4.2 Extracting the $\tilde{k}$ form factor 130

Understanding the semileptonic decay of a B to a charm mesons is of key importance to control the theoretical error on the CKM matrix element V_{cb}. It turns out, however, that there is a discrepancy between the inclusive [1] and the exclusive [127] determination (based on $B \to D^{(*)}\, \ell\, \nu$, see Chapter 2) of this matrix element. The difference is of the order of $1.5\,\sigma$ [1].

A non-negligible part of the total width $\Gamma(B \to X_c \ell\, \nu_\ell)$ comes from excited states. It was recently argued that the radial excitation D' might be particularly favored [63–65]. Another group of states, that contributes to the width (around one quarter of it), is the orbital excitations, in other words, the positive parity charmed mesons D^{**}.
As mentioned in Chapter 2, these states are not well understood: indeed there is a persistent conflict between theory and experiment concerning the semileptonic branching ratios of $B \to D^{**} \ell \bar{\nu}_\ell$.
However, the main limitation of almost all theoretical results is that they are derived in the heavy quark limit. Since the heavy mass corrections might be large, before getting any definitive conclusion on the disagreement between theory and experiment, it is mandatory to study the impact of the corrections arising from the finiteness of the heavy quark mass.

In the following, we will focus on the determination of $B \to D^{**}\, \ell \bar{\nu}_\ell$ form factors: we begin with the theoretical background of the subject and then proceed to the lattice setup. Subsequently we address the transition amplitudes governing the $B \to D^{**}$ decay and discuss results of our LQCD calculations.

The results discussed in this chapter are the object of a forthcoming publication [135].

7.1 The theoretical framework

Our work is devoted to the calculation of the decay rates of B mesons into the $\left|{}^3P_0\right\rangle$ (scalar D_0^*) and the $\left|{}^3P_2\right\rangle$ (tensor D_2^*) states[1].
Since the form factors enter the decay rates, we will start by describing the strategy used to determine explicitly the expressions of the $B \to\ D_0^*(D_2^*)$ form factors.

7.1.1 Definition of the form factors

This type of calculation requires the knowledge of the $B \to D_0^*$ (D_2^*) transition amplitudes which in turn are described using six form factors [136]

[1] We use the $\left|{}^{2S+1}L_J\right\rangle$ notation of the states, where S is the spin angular momentum, $L = 1$ the orbital angular momentum and $J = L + S$ the total angular momentum of the D^{**} state.

$^3P_2$ *state*

$$\begin{aligned}
\left\langle {}^3P_2\big(p_{D_2^*},\,\varepsilon(p_{D_2^*},\,\lambda)\big)\,\middle|\,V_\mu\,\middle|\,B(p_B)\right\rangle \;&=\; i\,\boxed{\tilde{h}}\,\epsilon_{\mu\nu\lambda\rho}\,\varepsilon^{*\nu\alpha}_{(p_{D_2^*})}\,p_{B\,\alpha}\,(p_B+p_{D_2^*})^\lambda\,(p_B-p_{D_2^*})^\rho \\
\left\langle {}^3P_2\big(p_{D_2^*},\,\varepsilon(p_{D_2^*},\,\lambda)\big)\,\middle|\,A_\mu\,\middle|\,B(p_B)\right\rangle &= \boxed{\tilde{k}}\,\varepsilon^{(p_{D_2^*})}_{\mu\nu}\,p_B{}^\nu \\
&\quad+\left(\varepsilon^{(p_{D_2^*})}_{\alpha\beta}\,p_B{}^\alpha p_B{}^\beta\right)\left[\boxed{\tilde{b}_+}\,(p_B+p_{D_2^*})_\mu+\boxed{\tilde{b}_-}\,(p_B-p_{D_2^*})_\mu\right]
\end{aligned} \tag{7.1}$$

In the above equations, $\varepsilon(p_{D_2^*},\,\lambda)$ is the polarization tensor of the $^3P_2$ state (λ being the projection of the $J=2$ total angular momentum along some quantification axis), V_μ denotes the vector current $\bar{c}\gamma_\mu b$ and A_μ stands for the axial current $\bar{c}\gamma_\mu\gamma_5 b$.

$^3P_0$ *state*

$$\begin{aligned}
\left\langle {}^3P_0(p_{D_0^*})\,\middle|\,V_\mu\,\middle|\,B(p_B)\right\rangle &= 0 \\
\left\langle {}^3P_0(p_{D_0^*})\,\middle|\,A_\mu\,\middle|\,B(p_B)\right\rangle &= \boxed{\tilde{u}_+}\,(p_B+p_{D_0^*})_\mu+\boxed{\tilde{u}_-}\,(p_B-p_{D_0^*})_\mu
\end{aligned} \tag{7.2}$$

The chosen normalization of the mesonic states is

$$\left\langle M\big(p'\big)\,\middle|\,M\big(p\big)\right\rangle \;=\; (2\pi)^3\,2E\,\delta^3(\vec{p}\,'-\vec{p}) \tag{7.3}$$

7.1.2 Extraction of the form factors

In order to calculate the semileptonic decay rates of the B to a D^{**}, one needs the momentum dependence of the form factors. On the lattice, the transition amplitudes can be determined at different momenta so that we are able to extract the corresponding form factors.
For practical convenience, we will work in the rest frame of the D^{**} meson and the B meson will carry a momentum having symmetric spatial components

$$p_{D^{**}} = (m_{D^{**}},\,\vec{0}) \qquad\qquad \text{and} \qquad\qquad p_B^\mu = (E_B,\,p,\,p,\,p)$$

Such kinematics greatly simplifies the expressions of the interpolating fields when we consider a fully propagating "charm" quark.

We proceed to implement the chosen kinematics to get the expressions of the form factors from the hadronic matrix elements.

$^3P_0$ form factors
We adopt the following notation

$$\mathscr{T}_\mu^A \overset{\text{def.}}{=} \left\langle {}^3P_0\,\middle|\,A_\mu\,\middle|\,B(p_B)\right\rangle$$

to represent the axial transition amplitude into the ${}^3P_0$ state. We explicitely get

$$\begin{cases} \mathscr{T}_0^A = \boxed{\tilde{u}_+}\,(E_B + m_{D^{**}}) + \boxed{\tilde{u}_-}\,(E_B - m_{D^{**}}) \\ \mathscr{T}_i^A = \boxed{\tilde{u}_+}\,p + \boxed{\tilde{u}_-}\,p \end{cases} \tag{7.4}$$

and so it is straightforward to express $\tilde{u}_+$ and $\tilde{u}_-$ in terms of $\mathscr{T}_\mu^A$s as follows

$$\begin{cases} \tilde{u}_+ = -\dfrac{1}{2\,m_{D^{**}}}\left[\dfrac{E_B - m_{D^{**}}}{p}\,\mathscr{T}_i^A - \mathscr{T}_0^A\right] = -\dfrac{1}{2\,m_{D^{**}}}\left[\dfrac{E_B - m_{D^{**}}}{3\,p}(\mathscr{T}_1^A + \mathscr{T}_2^A + \mathscr{T}_3^A) - \mathscr{T}_0^A\right] \\ \tilde{u}_- = \dfrac{1}{2\,m_{D^{**}}}\left[\dfrac{E_B + m_{D^{**}}}{p}\,\mathscr{T}_i^A - \mathscr{T}_0^A\right] = \dfrac{1}{2\,m_{D^{**}}}\left[\dfrac{E_B + m_{D^{**}}}{3\,p}(\mathscr{T}_1^A + \mathscr{T}_2^A + \mathscr{T}_3^A) - \mathscr{T}_0^A\right] \end{cases} \tag{7.5}$$

${}^3P_2$ form factors

To represent the axial and the vector transitions of the B meson into the ${}^3P_2$ state, we will use the notation

$$\mathscr{T}_{\mu(\lambda)}^A \overset{\text{def.}}{=} \big\langle {}^3P_2(\lambda)\,\big|\,A_\mu\,\big|\,B(p_B)\big\rangle \qquad \text{and} \qquad \mathscr{T}_{\mu(\lambda)}^V \overset{\text{def.}}{=} \big\langle {}^3P_2(\lambda)\,\big|\,V_\mu\,\big|\,B(p_B)\big\rangle \tag{7.6}$$

The strategy we follow in order to extract the corresponding form factors is described in Appendix C. In the following, we give some relevant expressions for the $\tilde{k}$, $\tilde{b}_\pm$ and $\tilde{h}$ form factors

form factor $\tilde{k}$

$$\begin{aligned} \boxed{\tilde{k}} &= -\frac{\sqrt{6}}{p}\,\mathscr{T}_{1(0)}^A = -\frac{\sqrt{6}}{p}\,\mathscr{T}_{2(0)}^A = \frac{\sqrt{6}}{2\,p}\,\mathscr{T}_{3(0)}^A \\ &= \frac{1}{p}\left[\mathscr{T}_{1(+2)}^A + \mathscr{T}_{1(-2)}^A\right] = -\frac{1}{p}\left[\mathscr{T}_{2(+2)}^A + \mathscr{T}_{2(-2)}^A\right] \end{aligned} \tag{7.7}$$

form factors $\tilde{b}_+$ and $\tilde{b}_-$

$$\begin{cases} \boxed{\tilde{b}_+} = -\dfrac{1+i}{4}\,\dfrac{1}{p^3\,m_{D^{**}}}\Big[(E_B - m_{D^{**}})(i\,\mathscr{T}_{1(+2)}^A + \mathscr{T}_{2(+2)}^A) - p(1+i)\mathscr{T}_{0(+2)}^A\Big] \\ \boxed{\tilde{b}_-} = \dfrac{1+i}{4}\,\dfrac{1}{p^3\,m_{D^{**}}}\Big[(E_B + m_{D^{**}})(i\,\mathscr{T}_{1(+2)}^A + \mathscr{T}_{2(+2)}^A) - p(1+i)\mathscr{T}_{0(+2)}^A\Big] \end{cases} \tag{7.8}$$

$$\begin{cases} \boxed{\tilde{b}_+} = \dfrac{1-i}{4}\,\dfrac{1}{p^3\,m_{D^{**}}}\Big[(E_B - m_{D^{**}})(i\,\mathscr{T}_{1(-2)}^A - \mathscr{T}_{2(-2)}^A) + p(1-i)\mathscr{T}_{0(-2)}^A\Big] \\ \boxed{\tilde{b}_-} = -\dfrac{1-i}{4}\,\dfrac{1}{p^3\,m_{D^{**}}}\Big[(E_B + m_{D^{**}})(i\,\mathscr{T}_{1(-2)}^A - \mathscr{T}_{2(-2)}^A) + p(1-i)\mathscr{T}_{0(-2)}^A\Big] \end{cases} \tag{7.9}$$

$$\begin{cases} \boxed{\tilde{b}_+} = \dfrac{1+i}{4}\,\dfrac{1}{p^3\,m_{D^{**}}}\Big[(E_B - m_{D^{**}})(\mathscr{T}^A_{1(+1)} + \mathscr{T}^A_{2(+1)} - \mathscr{T}^A_{3(+1)}) - p\,\mathscr{T}^A_{0(+1)}\Big] \\ \boxed{\tilde{b}_-} = -\dfrac{1+i}{4}\,\dfrac{1}{p^3\,m_{D^{**}}}\Big[(E_B + m_{D^{**}})(\mathscr{T}^A_{1(+1)} + \mathscr{T}^A_{2(+1)} - \mathscr{T}^A_{3(+1)}) - p\,\mathscr{T}^A_{0(+1)}\Big] \end{cases} \tag{7.10}$$

$$\begin{cases} \boxed{\tilde{b}_+} = -\dfrac{1-i}{4}\,\dfrac{1}{p^3\,m_{D^{**}}}\Big[(E_B - m_{D^{**}})(\mathscr{T}^A_{1(-1)} + \mathscr{T}^A_{2(-1)} - \mathscr{T}^A_{3(-1)}) - p\,\mathscr{T}^A_{0(-1)}\Big] \\ \boxed{\tilde{b}_-} = \dfrac{1-i}{4}\,\dfrac{1}{p^3\,m_{D^{**}}}\Big[(E_B + m_{D^{**}})(\mathscr{T}^A_{1(-1)} + \mathscr{T}^A_{2(-1)} - \mathscr{T}^A_{3(-1)}) - p\,\mathscr{T}^A_{0(-1)}\Big] \end{cases} \tag{7.11}$$

$$\begin{cases} \boxed{\tilde{b}_+} = \dfrac{1}{2\,i}\,\dfrac{1}{p^3\,m_{D^{**}}}\Big[(E_B - m_{D^{**}})\mathscr{T}^A_{3(+2)} - p\,\mathscr{T}^A_{0(+2)}\Big] \\ \boxed{\tilde{b}_-} = \dfrac{1}{2\,i}\,\dfrac{1}{p^3\,m_{D^{**}}}\Big[-(E_B + m_{D^{**}})\mathscr{T}^A_{3(+2)} + p\,\mathscr{T}^A_{0(+2)}\Big] \end{cases} \tag{7.12}$$

<u>form factor $\tilde{h}$</u>

$$\begin{aligned} \boxed{\tilde{h}} \;&=\; \frac{1}{2\,i}\,\frac{1}{p\,m_{D^{**}}}\,\frac{\mathscr{T}^V_{1(\lambda)}}{\varepsilon^{*3\alpha}_{(\lambda)}\,p_{B\alpha} - \varepsilon^{*2\alpha}_{(\lambda)}\,p_{B\alpha}} \\ &=\; \frac{1}{2\,i}\,\frac{1}{p\,m_{D^{**}}}\,\frac{\mathscr{T}^V_{2(\lambda)}}{\varepsilon^{*1\alpha}_{(\lambda)}\,p_{B\alpha} - \varepsilon^{*3\alpha}_{(\lambda)}\,p_{B\alpha}} \;=\; -\frac{1}{2\,i}\,\frac{1}{p\,m_{D^{**}}}\,\frac{\mathscr{T}^V_{3(\lambda)}}{\varepsilon^{*2\alpha}_{(\lambda)}\,p_{B\alpha} - \varepsilon^{*1\alpha}_{(\lambda)}\,p_{B\alpha}} \end{aligned} \tag{7.13}$$

where the values of the terms $\varepsilon^{*3\alpha}_{(\lambda)}\,p_{B\alpha} - \varepsilon^{*2\alpha}_{(\lambda)}\,p_{B\alpha}$, $\varepsilon^{*1\alpha}_{(\lambda)}\,p_{B\alpha} - \varepsilon^{*3\alpha}_{(\lambda)}\,p_{B\alpha}$ and $\varepsilon^{*2\alpha}_{(\lambda)}\,p_{B\alpha} - \varepsilon^{*1\alpha}_{(\lambda)}\,p_{B\alpha}$ are collected in the following table for each value of λ.

$\boldsymbol{\lambda}$	$\boldsymbol{\varepsilon^{*3\alpha}_{(\lambda)}\,p_{B\alpha} - \varepsilon^{*2\alpha}_{(\lambda)}\,p_{B\alpha}}$	$\boldsymbol{\varepsilon^{*1\alpha}_{(\lambda)}\,p_{B\alpha} - \varepsilon^{*3\alpha}_{(\lambda)}\,p_{B\alpha}}$	$\boldsymbol{\varepsilon^{*2\alpha}_{(\lambda)}\,p_{B\alpha} - \varepsilon^{*1\alpha}_{(\lambda)}\,p_{B\alpha}}$
+2	$-\dfrac{p}{2}(1+i)$	$-\dfrac{p}{2}(1-i)$	p
+1	$\dfrac{p}{2}$	$i\,\dfrac{p}{2}$	$-\dfrac{p}{2}(1+i)$
0	$-\,p\sqrt{\dfrac{3}{2}}$	$p\sqrt{\dfrac{3}{2}}$	0
-1	$-\dfrac{p}{2}$	$i\,\dfrac{p}{2}$	$\dfrac{p}{2}(1-i)$
-2	$-\dfrac{p}{2}(1-i)$	$-\dfrac{p}{2}(1+i)$	p

7.1.3 Decay rates

Our ultimate goal is to determine the decay widths of $B \to D^{**}\, \ell\bar{\nu}_\ell$ processes which have the general expression

$$\mathrm{d}\Gamma(B \to D^{**}\, \ell\, \bar{\nu}) = \frac{1}{2\, E_{_B}}\, |\bar{\mathscr{M}}|^2\, \mathrm{d}\Phi \tag{7.14}$$

with
$$\begin{cases} \mathrm{d}\Phi = \dfrac{d^3\vec{p}_{_{D^{**}}}}{(2\pi)^3\, 2E_{_{D^{**}}}}\, \dfrac{d^3\vec{p}_{_\ell}}{(2\pi)^3\, 2E_{_\ell}}\, \dfrac{d^3\vec{p}_{_\nu}}{(2\pi)^3\, 2E_{_\nu}}\, (2\pi)^4\, \delta^{(4)}(p_{_B} - p_{_{D^{**}}} - p_{_\ell} - p_{_\nu}) \\ |\bar{\mathscr{M}}|^2 = \displaystyle\sum_{\mu,\,\nu} W_{\mu\nu}\ell^{\mu\nu} \end{cases}$$

where $W_{\mu\nu}$ denotes the hadronic tensor, $l^{\mu\nu}$ is the leptonic one and $\mathrm{d}\Phi$ is the phase space element. In Appendix D, we have evaluated Eq. (7.14) in terms of the $B \to D_0^*$ (D_2^*) form factors considering both massive and massless charged leptons in the final state.

7.1.4 Strategy

Once we have constructed all the theoretical background which allows us to calculate the form factors and the decay rates of the semileptonic $B \to D^{**}$ channels, the following strategy consists of

a) computing, on the lattice, the transition amplitudes for the $B \to D^{**}$ processes.

b) extracting the form factors from them.

c) using the formulae in Appendix D to obtain the decay widths.

7.2 Going to the lattice

We present here some parameters and techniques used in the lattice to compute the energies and transition amplitudes participating in the form factor computations.

7.2.1 The setup

This analysis involves two ensembles of gauge configurations already used in Chapter 6 ($\beta = 3.90$ and $\beta = 4.05$). The parameters of the simulations are collected in Table 7.1. In the valence sector, we add two doublets of charm and "bottom" quarks. Moreover, we implement θ-boundary conditions for the b doublet

$$\chi_b(x + L\hat{e}_i) = e^{i\theta L}\chi_b(x) \tag{7.15}$$

which gives the B-meson the momentum

$$|\vec{p}_B| \;=\; \frac{|\vec{\theta}|\pi}{L} \tag{7.16}$$

with the particular choice

$$\vec{\theta} = (\theta_0, \theta_0, \theta_0) \tag{7.17}$$

Then, we determine the values of the twisting angle θ_0 (for each of our lattices) corresponding to the following chosen values of w

$$w = \sqrt{1 + \frac{3\theta_0^2\pi^2}{m_B^2 L^2}} \in \{1,\ 1.025,\ 1.05,\ 1.1,\ 1.15,\ 1.2,\ 1.3\} \tag{7.18}$$

β	$L^3 \times T$	a[fm]	# cnfgs	$\mu_{sea} = \mu_l$	μ_c	μ_b	θ $[\pi/L]$
3.9	$24^3 \times 48$	0.085(3)	240	0.0085	0.215	0.3498	0.0, 0.99, 1.41 2.02, 2.50, 2.92 3.66
						0.4839	0.0,1.21,1.72 2.46, 3.05, 3.56 4.46
						0.6694	0.0,1.48,2.11 3.01, 3.73, 4.36 5.46
4.05	$32^3 \times 64$	0.069(2)	160	0.006	0.1849	0.3008	0.0,1.09,1.56 2.23, 2.76, 3.23 4.04
						0.4162	0.0,1.35,1.92 2.74, 3.40, 3.97 4.97
						0.5757	0.0,1.67,2.37 3.39, 4.21, 4.91 6.15

Table 7.1: Parameters of the simulations. The quantities $a\mu_\ell$, $a\mu_c$ and $a\mu_b$ stand for light, charm and heavy bare valence quark mass values respectively, expressed in lattice units. The lattice spacing $a_{\beta=3.9}$ is fixed by the matching of f_π obtained on the lattice to its experimental value [2] and $a_{\beta=4.05}$ is rescaled using the parameter $\Lambda_{\overline{\rm MS}}^{\rm N_f=2}$ [3].

7.2.2 Computing the meson energies

The charmed meson masses and the B meson energies are relevant parameters that enter the lattice determination of the transition amplitudes. Such quantities are extracted from the two-point correlation functions as explained in Chapter 5.

Two-point correlation function

In this work, we compute the quark propagators entering the correlation functions, by using *all-to-all* propagators with stochastic sources already discussed in Chapter 4. The "*one-end-trick*", which is in this case generalized to include θ-boundary conditions, consists in solving the Dirac equations

$$\sum_y D\big[f,\, r,\, \vec{\theta}\big]^{ab}_{\alpha\beta}(x,y)\; \phi\big[i,\, f,\, r,\, \vec{\theta},\, \tilde{\alpha},\, \tilde{t}\big]^{b}_{\beta}(y) \;=\; \eta[i]^{a}_{\alpha}(x)\; \delta_{\alpha\,\tilde{\alpha}}\; \delta_{t_x\,\tilde{t}} \tag{7.19}$$

where $r = \pm 1$ and f represents the fermion flavor.

To create an operator of higher orbital angular momentum (the tensor meson D_2^*), and to improve the overlap of the interpolating fields for the ground states, we use a "derivative" smearing function where we incorporate, in the smearing function S, a covariant derivative of the form

$$\nabla_i \equiv \frac{1}{2a}\Big[U_i(x) - U_i^\dagger(x-\hat{\imath})\Big] \tag{7.20}$$

The Dirac equation then reads

$$\sum_y D\big[f,\, r,\, \vec{\theta}\big]^{ab}_{\alpha\beta}(x,y)\; \phi\big[i,\, f,\, r,\, S,\, \vec{\theta},\, \tilde{\alpha},\, \tilde{t}\big]^{b}_{\beta}(y) \;=\; \big(S\,\eta[i]\big)^{a}_{\alpha}(x)\; \delta_{\alpha\tilde{\alpha}}\; \delta_{t_x\tilde{t}} \tag{7.21}$$

After determining the relevant propagators, we combine them to compute the "charged" B or D two-point correlators $\mathscr{C}^{(2)\,hl}_{\vec{\theta};S_1\,\Gamma_1;S_2,\Gamma_2}(t)$, which read [137]

$$\begin{aligned}
\mathscr{C}^{(2)\,hl}_{\vec{\theta};S_1\,\Gamma_1;S_2,\Gamma_2}(t) &= \frac{1}{2}\sum_{r=\pm1}\left\langle \mathrm{Tr}\sum_{\vec{x},\vec{y}} \Gamma_1\, \mathscr{S}_l^{S_1}(r;\,\vec{y},\,\tilde{t};\,\vec{x},\,\tilde{t}+t)\,\Gamma_2\, \mathscr{S}_h^{S_2}(-r;\,\vec{x},\,\tilde{t}+t;\,\vec{y},\,\tilde{t})\right\rangle \\
&= \frac{1}{2}\sum_{r=\pm1}\frac{1}{N}\sum_{n=1}^{N}\left\langle \mathrm{Tr}\left\{\sum_{\vec{x}}(\Gamma_1\gamma_5)_{\tilde{\alpha}\tilde{\beta}}\,\phi^*\big[n,\,l,\,r,\,S_1,\,\vec{0},\,\tilde{\beta},\,\tilde{t}\big]^{b}_{\alpha}(\vec{x},\tilde{t}+t)\right.\right. \\
&\qquad\left.\left.\times(\gamma_5\Gamma_2)_{\alpha\beta}(S_2\,\phi\big[n,\,h,\,r,\,\vec{\theta},\,\tilde{\alpha},\,\tilde{t}\big])^{b}_{\beta}(\vec{x},\tilde{t}+t)\right\}\right\rangle
\end{aligned} \tag{7.22}$$

where $\langle ... \rangle$ stands for the gauge ensemble average and $\mathscr{S}_l$ denotes the light quark propagator while $\mathscr{S}_h$ (where $h \equiv c$ or b) is the heavy quark propagator. S_1 (S_2) represents the smearing function applied to the light (heavy) quark fields.

We recall that in tmQCD quark propagators have the hermiticity property

$$\mathscr{S}_q(r;\,x;\,y) \;=\; \gamma_5\,\mathscr{S}_q^\dagger(-r;\,y;\,x)\,\gamma_5 \tag{7.23}$$

The "charged" correlators are depicted in Figure 7.1. In the actual computation, we use Gaussian

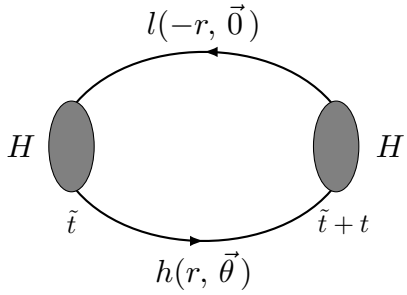


Figure 7.1: Kinematical configuration of the two-point correlators.

smeared interpolating fields [138] whose parameters are $\kappa_s = 0.15$ and $N = 30$ with an APE smearing of parameters $\alpha_{\rm APE} = 0.5$, $N_{\rm APE} = 10$. On each ensemble, we estimate the statistical error by a *Jackknife* procedure. An example of the input file containing the parameters used in the simulation at $\beta = 3.9$ can be found in Appendix B.

In this work we also choose to analyze smeared-smeared two-point correlation functions, since the benefit of such a technique has been already clearly observed in previous works.

B-meson energies

Masses and energies of pseudoscalar mesons are first extracted from a fit of the form

$$\mathscr{C}^{(2)}_{PP}(t,\vec{\theta}) = \frac{\mathscr{Z}^2}{2E_P(\vec{\theta})}\left(e^{-E(\vec{\theta})t} + e^{-E^{(\vec{\theta})}(T-t)}\right) \tag{7.24}$$

over a time range where the contribution from the first excitation is small compared to the statistical error. One can check the stability of the fit by enlarging the time interval and by adding a second exponential in the formula, i.e.

$$\mathscr{C}^{(2)}_{PP}(t,\vec{\theta}) = \sum_{i=1}^{2}\frac{\mathscr{Z}^{2\,(i)}}{2E^{(i)}_P(\vec{\theta})}\left(e^{-E^{(i)}(\vec{\theta})t} + e^{-E^{(i)}(\vec{\theta})(T-t)}\right) \tag{7.25}$$

in order to take into account the contributions of the radial excitations.
The effective energy $E_P \equiv E^{(1)}_P$ of the ground state is then measured from the ratio

$$\frac{\mathscr{C}^{(2)}_{PP}(t+1,\vec{\theta})}{\mathscr{C}^{(2)}_{PP}(t,\vec{\theta})} = \cosh(E_P(\vec{\theta})) + \sinh(E_P(\vec{\theta}))\tanh[E_P(\vec{\theta})(t-T/2)] \tag{7.26}$$

We compute the energies of the B-meson for all values of θs we considered in our simulations. In Figure 7.2, we show examples of energy plateaus for the lightest and the heaviest "B"-meson at three different momenta. From the plateaus obtained at $\theta = 0$ (the lowest ones), we can extract the "B" meson masses. The two highest plateaus represent the "B" energies corresponding to $w = 1.05$ and $w = 1.2$. After inspection, we fixed the plateaus to the intervals shown in Fig. 7.2 by the horizontal solid lines. The

dashed ones are the corresponding error bars.

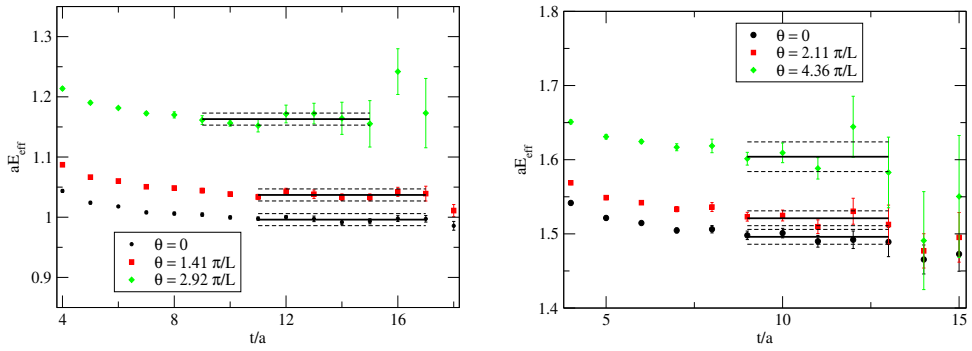


Figure 7.2: Effective energies of "B"-mesons measured with the ETMC ensemble ($\beta = 3.9$, $\mu_{\rm sea} = \mu_l = 0.0085$): $\mu_h = 0.3498$ (left) and $\mu_h = 0.6694$ (right).

The plateaus coming from the heaviest "b" quark mass as well as highest momenta are characterized by large fluctuations on the effective mass plateaus and thus by large uncertainties.
We collect in Table 7.2 all the masses and energies thus extracted and which we will need in our analysis. The error coming from the time range used to identify the plateau is estimated by changing the time interval $[t_{\rm min}, t_{\rm max}]$ by $t_{\rm min} \pm 1$ and $t_{\rm max} \pm 1$ and is included in the total error with the statistical one. Moreover, we include in the error the difference between the values obtained by using the two-state and the one-state exponential fits.

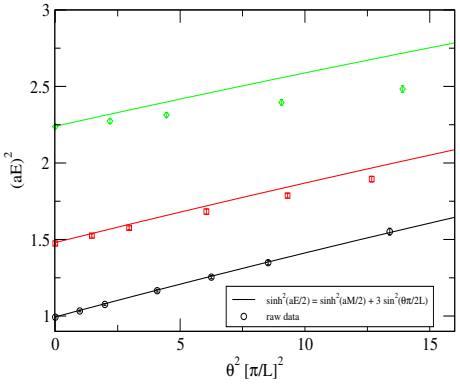


Figure 7.3: Comparison of the "B"-mesons energies with the dispersion relation, with the ETMC ensemble ($\beta = 3.9$, $\mu_{\rm sea} = \mu_l = 0.0085$).

In order to estimate the magnitude of the cut-off effects, we study the lattice dispersion relation of the meson. Figure 7.3 displays the "B" meson energies and the theoretical "energy-momentum" formula on the lattice (6.8). The agreement is good at the two lowest heavy masses but extremely poor for the heaviest one: in other words, the cut-off effects are important when we consider "moving B"-mesons.

	$\beta = 3.9$		$\beta = 4.05$	
meson	$\boldsymbol{\theta}$	$\boldsymbol{E(\theta)}$	$\boldsymbol{\theta}$	$\boldsymbol{E(\theta)}$
D	0	0.75(1)	0	0.62(1)
D_0^*	0	0.96(2)	0	0.76(2)
D_2^*	0	1.14(2)	0	0.93(2)
$B(\mu_{h_1})$	0	1.00(1)	0	0.82(1)
$B(\mu_{h_2})$	0	1.21(1)	0	1.01(1)
$B(\mu_{h_3})$	0	1.50(1)	0	1.25(1)
$B(\mu_{h_1})$	0.99	1.02(1)	1.09	0.84(1)
$B(\mu_{h_2})$	1.21	1.24(1)	1.35	1.02(1)
$B(\mu_{h_3})$	1.48	1.51(1)	1.67	1.26(1)
$B(\mu_{h_1})$	1.41	1.04(1)	1.56	0.85(1)
$B(\mu_{h_2})$	1.72	1.26(1)	1.92	1.04(1)
$B(\mu_{h_3})$	2.11	1.52(1)	2.37	1.28(1)
$B(\mu_{h_1})$	2.02	1.08(1)	2.23	0.89(1)
$B(\mu_{h_2})$	2.46	1.30(1)	2.74	1.08(1)
$B(\mu_{h_3})$	3.01	1.55(1)	3.39	1.31(1)
$B(\mu_{h_1})$	2.50	1.12(1)	2.76	0.92(2)
$B(\mu_{h_2})$	3.05	1.34(1)	3.40	1.11(2)
$B(\mu_{h_3})$	3.73	1.58(1)	4.21	1.34(1)
$B(\mu_{h_1})$	2.92	1.16(1)	3.23	0.95(2)
$B(\mu_{h_2})$	3.56	1.38(1)	3.97	1.15(2)
$B(\mu_{h_3})$	4.36	1.60(2)	4.91	1.38(2)
$B(\mu_{h_1})$	3.66	1.25(1)	4.04	1.00(3)
$B(\mu_{h_2})$	4.46	1.46(1)	4.97	1.22(3)
$B(\mu_{h_3})$	5.46	1.66(2)	6.15	1.45(1)

Table 7.2: Masses and energies extracted from the two-point correlation functions. The parameters μ_{h1}, μ_{h2} and μ_{h3} correspond to the heavy "b" quark masses given in Table 7.1. At $\beta = 3.9$, time intervals for the fits are [8, 23] (D), [6, 9] (D_0^* and D_2^*), [11, 17] (small momenta, $B(\mu_{h_1})$ and $B(\mu_{h_2})$), [9, 15] (large momenta, $B(\mu_{h_1})$ and $B(\mu_{h_2})$) and [9, 13] ($B(\mu_{h_3})$). At $\beta = 4.05$, time ranges for the fits are [10, 26] (D), [14, 26] (small momenta, $B(\mu_{h_1})$ and $B(\mu_{h_2})$), [9, 26] (large momenta, $B(\mu_{h_1})$ and $B(\mu_{h_2})$), [14, 22] (small momenta, $B(\mu_{h_3})$) and [9, 22] (large momenta, $B(\mu_{h_3})$).

The charmed meson masses

We have also computed the masses of the D_0^* and the D_2^*. They are given, in lattice units, in Table 7.2. We show in Fig. 7.4, the effective mass $m_{D_0^*}$ of the scalar meson for the ensemble ($\beta = 3.9$, $a\mu_{\text{sea}} = 0.0085$). It is calculated by solving the GEVP in the same manner as explained in Section 5.2.2. Here we set $t_0 = 3$. Although short, the signal is still acceptable for our qualitative study.

In the following, we will study the semileptonic B decays into the scalar D_0^* and the tensor D_2^* states.

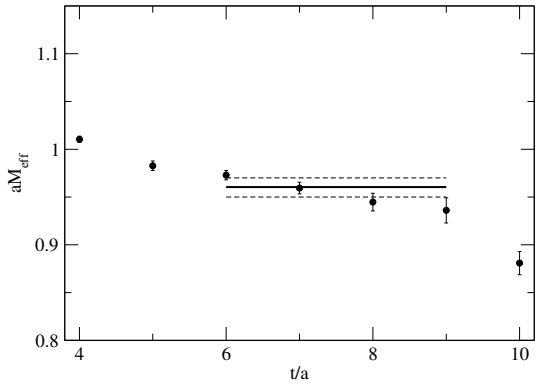


Figure 7.4: Effective mass of the D_0^* meson measured with the ETMC ensemble ($\beta = 3.9$, $\mu_{\rm sea} = \mu_l = 0.0085$).

7.3 B transitions to the scalar D_0^* ($J^P = 0^+$) meson

Hadron structure is explored by matrix elements of suitable operators between hadronic states or the vacuum providing information on semileptonic decays. Here we discuss the lattice calculation of the $B \to D_0^*$ transition amplitudes.

7.3.1 Three-point correlators

The first step to access matrix elements is to analyze the three-point correlation functions, cf. Chapter 6. To do so, we computed the "neutral" $B \to D$ three-point correlators $\mathscr{C}^{(3)\,b\Gamma c}_{\vec{\theta};S_1\,\Gamma_1;\Gamma;S_2,\Gamma_2}(t,t_s)$

$$\begin{aligned}\mathscr{C}^{(3)\,b\Gamma c}_{\vec{\theta};S_1\,\Gamma_1;\Gamma;S_2,\Gamma_2}(t,t_S) &= \frac{1}{2}\sum_{r=\pm1}\Bigg\langle \mathrm{Tr}\sum_{\vec{x},\vec{y},\vec{z}}\Gamma\,\mathscr{S}_c(r,\,\vec{0};\,\vec{z},\,\tilde{t}+t;\,\vec{y},\,\tilde{t})\,\Gamma_1\,\mathscr{S}_l^{S_1}(-r,\,\vec{0};\,\vec{y},\,\tilde{t};\,\vec{x},\,\tilde{t}+t_S)\\ &\qquad\qquad \times\Gamma_2\,\mathscr{S}_b^{S_2}(r,\,\vec{\theta};\,\vec{x},\,\tilde{t}+t_S;\,\vec{z},\,\tilde{t}+t)\Bigg\rangle\\ &= \frac{1}{2}\sum_{r=\pm1}\frac{1}{N}\sum_{n=1}^{N}\Bigg\langle \mathrm{Tr}\Bigg\{\sum_{\vec{x}}(\Gamma\gamma_5)_{\tilde{\alpha}\tilde{\beta}}\,(\phi\big[n,\,c,\,r,\,S_1,\,\vec{0},\,\tilde{\beta},\,\tilde{t}\big])^b_\alpha(\vec{x},\,\tilde{t}+t)\\ &\qquad \times(\gamma_5\Gamma_1)_{\alpha\beta}\,\Phi^*\big[n,\,b,\,-r,\,l,\,r,\,S_2,\,\Gamma_2,\,\vec{\theta},\,\vec{0},\,\tilde{\alpha},\,\tilde{t},\,\tilde{t}+t_S\big]^b_\beta(\vec{x},\,\tilde{t}+t)\Bigg\}\Bigg\rangle\end{aligned} \tag{7.27}$$

where Φ represents the *sequential propagator* determined by inverting the Dirac operator on the *sequential source* $\Gamma_{2\,\alpha\,\beta}\,\phi\big[i,\,f_1,\,r_1,\,\vec{\theta}_1,\,\tilde{\alpha},\,\tilde{t}\big]^a_\beta(x)\,\delta_{t_S,\,t_x-\tilde{t}}$

$$\begin{aligned}\sum_y D\big[f_2,\,r_2,\,\vec{\theta}_2\big]^{ab}_{\alpha\beta}(x,y)\;\Phi\big[i,\,f_2,\,r_2,\,f_1,\,r_1,\,\Gamma_2,\,\vec{\theta}_2,\,\vec{\theta}_1,\,\tilde{\alpha},\,\tilde{t},\,\tilde{t}+t_S\big]^b_\beta(y)&\\ = \;\Gamma_{2\,\alpha\,\beta}\;\phi\big[i,\,f_1,\,r_1,\,\vec{\theta}_1,\,\tilde{\alpha},\,\tilde{t}\big]^a_\beta(x)\;\delta_{t_S,\,t_x-\tilde{t}}&\end{aligned} \tag{7.28}$$

In Fig. 7.5, we show a schematic description of the computed three-point correlators.

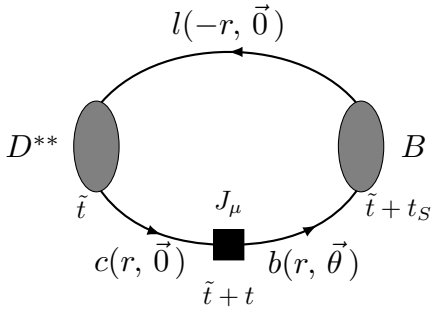


Figure 7.5: Kinematical configuration of the three-point correlators.

Unfortunately, it turns out that the three-point correlation functions of $B \to D_0^*$, computed with a B meson carrying a momentum p, are very noisy. At present, it is very challenging to discern the physical effects from lattice artifacts in the signal. So, we prefer to restrict our "scalar treatment" to the zero recoil kinematics where the B meson is at rest.
Indeed, the $B \to D_0^*$ amplitude at zero recoil holds an important phenomenological interpretation: at the infinite mass limit, it vanishes, forbidding, the decay into an S-wave and reducing significantly the phase space[2]. Any new results for this transition amplitude computed with a "real" charm quark will have an impact on experimentally measured observables, such as the ratio between $B \to D_2^*$ and $B \to D_0^*$ or the $\mathscr{B}(B \to D_0^*)/\mathscr{B}(B \to D)$ that will be discussed in the following.

7.3.2 Determination of $\dfrac{\mathscr{B}(B \to D_0^*)}{\mathscr{B}(B \to D)}$ at zero recoil

In order to estimate the ratio of the "scalar" and the "pseudoscalar" transitions of B mesons ($\mathscr{B}(B \to D_0^*)/\mathscr{B}(B \to D)$), we start by the evaluation of the hadronic matrix elements $\langle D|V_0|B\rangle$ and $\langle D_0^*|A_0|B\rangle$.

No scalar-pseudoscalar mixing

If, for the moment, we do not take into account that there is a mixing between scalar and pseudoscalar charmed meson states, the physical values of the matrix elements $\langle D|V_0|B\rangle$ and $\langle D_0^*|A_0|B\rangle$ are given by

$$\langle X_c^j|O|B\rangle = Z_O \frac{\mathscr{C}^{(3)}_{\mathrm{X_c^j OB}}(t_p, t, t_s)}{\dfrac{\sqrt{\mathscr{Z}_B}}{2E_B} \exp\left(-E_B\ (t - t_s)\right)\ \cdot \mathscr{C}^{(2)}_{X_c^j}(t_p - t)} \cdot \sqrt{\mathscr{Z}_{X_c^j}} \tag{7.29}$$

where $t_s < t < t_p$ are respectively the source, current and sink times (cf. Fig. 7.1), $Z_O = Z_V(Z_A)$ stands for the renormalisation constant of the vector (axial) operator and X_c^j represents the pseudoscalar D meson (X_c^1) and the scalar D_0^* (X_c^2). The quantities $\mathscr{Z}_{X_c^j}$ and $\mathscr{Z}_B$ are defined from the fit of the two-point correlators of the X_c^j and B mesons, assuming we are sufficiently far from the center of the lattice

[2]This can be shown using the transition amplitude of $B \to D_0^*$ at zero recoil.

to be able to neglect the backward exponential in time provided the contribution of the excited states is small

$$\mathscr{C}_B^{(2)}(t,0) = \frac{\mathscr{Z}_B}{2m_B}\exp\left(-m_B\, t\right) \qquad\qquad \mathscr{C}_{X_c^j}^{(2)}(t,0) = \frac{\mathscr{Z}_{X_c^j}}{2m_{X_c^j}}\exp\left(-m_{X_c^j}\, t\right) \tag{7.30}$$

Then we compute

$$\frac{\langle D_0^*|A_0|B\rangle}{\langle D|V_0|B\rangle} = \frac{\mathscr{C}^{(3)}_{D_0^* A_0 B}(t_p,t,t_s)\ \mathscr{C}_D^{(2)}(t_p-t)}{\mathscr{C}^{(3)}_{D V_0 B}(t_p,t,t_s)\ \mathscr{C}_{D_0^*}^{(2)}(t_p-t)}\ \frac{Z_A}{Z_V}\ \sqrt{\frac{\mathscr{Z}_{D_0^*}}{\mathscr{Z}_D}} \tag{7.31}$$

As a rough estimate, and if we neglect the dependence in the phase space, one can obtain the order of magnitude of $\mathscr{B}(B\to D_0^*)/\mathscr{B}(B\to D)$ from the above ratio squared, i.e. from $|\langle D_0^*|A_0|B\rangle/\langle D|V_0|B\rangle|^2$. However, we prefer to redetermine the ratio of the axial and vector matrix elements in the case where we take into account the mixing between the scalar and the pseudoscalar states due to the parity violation of the twisted mass action.

Addressing the scalar-pseudoscalar mixing

In Chapter 5, we have already detailed the GEVP method which we implement on two-point correlation functions in order to isolate the D and D_0^* states and extract their masses.
Let us recall that solving the GEVP means solving the following equations

$$\begin{cases} \mathscr{C}_{ij}^{(2)}(t)v_j^{(n)}(t,t_0) \ = \lambda^{(n)}(t,t_0)\,\mathscr{C}_{ij}^{(2)}(t_0)\,v_j^{(n)}(t,t_0) \\ \lambda^{(n)} = \ \dfrac{\cosh[E_n(T/2-t)]}{\cosh[E_n(T/2-t_0)]} \quad n=1,2 \end{cases} \tag{7.32}$$

where $\mathscr{C}_{ij}^{(2)}(t) = \left\langle \mathscr{O}_i^\dagger \mathscr{O}_j \right\rangle$ are the elements of a 2×2 matrix composed of two-point correlators having the interpolating fields $\mathscr{O}_i, \mathscr{O}_j \in \{\bar{\psi}_c\psi_l,\ \bar{\psi}_c\gamma_5\psi_l\}$.
Hereafter we denote by $\lambda^{(1)}$ the eigenvalues related to the D meson mass and by $\lambda^{(2)}$ the ones related to the D_0^* mass. The corresponding eigenvectors give the linear combination of $\bar{\psi}_c\gamma_5\psi_l$ and $\bar{\psi}_c\psi_l$ interpolating fields that have the largest coupling to the $D(D_0^*)$ state.
For a correlation matrix composed of $D,\ D_0^*$ meson interpolating fields, we can write

$$\begin{cases} \lambda^{(1)}(t_p-t,t_0)\ \displaystyle\sum_{i,j=1}^{2} v_i^{(1)\,\dagger}(t_p-t,t_0)\ \mathscr{C}_{ij}^{(2)}(t_0) v_j^{(1)}(t_p-t,t_0) \\ \qquad\qquad = \displaystyle\sum_{i,j=1}^{2} v_i^{(1)\,\dagger}(t_p-t,t_0)\ \mathscr{C}_{ij}^{(2)}(t_p-t) v_j^{(1)}(t_p-t,t_0); \\ \lambda^{(2)}(t_p-t,t_0)\ \displaystyle\sum_{i,j=1}^{2} v_i^{(2)\,\dagger}(t_p-t,t_0)\ \mathscr{C}_{ij}^{(2)}(t_0) v_j^{(2)}(t_p-t,t_0) \\ \qquad\qquad = \displaystyle\sum_{i,j=1}^{2} v_i^{(2)\,\dagger}(t_p-t,t_0)\ \mathscr{C}_{ij}^{(2)}(t_p-t) v_j^{(2)}(t_p-t,t_0) \end{cases}$$

where $t_0 \leq t_p - t$. The eigenvalues are fitted with

$$\begin{cases} \lambda^{(2)}(t_p - t, t_0) = \dfrac{\mathscr{Z}^2_{D_0^*}}{2m_{D_0^*}} \exp\left(-m_{D_0^*}(t_p - t - t_0)\right) \\ \lambda^{(1)}(t_p - t, t_0) = \dfrac{\mathscr{Z}^2_{D}}{2m_{D}} \exp\left(-m_{D}(t_p - t - t_0)\right) \end{cases} \tag{7.33}$$

The GEVP has many other applications. In the following we will implement the GEVP on the three-point correlators in order to extract the sought hadronic matrix elements.

Implementing GEVP in the matrix element extraction

We follow the application of the GEVP described in [139,140]. In this section we assume that $t_s < t < t_p$ and $t_0 < t_p - t$. The matrix element $\left\langle X_c^j | J_0 | B \right\rangle$, where J_0 expresses the temporal component of the axial A_μ (the vector V_μ) currents, can be written as

$$\begin{cases} \langle D|V_0|B\rangle \;=\; \dfrac{\mathscr{Z}'_D \mathscr{Z}_B \;\sum_j \; v_j^{(1)\dagger}(t_p - t, t_0)\; \mathscr{C}^{(3)}_{(X_c^j\, V_0\, B)}(t, t_s, t_p)}{\mathscr{C}^{(2)}_B(t - t_s)\; \sum_{ij} v_i^{(1)\dagger}(t_p - t, t_0) \mathscr{C}^{(2)}_{ij}(t_p - t)\; v_j^{(1)}(t_p - t, t_0)} \\ \langle D_0^*|A_0|B\rangle \;=\; \dfrac{\mathscr{Z}'_{D_0^*} \mathscr{Z}_B \;\sum_j \;\; v_j^{(2)\dagger}(t_p - t, t_0)\; \mathscr{C}^{(3)}_{(X_c^j\, A_0\, B)}(t, t_s, t_p)}{\mathscr{C}^{(2)}_B(t - t_s)\; \sum_{ij} v_i^{(2)\dagger}(t_p - t, t_0) \mathscr{C}^{(2)}_{ij\,,D}(t_p - t)\; v_j^{(2)}(t_p - t, t_0)} \end{cases} \tag{7.34}$$

The term $\sum_j \; v_j^{(1)\dagger}(t_p - t, t_0)\, \mathscr{C}^{(3)}_{(X_c^j\, V_0\, B)}(t, t_s, t_p)$ corresponds to the "projected" three-point correlators corresponding to $B \to X_c^j$ via the current V_0, and

$$\mathscr{C}^{(3)}_{(X_c^j\, V_0\, B)}(t, t_s, t_p) \;\equiv \left\langle \mathscr{O}_j^\dagger(t_p)\; V_0(t)\; \mathscr{O}_B(t_s) \right\rangle \tag{7.35}$$

is composed of the interpolating field $\mathscr{O}_B$ which creates a B meson at time t_s, the interpolating field $\mathscr{O}_j^\dagger$ annihilating a pseudoscalar D meson (scalar D_0^* meson) at time t_p (i.e. $\mathscr{O}_j(t_p) \;\in\; \{\bar\psi_c \psi_l(t_p),\, \bar\psi_c \gamma_5 \psi_l(t_p)\}$) and the current V_0 inserted at time t. The "projected" three-point correlation functions are then

$$\begin{aligned} \sum_j v_j^{(1)\dagger}(t_p - t, t_0)\; \mathscr{C}^{(3)}_{(X_c^j\, V_0\, B)}(t, t_s, t_p) = \;& v_1^{(1)\dagger}(t_p - t, t_0)\; \mathscr{C}^{(3)}_{(X_c^1\, V_0\, B)}(t, t_s, t_p) \\ & + v_2^{(1)\dagger}(t_p - t, t_0)\; \mathscr{C}^{(3)}_{(X_c^2\, V_0\, B)}(t, t_s, t_p) \end{aligned} \tag{7.36}$$

Similarly, the "projected" three-point correlation functions corresponding to the decay of B into D_0^* via the current A_0, $\sum_j \; v_j^{(2)\dagger}(t_p - t, t_0)\, \mathscr{C}^{(3)}_{(X_c^j\, A_0\, B)}$, read

$$\begin{aligned} \sum_j v_j^{(2)\dagger}(t_p - t, t_0)\, \mathscr{C}^{(3)}_{(X_c^j\, A_0\, B)}(t, t_s, t_p) = \;& v_1^{(2)\dagger}(t_p - t, t_0)\, \mathscr{C}^{(3)}_{(X_c^1\, A_0\, B)}(t, t_s, t_p) \\ & + v_2^{(2)\dagger}(t_p - t, t_0) \mathscr{C}^{(3)}_{(X_c^2\, A_0\, B)}(t, t_s, t_p) \end{aligned} \tag{7.37}$$

where

$$\begin{cases} \mathscr{C}^{(3)}_{(X_c^1\ A_0\ B)}(t,t_s,t_p) \equiv \left\langle \mathscr{O}_1^\dagger(t_p)\ A_0(t)\ \mathscr{O}_B(t_s)\right\rangle \\ \mathscr{C}^{(3)}_{(X_c^2\ A_0\ B)}(t,t_s,t_p) \equiv \left\langle \mathscr{O}_2^\dagger(t_p)\ A_0(t)\ \mathscr{O}_B(t_s)\right\rangle \end{cases} \tag{7.38}$$

Since the B meson goes through V_0 (A_0) only to a pure pseudoscalar D (scalar D_0^*), we can assume that

$$\begin{cases} \sum\limits_j v_j^{(1)\dagger}(t_p-t,t_0)\ \mathscr{C}^{(3)}_{(X_c^j\ V_0\ B)}(t,t_s,t_p) \simeq v_1^{(1)\dagger}(t_p-t,t_0)\mathscr{C}^{(3)}_{(X_c^1\ V_0\ B)}(t,t_s,t_p) \\ \sum\limits_j v_j^{(2)\dagger}(t_p-t,t_0)\ \mathscr{C}^{(3)}_{(X_c^j\ A_0\ B)}(t,t_s,t_p) \simeq v_2^{(2)\dagger}(t_p-t,t_0)\ \mathscr{C}^{(3)}_{(X_c^2\ A_0\ B)}(t,t_s,t_p) \end{cases} \tag{7.39}$$

This can be confirmed by looking at the actual computed values of the eigenvectors, such as the ones given in Table 7.3.

$v^{(1)}$	$v^{(2)}$
0.97	-0.3 i
-0.24 i	0.95

Table 7.3: Values of the eigenvectors $v^{(1)}$ and $v^{(2)}$, for $\beta = 3.9$, $t_0 = t_s = 3$, $t = 7$ and $t_p = 14$. We can notice that they are close to being orthogonal ($v^{(1)}v^{(2)\dagger} \simeq 0$).

The ratio of the axial and the vector hadronic matrix elements then reads

$$\begin{aligned} \frac{\langle D_0^*|A_0|B\rangle}{\langle D|V_0|B\rangle} = \frac{\mathscr{Z}'_{D_0^*}}{\mathscr{Z}'_D}\ & \frac{\sum_{ij} v_i^{(1)\dagger}(t_p-t,t_0)\mathscr{C}^{(2)}_{ij\ ,D}(t_p-t)\ v_j^{(1)}(t_p-t,t_0)}{\sum_{ij} v_i^{(2)\dagger}(t_p-t,t_0)\mathscr{C}^{(2)}_{ij\ ,D_0^*}(t_p-t)\ v_j^{(2)}(t_p-t,t_0)} \\ & \times \frac{v_2^{(2)\dagger}(t_p-t,t_0)\ \mathscr{C}^{(3)}_{(X_c^2\ A_0\ B)}(t,t_s,t_p)}{v_1^{(1)\dagger}(t_p-t,t_0)\ \mathscr{C}^{(3)}_{(X_c^1\ V_0\ B)}(t,t_s,t_p)} \end{aligned} \tag{7.40}$$

where the normalization constant $\mathscr{Z}'_D$ ($\mathscr{Z}'_{D_0^*}$) is obtained by performing a fit with the "projected" two-point correlation functions

$$\begin{cases} \sum\limits_{ij} v_i^{(1)\dagger}(t_p-t,t_0)\mathscr{C}^{(2)}_{ij}(t_p-t)\ v_j^{(1)}(t_p-t,t_0) = \dfrac{\mathscr{Z}'^2_D}{2m_D}\exp\left(-m_D(t_p-t)\right) \\ \sum\limits_{ij} v_i^{(2)\dagger}(t_p-t,t_0)\mathscr{C}^{(2)}_{ij}(t_p-t)\ v_j^{(2)}(t_p-t,t_0) = \dfrac{\mathscr{Z}'^2_{D_0^*}}{2m_{D_0^*}}\exp\left(-m_{D_0^*}(t_p-t)\right) \end{cases} \tag{7.41}$$

Finally, using (7.41), the ratio of Eq. (7.40) becomes

$$\frac{\langle D_0^*|A_0|B\rangle}{\langle D|V_0|B\rangle} = \sqrt{\frac{m_{D_0^*}}{m_D}}\ \frac{\sqrt{\sum_{ij} v_i^{(1)\dagger}(t_p-t,t_0)\mathscr{C}_{ij}^{(2)}(t_p-t)\ v_j^{(1)}(t_p-t,t_0)}}{\sqrt{\sum_{ij} v_i^{(2)\dagger}(t_p-t,t_0)\mathscr{C}_{ij}^{(2)}(t_p-t)\ v_j^{(2)}(t_p-t,t_0)}} \times \frac{v_2^{(2)\dagger}(t_p-t,t_0)\ \mathscr{C}^{(3)}_{(X_c^2\ A_0\ B)}(t,t_s,t_p)}{v_1^{(1)\dagger}(t_p-t,t_0)\ \mathscr{C}^{(3)}_{(X_c^1\ V_0\ B)}(t,t_s,t_p)} \times \frac{\exp\left(-m_D\,(t_p-t)/2\right)}{\exp\left(-m_{D_0^*}\,(t_p-t)/2\right)} \tag{7.42}$$

Estimation of the branching fractions ratio

We need the momentum dependence of the form factors in order to compute the decay rates of the semileptonic $B \to D_0^*$ decay channel. However, as indicated in the beginning of this section, we do not take into account the dependence on the recoil and we only estimated the zero recoil contribution. We will, in what follows, benefit from the ratio of hadronic transition amplitudes (7.42) written in terms of projected two- and three-point correlators to do a rough estimation (in the sense that we drop the contributions of the phase space) of the ratio of the corresponding branching fractions.

Symmetry properties

Let us recall that the tmQCD action preserves the parity symmetry if it is combined with the flip sign of the twisted mass terms (see Chapter 3). Here, we will call this symmetry the "flavor-parity symmetry" and we will denote it by $\mathscr{R}_5^{\rm sp}$

$$\mathscr{R}_5^{\rm sp} \equiv \mathscr{P} \otimes (\mu_l, \mu_c, \mu_b \rightsquigarrow -\mu_l, -\mu_c, -\mu_b) \tag{7.43}$$

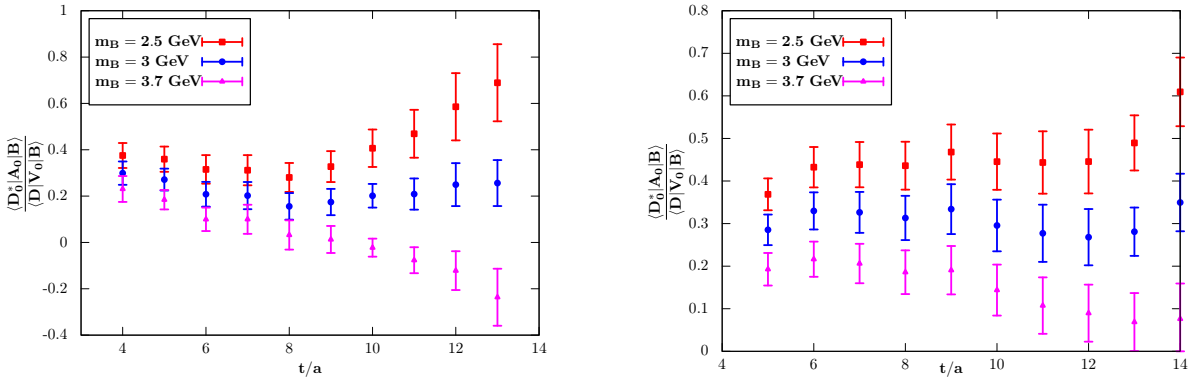
where $\mathscr{P}$ is the ordinary spatial parity and μ_l, μ_c, μ_b are the twisted mass terms for the light, charm and beauty quarks.
In the continuum limit, conservation of parity leads to vanishing $\langle D|A_0|B\rangle$ and $\langle D_0^*|V_0|B\rangle$ matrix elements. On the lattice this is no longer valid unless we use the "symmetrized" three-point correlation functions

$$\mathscr{C}_{i,j,k}^{(3)\,\rm sym}(t_p,t,t_s) \ \equiv\ \frac{1}{2}\ (1+\mathscr{R}_5^{\rm sp})\ \mathscr{C}_{i,j,k}^{(3)}(t_p,t,t_s) \tag{7.44}$$

This symmetrization will be assumed in what follows.

Results

We benefit from the symmetry property (7.43) to determine the hadronic matrix elements as well as the ratio (7.42) using the "symmetrized" three-point correlation functions. In Figure 7.6, we show the obtained results for the computed ratio $\frac{\langle D_0^*\,|\,A_0\,|\,B\rangle}{\langle D\,|\,V_0\,|\,B\rangle}$ as a function of time in lattice units. We identify acceptable plateaus which are in good agreement between the two gauge ensembles at small times ($t < 8$). However, this agreement is lost at larger times. Moreover, the ratio decreases with increasing B mass.



(a) $\beta = 3.9$ (b) $\beta = 4.05$

Figure 7.6: The ratio $\frac{\langle D_0^* \,|\, A_0 \,|\, B\rangle}{\langle D \,|\, V_0 \,|\, B\rangle}$ once symmetrized according to (7.44) for the three b quark masses (i.e. for the three B meson masses as indicated in the plots) and for both lattice spacings. Here, the values are computed using $t_0 = 4$ for $\beta = 3.9$ and $t_0 = 5$ for $\beta = 4.05$.

We list in Table 7.4 the values for the ratio (7.42) averaged over the time range $t \in [6, 8]$ ($t \in [5, 8]$) for $\beta = 3.9$ ($\beta = 4.05$).

β	ratio (μ_{h1})	ratio (μ_{h2})	ratio (μ_{h3})
3.9	0.29(2)	0.18(2)	0.08(2)
4.05	0.42(2)	0.30(2)	0.19(2)

Table 7.4: Ratios defined in Eq. (7.42). The b quark masses range from the lightest to the heaviest from left to right. They correspond to the B meson mass $m_B \in \{2.5, 3, 3.7\}$ GeV.

We then fit our data at different heavy meson masses as

$$\text{Ratio}(m_B) \;=\; \alpha + \frac{\gamma}{m_B} \tag{7.45}$$

Performing a preliminary extrapolation to the physical $m_B = 5.2$ GeV, we obtain:

$$\left.\frac{\langle D_0^* \,|\, A_0 \,|\, B\rangle}{\langle D \,|\, V_0 \,|\, B\rangle}\right|_{\substack{\text{guess estimate} \\ m_B = 5.2\text{GeV}}} \simeq \begin{cases} -0.02 & \text{at } \beta = 3.9 \\ 0.03 & \text{at } \beta = 4.05 \end{cases} \tag{7.46}$$

The ratio increases with the inverse of lattice spacing. However, with our available data, we are not able to estimate the uncertainty on these numbers nor to give reliable extrapolated values in the continuum. Performing a guess estimate of the extrapolated value at vanishing lattice spacing using

$$\text{Ratio}\,(a) \;= A + B \left(\frac{a}{a_{\beta=3.9}}\right)^2 \tag{7.47}$$

we obtain

$$\left.\frac{\langle D_0^* \,|\, A_0 \,|\, B\rangle}{\langle D \,|\, V_0 \,|\, B\rangle}\right|_{\substack{\text{guess estimate}\\ \text{in the contin.}}} \simeq 0.13 \tag{7.48}$$

which is compatible with the experimental results ($\simeq 0.1$) [1].

In the infinite mass limit, this ratio vanishes. Power corrections in the inverse of the heavy quark mass could contribute but they have never been studied. However, our fully non-perturbative computation has shown, for the first time, that this ratio has a non-vanishing value, in agreement with experimental results.

7.4 B decays to the tensor D_2^* state

In this section we want to estimate the amplitudes for $B \to D_2^* \ell \bar{\nu}_\ell$ ($B_s \to D_{s2}^* \ell \bar{\nu}_\ell$) decays. In the PDG [1], the naming scheme for these $J = 2$ state is $D_2^*(2460)$ ($D_{s2}^*(2573)$). Here, we use three heavy quarks corresponding to the three "B" mesons "$B_i,\ i = 1,\ 2,\ 3$" with increasing masses in the range 2.5, 3.0 and 3.7 GeV. Let us recall that we are working in the rest frame of the D_2^*.

7.4.1 Contribution of the form factors to the $^3P_2$ decay width

There are four form factors ($\tilde{k}$, $\tilde{b}_+$, $\tilde{b}_-$ and $\tilde{h}$) needed to describe the transition amplitudes from a B to a $^3P_2$ state. Computing each of them from lattice data would increase the difficulty of the work. Thus it is useful to have an idea of each contribution to the decay widths. To simplify the expressions, we introduce the two dimensionless parameters x and y defined as

$$x\, m_{_B} = 2\, E_\ell \qquad \text{as well as} \qquad y\, m_{_B}^2 = (p_{_B} - p_{_{D^{**}}})^2 = (p_\ell + p_\nu)^2 \tag{7.49}$$

where E_ℓ is the energy of the lepton in the B rest frame. We also define the mass ratio

$$r_{_{D^{**}}} = \frac{m_{_{D^{**}}}}{m_{_B}} \tag{7.50}$$

Relations between form factors and their infinite mass limit

In the limit where the heavy quark mass is infinite, new symmetries appear and thus additional conserved quantities. From a theoretical viewpoint [25], we get new commutators which relate the different matrix elements $\left\langle jJ^P \,\middle|\, J_\mu \,\middle|\, B\right\rangle$. Hence, the form factors, in this limit, are no longer independent

$$\begin{cases} \tilde{h} = \dfrac{\sqrt{3}}{2} \dfrac{1}{m_{_B}^2 \sqrt{r_{_{D_2^*}}}}\, \tau_{3/2} & \tilde{k} = \sqrt{3}\sqrt{r_{_{D_2^*}}}\,(1+w)\,\tau_{3/2} \\ \tilde{b}_+ = -\dfrac{\sqrt{3}}{2} \dfrac{1}{m_{_B}^2 \sqrt{r_{_{D_2^*}}}}\, \tau_{3/2} & \tilde{b}_- = \dfrac{\sqrt{3}}{2} \dfrac{1}{m_{_B}^2 \sqrt{r_{_{D_2^*}}}}\, \tau_{3/2} \end{cases} \tag{7.51}$$

where

$$m_B\, m_{D_2^*}\, w = p_B \cdot p_{D_2^*} \qquad \Longrightarrow \qquad y = 1 + r_{D^{**}}^2 - 2\, r_{D^{**}}\, w \tag{7.52}$$

and $\tau_{3/2}$, is one of IW functions which depend on the momentum transfer q^2, hence on y or w.

Quantitative estimate of the contribution of each form factor

Taking the limit of vanishing lepton masses, the partial decay width $\dfrac{\mathrm{d}^2\Gamma}{\mathrm{d}x\,\mathrm{d}y}$ of the $B \to D_2^*\,\ell\,\bar{\nu}_\ell$ decay channel, which we calculate in Appendix D, is written in terms of the four form factors and some coefficients $(C_1,\ C_2,\ C_3,\ \cdots\ ,\ C_8)$

$$\begin{aligned}\frac{\mathrm{d}^2\Gamma}{\mathrm{d}x\,\mathrm{d}y} \propto\ \Big\{ & C_1\,|\tilde{k}|^2 + C_2\,|\tilde{h}|^2 + C_3\,|\tilde{b}_+|^2 + C_4\,|\tilde{b}_-|^2 + C_5\,(\tilde{k}\,\tilde{b}_+^* + \tilde{k}^*\,\tilde{b}_+) \\ & + C_6\,(\tilde{k}\,\tilde{b}_-^* + \tilde{k}^*\,\tilde{b}_-) + C_7\,(\tilde{b}_+\,\tilde{b}_-^* + \tilde{b}_+^*\,\tilde{b}_-) + C_8\,(\tilde{h}\,\tilde{k}^* + \tilde{h}^*\,\tilde{k}) \Big\}\end{aligned} \tag{7.53}$$

Moreover, the IW function $\tau_{3/2}$ can be well fitted using [51]

$$\tau_{3/2}(y) = \tau_{3/2}(1)\ \left[\frac{4\, r_{D_2^*}}{(1 + r_{D_2^*})^2 - y}\right]^{2\,\sigma_{3/2}^2} \tag{7.54}$$

where the phase space is bounded by

$$(1 - r_{D_2^*})^2 \geq y \geq 0 \tag{7.55}$$

with $\tau_{3/2}(1) \simeq 0.539$ and $\sigma_{3/2}^2 \simeq 1.50$.
After integration over x and y, we obtain the following contribution of each form factor to the total width

$\boldsymbol{C_i}$	$C_1 \times \tilde{k}^2$	$C_2 \times \tilde{h}^2$	$C_3 \times \tilde{b}_+^2$	$C_5 \times 2\,\tilde{k}\,\tilde{b}_+$	C_8
$\iint \boldsymbol{C_i} \times \mathbf{FF^2}$	-61.3	-0.86	-4.43	29.1	0

The largest contributions to the decay width come from the terms where the $\tilde{k}$ form factor appears. Therefore, we will concentrate on its determination in the actual lattice computation.

7.4.2 Extracting the $\tilde{k}$ form factor

From the expressions of the polarization tensor of the D_2^*, we can relate the interpolating fields of the ${}^3P_2(\lambda)$ state (cf. Chapter 5) to its polarization states λ and thus to the corresponding transition amplitude $\langle {}^3P_2(\lambda)\,|\,J_\mu\,|\,B\rangle$. The results are listed in Table 7.5.

Since $\tilde{k}$ is given in terms of the amplitudes $\mathscr{T}^A_{i(\lambda)}$ and in the lattice we compute correlation functions of

IR	interpolating fields	polarization states λ	combination of $\mathscr{T}^A_{i(\lambda)}$
E^+	$\gamma_1 D_1 + \gamma_2 D_2 - 2\gamma_3 D_3$	(0)	$\mathscr{T}^A_{i(0)}$
	$\gamma_1 D_1 - \gamma_2 D_2$	$(+2) + (-2)$	$\mathscr{T}^A_{i(+2)} + \mathscr{T}^A_{i(-2)}$
T_2^+	$\gamma_2 D_3 + \gamma_3 D_2$	$(+1) + (-1)$	$\mathscr{T}^A_{i(+1)} + \mathscr{T}^A_{i(-1)}$
	$\gamma_1 D_3 + \gamma_3 D_1$	$(+1) - (-1)$	$\mathscr{T}^A_{i(+1)} - \mathscr{T}^A_{i(-1)}$
	$\gamma_1 D_2 + \gamma_2 D_1$	$(+2) - (-2)$	$\mathscr{T}^A_{i(+2)} - \mathscr{T}^A_{i(-2)}$

Table 7.5: Relations between interpolating fields and corresponding combinations of transition amplitudes for each IR ($\mathscr{T}^A_{i(\lambda)} = \langle {}^3P_2 \,|\, A_i \,|\, B\rangle$ where $i = 1, 2, 3$).

the interpolating fields, we need to express the form factor $\tilde{k}$ for each interpolating field. Let us list the relevant relations used

- $\gamma_1 D_1 + \gamma_2 D_2 - 2\gamma_3 D_3$

$$\tilde{k} = -\frac{\sqrt{6}}{p}\,\mathscr{T}^A_{1(0)} = -\frac{\sqrt{6}}{p}\,\mathscr{T}^A_{2(0)} = \frac{\sqrt{6}}{2\,p}\,\mathscr{T}^A_{3(0)} \tag{7.56}$$

- $\gamma_1 D_1 - \gamma_2 D_2$

$$\tilde{k} = \frac{1}{p}\left[\mathscr{T}^A_{1(+2)} + \mathscr{T}^A_{1(-2)}\right] = -\frac{1}{p}\left[\mathscr{T}^A_{2(+2)} + \mathscr{T}^A_{2(-2)}\right] \tag{7.57}$$

- $\gamma_1 D_2 + \gamma_2 D_1$ and $\gamma_2 D_3 + \gamma_3 D_2$

$$\begin{aligned}\tilde{k} = \frac{i}{p}\left\{\left[\mathscr{T}^A_{1(+2)} - \mathscr{T}^A_{1(-2)}\right] + \left[\mathscr{T}^A_{1(+1)} + \mathscr{T}^A_{1(-1)}\right]\right\} \\ = -\frac{i}{p}\left\{\left[\mathscr{T}^A_{3(+2)} - \mathscr{T}^A_{3(-2)}\right] + \left[\mathscr{T}^A_{3(+1)} + \mathscr{T}^A_{3(-1)}\right]\right\}\end{aligned} \tag{7.58}$$

- $\gamma_2 D_3 + \gamma_3 D_2$ and $\gamma_1 D_3 + \gamma_3 D_1$

$$\begin{aligned}\tilde{k} = \frac{i}{p}\left\{\left[\mathscr{T}^A_{1(+1)} + \mathscr{T}^A_{1(-1)}\right] + i\left[\mathscr{T}^A_{1(+1)} - \mathscr{T}^A_{1(-1)}\right]\right\} \\ = -\frac{i}{p}\left\{\left[\mathscr{T}^A_{2(+1)} + \mathscr{T}^A_{2(-1)}\right] + i\left[\mathscr{T}^A_{2(+1)} - \mathscr{T}^A_{2(-1)}\right]\right\}\end{aligned} \tag{7.59}$$

- $\gamma_1 D_2 + \gamma_2 D_1$ and $\gamma_1 D_3 + \gamma_3 D_1$

$$\begin{aligned}\tilde{k} = \frac{i}{p}\left\{\left[\mathscr{T}^A_{2(+2)} - \mathscr{T}^A_{2(-2)}\right] - i\left[\mathscr{T}^A_{2(+1)} - \mathscr{T}^A_{2(-1)}\right]\right\} \\ = -\frac{i}{p}\left\{\left[\mathscr{T}^A_{3(+2)} - \mathscr{T}^A_{3(-2)}\right] - i\left[\mathscr{T}^A_{3(+1)} - \mathscr{T}^A_{3(-1)}\right]\right\}\end{aligned} \tag{7.60}$$

Having all the above formulae of $\tilde{k}$, we proceed to analyze the three-point correlation functions.

Three-point correlators

In the case of a transition into the tensor D_2^* meson, we notice that the three-point correlation functions at higher momenta are not compatible with zero contrary to what was observed at small momenta where the signal practically vanishes. However, at large momenta p, it becomes difficult to get a sufficiently large signal over noise ratio. Therefore, one must devise a way to look for the source of the noise and reduce it as much as possible in order to get a clean signal and thus reliable results.
First, we consider all the combinations contributing to the determination of the $\tilde{k}$ form factor. Averaging the resulting value is analogous to increasing the statistics, i.e. doing the simulation with more configurations. Moreover, we apply the symmetry property (7.44) in order to eliminate the lattice artifacts as much as possible. Unfortunately, it seems that doing this is not sufficient and we will use a trick which consists in subtracting to every three-point correlator, computed at non zero momentum, the correlator obtained from the simulation on the same gauge configuration and containing the same operators but at zero momentum.
In the continuum, the $B \to D_2^*$ decay vanishes at zero recoil. Indeed, since we start with a B meson having angular momentum $J = 0$, the weak interaction operator cannot generate a $J = 2$ state (the axial current A_μ has $J = 0$ for A_0 and $J = 1$ for A_i).
Moreover, this vanishing is also exact on the lattice and the proof is the following. The three-point correlators contribution to $B \to D_2^*$ are linear combinations of correlators of the type

$$\mathscr{C}^{(3)}_{i,j,k}(t_p, t, t_s) \;=\; \left\langle \mathscr{O}^\dagger_{D_i\gamma_j}(t_p)\, A_k(t)\, \mathscr{O}_B(t_s) \right\rangle \tag{7.61}$$

where $O_{D_i\gamma_j}$ is a notation for $\mathscr{O}_{D_2^*}$ which exhibits the structure of the interpolating fields as seen in Table 7.5. Let us consider the rotation $\mathscr{R}_l(\pi)$ of angle π around one of the three spatial directions $\hat{l}$. Under $R_l(\pi)$, the spatial coordinates i as well as all vector operators (D_i, γ_i and A_i) change sign if i is perpendicular to $\hat{l}$. Besides, all the lattice actions (including tmLQCD since $\mathscr{R}_l(\pi)$ is parity even) are invariant under $\mathscr{R}_l(\pi)$ because it belongs to the cubic group. Hence, if an odd number of the induces i, j, k in Eq. (7.61) are orthogonal to[3] $\hat{l}$, then the correlator changes sign under $\mathscr{R}_l(\pi)$ and the amplitude must vanish. However, in the case where $i \neq j \neq k$, a different line of reasoning ensures the vanishing of the $B \to D_2^*$ decay. Parity changes the sign of the amplitude (7.61) but since it is not a symmetry of tmQCD, we must use the "flavor-parity symmetry" (7.43): invariance under $\mathscr{R}_5^{\rm sp}$ imposes that $\mathscr{C}^{(3)\rm sym}(t_p, t_s, t) = 0$ on the lattice at zero recoil.

So, we may subtract to the three point correlator at non vanishing recoil the same configuration at zero recoil. This reduces the noise, and indeed it turns out that the signal, although still very noisy, is significantly improved.

Using the three point correlation functions analyzed as described above, we will proceed to study the form factor $\tilde{k}$.

[3] This happens when: $i = j = k \neq \hat{l}$; $(i = j = \hat{l}) \neq k$ and $(i = j \neq k) \neq \hat{l}$.

Estimation of the ratio $\dfrac{\tilde{k}}{\tilde{k}_\infty}$

The estimate of $B \to D_2^*$ in the infinite mass limit is rather successful and in good agreement with experiment. We will thus profit from the signal quality of the three-point correlation functions to compute the ratio of the three-point correlators to the ones derived from the infinite mass limit formula of $\tau_{3/2}$, given in Section 7.4.1. The infinite mass limit expression of $\tilde{k}$ will be denoted $\tilde{k}_\infty$ and reads

$$\tilde{k}_\infty = \sqrt{3}\,\sqrt{r_{D_2^*}}\,(1+w)\,\tau_{3/2}(w) \tag{7.62}$$

The form factor $\tilde{k}_\infty$ will be used as a benchmark for $\tilde{k}$ extracted from our present calculations. Since the form factor $p\tilde{k}$ is proportional to the matrix elements (Eqs. (7.56), (7.57), (7.58), (7.59) and (7.60)), one can extract it by computing the ratio of three-point correlators and two-point correlators

$$p\tilde{k} \xrightarrow[(t_p-t_s)\to\infty]{} R(t_p,t,t_s) = \frac{\mathscr{C}^{(3)}(t_p,t,t_s)}{\mathscr{C}^{(2)}_{D_2^*}(t_p-t)\mathscr{C}^{(2)}_{B(\vec{\theta})}(t-t_s)}\;\mathscr{Z}_B\,\mathscr{Z}_{D_2^*} \tag{7.63}$$

where $\mathscr{C}^{(2)}_{D_2^*}(t_p-t)$, $\mathscr{C}^{(2)}_{B(\vec{\theta})}(t-t_s)$ are respectively the two-point correlators of the D_2^* (computed at zero momentum) and of the B (computed at different momentum $|\vec{p}| = \sqrt{3}\,\theta_0\,\pi/L$ i.e. different θ_0s). The D_2^* meson being annihilated at time t_p, the current inserted at time t and the B created at time t_s. From our benchmark $\tilde{k}_\infty$, we compute the corresponding three-point correlators at the infinite mass limit

$$p\tilde{k}_\infty \xrightarrow[(t_p-t_s)\to\infty]{} R(t_p,t,t_s) = \frac{\mathscr{C}^{(3)}_\infty(t_p,t,t_s)}{\mathscr{C}^{(2)}_{D_2^*}(t_p-t)\mathscr{C}^{(2)}_{B(\vec{\theta})}(t-t_s)}\;\mathscr{Z}_B\,\mathscr{Z}_{D_2^*} \tag{7.64}$$

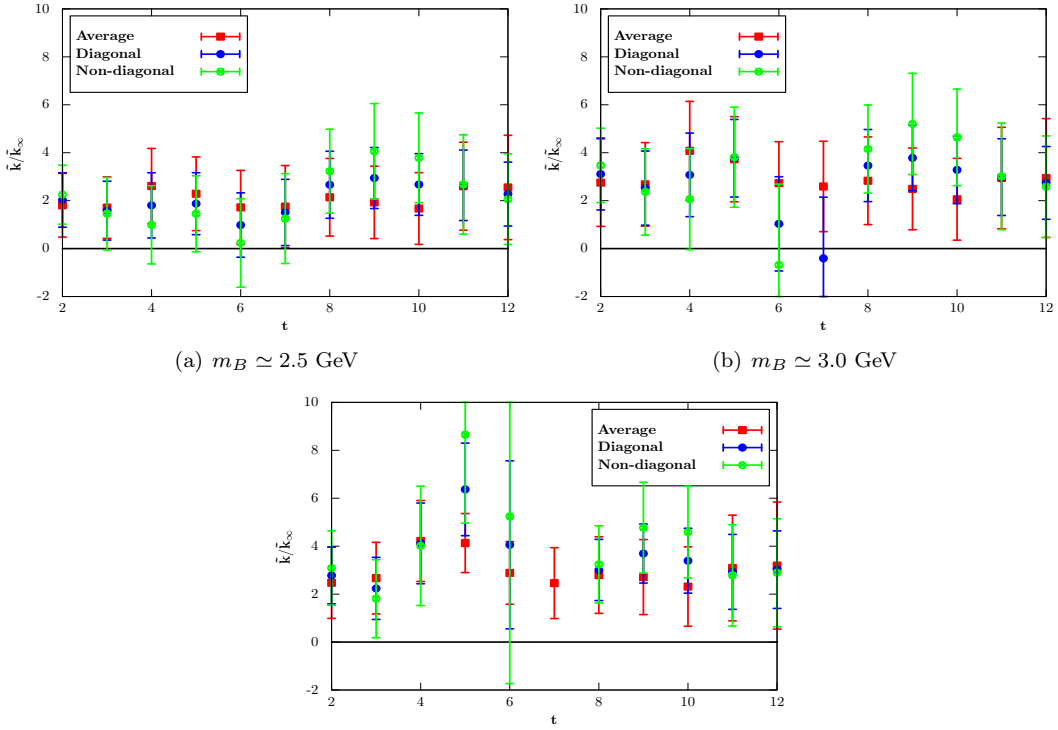
We then consider the ratio of $\tilde{k}$ and $\tilde{k}_\infty$ at the recoil $w = 1.3$ (the maximal recoil we consider in our simulations)

$$\left.\frac{\tilde{k}}{\tilde{k}_\infty}\right|_{w=1.3} = \left.\frac{\mathscr{C}^{(3)}_{D_2^* A_i B(\vec{\theta})}(t_p,t,t_s)}{\mathscr{C}^{(3)}_\infty(t_p,t,t_s)}\right|_{w=1.3} \tag{7.65}$$

We perform the computation of $\tilde{k}/\tilde{k}_\infty$ using the average of the diagonal contributions (Eqs. (7.56) and (7.57)) which correspond to the discrete representation E^+ for the D_2^* interpolating field. Also, we use the results obtained from the average of the non-diagonal contributions (Eqs. (7.58), (7.59) and (7.60)) corresponding to the discrete representation T_2^+. Finally, we average over all diagonal and non-diagonal contributions.

Figures 7.7 and 7.8 display the ratio $\dfrac{\tilde{k}}{\tilde{k}_\infty}$ in (7.65) computed respectively at $\beta = 3.9$ and $\beta = 4.05$, and for the three masses of the "B" meson, all taken at the maximum value of θ i.e. at $w = 1.3$.

At $\beta = 4.05$, there is a positive signal around 6 or even higher for heavier "B" masses. The signal over noise ratio goes up to 2.7, and around its maximum, the points are about two sigmas from zero. Although the three-point correlators $\mathscr{C}^{(3)}(t_p,t,t_s)$ show a signal, the ratio $\tilde{k}/\tilde{k}_\infty$ is characterized by



(a) $m_B \simeq 2.5$ GeV

(b) $m_B \simeq 3.0$ GeV

(c) $m_B \simeq 3.7$ GeV

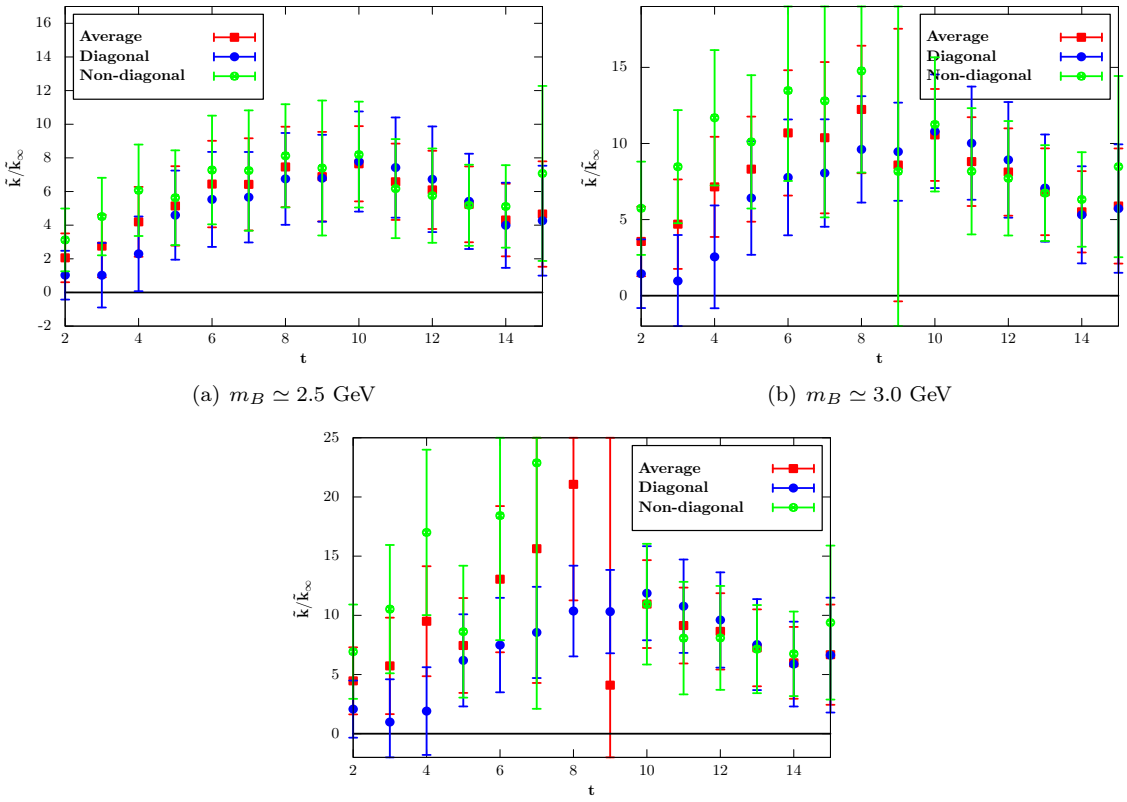
Figure 7.7: The ratio of $\tilde{k}/\tilde{k}_\infty$ for $B \to D_2^*$, at $\beta = 3.9$ and $t_p = 14$, to the value derived from the infinite mass limit as a function of time in lattice units for all "B" masses. We present results obtained by considering the average of the diagonal contributions ● (Eqs. (7.56) and (7.57)), and the non-diagonal contributions ● (Eqs. (7.58), (7.59) and (7.60)). The full average is presented by the ■ data points.

large statistical uncertainties. At $\beta = 3.9$, we observe a similar signal. However, the contribution of the diagonal and the non-diagonal correlation functions in the ratio are not very consistent in this case. This difference between the two contributions decreases when going to small lattice spacing at $\beta = 4.05$. So, one would interpret this as lattice artifacts.

Being unable to extract good plateaus, we have only analyzed the signal of the three-point correlators. The ratio $\tilde{k}/\tilde{k}_\infty$ gives somehow large estimates. Due to the large fluctuations of the three-point correlators, we are unable to check the amount of contributions coming from the finiteness of the heavy quark mass since the signal of the three-point correlators is also contaminated by the "B" meson energies which, as we showed, suffer from cut-off effects.

Concluding remarks

We have addressed for the first time the semileptonic decay of B into D^{**} states using fully propagating heavy quarks. We focused on two final states: the scalar charmed meson D_0^* and the tensor one D_2^*.



(a) $m_B \simeq 2.5$ GeV

(b) $m_B \simeq 3.0$ GeV

(c) $m_B \simeq 3.7$ GeV

Figure 7.8: Same as Fig. 7.7 but for $\beta = 4.05$ and $t_p = 18$.

We estimated the scalar matrix element at zero recoil having obtained a non vanishing value in contrast to what is predicted in the heavy quark limit. This will have a significant impact on any observable depending on this matrix element.

In the tensor case, we preferred to estimate the ratio of the form factor, which contributes the most to the decay width, over its predicted value in the infinite mass limit. We observed a signal at maximal recoil but the estimated statistical error is large at present.

In the future, we hope to get a cleaner signal for the three-point correlators in order to determine the q^2 dependence of the form factors.

Conclusion

B physics has been a field of intensive research over the past two decades. The main goal of experimental and theoretical investigations in the B sector is to test the Standard Model of particle physics. Semileptonic B decays are essential in that sense. Along with the experimental measurements of the decay rates, the theoretical predictions of some form factors participate in the accurate determination of the CKM matrix elements V_{cb} and V_{ub}.

In this thesis, we have carried out the determination of form factors contributing to the semileptonic B decays into the charm meson. Here we summarize the main results of this work.

Spectroscopy

Chapter 5 is dedicated to the spectroscopy of the fundamental and the excited charmed D meson. We have applied the GEVP to disentangle scalar and pseudoscalar states. For the orbitally excited D^{**} mesons, we followed a strategy based on group theory to find their corresponding effective masses. The difference between masses of excited and fundamental states is estimated to be 30% with respect to the experimental one.

This study serves as an introduction to the form factor extraction, especially those corresponding to $B \to D^{**}$ transitions. Also, it gives us an idea of the signal quality: results showed that working with excited states is a very delicate issue which demands a special effort.

Form factors

In Chapter 6, we presented a specific approach to deal with the b quark mass extrapolation, which has been applied to the $B_s \to D_s$ form factor determination. By building suitable ratios of appropriate quantities at zero recoil, it was possible to determine the factor

$$\mathscr{G}_s(1) \ = 1.052(47)$$

The above error bar can be significantly reduced if one imposes that the factor does not depend on the mass of the dynamical (sea) quark, which is essentially what we noticed from all of our lattice data (at all values of the lattice spacing).

Furthermore, we have determined $\mathscr{G}_s(w)$ at non zero recoils. From these data, we extracted the slope of $\mathscr{G}_s(w)$, ρ^2. In our case, we obtain

$$\rho^2 \ = 1.2(8)$$

Since we restrained our analysis to very small ws, we could not estimate the accurate value of the slope. However, the value is consistent with the experimental determination of ρ^2.

We also performed the first Lattice QCD estimate of the tensor form factor, which appears in some BSM models, with respect to the vector form factor $F_T(q^2)/F_+(q^2)$, for different non zero recoils. At the energy scale $\mu = m_b$ and in the $\overline{\text{MS}}$ scheme, we obtained

$$\frac{F_T(q^2)}{F_+(q^2)}_{q^2=11.5} = 1.08(7)$$

We are unable to say if the above ratio is a constant with the momentum, as predicted in the infinite mass limit, since the error estimate augments with increasing values of q^2.
We computed another form factor that has a significant contribution to the decay rate when there is a τ lepton in the final state. This contribution can be very important in various extensions of the SM. Using the same extrapolation strategy, the value at $q^2 = 11.5$ is

$$\frac{F_0(q^2)}{F_+(q^2)}_{q^2=11.5} = 0.77(2)$$

in agreement with the previous determination of the ratio $F_0(q^2)/F_+(q^2)$.

The form factors entering $B \to D^{**}$ decay channels were studied in Chapter 7. We have focused on the scalar D_0^* and the tensor D_2^* meson state contributions to the corresponding decay widths. Due to the lack in allocated computer time, we were unable to perform simulations on more than two gauge ensembles so that a reliable extrapolation to the continuum was not possible. Increasing the number of gauge configurations would help in getting more reliable results.

For the D_0^* states, we have guess-estimated the ratio $\mathscr{B}(B \to D_0^*)/\mathscr{B}(B \to D)$. The extrapolated value at vanishing lattice spacing gives 0.13. The main result here is the important fact that *at finite b and c masses, the $B \to D_0^*$ amplitude does not vanish at zero recoil.*

For the D_2^* state, we chose to estimate the ratio of $\tilde{k}$ to its value in the infinite mass limit since the latter is compatible with the experimental value. We have observed a signal for the $\tilde{k}$ ratio but the data points still displayed large uncertainties especially for the heaviest "b" quark masses.

Future perspective

In the past ten years, techniques and algorithms in LQCD have undergone a significant development; computing power has been massively increased and this is really encouraging for the Lattice community.

In order to calculate the physical observables and reach a precision on par with the experimental one, a more precise control of the uncertainties will be needed.
This work opens the door to explore different avenues

- with the increase in computational power, it will be possible to compute the momentum dependence of the $B \to D^{**}$ form factors. New Physics scenarios could also be added to study the semileptonic $B(B_s)$ decay to D^{**} (D_s^{**}). This would help in better understanding the NP effects.
- include the $J = 1$ $D^{**}(D_s^{**})$ states in the form factor computation. To this end one first needs to disentangle these two states.
- the exploration of the "ratio method" in the study of $B(B_s) \to D^{*,**}(D_s^{*,**})$ can help in reducing the uncertainties on the computed form factors.

Finally, there is an extensive list of interesting hadronic parameters relevant to heavy flavor phenomenology that can be determined using Lattice QCD. An essential step in all lattice computations is to find the source of uncertainty and try to reduce it as much as possible, in order to obtain more precise results.

Appendices

Appendix A

Quantum Field Theory on the Lattice

A.1 Short description of relevant notions in the continuum

In Quantum Field Theory (QFT), the partition function (which is also the generating functional of correlation functions) is expressed by

$$\mathscr{Z} \;=\; \int \mathscr{D}\phi \, e^{iS[\phi]}$$

where S is the action functional given in terms of the Lagrangian as

$$S \;=\; \int \mathscr{L} \, dt$$

Unlike the partition function in statistical mechanics, the partition function in QFT contains an extra factor of "i" in front of the action, making the integrand complex and hence, difficult to treat numerically (convergence problem).

Green's function: in real space, the scalar n-point Green's function, is defined as the functional expectation value of a time-ordered product of n scalar field operators

$$\mathscr{G}_n(x_1, x_2, ..., x_n) \;\equiv\; \big\langle T\{\, \phi(x_1)\phi(x_2)\cdots\phi(x_n)\,\}\big\rangle \;=\; \frac{1}{\mathscr{Z}} \int \mathscr{D}\phi \, e^{iS[\phi]}\, \phi(x_1)\cdots\phi(x_n) \tag{A.1}$$

The factor i in (A.1) is essential because it encodes the quantum feature of the theory. However, integrals of complex, oscillating functions are numerically uncontrollable.

Imaginary time: in order to avoid the convergence problem, a possible solution is to consider an imaginary time by performing the Wick rotation $\tau \rightsquigarrow it$. This rotation is a method for obtaining a solution to a mathematical problem in Minkowski space from its analogous version in Euclidean space.

Equation (A.1) then becomes

$$\begin{gathered}\mathscr{C}_n(x_1, x_2, ..., x_n) \equiv \left\langle T\{\, \phi(x_1)\phi(x_2)\cdots\phi(x_n)\,\}\right\rangle|_E = \frac{1}{\mathscr{Z}} \int \mathscr{D}\phi\, e^{-S_E[\phi]}\, \phi(x_1)\cdots\phi(x_n)|_E \\ \text{where} \quad \mathscr{Z} = \int \mathscr{D}\phi\, e^{-S_E[\phi]} \qquad \text{and} \qquad S_E = \int \mathscr{L}_E\, d\tau\end{gathered} \tag{A.2}$$

Furthermore, when comparing (A.1) and (A.2), we notice immediately how the path integral formulation of quantum field theory in Minkowski space is related to statistical physics in Euclidean space. Since $S[\phi]$ is real and bounded from above, $e^{-S[\phi]}$ could be interpreted as a probability density. Therefore, Eq. (A.2) is the statistical mean value (Maxwell–Boltzmann statistics) of the operator $\phi(x_1)\phi(x_2)\cdots\phi(x_n)$ and the Green's functions $\mathscr{G}_n$ are now equivalent to what is called *statistical correlation functions* $\mathscr{C}_n$.
This leads to many fruitful developments and makes numerical calculations and theoretical analyses much easier. Such integrals are sufficient to extract the relevant physical information, as for example the energy spectrum.

A.2 From Minkowski to Euclidean space

In order to evaluate numerically path integrals it is necessary to consider an imaginary time. To this end, we define the Wick rotation for any four-vector $\tilde{q}$

$$\begin{gathered}\tilde{q}_M\ (q^0_M,\, q^1_M,\, q^2_M,\, q^3_M) \qquad \longleftrightarrow \qquad \tilde{q}_E\ (q^1_E,\, q^2_E,\, q^3_E,\, q^4_E) \\ \text{where} \qquad q^4_E = i q^0_M \qquad \text{and} \qquad q^k_E = q^k_M\end{gathered}$$

The scalar product in Minkowski space is (with the choice of $g_{\mu\nu} = \text{diag}(+,-,-,-)$)

$$x \cdot y|_M = g_{\mu\nu} x^{\mu\nu} = x^0 y^0 - x^1 y^1 - x^2 y^2 - x^3 y^3$$

and in Euclidean space is

$$x \cdot y|_E = x^1 y^1 + x^2 y^2 + x^3 y^3 + x^4 y^4 = -x \cdot y|_M$$

For the sake of completeness, we give also the connection between the Dirac matrices in Euclidean and Minkowski space

$$\begin{aligned}\gamma_{1,2,3}|_E &\equiv -i\gamma_{1,2,3}|_M \\ \gamma_4|_E &\equiv -i\gamma_4|_M \equiv \gamma_0|_M\end{aligned}$$

The Euclidean Dirac matrices are chosen to be hermitian, and are simply denoted by $\gamma_\mu (\mu = 1, 2, 3, 4)$

$$\gamma_\mu \equiv \gamma_\mu|_E = \gamma^\dagger_\mu$$

They satisfy the anti-commutation relations

$$\{\gamma_\mu, \gamma_\nu\} = 2\delta_{\mu\nu}$$

For $\mu = 4$ and $\gamma_5 \equiv \gamma_1\gamma_2\gamma_3\gamma_4 = \gamma_5^\dagger$, one can take either the "non-relativistic" representation

$$\gamma_4 = \begin{pmatrix} 1 & 0 \\ 0 & -1 \end{pmatrix}, \qquad \gamma_5 = \begin{pmatrix} 0 & -1 \\ -1 & 0 \end{pmatrix}$$

or the "chiral representation"

$$\gamma_4 = \begin{pmatrix} 0 & 1 \\ 1 & 0 \end{pmatrix}, \qquad \gamma_5 = \begin{pmatrix} 1 & 0 \\ 0 & -1 \end{pmatrix}$$

A.3 Discretization of the scalar field

In order to better understand the discretization of a continuous space-time and introduce some useful notations, we propose to determine the propagator corresponding to a scalar field ϕ. The action corresponding to a free scalar field, in Euclidean space, reads

$$S[\phi] = -\frac{1}{2}\int d^4x \left(\partial_\mu\phi(x)\partial_\mu\phi(x) + m^2\phi^2(x)\right) \qquad \text{(the index } E \text{ will be dropped from now on.)}$$

Most of the time, a four-dimensional continuous space is discretized as a hypercubic box called *lattice* (see Fig. A.1) having a length L in spatial direction and T in time direction (T represents the Euclidean time slices). The distance "a" between sites is called *lattice spacing*. The spatial volume in lattice units is denoted by $\Omega = L^3$ and the total number of lattice points is $V = \Omega \times T$.

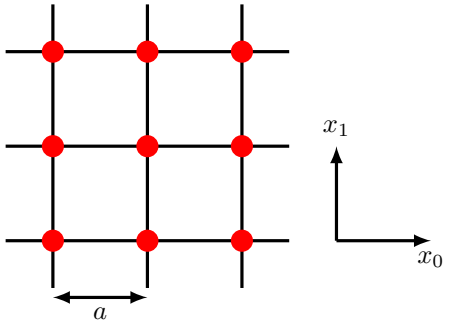


Figure A.1: The discretization of the lattice in two dimensions.

The points in a four dimensional hypercubic box are denoted by $x, y, \cdots$. They are usually chosen in

the interval

$$\begin{cases} 0 \le x_\mu \le L_\mu - 1 & \mu \in \{1,2,3\} \quad \text{are the three orthogonal spatial directions} \\ 0 \le x_4 \equiv \tau \le T - 1 & \text{the Euclidean time is the } 4^{\text{th}} \text{ coordinate} \end{cases}$$

For smooth functions $f(x)$, we have in the continuum limit

$$a^4 \sum_{n_1=0}^{N_L-1} \cdots \sum_{n_4=0}^{N_T-1} f(x_\mu) \quad \xrightarrow[a\to 0]{N_L, N_T \to \infty} \quad \int_0^V d^4x\, f(x) \quad \text{with fixed } L \text{ and } T$$

where N_L and N_T are the number of lattice points in spatial and time directions respectively.
The scalar field on the lattice is assigned to the sites x, so we write it ϕ_x. Derivatives in the continuum can be replaced by differences

$$\partial_\mu \phi_x = \frac{1}{2a}\left(\phi_{x+a\hat{\mu}} - \phi_{x-a\hat{\mu}}\right) \xrightarrow[a\to 0]{} \frac{\partial}{\partial x_\mu}\,\phi(x)$$

where $\hat{\mu}$ is a unit vector in the μ direction.
In the following, we will replace the notation $a^4 \sum_{n_1=0}^{N_L-1} \cdots \sum_{n_4=0}^{N_T-1}$ by $\sum_x$ for simplicity.

Momentum space

The usual plane waves in a finite volume with periodic boundary conditions are given by

$$e^{ip\cdot x} \qquad \text{where} \quad \begin{cases} p_\mu &= k_\mu \dfrac{2\pi}{L} \quad \mu \in \{1,2,3\} \quad \text{and } k_\mu \text{ are integers} \\ p_4 &= k_4 \dfrac{2\pi}{T} \quad k_4 \text{ is an integer} \end{cases}$$

There should not be more p_μ than x_μ, hence we take

$$\begin{cases} k_\mu \;=\; -\dfrac{N_L}{2}+1, -\dfrac{N_L}{2}+2, \cdots, \dfrac{N_L}{2} & \mu \in \{1,2,3\} \\ k_4 \;=\; -\dfrac{N_T}{2}+1, -\dfrac{N_T}{2}+2, \cdots, \dfrac{N_T}{2} \end{cases}$$

So, the momenta are restricted to the first Brillouin zone

$$\mathscr{B} \;=\; \left\{p:\; -\frac{\pi}{a} < p_\mu \le \frac{\pi}{a}\right\}$$

The Fourier transform (from position to momentum space) and its inverse are

$$\tilde{\phi}_p \;=\; \sum_x e^{-ip\cdot x}\,\phi_x \qquad \phi_x \;=\; \frac{1}{V}\sum_p e^{ip\cdot x}\,\tilde{\phi}_p \quad \text{where} \quad p\cdot x = \sum_\mu p_\mu\, x_\mu$$

For smooth functions $f(p)$, we have in the infinite-volume limit (we take $T = L = Na \to \infty$)

$$\frac{1}{V}\sum_p f(p) \;=\; \frac{1}{(2\pi)^4}\sum_k \left(\frac{2\pi}{L}\right)^4 f\left(\frac{2\pi}{L}k\right) \xrightarrow[N\to\infty]{a \text{ fixed}} \int_{-\frac{\pi}{a}}^{+\frac{\pi}{a}} f(p)\,\frac{d^4p}{(2\pi)^4}$$

The propagator of a free field can now be found in *momentum space*. After performing an integration by parts, we find that the action for the case under study can be written as

$$S \;=\; -\frac{1}{2}\sum_{x,y}\,\phi_x\,S_{xy}\,\phi_y$$

where

$$S_{xy} = \left(\sum_\mu \partial_\mu\partial_\mu + m^2\right)\delta_{x,y}$$

On the lattice, the second derivative of a function is usually taken as the following differences

$$-\sum_\mu \partial_\mu\partial_\mu\, f(x) \equiv \Box\, f(x) = +\frac{1}{a^2}\sum_\mu\,\left(f(x\,+\,a\hat{\mu})\,-\,2f(x)\,+\,f(x-a\hat{\mu})\right)$$

where $\Box$ is the d'Alembert operator. The matrix indices of S_{xy} correspond to lattice points. The propagator on the lattice is the inverse of S_{xy}

$$\sum_y\, S_{xy}G_{yz} \;=\; \delta_{x,z} \tag{A.3}$$

Substituting the Fourier transform

$$G_{yz} \;=\; \frac{1}{V}\sum_p\, e^{ip\cdot(y-z)}\,\tilde{G}(p)$$

in Eq. (A.3) gives

$$\frac{1}{V}\sum_p\,(-\Box + m^2)\,e^{ip\cdot(x-z)}\,\tilde{G}(p) \;=\; \delta_{x,z}$$

Applying the derivative $\Box$ on $e^{ip\cdot(x-z)}$ with respect to x, and replacing $\delta_{x,z}$ by $\frac{1}{V}\sum_p e^{ip\cdot(x-z)}$, we get

$$\frac{1}{V}\sum_p\,(m^2\,+\,a^{-2}\sum_\mu\big(2-2\cos(a\,p_\mu)\big)\,e^{ip\cdot(x-z)}\,\tilde{G}(p) \;=\; \frac{1}{V}\sum_p\,e^{ip\cdot(x-z)}$$

Finally, the discretized scalar field propagator reads

$$\boxed{\tilde{G}(p) \;=\; \frac{1}{m^2\,+\,a^{-2}\sum_\mu(2-2\cos(ap_\mu))}}$$

When $a \to 0$, $\tilde{G}(p)$ goes to

$$\frac{1}{m^2 + p^2 + O(a^2)} \tag{A.4}$$

which is the usual covariant expression for the scalar field propagator in Euclidean space

Back to Minkowski: we want to find the propagator of the scalar field in Minkowski space so, from (A.4) we use

$$p^2|_M = p_0^2 - p_k^2 = -p_4^2 - p_k^2 = -p^2|_E$$

and we obtain

$$\boxed{\tilde{G}(p)|_M = \frac{1}{m^2 - p^2}} \tag{A.5}$$

which is indeed the scalar propagator in Minkowski space.

Appendix B

Input file

We show here an example of the input file used when computing $B \to D^{**}$ two- and three-point correlation functions.

```
L 24
T 48
WallTime 2000000
Kappa 0.160856

SEED
NoiseType 4


ApeAlpha 0.5
ApeNiter 10
JacobiKappa 0.15
JacobiNiterSo 2  0 30
JacobiNiterSe 2  0 30
JacobiNiterSi 2  0 30

MassResiduesS0 2
0.0085 1.e-12
0.215 1.e-20

NThetaS0 1
0.00

MassResidueswS0 3
0.3498 1.e-20
0.4839 1.e-20
0.6694 1.e-20
```

```
NwThetaS0 21
0.00 0.00 0.00 0.99 1.21 1.48 1.41 1.72 2.11 2.02 2.46 3.01 2.50 3.05 3.73
2.92 3.56 4.36 3.66 4.46 5.46
NwThetaS0 7

ComputeDerivativeCorrelations 1
StartDerivativeInversionFromIMass 1


NContrTwoPoints 13
5 5
5 0
0 5
0 0
1 1
1 2
1 3
2 1
2 2
2 3
3 1
3 2
3 3

NChromoContrTwoPoints 0

MassResiduesS1 0

NThetaS1 0

MassResidueswS1 3
0.3498 1.e-20
0.4839 1.e-20
0.6694 1.e-20

NwThetaS1 21
0.00 0.00 0.00 0.99 1.21 1.48 1.41 1.72 2.11 2.02 2.46 3.01 2.50 3.05 3.73
2.92 3.56 4.36 3.66 4.46 5.46
NwThetaS1 7

TSep 18
NSpec 2
```

```
iThetaMassR 0 0 0
iThetaMassR 0 0 1



NContrThreePoints 29
0 9
0 6
0 7
0 8
1 9
1 6
1 7
1 8
2 9
2 6
2 7
2 8
3 9
3 6
3 7
3 8
1 1
1 2
1 3
2 1
2 2
2 3
3 1
3 2
3 3
5 1
5 2
5 3
5 4

NChromoContrThreePoints 0

NGaugeConf 1

conf.44
TSOURCE
outp_BDstar_wnonzero_tsource18
```

Appendix C

Extraction of the $B \to D^{**}$ form factors

The goal is to extract the form factors entering the transition amplitudes of $B \to D_2^*$ decays. Since these matrix elements are written in terms of the polarization tensor of a spin-2 state, one needs to construct an expression for such a polarization tensor using the chosen kinematics (in our case, in the D^{**} rest frame).
We start by finding the polarization tensors of ${}^3P_2(\lambda)$ state. Then, we will proceed to describe the strategy we followed to find the expressions of the desired form factors.

C.1 Polarization tensor for the ${}^3P_2$ state

The idea is to construct a spin-2 state by combining two spin-1 states. Explicitly, we have

$$\boxed{\varepsilon^{\mu\nu}(\vec{p},\,\lambda) = \sum_{s,\,s'} \langle 1\;1\;s\;s' \,|\, 2\;\lambda\rangle\, \varepsilon^{\mu}(\vec{p},\,s)\, \varepsilon^{\nu}(\vec{p},\,s')} \tag{C.1}$$

where $\vec{p}$ represents the spatial components of the four-momentum of the spin-2 state, λ (s and s') the spin projection of the spin-2 (spin-1) state along a quantification axis chosen to be the z axis[1] and, finally, with

$$\begin{cases} \varepsilon^{\mu\nu}(\vec{p},\,\lambda): & \text{polarisation tensor (spin 2)} \\ \varepsilon^{\mu}(\vec{p},\,s): & \text{polarisation vector (spin 1)} \\ \langle 1\;1\;s\;s' \,|\, 2\;\lambda\rangle: & \text{Clebsch-Gordan coefficients for } 1+1 \to 2 \end{cases}$$

Since we do the lattice computations in the D^{**} rest frame, the polarization vector and tensor will be calculated at zero three-momentum.

[1] $\lambda = \pm 2,\, \pm 1,\, 0$ and $s^{(\prime)} = \pm 1,\, 0$.

C.1.1 Polarisation vector $\varepsilon^{\mu}(\vec{0},\, s)$

The polarization vector $\varepsilon^{\mu}(\vec{0},\, s)$ four-vector reads [141]

$$\varepsilon^{\mu}(0) = \begin{pmatrix} 0 \\ 0 \\ 0 \\ -1 \end{pmatrix} \qquad \varepsilon^{\mu}(+1) = \frac{1}{\sqrt{2}} \begin{pmatrix} 0 \\ 1 \\ i \\ 0 \end{pmatrix} \qquad \varepsilon^{\mu}(-1) = \frac{1}{\sqrt{2}} \begin{pmatrix} 0 \\ -1 \\ i \\ 0 \end{pmatrix}$$

where the chosen quantification axis is the z axis.

C.1.2 Polarisation tensor $\varepsilon^{\mu\nu}(\vec{0},\, \lambda)$

- *First case*: $\boxed{\lambda = \pm 2}$

  Using (C.1)

$$\varepsilon^{\mu\nu}_{(\pm 2)} = \varepsilon^{\mu}(\pm 1)\, \varepsilon^{\nu}(\pm 1) \qquad \Longrightarrow \qquad \boxed{\varepsilon^{\mu\nu}_{(+2)} = \frac{1}{2} \begin{pmatrix} 0 & 0 & 0 & 0 \\ 0 & 1 & i & 0 \\ 0 & i & -1 & 0 \\ 0 & 0 & 0 & 0 \end{pmatrix}} \quad \text{and} \quad \boxed{\varepsilon^{\mu\nu}_{(-2)} = \frac{1}{2} \begin{pmatrix} 0 & 0 & 0 & 0 \\ 0 & 1 & -i & 0 \\ 0 & -i & -1 & 0 \\ 0 & 0 & 0 & 0 \end{pmatrix}}$$

- *Second case*: $\boxed{\lambda = \pm 1}$

  We have here

$$\varepsilon^{\mu\nu}_{(\pm 1)} = \frac{1}{2} \Big[\varepsilon^{\mu}(\pm 1)\, \varepsilon^{\nu}(0) + \varepsilon^{\mu}(0)\, \varepsilon^{\nu}(\pm 1) \Big]$$

$$\Longrightarrow \qquad \boxed{\varepsilon^{\mu\nu}_{(+1)} = \frac{1}{2} \begin{pmatrix} 0 & 0 & 0 & 0 \\ 0 & 0 & 0 & -1 \\ 0 & 0 & 0 & -i \\ 0 & -1 & -i & 0 \end{pmatrix}} \quad \text{and} \quad \boxed{\varepsilon^{\mu\nu}_{(-1)} = \frac{1}{2} \begin{pmatrix} 0 & 0 & 0 & 0 \\ 0 & 0 & 0 & 1 \\ 0 & 0 & 0 & -i \\ 0 & 1 & -i & 0 \end{pmatrix}}$$

- *Third case*: $\boxed{\lambda = 0}$

  Finally

$$\varepsilon^{\mu\nu}_{(0)} = \frac{1}{\sqrt{6}} \Big[\varepsilon^{\mu}(+1)\, \varepsilon^{\nu}(-1) + \varepsilon^{\mu}(-1)\, \varepsilon^{\nu}(+1) + 2\, \varepsilon^{\mu}(0)\, \varepsilon^{\nu}(0) \Big] \qquad \Longrightarrow \qquad \boxed{\varepsilon^{\mu\nu}_{(0)} = \frac{1}{\sqrt{6}} \begin{pmatrix} 0 & 0 & 0 & 0 \\ 0 & -1 & 0 & 0 \\ 0 & 0 & -1 & 0 \\ 0 & 0 & 0 & 2 \end{pmatrix}}$$

Notice that the transversality of $\varepsilon^{\mu\nu}$ implies

$$\sum_{\nu} \varepsilon^{\mu\nu}_{(p_{D^{**}})}\, p_{D^{**}\nu} \;=\; 0 \qquad \Longrightarrow \qquad m_{D^{**}}\, \varepsilon^{\mu 0}_{(\lambda)} = 0 \qquad \Longrightarrow \qquad \boxed{\varepsilon^{0\mu}_{(\lambda)} = 0} \qquad \text{since} \;\; \varepsilon^{\mu\nu}_{(\lambda)} = \varepsilon^{\nu\mu}_{(\lambda)}$$

This property could have been directly observed in the explicit form of the matrices $\varepsilon^{\mu\nu}_{(\lambda)}$. Also, owing to the Minkowski metrics we have $\varepsilon^{\mu\nu}_{(\lambda)} = \varepsilon^{(\lambda)}_{\mu\nu}$.

C.2 $B \to D_2^*$ form factors

Let us recall the following notations to represent the vector and the axial hadronic matrix elements

$$\mathscr{T}^A_{\mu(\lambda)} \stackrel{\text{def.}}{=} \left\langle {}^3P_2(\lambda) \,\middle|\, A_\mu \,\middle|\, B(p_{_B}) \right\rangle \qquad \text{and} \qquad \mathscr{T}^V_{\mu(\lambda)} \stackrel{\text{def.}}{=} \left\langle {}^3P_2(\lambda) \,\middle|\, V_\mu \,\middle|\, B(p_{_B}) \right\rangle$$

They are parametrized in terms of weak form factors as

$$\begin{aligned}
\mathscr{T}^V_{\mu(\lambda)} &= \; i\boxed{\tilde{h}}\,\epsilon_{\mu\rho\sigma\tau}\,\varepsilon^{\rho\alpha *}_{(p_{_{D^{**}}})}\,p_{_{B\alpha}}\,(p_{_B}+p_{_{D^{**}}})^\sigma\,(p_{_B}-p_{_{D^{**}}})^\tau = 2\,i\boxed{\tilde{h}}\,\epsilon_{\mu\rho\sigma\tau}\,\varepsilon^{\rho\alpha *}_{(p_{_{D^{**}}})}\,p_{_{B\alpha}}\,p^\sigma_{_{D^{**}}}\,p^\tau_{_B} \\
\mathscr{T}^A_{\mu(\lambda)} &= \boxed{\tilde{k}}\,\varepsilon^{(p_{_{D^{**}}})}_{\mu\rho}\,p^\rho_{_B} + \left(\varepsilon^{(p_{_{D^{**}}})}_{\alpha\beta}\,p^\alpha_{_B}p^\beta_{_B}\right)\left[\boxed{\tilde{b}_+}\,(p_{_B}+p_{_{D^{**}}})_\mu + \boxed{\tilde{b}_-}\,(p_{_B}-p_{_{D^{**}}})_\mu\right]
\end{aligned} \tag{C.2}$$

Expanding the above matrix elements in the D^{**} rest frame gives rise to expressions written in terms of the polarization tensor $\varepsilon^{(\lambda)}_{\mu\nu}$ and of the four momenta $p_{_B}$. As an example we show the matrix element

$$\mathscr{T}^A_{i(\lambda)} = \boxed{\tilde{k}}\,\varepsilon^{(\lambda)*}_{i\rho}\,p^\rho_{_B} + \left(\varepsilon^{(\lambda)*}_{\alpha\beta}\,p^\alpha_{_B}p^\beta_{_B}\right)\left[\boxed{\tilde{b}_+}\,p_{_{B\,i}} + \boxed{\tilde{b}_-}\,p_{_{B\,i}}\right] \tag{C.3}$$

used to extract the form factor $\tilde{k}$. So, the first step is to calculate the contributions

$$\varepsilon^{(\lambda)}_{\mu\nu}p^\nu_{_B}, \quad \varepsilon^{\mu\nu}_{(\lambda)}p_{_{B\,\nu}} \quad \text{and} \quad \varepsilon^{\mu\nu}_{(\lambda)}p_{_{B\,\mu}}p_{_{B\,\nu}} \tag{C.4}$$

by making use of the explicit expressions of the polarization tensors for a spin-2 state, determined in Section C.1, along with expressions of the B four momenta

$$p^\mu_{_B} = (E_{_B},\, p,\, p,\, p) \qquad \Longrightarrow \qquad p_{_{B\,\mu}} = (E_{_B},\, -p,\, -p,\, -p)\,,$$

The expressions of the contributions are listed in Tables C.1 and C.2.

The next step is to use the above contributions to obtain the explicit expressions of form factors in terms of the transition amplitudes. If we carry on with our example, let us illustrate how one can extract $\tilde{k}$ from Eq. (C.3). The strategy is to choose combinations listed in Tables C.1 and C.2 so that the contribution of the other form factors in Eq. (C.3), $\tilde{b}_\pm$, vanishes. In other words, the contribution of the term $\left(\varepsilon^{(\lambda)*}_{\alpha\beta}\,p^\alpha_{_B}p^\beta_{_B}\right)$ must go to zero. One can see from Table C.2 that $\varepsilon^{\mu\nu}_{(\lambda=0)}p_{_{B\,\mu}}p_{_{B\,\nu}} = 0$. So, for the ${}^3P_2(\lambda=0)$ state, it is possible to express $\tilde{k}$ by considering the amplitudes

$$\mathscr{T}^A_{i(0)} = \boxed{\tilde{k}}\,\varepsilon^{(0)}_{i\rho}\,p^\rho_{_B} = -\boxed{\tilde{k}}\,\frac{p}{\sqrt{6}}\left(1,\,1,\,-2\right) \tag{C.5}$$

$\varepsilon^{(\lambda)}_{\mu\nu}$	$\varepsilon^{(\lambda)}_{\mu\nu} p_B^\nu$
$\varepsilon^{(+2)}_{\mu\nu}$	$\frac{p}{2}\Big(0,\, 1+i,\, i-1,\, 0\Big)$
$\varepsilon^{(+1)}_{\mu\nu}$	$-\frac{p}{2}\Big(0,\, 1,\, i,\, 1+i\Big)$
$\varepsilon^{(0)}_{\mu\nu}$	$-\frac{p}{\sqrt{6}}\Big(0,\, 1,\, 1,\, -2\Big)$
$\varepsilon^{(-1)}_{\mu\nu}$	$\frac{p}{2}\Big(0,\, 1,\, -i,\, 1-i\Big)$
$\varepsilon^{(-2)}_{\mu\nu}$	$\frac{p}{2}\Big(0,\, 1-i,\, -1-\, i,\, 0\Big)$
$\varepsilon^{(+2)}_{\mu\nu} + \varepsilon^{(-2)}_{\mu\nu}$	$p\Big(0,\, 1,\, -1,\, 0\Big)$
$\varepsilon^{(+2)}_{\mu\nu} - \varepsilon^{(-2)}_{\mu\nu}$	$p\Big(0,\, i,\, i,\, 0\Big)$
$\varepsilon^{(+1)}_{\mu\nu} + \varepsilon^{(-1)}_{\mu\nu}$	$p\Big(0,\, 0,\, -i,\, -i\Big)$
$\varepsilon^{(+1)}_{\mu\nu} - \varepsilon^{(-1)}_{\mu\nu}$	$p\Big(0,\, -1,\, 0,\, -1\Big)$

$\varepsilon^{\mu\nu}_{(\lambda)}$	$\varepsilon^{\mu\nu}_{(\lambda)} p_{B\,\nu}$
$\varepsilon^{\mu\nu}_{(+2)}$	$-\frac{p}{2}\Big(0,\, 1+i,\, -1+i,\, 0\Big)$
$\varepsilon^{\mu\nu}_{(+1)}$	$\frac{p}{2}\Big(0,\, 1,\, i,\, 1+i\Big)$
$\varepsilon^{\mu\nu}_{(0)}$	$\frac{p}{\sqrt{6}}\Big(0,\, 1,\, 1,\, -2\Big)$
$\varepsilon^{\mu\nu}_{(-1)}$	$\frac{p}{2}\Big(0,\, -1,\, i,\, -1+i\Big)$
$\varepsilon^{\mu\nu}_{(-2)}$	$\frac{p}{2}\Big(0,\, -1+i,\, 1+i,\, 0\Big)$
$\varepsilon^{\mu\nu}_{(+2)} + \varepsilon^{\mu\nu}_{(-2)}$	$p\Big(0,\, -1,\, 1,\, 0\Big)$
$\varepsilon^{\mu\nu}_{(+2)} - \varepsilon^{\mu\nu}_{(-2)}$	$p\Big(0,\, -i,\, -i,\, 0\Big)$
$\varepsilon^{\mu\nu}_{(+1)} + \varepsilon^{\mu\nu}_{(-1)}$	$p\Big(0,\, 0,\, i,\, i\Big)$
$\varepsilon^{\mu\nu}_{(+1)} - \varepsilon^{\mu\nu}_{(-1)}$	$p\Big(0,\, 1,\, 0,\, 1\Big)$

Table C.1: Contribution of the terms $\varepsilon^{(\lambda)}_{\mu\nu} p_B^\nu$ and $\varepsilon^{\mu\nu}_{(\lambda)} p_{B\,\nu}$ to the $B \to {}^3P_2$ transition amplitude.

$\varepsilon^{\mu\nu}_{(\lambda)}$	$\varepsilon^{\mu\nu}_{(\lambda)} p_{B\,\mu} p_{B\,\nu}$
$\varepsilon^{\mu\nu}_{(+2)}$	$i\,p^2$
$\varepsilon^{\mu\nu}_{(+1)}$	$-\,(1+i)\,p^2$
$\varepsilon^{\mu\nu}_{(0)}$	0
$\varepsilon^{\mu\nu}_{(-1)}$	$(1-i)\,p^2$
$\varepsilon^{\mu\nu}_{(-2)}$	$-\,i\,p^2$
$\varepsilon^{\mu\nu}_{(+2)} + \varepsilon^{\mu\nu}_{(-2)}$	0
$\varepsilon^{\mu\nu}_{(+2)} - \varepsilon^{\mu\nu}_{(-2)}$	$2\,i\,p^2$
$\varepsilon^{\mu\nu}_{(+1)} + \varepsilon^{\mu\nu}_{(-1)}$	$-\,2\,i\,p^2$
$\varepsilon^{\mu\nu}_{(+1)} - \varepsilon^{\mu\nu}_{(-1)}$	$-\,2\,p^2$

Table C.2: Contribution of the term $\varepsilon^{\mu\nu}_{(\lambda)} p_{B\,\mu} p_{B\,\nu}$ to the $B \to {}^3P_2$ transition amplitude.

The relation (C.5) implies

$$\tilde{k} = -\,\frac{\sqrt{6}}{p}\,\mathscr{T}^A_{1(0)} = -\,\frac{\sqrt{6}}{p}\,\mathscr{T}^A_{2(0)} = \frac{\sqrt{6}}{2\,p}\,\mathscr{T}^A_{3(0)}$$

Moreover, the sum of these two terms

$$\varepsilon^{\mu\nu}_{(\lambda=+2)} p_{B\,\mu} p_{B\,\nu} \; + \varepsilon^{\mu\nu}_{(\lambda=-2)} p_{B\,\mu} p_{B\,\nu}$$

is zero. Therefore, combining $\mathscr{T}^A_{i(+2)}$ and $\mathscr{T}^A_{i(-2)}$ leads to the form factor $\tilde{k}$

$$\mathscr{T}^A_{i(+2)} + \mathscr{T}^A_{i(-2)} = \boxed{\tilde{k}} \left(\varepsilon^{(+2)}_{i\rho} p_B^\rho + \varepsilon^{(-2)}_{i\rho} p_B^\rho \right) = \boxed{\tilde{k}}\, p \left(1,\, -1,\, 0 \right) \tag{C.6}$$

With the relation (C.6), we obtain

$$\tilde{k} = \frac{1}{p} \left[\mathscr{T}^A_{1(+2)} + \mathscr{T}^A_{1(-2)} \right] = -\frac{1}{p} \left[\mathscr{T}^A_{2(+2)} + \mathscr{T}^A_{2(-2)} \right]$$

Notice that these are not the only possible expressions. One can eliminate the form factors $\tilde{b}_\pm$ by using other vanishing contributions from Table C.2. The above strategy is the same for all $B \to D_2^*$ form factors.

Appendix D

Semileptonic decay widths

In this appendix, we will consider the semileptonic decay of B into the D^{**} mesons and we will find the expressions of the corresponding differential decay widths. We will also take into account massive charged leptons.

D.1 Stating the problem

We aim to evaluate the differential decay width $\mathrm{d}\Gamma(B \to D^{**}\,\ell\,\bar{\nu}_\ell)$, whose general expression is

$$\mathrm{d}\Gamma(B \to D^{**}\,\ell\,\bar{\nu}_\ell) = \frac{1}{2\,E_{_B}}\,|\bar{\mathscr{M}}|^2\,\mathrm{d}\Phi \tag{D.1}$$

$$\text{with} \quad \begin{cases} \mathrm{d}\Phi = \dfrac{d^3\vec{p}_{_{D^{**}}}}{(2\pi)^3\,2E_{_{D^{**}}}}\,\dfrac{d^3\vec{p}_{\ell}}{(2\pi)^3\,2E_{\ell}}\,\dfrac{d^3\vec{p}_{\nu}}{(2\pi)^3\,2E_{_\nu}}\,(2\pi)^4\,\delta^{(4)}(p_{_B} - p_{_{D^{**}}} - p_\ell - p_{_\nu}) \\ |\bar{\mathscr{M}}|^2 = \displaystyle\sum_{\mu,\,\nu} W_{\mu\nu}\ell^{\mu\nu} \end{cases}$$

where $W_{\mu\nu}$ denotes the hadronic tensor

$$W_{\mu\nu}(p_{_B},\,p_{_{D^{**}}}) = \frac{G_F^2\,|V_{cb}|^2}{2} \sum_{\text{final spins}} \big\langle D^{**}(p_{_{D^{**}}})\,\big|\,V_\mu - A_\mu\,\big|\,B(p_{_B})\big\rangle\,\big\langle B(p_{_B})\,\big|\,V_\nu - A_\nu\,\big|\,D^{**}(p_{_{D^{**}}})\big\rangle$$

(let us note that there is no summation nor average over the initial spins since the B meson has a spin equal to zero); $\ell^{\mu\nu}$ represents the leptonic tensor

$$\ell^{\mu\nu}(p_\ell,\,p_{_\nu}) = \sum_s \big[\bar{u}_\ell(p_\ell,s)\,\gamma^\mu\big(1-\gamma^5\big)v_\nu(p_{_\nu})\big]\cdot\big[\bar{u}_\ell(p_\ell,s)\,\gamma^\nu\big(1-\gamma^5\big)v_\nu(p_{_\nu})\big]^* \tag{D.2}$$

In this last formula, $u_\ell(p_\ell,s)$ is the lepton ℓ spinor (s denotes the usual projection of its spin), while $v_\nu(p_{_\nu})$ represents the antineutrino $\bar{\nu}$ spinor.

All that remains is to compute the leptonic and the hadronic tensors as well as the measure $\mathrm{d}\Phi$ of the phase space in order to obtain the expression of the differential decay widths.

D.1.1 Leptonic tensor $\ell^{\mu\nu}$

Starting from (D.2), the second term between brackets reads

$$\begin{aligned}\left[\bar{u}_\ell(p_\ell,s)\,\gamma^\nu\big(1-\gamma^5\big)v_\nu(p_\nu)\right]^* &= \left[\bar{u}_\ell(p_\ell,s)\,\gamma^\nu\big(1-\gamma^5\big)v_\nu(p_\nu)\right]^\dagger \\ &= \bar{v}_\nu(p_\nu)\,\gamma^\nu\big(1-\gamma^5\big)u_\ell(p_\ell,s)\end{aligned}$$

Therefore, relation (D.2) becomes

$$\ell^{\mu\nu} = \sum_s \left[u_\ell(p_\ell,s)\right]_d \left[\bar{u}_\ell(p_\ell,s)\right]_a \left[\gamma^\mu\big(1-\gamma^5\big)\right]_{ab} \left[v_\nu(p_\nu)\right]_b \left[\bar{v}_\nu(p_\nu)\right]_c \left[\gamma^\nu\big(1-\gamma^5\big)\right]_{cd}$$

where, in the last two relations, we have explicitly introduced the Lorentz indices (a summation over a, b, c and d is implied).

Using the following relations

$$\begin{cases} \displaystyle\sum_s u_\ell(p_\ell,s)\,\bar{u}_\ell(p_\ell,s) = (\not{p}_\ell + m_\ell) \quad\Longrightarrow\quad \sum_s \left[u_\ell(p_\ell,s)\right]_d \left[\bar{u}_\ell(p_\ell,s)\right]_a = (\not{p}_\ell + m_\ell)_{da} & \text{for the massive lepton} \\ v_\nu(p_\nu)\,\bar{v}_\nu(p_\nu) = \dfrac{1}{2}(1-\gamma^5)\not{p}_\nu \quad\Longrightarrow\quad \left[v_\nu(p_\nu)\right]_b \left[\bar{v}_\nu(p_\nu)\right]_c = \left[\dfrac{1}{2}(1-\gamma^5)\not{p}_\nu\right]_{bc} & \text{for the massless antineutrino} \end{cases}$$

one finally obtains

$$\boxed{\ell^{\mu\nu} = 8\left[p_\ell^\mu\,p_\nu^\nu \;+\; p_\ell^\nu\,p_\nu^\mu \;-\; (p_\ell\cdot p_\nu)\,g^{\mu\nu} \;-\; i\,\epsilon^{\mu\nu\rho\sigma}(p_\ell)_\rho(p_\nu)_\sigma\right]} \tag{D.3}$$

Notice that the mass of the charged lepton has vanished, which renders the expression valid in the situations where $m_\ell = 0$ as well as $m_\ell \neq 0$.

D.2 Hadronic tensor $W_{\mu\nu}$

D.2.1 Generalities

From the expressions of the transition amplitudes given in Chapter 7, the general structure of the hadronic tensor can be inferred and put into the form [136]

$$\begin{aligned}W_{\mu\nu} = \frac{G_F^2\,|V_{cb}|^2}{2}\Big[&\boxed{\alpha}\,g_{\mu\nu} \;+\; \boxed{\beta_{++}}(p_B+p_{D^{**}})_\mu(p_B+p_{D^{**}})_\nu \;+\; \boxed{\beta_{+-}}(p_B+p_{D^{**}})_\mu(p_B-p_{D^{**}})_\nu \\ &+\; \boxed{\beta_{-+}}(p_B-p_{D^{**}})_\mu(p_B+p_{D^{**}})_\nu \;+\; \beta_{--}(p_B-p_{D^{**}})_\mu(p_B-p_{D^{**}})_\nu \;+\; i\boxed{\gamma}\,\epsilon_{\mu\nu\rho\sigma}(p_B+p_{D^{**}})^\rho(p_B-p_{D^{**}})^\sigma\Big]\end{aligned} \tag{D.4}$$

In order to compute explicitly the coefficients $\boxed{\alpha}$, $\boxed{\beta_{++}}$, $\boxed{\beta_{+-}}$, $\boxed{\beta_{-+}}$, $\boxed{\beta_{--}}$ and $\boxed{\gamma}$, we have to evaluate the possible summation over the D^{**} spin

- *Scalar meson*: there is no summation

- *Vector meson*: the polarisation tensor $\varepsilon_\mu^{(p)}$ satisfies $\sum_s \varepsilon_\mu^{(p)*}\,\varepsilon_\nu^{(p)} = -\,g_{\mu\nu} + \dfrac{p_\mu\,p_\nu}{p^2}$

- *Tensor meson $J = 2$*: the polarisation tensor $\varepsilon_{\mu\nu}^{(p)}$ satisfies [142]

$$\sum_s \varepsilon_{\mu\nu}^{(p)*}\,\varepsilon_{\rho\sigma}^{(p)} = -\,\frac{1}{3}\left(g_{\mu\nu} - \frac{p_\mu\,p_\nu}{p^2}\right)\left(g_{\rho\sigma} - \frac{p_\rho\,p_\sigma}{p^2}\right) + \frac{1}{2}\left(g_{\mu\rho} - \frac{p_\mu\,p_\rho}{p^2}\right)\left(g_{\nu\sigma} - \frac{p_\nu\,p_\sigma}{p^2}\right) + \frac{1}{2}\left(g_{\mu\sigma} - \frac{p_\mu\,p_\sigma}{p^2}\right)\left(g_{\nu\rho} - \frac{p_\nu\,p_\rho}{p^2}\right)$$

D.2.2 $^3P_0$ case

We expand the relation

$$W_{\mu\nu} = \frac{G_F^2\,|V_{cb}|^2}{2}\,[\tilde{u}_+(p_B + p_{D^{**}})_\mu + \tilde{u}_-(p_B - p_{D^{**}})_\mu]\cdot[\tilde{u}_+(p_B + p_{D^{**}})_\nu + \tilde{u}_-(p_B - p_{D^{**}})_\nu]^*$$

and then identify the terms according to Eq. (D.4). We find

$$^3P_0 \begin{cases} \boxed{\alpha} = 0 \\ \boxed{\beta_{++}} = |\tilde{u}_+|^2 \qquad \boxed{\beta_{+-}} = \tilde{u}_+\tilde{u}_-^* \qquad \boxed{\beta_{-+}} = \tilde{u}_+^*\tilde{u}_- \qquad \boxed{\beta_{--}} = |\tilde{u}_-|^2 \\ \boxed{\gamma} = 0 \end{cases}$$

D.2.3 $^3P_2$ case

We proceed analogously as before and we obtain

$$\boxed{\alpha} = -\,\frac{(p_B\cdot p_{D_2^*})^2 - m_B^2 m_{D_2^*}^2}{2\,m_{D_2^*}^2}\left[|\tilde{k}|^2 + 4\,|\tilde{h}|^2\Big((p_B\cdot p_{D_2^*})^2 - m_B^2 m_{D_2^*}^2\Big)\right]$$

$$\boxed{\beta_{++}} = \frac{\tilde{k}\,\tilde{b}_+^* + \tilde{k}^*\,\tilde{b}_+}{3\,m_{D_2^*}^4}\Big(p_B\cdot p_{D_2^*} - m_{D_2^*}^2\Big)\Big((p_B\cdot p_{D_2^*})^2 - m_B^2 m_{D_2^*}^2\Big) + \frac{2\,|\tilde{b}_+|^2}{3\,m_{D_2^*}^4}\Big((p_B\cdot p_{D_2^*})^2 - m_B^2 m_{D_2^*}^2\Big)^2 - \frac{|\tilde{h}|^2}{2\,m_{D_2^*}^2}\Big((p_B\cdot p_{D_2^*})^2 - m_B^2 m_{D_2^*}^2\Big)(p_B - p_{D_2^*})^2 + \frac{|\tilde{k}|^2}{24\,m_{D_2^*}^4}\left[m_{D_2^*}^2(p_B - p_{D_2^*})^2 + 4\Big((p_B\cdot p_{D_2^*})^2 - m_B^2 m_{D_2^*}^2\Big)\right]$$

$$\boxed{\beta_{+-}} = \frac{2\,\tilde{b}_+\,\tilde{b}_-^*}{3\,m_{D_2^*}^4}\Big((p_B\cdot p_{D_2^*})^2 - m_B^2 m_{D_2^*}^2\Big)^2 + \frac{\tilde{k}\,\tilde{b}_-^*}{3\,m_{D_2^*}^4}\Big(p_B\cdot p_{D_2^*} - m_{D_2^*}^2\Big)\Big((p_B\cdot p_{D_2^*})^2 - m_B^2 m_{D_2^*}^2\Big)$$
$$- \frac{\tilde{k}^*\tilde{b}_+}{3\,m_{D_2^*}^4}\Big(p_B\cdot p_{D_2^*} + m_{D_2^*}^2\Big)\Big((p_B\cdot p_{D_2^*})^2 - m_B^2 m_{D_2^*}^2\Big) + \frac{|\tilde{h}|^2}{2\,m_{D_2^*}^2}(m_B^2 - m_{D_2^*}^2)\Big((p_B\cdot p_{D_2^*})^2 - m_B^2 m_{D_2^*}^2\Big)$$
$$+ \frac{|\tilde{k}|^2}{24\,m_{D_2^*}^4}\Big(3\,m_B^2\,m_{D_2^*}^2 - 4\,(p_B\cdot p_{D_2^*})^2 + m_{D_2^*}^4\Big)$$

$$\boxed{\beta_{-+}} = \boxed{\beta_{+-}^*}$$

$$\boxed{\beta_{--}} = -\frac{\tilde{k}\,\tilde{b}_-^* + \tilde{k}^*\,\tilde{b}_-}{3\,m_{D_2^*}^4}\Big(p_B\cdot p_{D_2^*} + m_{D_2^*}^2\Big)\Big((p_B\cdot p_{D_2^*})^2 - m_B^2 m_{D_2^*}^2\Big) + \frac{2\,|\tilde{b}_-|^2}{3\,m_{D_2^*}^4}\Big((p_B\cdot p_{D_2^*})^2 - m_B^2 m_{D_2^*}^2\Big)^2$$
$$- \frac{|\tilde{h}|^2}{2\,m_{D_2^*}^2}\Big((p_B\cdot p_{D_2^*})^2 - m_B^2 m_{D_2^*}^2\Big)(p_B + p_{D_2^*})^2$$
$$+ \frac{|\tilde{k}|^2}{24\,m_{D_2^*}^4}\Big[m_{D_2^*}^2(p_B + p_{D_2^*})^2 + 4\Big((p_B\cdot p_{D_2^*})^2 - m_B^2 m_{D_2^*}^2\Big)\Big]$$

$$\boxed{\gamma} = \frac{\tilde{k}^*\,\tilde{h} + \tilde{k}\,\tilde{h}^*}{2\,m_{D_2^*}^2}\Big((p_B\cdot p_{D_2^*})^2 - m_B^2 m_{D_2^*}^2\Big)$$

D.2.4 Contraction $|\bar{\mathscr{M}}|^2 = W_{\mu\nu}\ell^{\mu\nu}$

Finally, the contraction of the Eqs. (D.3) and (D.4) gives

$$|\bar{\mathscr{M}}|^2 = \frac{G_F^2\,|V_{cb}|^2}{2}\Big[-16\boxed{\alpha}\,p_\ell\cdot p_\nu + 8\boxed{\beta_{++}}\Big\{2\,[(p_B + p_{D^{**}})\cdot p_\ell]\,[(p_B + p_{D^{**}})\cdot p_\nu] - (p_\ell\cdot p_\nu)(p_B + p_{D^{**}})^2\Big\}$$
$$+8\boxed{\beta_{+-}}\Big\{-(p_\ell\cdot p_\nu)(m_B^2 - m_{D^{**}}^2) - 2\,i\,\epsilon_{\mu\nu\rho\sigma}p_B^\mu p_{D^{**}}^\nu p_\ell^\rho p_\nu^\sigma + 2\,(p_B\cdot p_\ell)(p_B\cdot p_\nu) - 2\,(p_{D^{**}}\cdot p_\ell)(p_{D^{**}}\cdot p_\nu)\Big\}$$
$$+8\boxed{\beta_{-+}}\Big\{-(p_\ell\cdot p_\nu)(m_B^2 - m_{D^{**}}^2) + 2\,i\,\epsilon_{\mu\nu\rho\sigma}p_B^\mu p_{D^{**}}^\nu p_\ell^\rho p_\nu^\sigma + 2\,(p_B\cdot p_\ell)(p_B\cdot p_\nu) - 2\,(p_{D^{**}}\cdot p_\ell)(p_{D^{**}}\cdot p_\nu)\Big\}$$
$$+8\boxed{\beta_{--}}\Big\{2\,[(p_B - p_{D^{**}})\cdot p_\ell]\,[(p_B - p_{D^{**}})\cdot p_\nu] - (p_\ell\cdot p_\nu)(p_B - p_{D^{**}})^2\Big\}$$
$$+32\boxed{\gamma}\Big\{(p_B\cdot p_\nu)(p_{D^{**}}\cdot p_\ell) - (p_B\cdot p_\ell)(p_{D^{**}}\cdot p_\nu)\Big\}\Big]$$

D.3 Measure dΦ of the phase space

For simplicity, we will work from now on in the rest frame of the B meson. The momenta involved are

$$p_B(m_B,\vec{0}) \quad ; \quad p_{D^{**}}(E_{D^{**}},\vec{p}_{D^{**}}) \quad ; \quad p_\ell(E_\ell,\vec{p}_\ell) \quad ; \quad p_\nu(E_\nu,\vec{p}_\nu) \ \text{ with } m_\nu = 0$$

The different scalar products can be written as

$$\begin{cases} p_B \cdot p_\ell = m_B\, E_\ell \\ p_B \cdot p_{D^{**}} = m_B\, E_{D^{**}} \\ p_\ell \cdot p_{D^{**}} = E_\ell\, E_{D^{**}} - \vec{p}_\ell \cdot \vec{p}_{D^{**}} \end{cases}$$

Let us also introduce the x and y parameters, defined by

$$x\, m_B = 2\, E_\ell \qquad \text{as well as} \qquad y\, m_B^2 = (p_B - p_{D^{**}})^2 = (p_\ell + p_\nu)^2$$

Knowing these two parameters is equivalent to knowing the energies E_ℓ and $E_{D^{**}}$. Indeed

$$y\, m_B^2 = (p_B - p_{D^{**}})^2 = m_B^2 + m_{D^{**}}^2 - 2\, \underbrace{p_B \cdot p_{D^{**}}}_{m_B\, E_{D^{**}}} \qquad \Longrightarrow \qquad E_{D^{**}} = \frac{m_B^2(1-y) + m_{D^{**}}^2}{2\, m_B} \tag{D.5}$$

while the product of p_ℓ with p_ν is given by

$$y\, m_B^2 = (p_\ell + p_\nu)^2 = m_\ell^2 + \underbrace{m_\nu^2}_{0} + 2\, p_\ell \cdot p_\nu \qquad \Longrightarrow \qquad p_\ell \cdot p_\nu = \frac{1}{2}\left(y\, m_B^2 - m_\ell^2\right)$$

Conservation of total momentum then leads to

$$\frac{1}{2}\left(y\, m_B^2 - m_\ell^2\right) = p_\ell \cdot (p_B - p_{D^{**}} - p_\ell) \qquad \Longrightarrow \qquad p_\ell \cdot p_{D^{**}} = \frac{1}{2}\left[m_B^2(x-y) - m_\ell^2\right]$$

Finally, differentiating the relations (D.3) and (D.5) gives

$$\boxed{\mathrm{d}E_\ell = \frac{m_B}{2}\,\mathrm{d}x} \qquad \text{and} \qquad \boxed{\mathrm{d}E_{D^{**}} = -\,\frac{m_B}{2}\,\mathrm{d}y} \tag{D.6}$$

Notice that $E_{D^{**}}$ and y vary in opposite directions.

D.3.1 Starting point

Our goal is to calculate the differential widths with respect to the lepton energy E_ℓ and the transfer $(p_B - p_{D^{**}})^2$, in other words with respect to the variables x and y ($\mathrm{d}^2\Gamma/\mathrm{d}x\,\mathrm{d}y$). We start from the general expression of the elementary volume of the phase space

$$\mathrm{d}\Phi = \frac{d^3\vec{p}_{D^{**}}}{(2\pi)^3\, 2E_{D^{**}}}\, \frac{d^3\vec{p}_\ell}{(2\pi)^3\, 2E_\ell}\, \frac{d^3\vec{p}_\nu}{(2\pi)^3\, 2E_\nu}\, (2\pi)^4\, \delta^{(4)}(p_B - p_{D^{**}} - p_\ell - p_\nu)$$

First step

We begin by integrating out the antineutrino momentum $\vec{p}_\nu$. To do so, we transform the 3D-integral into a 4D-integral by using

$$\int \frac{d^3\vec{p}_\nu}{2E_\nu} = \int d^4p_\nu\, \delta(p_\nu^2)\, \theta(E_\nu)$$

where $\theta(E_\nu)$ denotes the Heaviside "function". The new phase space element, averaged over the antineutrino momenta, is

$$\mathrm{d}\Phi = \frac{1}{(2\pi)^5}\frac{d^3\vec{p}_{D^{**}}}{2E_{D^{**}}}\,\frac{d^3\vec{p}_\ell}{2E_\ell}\,\delta\big[(p_B - p_{D^{**}} - p_\ell)^2\big]\;\theta(m_B - E_{D^{**}} - E_\ell)$$

From now on, p_ν must be replaced by $p_B - p_{D^{**}} - p_\ell$ in the expression of $|\bar{\mathscr{M}}|^2$.

Second step

We now proceed to integrate over all possible orientations of $\vec{p}_\ell$ so that only the dependence on E_ℓ (i.e. on x) remains. We will use the spherical coordinates where the Oz axis is given by the direction of $\vec{p}_{D^{**}}$, and we will denote by α the angle between $\vec{p}_\ell$ and $\vec{p}_{D^{**}}$.
Therefore

$$d^3\vec{p}_\ell = 2\pi\,\sin\alpha\,\mathrm{d}\alpha\,\|\vec{p}_\ell\|^2\mathrm{d}\|\vec{p}_\ell\| = 2\pi\,\mathrm{d}(-\cos\alpha)\,\|\vec{p}_\ell\|^2\mathrm{d}\|\vec{p}_\ell\|$$

where the integration over α remains to be performed.

- *Integration over α*: this integration can be performed owing to $\delta\big[(p_B - p_{D^{**}} - p_\ell)^2\big]$

$$\begin{aligned}(p_B - p_{D^{**}} - p_\ell)^2 &= m_B^2 + m_{D^{**}}^2 + m_\ell^2 - 2\,p_{D^{**}}\cdot p_B - 2\,p_\ell\cdot p_B + 2\,p_{D^{**}}\cdot p_\ell \\ &= m_B^2 + m_{D^{**}}^2 + m_\ell^2 - 2\,m_B\,E_{D^{**}} - 2\,m_B\,E_\ell \\ &\quad + 2\,(E_{D^{**}}\,E_\ell - \|\vec{p}_\ell\|\,\|\vec{p}_{D^{**}}\|\,\cos\alpha)\end{aligned} \tag{D.7}$$

  Due to $\delta\big[(p_B - p_{D^{**}} - p_\ell)^2\big]$ (or, equivalently, to the conservation of the total momentum), the squared term in Eq. (D.7) must vanish. The solution of the equation is given by the value α_o such that

$$-\cos\alpha_o = \frac{2\,m_B\,(E_{D^{**}} + E_\ell) - 2\,E_{D^{**}}\,E_\ell - m_B^2 - m_{D^{**}}^2 - m_\ell^2}{2\,\|\vec{p}_\ell\|\,\|\vec{p}_{D^{**}}\|}$$

  Consequently, we have

$$\delta\big[(p_B - p_{D^{**}} - p_\ell)^2\big] = \frac{1}{2\,\|\vec{p}_\ell\|\,\|\vec{p}_{D^{**}}\|}\,\delta(-\cos\alpha + \cos\alpha_o)$$

  The integration over α then leads to the following expression of the new phase space element averaged over the antineutrino momentum and the direction of the outgoing lepton

$$\mathrm{d}\Phi = \frac{1}{(2\pi)^4}\frac{d^3\vec{p}_{D^{**}}}{2E_{D^{**}}}\,\theta(m_B - E_{D^{**}} - E_\ell)\times\frac{1}{4\,E_\ell}\,\frac{\|\vec{p}_\ell\|\mathrm{d}\|\vec{p}_\ell\|}{\|\vec{p}_{D^{**}}\|}$$

- *$\|\vec{p}_\ell\|$ manipulation*: with the help of the usual formulae and in terms of x defined in (D.3),

$$\|\vec{p}_\ell\|^2 = E_\ell^2 - m_\ell^2 = \frac{1}{4}\,x^2\,m_B^2 - m_\ell^2 \qquad\Longrightarrow\qquad 2\,\|\vec{p}_\ell\|\mathrm{d}\|\vec{p}_\ell\| = \frac{1}{2}\,m_B^2\,x\,\mathrm{d}x \qquad\text{and}\qquad 2\,E_\ell = x\,m_B$$

- *Summary for this second step*:

$$\mathrm{d}\Phi = \frac{m_{_B}}{(2\pi)^4}\,\frac{\mathrm{d}x}{8\,\|\vec{p}_{_{D^{**}}}\|}\,\frac{d^3\vec{p}_{_{D^{**}}}}{2E_{_{D^{**}}}}\,\theta(m_{_B}-E_{_{D^{**}}}-E_{_\ell})$$

Third step

Finally we will carry the integration over $\vec{p}_{_{D^{**}}}$. Since we want to keep the dependence on $E_{_{D^{**}}}$, we need to integrate over all possible directions of the three-vector $\vec{p}_{_{D^{**}}}$. Since all the directions are equiprobable, the volume element $d^3\vec{p}_{_{D^{**}}}$ reads

$$d^3\vec{p}_{_{D^{**}}} = 4\,\pi\,\|\vec{p}_{_{D^{**}}}\|^2\,\mathrm{d}\|\vec{p}_{_{D^{**}}}\| = 4\,\pi\,\|\vec{p}_{_{D^{**}}}\|\,E_{_{D^{**}}}\,\mathrm{d}E_{_{D^{**}}}$$

The phase space volume element *averaged over the momentum of the antineutrino and the directions of the lepton and the meson* D^{**} is given by

$$\mathrm{d}\Phi = \frac{m_{_B}}{(2\pi)^3}\,\frac{1}{8}\,\mathrm{d}x\,\mathrm{d}E_{_{D^{**}}}\,\theta(m_{_B}-E_{_{D^{**}}}-E_{_\ell})$$

Finally, we get the expression in terms of y, owing to the relation (D.6)

$$\boxed{\mathrm{d}\Phi = -\,\frac{m_{_B}^2}{128\pi^3}\,\mathrm{d}x\,\mathrm{d}y\;\times\;\theta(m_{_B}-E_{_{D^{**}}}-E_{_\ell})}$$

D.3.2 Differential decay widths dΓ

General expression in the rest frame of the *B* meson

Using the definition of dΓ as well as the preceding results, the construction of the differential decay widths proceeds in the following way

$$\boxed{\frac{\mathrm{d}\Gamma}{\mathrm{d}x\,\mathrm{d}y}(\bar{B}\to D^{**}\,\ell\,\bar{\nu}) = -\,\frac{m_{_B}}{256\pi^3}\,|\bar{\mathscr{M}}|^2}$$

knowing that the following substitutions need to be performed in the general expression of $|\bar{\mathscr{M}}|^2$:

$$\begin{cases} p_{_\nu} \rightsquigarrow & p_{_B}-p_{_{D^{**}}}-p_{_\ell} \\ p_{_B}\cdot p_{_\ell} \rightsquigarrow & \dfrac{1}{2}\,m_{_B}^2\,x \\ p_{_B}\cdot p_{_{D^{**}}} \rightsquigarrow & \dfrac{1}{2}\,\left[m_{_B}^2(1-y)+m_{_{D^{**}}}^2\right] \\ p_{_\ell}\cdot p_{_{D^{**}}} \rightsquigarrow & \dfrac{1}{2}\,\left[m_{_B}^2(x-y)-m_{_\ell}^2\right] \end{cases}$$

With our choice of kinematics and notations, $|\bar{\mathscr{M}}|^2$ is given by

$$
\boxed{
\begin{aligned}
|\bar{\mathscr{M}}|^2 = 2\,G_F^2\,|V_{cb}|^2\,m_B^2 \Big\{ & -2\boxed{\alpha}\,(y - r_\ell^2) \\
& - \boxed{\beta_{++}}\, m_B^2 \Big[4\big[x\,r_{D^{**}}^2 + (1-x)(y-x)\big] + r_\ell^2\big[3\,y - 4(x + r_{D^{**}}^2) + r_\ell^2\big]\Big] \\
& + \Big(\boxed{\beta_{+-}} + \boxed{\beta_{-+}}\Big)\, m_B^2\, r_\ell^2 \Big[2(1 - x - r_{D^{**}}^2) + y + r_\ell^2\Big] \\
& + \boxed{\beta_{--}}\, m_B^2\, r_\ell^2\,(y - r_\ell^2) \\
& - 2\boxed{\gamma}\, m_B^2 \Big[y\,(1 + y - 2\,x - r_{D^{**}}^2) + r_\ell^2(1 + y - r_{D^{**}}^2)\Big] \Big\}
\end{aligned}
}
$$

Notice that, for a zero mass lepton, only the coefficients $\boxed{\alpha}$, $\boxed{\beta_{++}}$ and $\boxed{\gamma}$ remain.

Notation

$$
\boxed{2\,E_\ell = x\,m_B} \qquad\qquad \boxed{2\,m_B\,E_{D^{**}} = m_B^2(1-y) + m_{D^{**}}^2}
$$

We also express all the masses in terms of the B mass through the dimensionless coefficients r_i, defined by

$$
\boxed{r_{D^{**}} = \frac{m_{D^{**}}}{m_B}} \qquad \text{as well as} \qquad \boxed{r_\ell = \frac{m_\ell}{m_B}}
$$

Constraints on the x and y parameters

The parameters x and y, that is the lepton energy (E_ℓ) and the D^{**} meson energy ($E_{D^{**}}$), cannot be arbitrary. These are real numbers satisfying

- *First constraint*: we previously obtained

$$
\cos\alpha = \frac{m_B^2 + m_{D^{**}}^2 + m_\ell^2 - 2\,m_B\,(E_{D^{**}} + E_\ell) + 2\,E_{D^{**}}\,E_\ell}{2\,\sqrt{E_\ell^2 - m_\ell^2}\,\sqrt{E_{D^{**}}^2 - m_{D^{**}}^2}} \tag{D.8}
$$

  which leads to conditions on the accessible values of E_ℓ (i.e. x) in terms of $E_{D^{**}}$ (i.e. y), or conversely. This first constraint provides the variation domain of one parameter in terms of the other.

- *Second constraint*: the Heaviside "function" which appeared in the phase space volume element implies

$$
m_B - E_{D^{**}} - E_\ell \geqslant 0 \qquad \Longrightarrow \qquad 1 + y - x \geqslant r_{D^{**}}^2 \tag{D.9}
$$

  The above inequality fixes the authorized variation domain for the so far unconstrained parameter.

First kind of constraints: $x = x(y)$

In this case, we solve the equation (D.8) as a function of the energy E_ℓ (or x) expressed in terms of $E_{D^{**}}$ (or y), and we then impose condition (D.9) on $E_{D^{**}}$ (or y).

Non-zero mass lepton:

$$(m_\ell \neq 0) \qquad \begin{cases} x_{\max} = \dfrac{1}{2}\left\{1+y-r_{D^{**}}^2+r_\ell^2\left[1+\dfrac{1}{y}\left(1-r_{D^{**}}^2\right)\right]\right. \\ \qquad\qquad \left.+\left(1-\dfrac{r_\ell^2}{y}\right)\sqrt{\left[y-(1-r_{D^{**}})^2\right]\left[y-(1+r_{D^{**}})^2\right]}\right\} \\ x_{\min} = \dfrac{1}{2}\left\{1+y-r_{D^{**}}^2+r_\ell^2\left[1+\dfrac{1}{y}\left(1-r_{D^{**}}^2\right)\right]\right. \\ \qquad\qquad \left.\left(1-\dfrac{r_\ell^2}{y}\right)\sqrt{\left[y-(1-r_{D^{**}})^2\right]\left[y-(1+r_{D^{**}})^2\right]}\right\} \end{cases}$$

$$\text{with} \qquad r_\ell^2 \leqslant y \leqslant (1-r_{D^{**}})^2$$

Zero mass lepton:

$$(m_\ell = 0) \qquad \begin{cases} x_{\max} = \dfrac{1}{2}\left[1+y-r_{D^{**}}^2+\sqrt{\left[y-(1-r_{D^{**}})^2\right]\left[y-(1+r_{D^{**}})^2\right]}\right] \\ x_{\min} = \dfrac{1}{2}\left[1+y-r_{D^{**}}^2-\sqrt{\left[y-(1-r_{D^{**}})^2\right]\left[y-(1+r_{D^{**}})^2\right]}\right] \end{cases}$$

$$\text{with} \qquad 0 \leqslant y \leqslant (1-r_{D^{**}})^2$$

Second kind of contraints: $y = y(x)$

We now solve the equation (D.8) as a function of the energy $E_{D^{**}}$ (or y) expressed in terms of E_ℓ (or x) and we then impose the condition (D.9) on E_ℓ (or x).

Non-zero mass lepton:

$$(m_\ell \neq 0) \qquad \begin{cases} y_{\max} = \dfrac{1}{2}\left[x-\dfrac{r_{D^{**}}^2(x-2r_\ell^2)}{1-x+r_\ell^2}+\left(1-\dfrac{r_{D^{**}}^2}{1-x+r_\ell^2}\right)\sqrt{x^2-4r_\ell^2}\right] \\ y_{\min} = \dfrac{1}{2}\left[x-\dfrac{r_{D^{**}}^2(x-2r_\ell^2)}{1-x+r_\ell^2}-\left(1-\dfrac{r_{D^{**}}^2}{1-x+r_\ell^2}\right)\sqrt{x^2-4r_\ell^2}\right] \end{cases}$$

$$\text{with} \qquad 2\,r_\ell \leqslant x \leqslant 1-r_{D^{**}}^2+r_\ell^2$$

Zero mass lepton:

$$\boxed{(m_\ell = 0) \qquad \begin{cases} y_{\max} = x\left(1 - \dfrac{r_{D^{**}}^2}{1-x}\right) \\ y_{\min} = 0 \end{cases} \qquad \text{with} \qquad 0 \leqslant x \leqslant 1 - r_{D^{**}}^2}$$

$\dfrac{\mathrm{d}^2\Gamma}{\mathrm{d}x\,\mathrm{d}y}$ differential decay width

▶ $\boxed{{}^3P_0 \text{ states}}$

Non-zero mass lepton

$$\boxed{\begin{aligned}\frac{\mathrm{d}^2\Gamma}{\mathrm{d}x\,\mathrm{d}y} = -\frac{G_F^2\,|V_{cb}|^2}{128\pi^3}\; m_B^5 \Bigg\{ & -|\tilde{u}_+|^2\left[4\left[x\,r_{D_0^*}^2 + (1-x)(y-x)\right] + r_\ell^2\left[3\,y - 4(x + r_{D_0^*}^2) + r_\ell^2\right]\right] \\ & + \left(\tilde{u}_+\tilde{u}_-^* + \tilde{u}_+^*\tilde{u}_-\right) r_\ell^2\left[2(1 - x - r_{D_0^*}^2) + y + r_\ell^2\right] \\ & + |\tilde{u}_-|^2\, r_\ell^2\,(y - r_\ell^2)\Bigg\}\end{aligned}}$$

Zero mass lepton

$$\boxed{\frac{\mathrm{d}^2\Gamma}{\mathrm{d}x\,\mathrm{d}y} = \frac{G_F^2\,|V_{cb}|^2}{32\pi^3}\; m_B^5\,|\tilde{u}_+|^2\left[x\,r_{D_0^*}^2 + (1-x)(y-x)\right]}$$

▶ $\boxed{{}^3P_2 \text{ states}}$

Non-zero mass lepton

$$\boxed{\begin{aligned}\frac{\mathrm{d}^2\Gamma}{\mathrm{d}x\,\mathrm{d}y} = -\frac{m_B}{256\pi^3}\,\frac{G_F^2\,|V_{cb}|^2}{2} \Bigg\{ & C_1\,|\tilde{k}|^2 + C_2\,|\tilde{h}|^2 + C_3\,|\tilde{b}_+|^2 + C_4\,|\tilde{b}_-|^2 + C_5\,(\tilde{k}\,\tilde{b}_+^* + \tilde{k}^*\,\tilde{b}_+) \\ & + C_6\,(\tilde{k}\,\tilde{b}_-^* + \tilde{k}^*\,\tilde{b}_-) + C_7\,(\tilde{b}_+\,\tilde{b}_-^* + \tilde{b}_+^*\,\tilde{b}_-) + C_8\,(\tilde{h}\,\tilde{k}^* + \tilde{h}^*\,\tilde{k})\Bigg\}\end{aligned}}$$

where the C_i coefficients are given by

$$C_1 = \frac{m_B^4}{3\,r_{D_2^*}^4}\Bigg\{\Big[y^2-(2+r_{D_2^*}^2)\,y+(1-r_{D_2^*}^2)^2\Big]\Big[2(1-x)(x-y)+r_{D_2^*}^2(3\,y-2\,x)\Big]-3\,y^2\,r_{D_2^*}^4 \\ -r_\ell^2\Big[(1-2\,x+y)\Big[2(1-y)^2-3\,r_{D_2^*}^2(1+y)\Big]-r_{D_2^*}^4(2\,x-r_{D_2^*}^2)\Big] \\ -2\,r_\ell^4\Big[y^2-2(1+r_{D_2^*}^2)\,y+1-r_{D_2^*}^2+r_{D_2^*}^4\Big]\Bigg\}$$

$$C_2 = \frac{m_B^8}{r_{D_2^*}^2}\Big[y-(1-r_{D_2^*})^2\Big]\Big[y-(1+r_{D_2^*})^2\Big] \\ \times\Big[y\Big[2(1-x+r_{D_2^*})(1-x-r_{D_2^*})-(1-y+r_{D_2^*}^2)(1+y-2\,x-r_{D_2^*}^2)\Big] \\ +r_\ell^2\Big[(1+y-r_{D_2^*}^2)(1+y-2\,x-r_{D_2^*}^2)+2\,r_\ell^2\Big]\Big]$$

$$C_3 = \frac{m_B^8}{6\,r_{D_2^*}^4}\Big[y-(1-r_{D_2^*})^2\Big]^2\Big[y-(1+r_{D_2^*})^2\Big]^2\Big[4\,x(1-x-r_{D_2^*}^2)-4\,y(1-x) \\ +r_\ell^2\Big[4(x+r_{D_2^*}^2)-3\,y-r_\ell^2\Big]\Big]$$

$$C_4 = \frac{m_B^8}{6\,r_{D_2^*}^4}\,r_\ell^2\,(y-r_\ell^2)\Big[y-(1-r_{D_2^*})^2\Big]^2\Big[y-(1+r_{D_2^*})^2\Big]^2$$

$$C_5 = \frac{m_B^6}{3\,r_{D_2^*}^4}\Big[y-(1-r_{D_2^*})^2\Big]\Big[y-(1+r_{D_2^*})^2\Big] \\ \times\Big[2(1-y-r_{D_2^*}^2)\Big[(1-x)(x-y)-x\,r_{D_2^*}^2\Big] \\ -r_\ell^2\Big[(1-y+r_{D_2^*}^2)(1-3\,x+2\,y-r_{D_2^*}^2+r_\ell^2)+2\,x\,r_{D_2^*}^2\Big]\Big]$$

$$C_6 = \frac{m_B^6}{3\,r_{D_2^*}^4}\,r_\ell^2\,\Big[y-(1-r_{D_2^*})^2\Big]\Big[y-(1+r_{D_2^*})^2\Big] \\ \times\Big[(1-y+r_{D_2^*}^2)(1-x+r_{D_2^*}^2)+2r_{D_2^*}^2(x-2)+r_\ell^2(1-y+r_{D_2^*}^2)\Big]$$

$$C_7 = \frac{m_B^8}{6\,r_{D_2^*}^4}\,r_\ell^2\,\Big[y-(1-r_{D_2^*})^2\Big]^2\Big[y-(1+r_{D_2^*})^2\Big]^2\Big[2(1-x-r_{D_2^*}^2)+y+r_\ell^2\Big]$$

$$C_8 = -\frac{m_B^6}{r_{D_2^*}^2}\Big[y-(1-r_{D_2^*})^2\Big]\Big[y-(1+r_{D_2^*})^2\Big]\Big[y(1+y-2\,x-r_{D_2^*}^2)+r_\ell^2(1+y-r_{D_2^*}^2)\Big]$$

Zero mass lepton

The coefficients of C_4, C_6 and C_7 cancel in this limit, leading to

$$\boxed{\frac{\mathrm{d}^2\Gamma}{\mathrm{d}x\,\mathrm{d}y} = -\frac{m_{_B}}{256\pi^3}\,\frac{G_F^2\,|V_{cb}|^2}{2}\,\Big[C_1\,|\tilde{k}|^2 + C_2\,|\tilde{h}|^2 + C_3\,|\tilde{b}_+|^2 + C_5\,(\tilde{k}\,\tilde{b}_+^* + \tilde{k}^*\,\tilde{b}_+) + C_8\,(\tilde{h}\,\tilde{k}^* + \tilde{h}^*\,\tilde{k})\Big]}$$

where the C_i coefficients are given by

$$\boxed{C_1 = \frac{m_{_B}^4}{3\,r_{_{D_2^*}}^4}\Big[\,\Big[y^2 - (2 + r_{_{D_2^*}}^2)\,y + (1 - r_{_{D_2^*}}^2)^2\Big]\,\Big[2(1-x)(x-y) + r_{_{D_2^*}}^2(3\,y - 2\,x)\Big] - 3\,y^2\,r_{_{D_2^*}}^4\Big]}$$

$$\boxed{\begin{aligned}C_2 = {}& \frac{m_{_B}^8}{r_{_{D_2^*}}^2}\Big[y - (1 - r_{_{D_2^*}})^2\Big]\Big[y - (1 + r_{_{D_2^*}})^2\Big] \\ & \times y\,\Big[2(1 - x + r_{_{D_2^*}})(1 - x - r_{_{D_2^*}}) - (1 - y + r_{_{D_2^*}}^2)(1 + y - 2\,x - r_{_{D_2^*}}^2)\Big]\end{aligned}}$$

$$\boxed{C_3 = \frac{m_{_B}^8}{6\,r_{_{D_2^*}}^4}\Big[y - (1 - r_{_{D_2^*}})^2\Big]^2\Big[y - (1 + r_{_{D_2^*}})^2\Big]^2\Big[4\,x(1 - x - r_{_{D_2^*}}^2) - 4\,y(1-x)\Big]}$$

$$\boxed{C_5 = \frac{m_{_B}^6}{3\,r_{_{D_2^*}}^4}\Big[y - (1 - r_{_{D_2^*}})^2\Big]\Big[y - (1 + r_{_{D_2^*}})^2\Big]\Big[2(1 - y - r_{_{D_2^*}}^2)\,\Big[(1-x)(x-y) - x\,r_{_{D_2^*}}^2\Big]\Big]}$$

$$\boxed{C_8 = -\frac{m_{_B}^6}{r_{_{D_2^*}}^2}\Big[y - (1 - r_{_{D_2^*}})^2\Big]\Big[y - (1 + r_{_{D_2^*}})^2\Big]y\,(1 + y - 2\,x - r_{_{D_2^*}}^2)}$$

$\dfrac{\mathbf{d\Gamma}}{\mathbf{d}y}$ differential decay width

The form factors only depend (although in an unknown way) on the y parameter. To do the integration over the x variable, we will use the expressions of the kind $x = x(y)$.

► $\boxed{^3P_0\ states}$

Non-zero mass lepton: in this situation, the integration is performed from

$$x_{\min} = \frac{1}{2}\left\{1 + y - r_{_{D_0^*}}^2 + r_\ell^2\left[1 + \frac{1}{y}\left(1 - r_{_{D_0^*}}^2\right)\right] - \left(1 - \frac{r_\ell^2}{y}\right)\sqrt{\left[y - (1 - r_{_{D_0^*}})^2\right]\left[y - (1 + r_{_{D_0^*}})^2\right]}\right\}$$

to

$$x_{\max} = \frac{1}{2}\left\{1 + y - r_{_{D_0^*}}^2 + r_\ell^2\left[1 + \frac{1}{y}\left(1 - r_{_{D_0^*}}^2\right)\right] + \left(1 - \frac{r_\ell^2}{y}\right)\sqrt{\left[y - (1 - r_{_{D_0^*}})^2\right]\left[y - (1 + r_{_{D_0^*}})^2\right]}\right\}$$

We obtain

$$\boxed{\frac{\mathrm{d}\Gamma}{\mathrm{d}y} = -\frac{G_F^2\,|V_{cb}|^2}{128\pi^3}\,m_B^5\,\left[D_1\,|\tilde{u}_+|^2 + D_2\,(\tilde{u}_+\,\tilde{u}_-^* + \tilde{u}_+^*\,\tilde{u}_-) + D_3\,|\tilde{u}_-|^2\right]}$$

where the D_i coefficients are function of y and are given by

$$D_i(y) = \int_{x_{\min}}^{x_{\max}} C_i(x,\,y)\,\mathrm{d}x \qquad \text{with} \quad \begin{cases} C_1 = -4\left[x\,r_{D_0^*}^2 + (1-x)(y-x)\right] - r_\ell^2\left[3\,y - 4(x + r_{D_0^*}^2) + r_\ell^2\right] \\ C_2 = r_\ell^2\left[2(1 - x - r_{D_0^*}^2) + y + r_\ell^2\right] \\ C_3 = r_\ell^2\,\left(y - r_\ell^2\right) \end{cases}$$

After performing these integrations, we find

$$\boxed{\begin{aligned} D_1 = {} & \frac{1}{3\,y^3}\,\left(y - r_\ell^2\right)^2\,\left[\left[y - (1 - r_{D_0^*})^2\right]\left[y - (1 + r_{D_0^*})^2\right]\right]^{1/2} \\ & \times\left\{2\,y\left[y - (1 - r_{D_0^*})^2\right]\left[y - (1 + r_{D_0^*})^2\right] + r_\ell^2\left[y^2 - 2\,y\,(1 + r_{D_0^*}^2) + 4\,(1 - r_{D_0^*}^2)^2\right]\right\} \end{aligned}}$$

$$\boxed{D_2 = \frac{1}{y^2}\,r_\ell^2\,\left(y - r_\ell^2\right)^2\,(1 - r_{D_0^*}^2)\,\left[\left[y - (1 - r_{D_0^*})^2\right]\left[y - (1 + r_{D_0^*})^2\right]\right]^{1/2}}$$

$$\boxed{D_3 = \frac{1}{y}\,r_\ell^2\,\left(y - r_\ell^2\right)^2\,\left[\left[y - (1 - r_{D_0^*})^2\right]\left[y - (1 + r_{D_0^*})^2\right]\right]^{1/2}}$$

Recall that, in the expression of $\mathrm{d}\Gamma/\mathrm{d}y$, the y parameter varies in the interval: $r_\ell^2 \leqslant y \leqslant (1 - r_{D_0^*})^2$.

Zero mass lepton

The integration is now to be performed from

$$x_{\min} = \frac{1}{2}\left\{1 + y - r_{D_0^*}^2 + -\sqrt{\left[y - (1 - r_{D_0^*})^2\right]\left[y - (1 + r_{D_0^*})^2\right]}\right\}$$

to

$$x_{\max} = \frac{1}{2}\left\{1 + y - r_{D_0^*}^2 + +\sqrt{\left[y - (1 - r_{D_0^*})^2\right]\left[y - (1 + r_{D_0^*})^2\right]}\right\}$$

and we get (we can take the limit $r_\ell \to 0$), with $0 \leqslant y \leqslant (1 - r_{D_0^*})^2$

$$\boxed{\frac{\mathrm{d}\Gamma}{\mathrm{d}y} = -\frac{G_F^2\,|V_{cb}|^2}{128\pi^3}\,m_B^5\,\,|\tilde{u}_+|^2\,D_1} \qquad \text{where} \qquad \boxed{D_1 = \frac{2}{3}\,\left[\left[y - (1 - r_{D_0^*})^2\right]\left[y - (1 + r_{D_0^*})^2\right]\right]^{3/2}}$$

since the other coefficients D_2 and D_3 are zero in this case.

► $\boxed{{}^3P_2 \text{ states}}$

Non-zero mass lepton: proceeding analogously we find

$$\boxed{\frac{\mathrm{d}\Gamma}{\mathrm{d}y} = -\frac{m_{_B}}{256\pi^3}\,\frac{G_F^2\,|V_{cb}|^2}{2}\,\Big\{D_1\,|\tilde{k}|^2 + D_2\,|\tilde{h}|^2 + D_3\,|\tilde{b}_+|^2 + D_4\,|\tilde{b}_-|^2 + D_5\,(\tilde{k}\,\tilde{b}_+^* + \tilde{k}^*\,\tilde{b}_+) + D_6\,(\tilde{k}\,\tilde{b}_-^* + \tilde{k}^*\,\tilde{b}_-) + D_7\,(\tilde{b}_+\,\tilde{b}_-^* + \tilde{b}_+^*\,\tilde{b}_-) + D_8\,(\tilde{h}\,\tilde{k}^* + \tilde{h}^*\,\tilde{k})\Big\}}$$

where the D_i coefficients are given by

$$\boxed{D_1 = \frac{m_{_B}^4}{r_{_{D_2^*}}^4}\,\frac{1}{9\,y^3}\,\big(y - r_\ell^2\big)^2\,\Big[\Big[y - (1 - r_{_{D_2^*}})^2\Big]\,\Big[y - (1 + r_{_{D_2^*}})^2\Big]\Big]^{3/2} \times \Big\{y\,\Big[y^2 - 2\,y\,(1 - 4\,r_{_{D_2^*}}^2) + (1 - r_{_{D_2^*}}^2)^2\Big] + r_\ell^2\,\Big[2\,y^2 - y\,(4 - r_{_{D_2^*}}^2) + 2\,(1 - r_{_{D_2^*}}^2)^2\Big]\Big\}}$$

$$\boxed{D_2 = \frac{m_{_B}^8}{r_{_{D_2^*}}^2}\,\frac{1}{3\,y^2}\,\big(y - r_\ell^2\big)^2\,(2\,y + r_\ell^2)\,\Big[\Big[y - (1 - r_{_{D_2^*}})^2\Big]\,\Big[y - (1 + r_{_{D_2^*}})^2\Big]\Big]^{5/2}}$$

$$\boxed{D_3 = \frac{m_{_B}^8}{r_{_{D_2^*}}^4}\,\frac{1}{18\,y^3}\,\big(y - r_\ell^2\big)^2\,\Big[\Big[y - (1 - r_{_{D_2^*}})^2\Big]\,\Big[y - (1 + r_{_{D_2^*}})^2\Big]\Big]^{5/2} \times \Big\{2\,y\,\Big[y - (1 - r_{_{D_2^*}})^2\Big]\,\Big[y - (1 + r_{_{D_2^*}})^2\Big] + r_\ell^2\,\Big[y^2 - 2\,y\,(1 + r_{_{D_2^*}}^2) + 4\,(1 - r_{_{D_2^*}}^2)^2\Big]\Big\}}$$

$$\boxed{D_4 = \frac{m_{_B}^8}{r_{_{D_2^*}}^4}\,\frac{1}{6\,y}\,r_\ell^2\,\big(y - r_\ell^2\big)^2\,\Big[\Big[y - (1 - r_{_{D_2^*}})^2\Big]\,\Big[y - (1 + r_{_{D_2^*}})^2\Big]\Big]^{5/2}}$$

$$\boxed{D_5 = \frac{m_{_B}^6}{r_{_{D_2^*}}^4}\,\frac{1}{18\,y^3}\,\big(y - r_\ell^2\big)^2\,\Big[\Big[y - (1 - r_{_{D_2^*}})^2\Big]\,\Big[y - (1 + r_{_{D_2^*}})^2\Big]\Big]^{5/2}\Big[2\,y\,\Big(1 - y - r_{_{D_2^*}}^2\Big) + r_\ell^2\,\Big(4 - y - 4\,r_{_{D_2^*}}^2\Big)\Big]}$$

$$\boxed{D_6 = \frac{m_{_B}^6}{r_{_{D_2^*}}^4}\,\frac{1}{6\,y^2}\,r_\ell^2\,\big(y - r_\ell^2\big)^2\,\Big[\Big[y - (1 - r_{_{D_2^*}})^2\Big]\,\Big[y - (1 + r_{_{D_2^*}})^2\Big]\Big]^{5/2}}$$

$$\boxed{D_7 = \frac{m_{_B}^8}{r_{_{D_2^*}}^4}\,\frac{1}{6\,y^2}\,r_\ell^2\,\big(y - r_\ell^2\big)^2\,(1 - r_{_{D_2^*}}^2)\,\Big[\Big[y - (1 - r_{_{D_2^*}})^2\Big]\,\Big[y - (1 + r_{_{D_2^*}})^2\Big]\Big]^{5/2}}$$

$$\boxed{D_8 = 0}$$

Recall that, in these formulae, the y parameter varies in the interval $\;r_\ell^2 \leqslant y \leqslant (1 - r_{_{D_2^*}})^2$.

Zero mass lepton: we obtain

$$\boxed{\frac{\mathrm{d}\Gamma}{\mathrm{d}y} = -\frac{m_B}{256\pi^3}\,\frac{G_F^2\,|V_{cb}|^2}{2}\,\Big[D_1\,|\tilde{k}|^2 + D_2\,|\tilde{h}|^2 + D_3\,|\tilde{b}_+|^2 + D_5\,(\tilde{k}\,\tilde{b}_+^* + \tilde{k}^*\,\tilde{b}_+) + D_8\,(\tilde{h}\,\tilde{k}^* + \tilde{h}^*\,\tilde{k})\Big]}$$

where the D_i coefficients are given by

$$\boxed{D_1 = \frac{m_B^4}{r_{D_2^*}^4}\,\frac{1}{9}\,\Big[\Big[y-(1-r_{D_2^*})^2\Big]\,\Big[y-(1+r_{D_2^*})^2\Big]\Big]^{3/2}\Big[y^2 - 2\,y\,(1-4\,r_{D_2^*}^2) + (1-r_{D_2^*}^2)^2\Big]}$$

$$\boxed{D_2 = \frac{m_B^8}{r_{D_2^*}^2}\,\frac{2}{3}\,y\,\Big[\Big[y-(1-r_{D_2^*})^2\Big]\,\Big[y-(1+r_{D_2^*})^2\Big]\Big]^{5/2}}$$

$$\boxed{D_3 = \frac{m_B^8}{r_{D_2^*}^4}\,\frac{1}{9}\,\Big[\Big[y-(1-r_{D_2^*})^2\Big]\,\Big[y-(1+r_{D_2^*})^2\Big]\Big]^{7/2}}$$

$$\boxed{D_5 = \frac{m_B^6}{r_{D_2^*}^4}\,\frac{1}{9}\,(1-y-r_{D_2^*}^2)\,\Big[\Big[y-(1-r_{D_2^*})^2\Big]\,\Big[y-(1+r_{D_2^*})^2\Big]\Big]^{5/2}}$$

$$\boxed{D_8 = 0}$$

Here, the y parameter lies in the domain $0 \leqslant y \leqslant (1-r_{D_2^*})^2$.

$\dfrac{\mathbf{d\Gamma}}{\mathbf{d}x}$ differential decay width

It is impossible to give *a priori* expressions for the leptonic spectra $\dfrac{\mathrm{d}\Gamma}{\mathrm{d}x}$: since the dependence of the form factors on y is unknown, we cannot perform the integration over y. Nevertheless, the procedure to do those calculations is the following

1. We start from the expressions of the $\dfrac{\mathrm{d}^2\Gamma}{\mathrm{d}x\,\mathrm{d}y}$ decay widths given above.

2. We use the constraints of the kind $y = y(x)$ in order to perform the integration over y from $y_{\min}$ to $y_{\max}$. Recall that, due to (D.5), the maximum of $E_{D^{**}}$ corresponds to the minimum of y and vice-versa. So, to integrate over $E_{D^{**}}$ from $E_{D^{**}}^{\min}$ to $E_{D^{**}}^{\max}$, we have to integrate over y from $y_{\max}$ to $y_{\min}$

$$\frac{\mathrm{d}\Gamma}{\mathrm{d}x} = \int_{y_{\max}}^{y_{\min}} \frac{\mathrm{d}^2\Gamma}{\mathrm{d}x\,\mathrm{d}y}\,\mathrm{d}y$$

with

$$\begin{cases} y_{\max} = \dfrac{1}{2}\left[x - \dfrac{r_{D^{**}}^2(x-2r_\ell^2)}{1-x+r_\ell^2} + \left(1 - \dfrac{r_{D^{**}}^2}{1-x+r_\ell^2}\right)\sqrt{x^2-4r_\ell^2}\right] \\ y_{\min} = \dfrac{1}{2}\left[x - \dfrac{r_{D^{**}}^2(x-2r_\ell^2)}{1-x+r_\ell^2} - \left(1 - \dfrac{r_{D^{**}}^2}{1-x+r_\ell^2}\right)\sqrt{x^2-4r_\ell^2}\right] \end{cases}$$

(Setting $r_\ell = 0$ corresponds to the case of a zero mass lepton.)

3. The last free parameter x lies in the domain

$$2\,r_\ell \leqslant x \leqslant 1 - r_{D^{**}}^2 + r_\ell^2$$

(Once again, $r_\ell = 0$ gives the variation domain in the case of a massless lepton.)

Total decay width Γ

The problem which was encountered when computing the leptonic spectra also occurs here, as one must conduct some integration over y.

Bibliography

[1] J. Beringer et al. Review of particle physics. *Phys. Rev. D*, 86:010001, Jul 2012.

[2] B. Blossier, P. Dimopoulos, R. Frezzotti, V. Lubicz, M. Petschlies, F. Sanfilippo, S. Simula, and C. Tarantino. Average up/down, strange, and charm quark masses with $N_f = 2$ twisted-mass lattice QCD. *Phys. Rev. D*, 82:114513, Dec 2010.

[3] B. Blossier, Ph. Boucaud, F. De soto, V. Morenas, M. Gravina, O. Pène, and J. Rodríguez-Quintero. Ghost-gluon coupling, power corrections, and $\Lambda_{\overline{\text{ms}}}$ from twisted-mass lattice QCD at $N_f = 2$. *Phys. Rev. D*, 82:034510, Aug 2010.

[4] Damir Becirevic, Nejc Kosnik, and Andrey Tayduganov. $\bar{B} \to D\tau\bar{\nu}_\tau$ vs. $\bar{B} \to D\mu\bar{\nu}_\mu$. *Phys.Lett.*, B716:208–213, 2012.

[5] Bogdan A. Dobrescu and Andreas S. Kronfeld. Accumulating evidence for nonstandard leptonic decays of D_s mesons. *Phys.Rev.Lett.*, 100:241802, 2008.

[6] Enrico Lunghi and Amarjit Soni. Possible Indications of New Physics in B_d -mixing and in sin(2 beta) Determinations. *Phys.Lett.*, B666:162–165, 2008.

[7] Martin Beneke, Gerhard Buchalla, Alexander Lenz, and Ulrich Nierste. CP asymmetry in flavor specific B decays beyond leading logarithms. *Phys.Lett.*, B576:173–183, 2003.

[8] S.L. Glashow. Partial Symmetries of Weak Interactions. *Nucl.Phys.*, 22:579–588, 1961.

[9] F. Englert and R. Brout. Broken Symmetry and the Mass of Gauge Vector Mesons. *Phys. Rev. Lett.*, 13:321–323, Aug 1964.

[10] G. S. Guralnik, C. R. Hagen, and T. W. B. Kibble. Global conservation laws and massless particles. *Phys. Rev. Lett.*, 13:585–587, Nov 1964.

[11] Peter W. Higgs. Broken symmetries and the masses of gauge bosons. *Phys. Rev. Lett.*, 13:508–509, Oct 1964.

[12] Peter W. Higgs. Spontaneous symmetry breakdown without massless bosons. *Phys. Rev.*, 145:1156–1163, May 1966.

[13] Nicola Cabibbo. Unitary Symmetry and Leptonic Decays. *Phys.Rev.Lett.*, 10:531–533, 1963.

[14] Makoto Kobayashi and Toshihide Maskawa. CP Violation in the Renormalizable Theory of Weak Interaction. *Prog.Theor.Phys.*, 49:652–657, 1973.

[15] Ling-Lie Chau and Wai-Yee Keung. Comments on the Parametrization of the Kobayashi-Maskawa Matrix. *Phys.Rev.Lett.*, 53:1802, 1984.

[16] Lincoln Wolfenstein. Parametrization of the Kobayashi-Maskawa Matrix. *Phys.Rev.Lett.*, 51:1945, 1983.

[17] J.C. Hardy and I.S. Towner. Superallowed $0^+ \to 0^+$ nuclear beta decays: A New survey with precision tests of the conserved vector current hypothesis and the standard model. *Phys.Rev.*, C79:055502, 2009.

[18] C. Jarlskog. Commutator of the quark mass matrices in the standard electroweak model and a measure of maximal CP nonconservation. *Phys. Rev. Lett.*, 55:1039–1042, Sep 1985.

[19] Denis Derkach. Unitarity Triangle Fitter Results for CKM Angles. 2013.

[20] CKMfitter Collaboration. State-of-the-Art Results (2013 FPCP conference: Rio de Janeiro, Brazil). `http://www.ckmfitter.in2p3.fr`. May, 2013.

[21] A. Le Yaouanc, L. Oliver, O. Pène, J.-C. Raynal, and V. Morénas. Uraltsev sum rule in Bakamjian-Thomas quark models. *Physics Letters B*, 520(1-2):25 – 32, 2001.

[22] A. Le Yaouanc, L. Oliver, O. Pène, J.-C Raynal, and V. Morénas. On P-wave meson decay constants in the heavy quark limit of QCD. *Physics Letters B*, 520(1-2):59 – 62, 2001.

[23] D. Bečirević, A. Le Yaouanc, L. Oliver, J.-C. Raynal, P. Roudeau, and J. Serrano. Proposal to study $B_s \to \bar{D}_{sJ}$ transitions. *Phys. Rev. D*, 87:054007, Mar 2013.

[24] Aneesh V. Manohar and Mark B. Wise. *Heavy Quark Physics*. Cambridge University Press, 2000.

[25] Nathan Isgur and Mark B. Wise. Excited charm mesons in semileptonic $\overline{B}$ decay and their contributions to a Bjorken sum rule. *Phys. Rev. D*, 43:819–828, Feb 1991.

[26] A. R. Edmonds. *Angular Momentum in Quantum Mechanics*. Princeton University Press, 1985.

[27] K. Abe et al. Study of $B^- \to D^{**0}\pi^-(D^{**0} \to D^{(*)+}\pi^-)$ decays. *Phys.Rev.*, D69:112002, 2004.

[28] Nathan Isgur and Mark B. Wise. Weak Decays of Heavy Mesons in the Static Quark Approximation. *Phys.Lett.*, B232:113, 1989.

[29] M. Okamoto, C. Aubin, C. Bernard, Carleton E. DeTar, M. Di Pierro, et al. Semileptonic $D \to \pi/K$ and $B \to \pi/D$ decays in 2+1 flavor lattice QCD. *Nucl.Phys.Proc.Suppl.*, 140:461–463, 2005.

[30] D. Asner et al. Averages of b-hadron, c-hadron, and τ-lepton properties. 2012.

[31] Jon A. Bailey et al. $B \to D^* \ell\nu$ at zero recoil: an update. *PoS*, LATTICE2010:311, 2010.

[32] C. Bernard, Carleton E. DeTar, M. Di Pierro, A.X. El-Khadra, R.T. Evans, et al. The $\bar{B} \to D^* \ell \bar{\nu}$ form factor at zero recoil from three-flavor lattice QCD: A Model independent determination of $|V_{cb}|$. *Phys.Rev.*, D79:014506, 2009.

[33] G.M. de Divitiis, E. Molinaro, R. Petronzio, and N. Tantalo. Quenched lattice calculation of the $B \to D\ell\nu$ decay rate. *Phys.Lett.*, B655:45–49, 2007.

[34] G.M. de Divitiis, R. Petronzio, and N. Tantalo. Quenched lattice calculation of semileptonic heavy-light meson form factors. *JHEP*, 0710:062, 2007.

[35] Bernard Aubert et al. Measurement of $|V_{(cb)}|$ and the Form-Factor Slope in $\bar{B} \to D\,\ell\bar{\nu}$ Decays in Events Tagged by a Fully Reconstructed B Meson. *Phys.Rev.Lett.*, 104:011802, 2010.

[36] Nikolai Uraltsev. A 'BPS' expansion for B and D mesons. *Phys.Lett.*, B585:253–262, 2004.

[37] A. Matyja et al. Observation of $B_0 \to D^{*-}\tau^+\nu_\tau$ decay at Belle. *Phys.Rev.Lett.*, 99:191807, 2007.

[38] Bernard Aubert et al. Observation of the semileptonic decays $B \to D^*\tau^-\bar{\nu}(\ \tau^)$ and evidence for $B \to D\tau^-\bar{\nu}(\ \tau^)$. *Phys.Rev.Lett.*, 100:021801, 2008.

[39] A. Bozek et al. Observation of $B^+ \to \bar{D}^{*0}\tau^+\nu_\tau$ and Evidence for $B^+ \to \bar{D}^0\tau^+\nu_\tau$ at Belle. *Phys.Rev.*, D82:072005, 2010.

[40] Svjetlana Fajfer, Jernej F. Kamenik, and Ivan Nisandzic. On the $B \to D * \tau\bar{n}u_\tau$ Sensitivity to New Physics. *Phys.Rev.*, D85:094025, 2012.

[41] Jernej F. Kamenik and Federico Mescia. $B \to D\tau\nu$ Branching Ratios: Opportunity for Lattice QCD and Hadron Colliders. *Phys.Rev.*, D78:014003, 2008.

[42] Jon A. Bailey, A. Bazavov, C. Bernard, C.M. Bouchard, C. DeTar, et al. Refining new-physics searches in $B \to D\tau\nu$ decay with lattice QCD. *Phys.Rev.Lett.*, 109:071802, 2012.

[43] Bob Kowalewski. Evidence for an excess of B ? $D^{(*)}\tau\nu$ decays. *J.Phys.Conf.Ser.*, 455:012039, 2013.

[44] Wolfgang Altmannshofer, Marcela Carena, Nausheen R. Shah, and Felix Yu. Indirect Probes of the MSSM after the Higgs Discovery. *JHEP*, 1301:160, 2013.

[45] Andreas Crivellin, Christoph Greub, and Ahmet Kokulu. Explaining $B \to D\tau\nu$, $B \to D^*\tau\nu$ and $B \to \tau\nu$ in a 2HDM of type III. *Phys.Rev.*, D86:054014, 2012.

[46] Alejandro Celis, Martin Jung, Xin-Qiang Li, and Antonio Pich. Sensitivity to charged scalars in $B \to D^{(*)}\tau\nu_\tau$ and $B \to \tau\nu_\tau$ decays. *JHEP*, 1301:054, 2013.

[47] Svjetlana Fajfer, Jernej F. Kamenik, and Ivan Nišandžić. $b \to D^*\tau\overline{\nu}_\tau$ sensitivity to new physics. *Phys. Rev. D*, 85:094025, May 2012.

[48] Nikolai Uraltsev. New exact heavy quark sum rules. *Physics Letters B*, 501(1-2):86 – 91, 2001.

[49] A. Le Yaouanc, D. Melikhov, V. Morenas, L. Oliver, O. Pene, et al. One interesting new sum rule extending Bjorken's to order 1 / m(Q). *Phys.Lett.*, B480:119–128, 2000.

[50] A. Le Yaouanc, L. Oliver, O. Pene, and J.C. Raynal. Covariant quark model of form-factors in the heavy mass limit. *Phys.Lett.*, B365:319–326, 1996.

[51] V. Morénas, A. Le Yaouanc, L. Oliver, O. Pène, and J.-C. Raynal. Quantitative predictions for B semileptonic decays into D, D^*, and the orbitally excited D^{**} in quark models in the manner of Bakamjian and Thomas. *Phys. Rev. D*, 56:5668–5680, Nov 1997.

[52] Stephen Godfrey and Nathan Isgur. Mesons in a relativized quark model with chromodynamics. *Phys. Rev. D*, 32:189–231, Jul 1985.

[53] V. Morenas, A. Le Yaouanc, L. Oliver, O. Pene, and J.C. Raynal. Slope of the Isgur-Wise function in the heavy mass limit of quark models a la Bakamjian-Thomas. *Phys.Lett.*, B408:357–366, 1997.

[54] D. Bečirević, B. Blossier, Ph. Boucaud, G. Herdoiza, J.P. Leroy, A. Le Yaouanc, V. Morénas, and O. Pène. Lattice measurement of the Isgur-Wise functions $\tau(1/2)$ and $\tau(3/2)$. *Physics Letters B*, 609(3-4):298 – 308, 2005.

[55] Benoit Blossier, Marc Wagner, and Olivier Pene. Lattice calculation of the Isgur-Wise functions $\tau(1/2)$ and $\tau(3/2)$ with dynamical quarks. *JHEP*, 0906:022, 2009.

[56] D. Bećirević, E. Chang, L. Oliver, J.-C. Raynal, and A. Le Yaouanc. Spatial distributions in static heavy-light mesons: A comparison of quark models with lattice qcd. *Phys. Rev. D*, 84:054507, Sep 2011.

[57] Pietro Colangelo, Giuseppe Nardulli, and Nello Paver. Semileptonic b decays into charmed p-wave mesons and the heavy-quark symmetry. *Physics Letters B*, 293(1-2):207 – 215, 1992.

[58] P. Colangelo, F. De Fazio, and N. Paver. Universal $\tau_{1/2}(y)$ isgur-wise function at the next-to-leading order in qcd sum rules. *Phys. Rev. D*, 58:116005, Nov 1998.

[59] Ming-Qiu Huang and Yuan-Ben Dai. Semileptonic b decays into excited charmed mesons from qcd sum rules. *Phys. Rev. D*, 59:034018, Jan 1999.

[60] I.I. Bigi, B. Blossier, A. Le Yaouanc, L. Oliver, O. Pene, et al. Memorino on the '1/2 vs. 3/2 Puzzle' in $\bar{B} \to \ell\bar{\nu}\, X_c$: A Year Later and a Bit Wiser. *Eur.Phys.J.*, C52:975–985, 2007.

[61] Nikolai Uraltsev. New exact heavy quark sum rules. *Phys.Lett.*, B501:86–91, 2001.

[62] Adam K. Leibovich, Zoltan Ligeti, Iain W. Stewart, and Mark B. Wise. Semileptonic B decays to excited charmed mesons. *Phys.Rev.*, D57:308–330, 1998.

[63] Paolo Gambino, Thomas Mannel, and Nikolai Uraltsev. $B \to D^*$ Zero-Recoil Formfactor and the Heavy Quark Expansion in QCD: A Systematic Study. *JHEP*, 1210:169, 2012.

[64] Florian U. Bernlochner, Zoltan Ligeti, and Sascha Turczyk. A proposal to solve some puzzles in semileptonic b decays. *Phys. Rev. D*, 85:094033, May 2012.

[65] Damir Becirevic, Benoit Blossier, Antoine Gerardin, Alain Le Yaouanc, and Francesco Sanfilippo. On the significance of B-decays to radially excited D. *Nucl.Phys.*, B872:313–332, 2013.

[66] Michael E.Peskin and Daniel V.Schroeder. *An introduction to quantum field theory.* Westview Press., 1995.

[67] K. Symanzik. Continuum Limit and Improved Action in Lattice Theories. 1. Principles and phi**4 Theory. *Nucl.Phys.*, B226:187, 1983.

[68] K. Symanzik. Continuum Limit and Improved Action in Lattice Theories. 2. $O(N)$ Nonlinear Sigma Model in Perturbation Theory. *Nucl.Phys.*, B226:205, 1983.

[69] P. Weisz. Continuum limit improved lattice action for pure yang-mills theory (i). *Nuclear Physics B*, 212(1):1 – 17, 1983.

[70] Y. Iwasaki. Four-dimensional non-abelian SU(N) gauge model. *UTHEP*, page 118.

[71] Kenneth G. Wilson. Quarks and Strings on a Lattice. 1975.

[72] H. B. Nielsen and M.Ninomiya. A no-go theorem for regularizing chiral fermions. *Phys. Lett. B*, 105:219, 1981.

[73] H. B. Nielsen and M.Ninomiya. Absence of neutrinos on a lattice: (II). intuitive topological proof. *Nucl. Phys. B*, 193:173, 1981.

[74] Paul H. Ginsparg and Kenneth G. Wilson. A remnant of chiral symmetry on the lattice. *Phys. Rev. D*, 25:2649–2657, May 1982.

[75] M. Lusher. Exact chiral symmetry on the lattice and the ginsparg-wilson relation. *Phys. lett. B*, 428:342, 1998.

[76] D. B. Kaplan. A method for simulating chiral fermions on the lattice. *Phys. lett. B*, 288:342, 1992.

[77] Y. Shamir. Anomalies and chiral defect fermions. *Nucl. Phys. B*, 417:167, 1994.

[78] Y. Shamir. Chiral fermions from lattice boundaries. *Nucl. Phys. B*, 406:90, 1993.

[79] Roberto Frezzotti, Pietro Antonio Grassi, Stefan Sint, and Peter Weisz. Lattice QCD with a chirally twisted mass term. *JHEP*, 0108:058, 2001.

[80] Andrea Shindler. Twisted mass lattice QCD. *Phys.Rept.*, 461:37–110, 2008.

[81] C. Pena, S. Sint, and A. Vladikas. Towards a determination of g(8) and g(27) from twisted mass lattice QCD. *Nucl.Phys.Proc.Suppl.*, 129:263–265, 2004.

[82] R. Frezzotti and G.C. Rossi. Twisted mass lattice QCD with mass nondegenerate quarks. *Nucl.Phys.Proc.Suppl.*, 128:193–202, 2004.

[83] R. Frezzotti and C. Rossi. Chirally improving wilson fermions i: O(a) improvement. *Nucl.Phys.Proc.Suppl.*, 129:880, 2004.

[84] Roberto Frezzotti, Pietro Antonio Grassi, Stefan Sint, and Peter Weisz. A local formulation of lattice QCD without unphysical fermion zero modes. *Nucl.Phys.Proc.Suppl.*, 83:941–946, 2000.

[85] R. Frezzotti. Wilson fermions with chirally twisted mass. *Nucl.Phys.Proc.Suppl.*, 119:140–148, 2003.

[86] Thomas DeGrand and Carleton DeTar. *Lattice methods for Quantum Chromodynammics*. World Scientific., 2006.

[87] R. Frezzotti and G. C. Rossi. cutoff effects in lattice wilson fermion simulations. *ETMC Internal notes*, 2009.

[88] Christof Gattringer and Christian B. Lang. *Quantum Chromodynamics on the Lattice.* Springer., 2010.

[89] Simon Duane, A.D. Kennedy, Brian J. Pendleton, and Duncan Roweth. Hybrid monte carlo. *Physics Letters B*, 195(2):216 – 222, 1987.

[90] P.A. Boyle, A. Juttner, C. Kelly, and R.D. Kenway. Use of stochastic sources for the lattice determination of light quark physics. *JHEP*, 0808:086, 2008.

[91] E. Endress, A. Juttner, and H. Wittig. On the efficiency of stochastic volume sources for the determination of light meson masses. 2011.

[92] M. Foster and Christopher Michael. Quark mass dependence of hadron masses from lattice QCD. *Phys.Rev.*, D59:074503, 1999.

[93] C. R. Allton et al. Gauge-invariant smearing and matrix correlators using Wilson fermions at $\beta = 6.2$. *Phys.Rev.*, D74, 1993.

[94] M. Albanese et al. Glueball Masses and String Tension in Lattice QCD. *Phys.Lett.*, B192:163–169, 1987.

[95] N. Carrasco, M. Ciuchini, P. Dimopoulos, R. Frezzotti, V. Gimenez, et al. B-physics from Nf=2 tmQCD: the Standard Model and beyond. 2013.

[96] Beat Jegerlehner. Krylov space solvers for shifted linear systems. 1996.

[97] D.R.T. Jones. Two loop diagrams in yang-mills theory. *Nucl.Phys.*, B75:531, 1974.

[98] R. Sommer. A new way to set the energy scale in lattice gauge theories and its application to the static force and α_s in SU(2) yang–mills theory. *Nucl.Phys.*, B411:839, 1994.

[99] Gilberto Colangelo, Stephan Durr, and Christoph Haefeli. Finite volume effects for meson masses and decay constants. *Nucl.Phys.*, B721:136–174, 2005.

[100] M. Luscher. Volume Dependence of the Energy Spectrum in Massive Quantum Field Theories. 1. Stable Particle States. *Commun.Math.Phys.*, 104:177, 1986.

[101] A. Bode and H. Panagopoulos. The Three loop beta function of QCD with the clover action. *Nucl.Phys.*, B625:198–210, 2002.

[102] A. Skouroupathis and H. Panagopoulos. Two-loop renormalization of scalar and pseudoscalar fermion bilinears on the lattice. *Phys.Rev.*, D76:094514, 2007.

[103] A. Skouroupathis and H. Panagopoulos. Two-loop renormalization of vector, axial-vector and tensor fermion bilinears on the lattice. *Phys.Rev.*, D79:094508, 2009.

[104] C. Alexandrou, M. Constantinou, T. Korzec, H. Panagopoulos, and F. Stylianou. Renormalization constants of local operators for Wilson type improved fermions. *Phys.Rev.*, D86:014505, 2012.

[105] G. Martinelli, C. Pittori, Christopher T. Sachrajda, M. Testa, and A. Vladikas. A General Method for Non-Perturbative Renormalization of Lattice Operators. *Nucl.Phys.*, B445:81–108, 1995.

[106] Enrico Franco and Vittorio Lubicz. Quark mass renormalization in the MS and RI schemes up to the NNLO order. *Nuclear Physics B*, 531(1-3):641 – 651, 1998.

[107] T. Inui, Y. Tanabe, and Y. Onodera. *Group Theory and its Applications in Physics.* Springer-Verlag., 1990.

[108] Kari Rummukainen. *Monte Carlo simulations in physics.* Department of physical sciences, University of Oulu, 2008.

[109] Marc Wagner and Martin Kalinowski. Twisted mass lattice computation of charmed mesons with focus on D^{**}. 2013.

[110] Benoit Blossier, Michele Della Morte, Georg von Hippel, Tereza Mendes, and Rainer Sommer. On the generalized eigenvalue method for energies and matrix elements in lattice field theory. *JHEP*, 0904:094, 2009.

[111] Ph. Boucaud, P. Dimopoulos, F. Farchioni, R. Frezzotti, V. Gimenez, G. Herdoiza, K. Jansen, V. Lubicz, G. Martinelli, C. McNeile, C. Michael, I. Montvay, D. Palao, M. Papinutto, J. Pickavance, G.C. Rossi, L. Scorzato, A. Shindler, S. Simula, C. Urbach, and U. Wenger. Dynamical twisted mass fermions with light quarks. *Physics Letters B*, 650(4):304 – 311, 2007.

[112] Ph. Boucaud, P. Dimopoulos, F. Farchioni, R. Frezzotti, V. Gimenez, G. Herdoiza, K. Jansen, V. Lubicz, C. Michael, G. M′unster, D. Palao, G.C. Rossi, L. Scorzato, A. Shindler, S. Simula, T. Sudmann, C. Urbach, and U. Wenger. Dynamical twisted mass fermions with light quarks: simulation and analysis details. *Computer Physics Communications*, 179(10):695 – 715, 2008.

[113] R. Frezzotti and G.C. Rossi. Chirally improving Wilson fermions. II. Four-quark operators. *JHEP*, 0410:070, 2004.

[114] Damir Becirevic and Francesco Sanfilippo. Lattice QCD study of the radiative decays $J/\psi \to \eta_c\gamma$ and $h_c \to \eta_c\gamma$. *JHEP*, 1301:028, 2013.

[115] Damir Becirevic and Nejc Kosnik. Soft photons in semileptonic $B \to D$ decays. *Acta Phys.Polon.Supp.*, 3:207–214, 2010.

[116] C. Aubin. Lattice studies of hadrons with heavy flavors. *PoS*, LAT2009:007, 2009.

[117] Mariam Atoui, Damir Becirevic, Vincent Morenas, and Francesco Sanfilippo. '$B_s \to D_s\ell\nu$' near zero recoil in and beyond the Standard Model. 2013.

[118] D. Becirevic, V. Lubicz, G. Martinelli, and F. Mescia. First lattice calculation of the electromagnetic operator amplitude $\langle \pi^0 | Q_\gamma^+ | K^0 \rangle$. *Phys.Lett.*, B501:98–105, 2001.

[119] Paulo F. Bedaque. Aharonov-Bohm effect and nucleon nucleon phase shifts on the lattice. *Phys.Lett.*, B593:82–88, 2004.

[120] G.M. de Divitiis, R. Petronzio, and N. Tantalo. On the discretization of physical momenta in lattice QCD. *Phys.Lett.*, B595:408–413, 2004.

[121] M. Constantinou et al. Non-perturbative renormalization of quark bilinear operators with $N_f = 2$ (tmQCD) Wilson fermions and the tree-level improved gauge action. *JHEP*, 1008:068, 2010.

[122] M. Foster and C. Michael. Hadrons with a heavy color-adjoint particle. *Phys. Rev. D*, 59:094509, Apr 1999.

[123] C. McNeile and C. Michael. Decay width of light quark hybrid meson from the lattice. *Phys. Rev. D*, 73:074506, Apr 2006.

[124] S. Gusken. A Study of smearing techniques for hadron correlation functions. *Nucl.Phys.Proc.Suppl.*, 17:361–364, 1990.

[125] Karl Jansen, Chris Michael, Andrea Shindler, and Marc Wagner. The Static-light meson spectrum from twisted mass lattice QCD. *JHEP*, 0812:058, 2008.

[126] P. Dimopoulos et al. Lattice QCD determination of m_b, f_B and f_{B_s} with twisted mass Wilson fermions. *JHEP*, 1201:046, 2012.

[127] Irinel Caprini, Laurent Lellouch, and Matthias Neubert. Dispersive bounds on the shape of $\bar{B} \to D^{(*)}$ lepton anti-neutrino form-factors. *Nucl.Phys.*, B530:153–181, 1998.

[128] A. Le Yaouanc, L. Oliver, and J.C. Raynal. Lower bounds on the curvature of the Isgur-Wise function. *Phys.Rev.*, D69:094022, 2004.

[129] D. Melikhov and B. Stech. Weak form-factors for heavy meson decays: An Update. *Phys.Rev.*, D62:014006, 2000.

[130] Matthias Neubert. Heavy-quark symmetry. *Physics Reports*, 245(5-6):259 – 395, 1994.

[131] Jon A. Bailey, A. Bazavov, C. Bernard, C.M. Bouchard, C. DeTar, et al. $B_s \to D_s / B \to D$ Semileptonic Form-Factor Ratios and Their Application to BR($B_s^0 \to \mu^+ \mu^-$). *Phys.Rev.*, D85:114502, 2012.

[132] S. Faller, A. Khodjamirian, Ch. Klein, and Th. Mannel. $B \to D^{(*)}$ Form Factors from QCD Light-Cone Sum Rules. *Eur.Phys.J.*, C60:603–615, 2009.

[133] K. Azizi. QCD Sum Rules Study of the Semileptonic $B(s)(B^{+-})(B^0) \to D(s)[1968](D^0)(D^{+-})\ell\nu$ Decays. *Nucl.Phys.*, B801:70–80, 2008.

[134] R.N. Faustov and V.O. Galkin. Weak decays of B_s mesons to D_s mesons in the relativistic quark model. *Phys.Rev.*, D87:034033, 2013.

[135] M. Atoui, B. Blossier, V. Morénas, O. Pène, and K. Petrov. Semileptonic $B \to D^{**}$ decays in Lattice QCD : a feasibility study and first results. 2013.

[136] Nathan Isgur, Daryl Scora, Benjamin Grinstein, and Mark B. Wise. Semileptonic B and D decays in the quark model. *Phys. Rev. D*, 39:799–818, Feb 1989.

[137] R. Frezzotti, V. Lubicz, and S. Simula. Electromagnetic form factor of the pion from twisted-mass lattice QCD at $N_f = 2$. *Phys. Rev. D*, 79:074506, Apr 2009.

[138] S. Gusken, U. Low, K.-H. Mutter, R. Sommer, A. Patel, and K. Schilling. Non-singlet axial vector couplings of the baryon octet in lattice QCD. *Physics Letters B*, 227(2):266 – 269, 1989.

[139] John Bulava, Michael Donnellan, and Rainer Sommer. On the computation of hadron-to-hadron transition matrix elements in lattice QCD. *JHEP*, 1201:140, 2012.

[140] Benoit Blossier et al. HQET at order 1/m: III. Decay constants in the quenched approximation. *JHEP*, 1012:039, 2010.

[141] Steven Weinberg. *The Quantum Theory of fields*, volume I: Foundations. Cambridge University Press., May 2005.

[142] D. Spehler and S.F. Novaes. Helicity wave functions for massless and massive spin-2 particles. *Phys.Rev.*, D44:3990–3993, 1991.

Résumé

Les désintégrations semileptoniques du méson B participent à la détermination de certains paramètres fondamentaux du Modèle Standard. Ce travail décrit essentiellement l'étude des deux canaux de désintégrations $B_s \to D_s \ell \bar{\nu}_\ell$ et $B \to D^{**} \ell \bar{\nu}_\ell$ (où les D^{**} sont les premières excitations orbitales des mésons D ayant une parité positive). La cadre théorique est celui de la QCD sur réseau qui, en discrétisant l'espace-temps, permet de calculer non perturbativement les fonctions de Green de la théorie. En utilisant l'action à masse twistée avec deux saveurs dégénérées de quarks dynamiques ($N_f = 2$), nous avons commencé par étudier la spectroscopie des états charmés scalaires D_0^* et tenseurs D_2^*. Ensuite, nous avons réalisé la détermination du facteur de forme $\mathscr{G}_s(1)$ décrivant le processus $B_s \to D_s \ell \bar{\nu}_\ell$ dans le Modèle Standard. Ce paramètre offre un moyen d'extraire l'élément de la matrice CKM V_{cb}. Par ailleurs, et pour la première fois en QCD sur réseau, nous avons déterminé les rapports $F_0(q^2)/F_+(q^2)$ et $F_T(q^2)/F_+(q^2)$ dans la région proche du recul nul: ces contributions sont en effet nécessaires afin de discuter ce canal de désintégration dans certains modèles au-delà du Modèle Standard. Enfin, une étude préliminaire du canal de désintégration $B \to D^{**}$ a été abordée où nous avons trouvé une valeur non nulle de l'élément de matrice décrivant la désintégration $B \to D_0^*$ à recul nul contrairement de ce qui est connu à la limite des quarks lourds. Dans le cas du $B \to D_2^*$, nos résultats ont montré un signal indiquant une différence par rapport aux prédictions de masse infinie. Ces calculs sont indispensables afin de tirer une conclusion plus solide concernant le "puzzle 1/2 vs 3/2".

Abstract

Semileptonic decays of B mesons provide a rich source of knowledge for determining fundamental parameters of the Standard Model. This work reports mainly on the study of two semileptonic decay channels: the $B_s \to D_s \ell \bar{\nu}_\ell$ and $B \to D^{**} \ell \bar{\nu}_\ell$ (where the D^{**} are the first orbitally excited states of the D mesons having a positive parity). The theoretical framework is Lattice QCD which is considered as the only satisfying approach which calculates in a non perturbative way the transition amplitudes from first principles. By using the twisted mass QCD on the lattice with $N_f = 2$ dynamical flavors we studied, first, the spectroscopy of the scalar D_0^* and the tensor D_2^* states. Then, we determined the normalization $\mathscr{G}_s(1)$ of the form factor dominating $B_s \to D_s \ell \bar{\nu}_\ell$ in the Standard Model which provides a means of extracting the CKM matrix element V_{cb}. Next, we make the first lattice determination of $F_0(q^2)/F_+(q^2)$ and $F_T(q^2)/F_+(q^2)$ near the zero recoil. The obtained results are important for the discussion of this decay in various scenarios of physics beyond the Standard Model. Finally, we did a preliminary study of $B \to D^{**}$ where we have obtained a non vanishing matrix element corresponding to the decay of B into the D_0^* at zero recoil contrary to what was known in the heavy quark limit. Moreover, the computations corresponding to $B \to D_2^*$ show a signal indicating a difference with respect to the infinite mass limit prediction. These results are important to draw a firm conclusion on the "1/2 vs 3/2 puzzle".

Keywords:

Heavy Flavor Physics - Lattice QCD - Phenomenology of B mesons - Standard Model - Semileptonic form factors - Orbital excitations D^{**} - Heavy-light mesons